МИНИСТЕРСТВО НАУКИ И ВЫСШЕГО ОБРАЗОВАНИЯ
РЕСПУБЛИКИ КАЗАХСТАН

Некоммерческое акционерное общество «Казахский национальный
исследовательский технический университет
имени К.И.Сатпаева»

Институт геологии и нефтегазового дела им.К.Турысова

УДК 547.458; 541.64; 651.454

На правах рукописи

Гизатуллина Наргиз Нурмухаметовна

МАГИСТЕРСКАЯ ДИССЕРТАЦИЯ

На соискание академической степени магистра

Название диссертации	«Исследование и модификация фракционированного низкомолекулярного биополимера геллана для применения в разработке лекарственных форм»
Направление подготовки	7М07142 – «Химическая технология органических веществ»

Научный руководитель
к.х.н., ассоциированный профессор
_____ Татыханова Г.С.
"13" 06 2025 г.

Рецензент
PhD, ведущий научный сотрудник, National Laboratory Astana
_____ Әбутәліп Мунзия
"12" 06 2025 г.

Нормоконтроль
к.х.н., ассоциированный профессор
_____ Татыханова Г.С.
"13" 06 2025 г.

ДОПУЩЕНА К ЗАЩИТЕ
Заведующий кафедрой «Химической
и биохимической инженерии»
к.х.н, ассоциированный профессор
_____ Р.А. Мангазбаева
"17" 06 2025 г.

Алматы 2025

МИНИСТЕРСТВО НАУКИ И ВЫСШЕГО ОБРАЗОВАНИЯ
РЕСПУБЛИКИ КАЗАХСТАН

Некоммерческое акционерное общество «Казахский национальный исследовательский технический университет имени К.И.Сатпаева»

Институт геологии и нефтегазового дела им. К.Турысова
Кафедра Химической и биохимической инженерии

7М07142 – «Химическая технология органических веществ»

УТВЕРЖДАЮ
Заведующий кафедрой Химической
и биохимической инженерии
к.х.н., ассоциированный профессор
_____ Мангазбаева Р.А.
"17" 06 2025 г.

ЗАДАНИЕ
на выполнение магистерской диссертации

Магистранту: *Гизатуллиной Наргиз Нурмухаметовне*

Тема: *«Исследование и модификация фракционированного низкомолекулярного биополимера геллана для применения в разработке лекарственных форм»*

Утверждена приказом Проректора Университета № 548-П/Ө от 4 декабря 2023 г.

Срок сдачи законченной диссертации: 06.06.2025 г.

Исходные данные к магистерской диссертации: *Исследование и модификация фракционированного низкомолекулярного биополимера геллана для применения в разработке лекарственных форм*

Перечень подлежащих разработке в магистерской диссертации вопросов:

а) Теоретические основы применения и модификации биополимера геллана в разработке лекарственных форм;

б) Экспериментальные исследования по фракционированию и модификации геллана для разработки офтальмологической лекарственной формы;

в) *Результаты фракционирования коммерческого геллана с получением низкомолекулярных фракций, их структурной и молекулярной характеристики, включая определение молекулярных масс, полидисперсности, среднегидродинамических размеров и дзета-потенциалов. Также обсуждаются особенности гелеобразования в различных условиях, модификация геллана поли(2-этил-2-оксазолином), а также исследование иммобилизации офлоксацина в полученные матрицы и оценка кинетики его высвобождения.*

Перечень графического материала: представлены 22 слайда презентации работы, 35 рисунков и 9 таблиц.

Рекомендуемая основная литература: из 105 предложенных, 6 отечественных и 99 зарубежных источников.

ГРАФИК

подготовки магистерской диссертации

Наименование разделов, перечень разрабатываемых вопросов	Сроки представления научному руководителю	Примечание
Анализ литературного обзора, подбор подходящих источников.	20.10.2023 г. – 22.12.2023 г.	Отчет в формате MS Word и презентация MS PowerPoint.
Подбор и обоснование исследовательских методов, проведение пробоподготовки и лабораторных анализов, анализ и интерпретация экспериментальных данных.	25.12.2023 г. – 27.12.2024 г.	Отчет в формате MS Word и презентация MS PowerPoint.
Анализ и интерпретация результатов, обоснование выводов и завершение исследования.	30.12.2024 г. – 23.05.2024 г.	Отчет в формате MS Word и презентация MS PowerPoint.

Подписи

консультантов и норм контролера на законченную магистерскую диссертацию с указанием относящихся к ним разделов работы

Наименования разделов	Консультанты, И.О.Ф. (уч. степень, звание)	Дата подписания	Подпись
Норм контролер	Татыханова Г.С. к.х.н., ассоциированный профессор	13.06.2025	

Научный руководитель _____ Татыханова Г.С.

Задание принял к исполнению обучающийся _____ Гизатуллина Н.Н.

Дата «20» 10 2023г

АҢДАТПА

Диссертациялық жұмыс 116 беттен тұрады, оның ішінде 35 сурет, 9 кесте, 105 дереккөз қамтылған.

Түйінді сөздер: геллан, золь-гель ауысуы, офлоксацин, фракциялау, көз тамшылары, офтальмология.

Зерттеу нысаны: Геллан биополимері – бактерия Sphingomonas elodea (кейде Pseudomonas elodea) арқылы ферментативті жолмен синтезделетін табиғи полисахарид.

Жұмыстың мақсаты: Жоғары молекулалық биополимер гелланды фракциялау әдісі арқылы төмен молекулалы гелланды алу, оның физика-химиялық қасиеттерін анықтау және оны фармацевтикада дәрілік зат ретінде қолдану үшін модификациялау.

Зерттеу әдістері: Фракциялау, идентификация, модификация және гель түзілу процесін, мукоадгезивтік қасиеттер мен дәрілік заттың бөліну кинетикасын зерттеу.

Жұмыстың нәтижелері мен жаңалығы: Зерттеу барысында төмен молекулалық фракцияларды алу үшін гелланды фракциялау әдістемесі қолданды. Барлық алынған фракциялар зерттеліп, олардың молекулалық массалары анықталды. Әсіресе геллан фракцияларының гель түзушілік қасиеттері зерттеліп, оңтайлы төмен молекулалық фракция таңдалды. Гелланның бастапқы және модификацияланған түрлерінің мукоадгезивтік қасиеттері мен дәрілік заттың ультражұқа гелландық үлбірлерден бөлінуі зерттелді.

Жалпы, алынған нәтижелер жаңашыл сипатқа ие және төмен молекулалық массалы геллан фракцияларын медицина мен фармацевтикада қолданудың жаңа мүмкіндіктерін ашады.

Мемлекеттік ғылыми-зерттеу бағдарламаларымен байланысы: Диссертациялық жұмыс AP13067773-ОТ-24 «Геллан мен офлоксацин негізінде ұзақ әсер ететін көз тамшыларын дайындаудың ғылыми негіздері мен технологиясын әзірлеу» (2022–2024 жж.) жоба аясында орындалды.

АННОТАЦИЯ

Диссертация содержит: 116 с., 35 рис., 9 табл., 105 источников.

Ключевые слова: геллан, золь-гель переход, офлоксацин, фракционирование, глазные капли, офтальмалогия.

Объект исследования: биополимер геллан - природный полисахарид, производимый ферментативным путем с помощью бактерии *Sphingomonas (*иногда *Pseudomonas) elodea.*

Цель исследования: получение фракционированного низкомолекулярного биополимера геллана, определение его физико-химических характеристик и модификация для применения в фармацевтической разработке лекарственных средств.

Метод или методология проведения работы: Фракционирование, идентификация, модификация и изучение гелеобразование, мукоадгезивных свойств и кинетика выхода лекарственных веществ.

Результаты работы и их новизна были представлены в исследовании, в котором разработана методика фракционирования для получения низкомолекулярных фракций геллана. В ходе работы были изучены все полученные фракции геллана, а также определена их молекулярная масса. Особое внимание было уделено изучению гелеобразования фракции геллана, с целью выбрать оптимальную фракцию с низкой молекулярной массой. Также были проведены исследования мукоадгезивных свойств геллана и модифицированного геллана. Были изучены выходы лекарственного вещества из ультратонких геллановых пленок.

В целом, полученные результаты являются новаторскими и открывают новые возможности в использовании геллановых фракций с низкой молекулярной массой в медицине и фармацевтике.

Связь с государственными научно-исследовательскими программами: Диссертационная работа выполнена в рамках проекта AP13067773-OT-24 «Разработка научных основ и технологии приготовления глазных капель пролонгированного действия на основе геллана и офлоксацина» (2022-2024гг.)

SUMMARY

The dissertation consists of 116 pages, including 35 figures, 9 tables, and 105 references.

Keywords: gellan, sol-gel transition, ofloxacin, fractionation, eye drops, ophthalmology.

Object of the study: The object of the research is the biopolymer gellan – a natural polysaccharide produced enzymatically by the bacterium Sphingomonas elodea (sometimes Pseudomonas elodea).

Aim of the study: To obtain a fractionated low-molecular-weight gellan biopolymer, determine its physicochemical properties, and modify it for use in the pharmaceutical development of drug formulations.

Method or methodology: Fractionation, identification, modification, and the study of gelation behavior, mucoadhesive properties, and drug release kinetics.

Results and novelty: The research presents a methodology for fractionating gellan to obtain low-molecular-weight fractions. All obtained gellan fractions were studied, and their molecular weights were determined. Special attention was given to studying the gelation capacity of the gellan fractions to identify the optimal low-molecular-weight fraction. The mucoadhesive properties of both native and modified gellan were investigated, along with drug release from ultrathin gellan-based films.

Overall, the results are innovative and open new prospects for the application of low-molecular-weight gellan fractions in medicine and pharmaceutical formulations.

Relevance to state scientific research programs: The dissertation was carried out within the framework of the project AP13067773-OT-24 "Development of scientific foundations and technology for the preparation of prolonged-release eye drops based on gellan and ofloxacin" (2022–2024).

СОДЕРЖАНИЕ

ВВЕДЕНИЕ

Гелловая камедь привлекает большое внимание исследователей благодаря широкому применению в биотехнологии, медицине и нефтедобыче.[1-3] Повторяющиеся мономерные звенья геллановой камеди состоят из следующих остатков: 1,3-β-D-глюкозы, 1,4-β-D-глюкуроновой кислоты, 1,4-β-D-глюкозы и 1,4-α-L-рамнозы.[4] Геллан, содержащий лекарственные вещества, может быть использован в фармацевтике в пероральной, буккальной, назальной, офтальмологической, вагинальной и других формах[2]. Ранее была разработана система доставки офтальмологических лекарственных средств на основе комплекса геллана с антимикробным препаратом – офлоксацином[5]. Было обнаружено, что гелеобразование геллана в ответ на имитацию слезной жидкости подходит для офтальмологических препаратов в условиях *in vitro* в качестве загущающего компонента, препятствующего дренажу из глаза и продлевающего время удержания лекарственного средства[6]. Однако чрезвычайно высокая молекулярная масса первозданного геллана[7] в диапазоне $(5\text{-}10)\cdot10^5$ ограничивает широкое применение геллана, в качестве системы доставки лекарственных средств.

С целью расширить применение геллана для создания высокоэффективных систем доставки лекарств, были поставлены следующие задачи:

- Фракционировать коммерческий геллан для получения низкомолекулярных фракций разными методами и провести их физико-химическую идентификацию;
- Исследовать золь-гель переход и реологические характеристики геллана и его фракций в условиях смоделированной искусственной слезной жидкости (в присутствии низкомолекулярных солей, при варьировании pH и температуры);
- Оценить влияние офтальмологического лекарственного препарата на процесс гелеобразования геллана и его фракций;
- Модифицировать низкомолекулярные фракции геллана, исследовать полученные образцы и сравнить их свойства с исходными с целью оптимизации гелеобразующих и реологических характеристик.

Коммерческий низкомолекулярный геллан был очищен методом фракционного растворения. Водный раствор очищенного коммерческого низкомолекулярного геллана обладал полиэлектролитными свойствами благодаря высокой молярной массе и карбоновым группам во фрагментах глюкуроновой кислоты. Эмпирическое уравнение Фуосса определило внутреннюю вязкость очищенного геллана в воде без соли. Фракционирование коммерческого геллана осуществлялось с помощью ультразвуковой обработки и методом дробного осаждения. Фракции геллана были охарактеризованы с помощью протонной ЯМР- и ИК- спектроскопии. Внутреннюю вязкость образцов низкомолеклярного геллана измеряли в 0,025

М хлорида тетраметиламмония. Молекулярные массы фракций геллана были определены с помощью уравнения Марка-Куна-Хоувинка. Кроме того, осуществлена модификация геллана с помощью полиоксазолина и подтверждена привязка сополимеров Геллан-PEtOx при помощи ИК-спектроскопии.

1 Основная часть

1.1 Биополимер геллан

В течение последних нескольких десятилетий микробные полисахариды интенсивно изучались благодаря их выгодным физико-химическим свойствам. В настоящее время одним из наиболее широко изученных и всесторонне описанных представителей этой группы является геллан - линейный полимер, природный полисахарид, производимый ферментативным путем с помощью бактерии *Sphingomonas (*иногда *Pseudomonas) elodea* [8, 9], повторяющееся звено в макромолекулярной структуре состоит из остатков 4 полисахаридов: 2х β-D-глюкоз, β-D-глюкуроновой кислоты и α-L-рамнозы (Рис. 1):

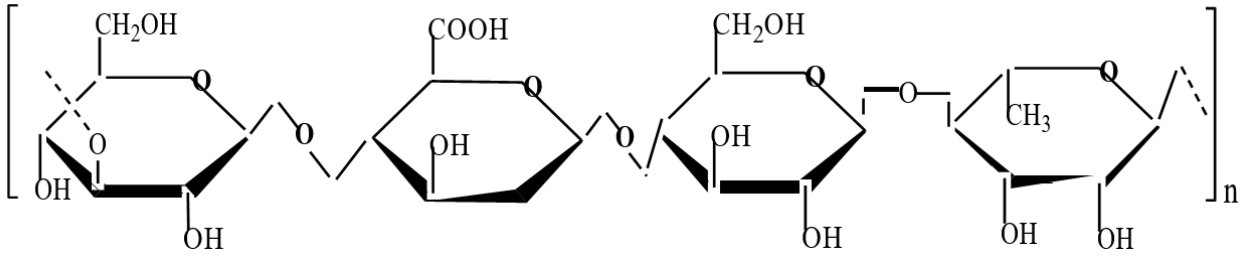

Рисунок 1 – Структура повторяющегося звена геллана

В работе[10] представлены химические и физические свойства геллана. Нативный геллан состоит из высокоацильных и низкоацильных предшественников [9]. Основное различие между ними заключается в том, что высокоацильный геллан содержит два ацильных заместителя: ацетил и L-глицерил [11]. Низкоацильный геллан получают путем удаления ацильных остатков щелочным гидролизом [12]. Различия между гелланом с высоким и низким содержанием ацила описаны в работе [13]

Авторы Morris et al. [14] всесторонне рассмотрели структуру, конформацию, гелеобразование, топологию, реологию и аспекты применения геллана. Конформационные и золь-гель-фазовые переходы геллановых смол , индуцированные температурой, добавлением соли, изменением pH и т.д., стали основным предметом многих исследований [15-20].

До сих пор большинство исследований было сосредоточено на применении геллана в качестве пищевого ингредиента – геллановая камедь применяется в качестве желирующего агента. Кроме того, применяется в различных отраслях науки, например, в качестве желирующего агента бактериологических сред, а также в качестве гелеобразующего агента в соленой воде (пластовые воды) для повышения нефтеотдачи пластов. Однако в последние годы наблюдается рост исследований на применение геллана в медицине[21-29].

1.2 Применение геллана в промышленности и науке

Биополимер геллан имеет широкое применение в различных отраслях промышленности и науки, а именно пищевой промышленности, микробиологии, биомедицине и тканевой инженерии, фармацевтике и .

Геллан используется в качестве желирующего агента в производстве пищевых продуктов[30-32], а именно молочных и растительных напитков, различных десертов, джемов и мармелада. Кроме того, геллан является хорошей альтернативой желатину в производстве веганских продуктах, например жевательных конфет. Не таким распространенным, но не менее важным является применение геллана в производстве макаронных изделий для улучшения текстуры, повышения упругости и снижению ломкости. Применение геллана в пищевой промышленности обусловлено уникальными физико-химическими и технологическими свойствами, которые выгодно отличают его от традиционных желирующих агентов.

Гелановая камедь активно применяется в качестве альтернативного желирующего агента в микробиологических и бактериологических средах, особенно в случаях, когда требуется высокая прозрачность, термостабильность или низкое содержание ионов, таких как натрий. В своей работе Tamaki et al. [33] обсуждают преимущества геллана по сравнению с агаром, включая более высокую прозрачность, термостабильность и возможность формирования прочных гелей в присутствии катионов. Эти свойства делают геллан подходящим для культивирования термофильных бактерий и других микроорганизмов, требующих специфических условий. В исследовании Shandera et al. [34], была разработана среда с 1% геллана (Gel-Gro™) с низким содержанием натрия (<2 мМ) для оценки потребности бактерий Vibrio в Na^+. Результаты показали, что большинство штаммов Vibrio не росли без добавления Na^+, в то время как Aeromonas, не требующие Na^+, росли хорошо. Это подчеркивает пригодность геллана для создания сред с контролируемым содержанием ионов. Кроме того, изучено, что геллан, заменяющий агар в микологических средах, не только является подходящим желирующим агентом в микробиологических средах, используемых для ПЦР-приложений, благодаря своей чистоте и способности не ингибировать ферментативные реакции [35], но и позволяет ускорить идентификацию видов Aspergillus с использованием ПЦР, обеспечивая точные результаты в течение 24 часов после пересевания[36, 37]. Все эти исследования демонстрируют, что гелановая камедь является эффективной альтернативой агар-агару в различных микробиологических приложениях, особенно когда требуются специфические физико-химические свойства среды.

Высокая биологическая совместимость, а также способность формировать прочные устойчивые гели в присутствии различных ионов способствовала применению биополимера геллана в различных областях биомедицины и тканевой инженерии[38-40].

Кроме того, в настоящее время активно ведется изучение перспектив применения геллана в нефтедобывающей промышленности в качестве агента для повышения нефтеотдачи пластов[41]. Гелановая камедь, обладающая высокой ионной чувствительностью и способностью формировать прочные гели в условиях высокой минерализации, рассматривается как перспективный полимер для применения в технологиях повышения нефтеотдачи пластов. Исследования показывают, что растворы геллана устойчивы в присутствии солей, характерных для пластовых вод, и могут использоваться для создания плотных гелевых барьеров, эффективно перекрывающих высокопроницаемые зоны коллекторов[42]. Применение геллана в таких условиях обеспечивает улучшенное вытеснение остаточной нефти за счёт перераспределения потоков и увеличения эффективности закачки.

1.3 Применение геллана в медицине

Уникальная структура и гелеобразующие свойства геллана в настоящее время позволяют выступать данному полимеру в качестве мощной многофункциональной фармацевтической добавки. Особенность свойств гелеобразования в различных средах привели к разработке лекарственных форм с контролируемым пролонгированным высвобождением действующих веществ на основе биополимера геллана, а именно были изучены такие формы, как пероральные, назальные, офтальмолагические и др.[43, 44]. *Osmalek et al.* [43] в своей работе указывают на то, что материалы на основе биополимера геллана применяемы в регенеративной медицине, стоматологии, а также генной инженерии, а именно в технологии переноса генов. Гелановые гидрогели показывают превосходные результаты экспериментов на биосовместимость *in vivo* и *in vitro*[44], а также контролируемые физико-механические и инъекционные свойства[46-48] для применения в регенерации хрящей[46, 47], тканевой инженерии[49], инкапсуляции клеток[50], а также регенерации пульпозного ядра[51].

Широко известно, что рак является одной из ведущих причин смертности в мире, ежегодно регистрируется более 10 миллионов новых случаев заболевания. В настоящее время обширными являются исследования наночастиц золота AuNPs, стабилизированных гелановой камедью, в противоопухолевой терапии[52-70].

Гелеобразующие свойства геллана позволяют использовать его в фармацевтической разраотке офтальмолагических препаратов. Геллан являтеся не токсичным[71] для организма человека. В настоящее время наиболее известным препаратом на основе геллана является Timoptic XE®. В сравнении со стандартным раствором Timolol, Timoptic XE® нанесенный на роговицу кролика повышает биодоступность лекарственного средства в три-четыре раза и снижает частоту проявления нежелательных эффектов [72, 73].

Системы, состоящие из модельного препарата Gatifloxacin 0,3% и Геллана или смеси Геллан:Альгинат натрия:Карбоксиметилцеллюлоза обладают мукоадгезивными свойствами. Продолжительность выделения лекарственного препарата в условиях in vitro превышала 12 ч. [74]. Комбинации Gerlite®: альгинат содержащие matrine, в предварительных исследованиях на роговице, в условиях in vivo обладают пролонгирующей способностью высвобождать активную субстанцию. Реологические исследования показали, что подобные смеси обладают псевдопластичным характером жидкости при контакте с искусственной слезной жидкостью. Данное свойство благоприятно сказывается на доставку офтальмологических препаратов на поверхность глаза [75]. Изучение вязкости микроэмульсионных систем, содержащих terbinafine hydrochloride, и в комбинации с муцином (mucine) позволило установить возможные взаимодействия между макромолекулами Геллана и муцина, доказывающие возможность адгезии к биоповерхностям [76].

1.4 Проблемы традиционных глазных капель

В лечении глазных заболеваний широкое применение имеют глазные капли. Данная лекарственная форма(ЛФ) на ряду со всеми преимуществами имеет один существенный недостаток – низкую или ограниченную биодоступность. Капли при попадании на слизистую глаза достаточно быстро вымываются слезной жидкостью и выводятся через носослезной канал, при этом эффективность препаратов снижается, что подтверждают исследования. Лишь 0,1-5% ЛВ проникает через роговицу и такого количество недостаточно для эффективной доставки к тканям глаза[77, 78].

Данная проблема требует создания новых глазных ЛФ, которые будут обладать повышенной биодоступностью и эффективностью лечения офтальмологических заболеваний.

Увеличение времени контакта лекарственного средства(ЛС) с поверхностью слизистой оболочки глаза – один из наиболее простых, удобных и эффективных способов повыить биодоступность. Для это применимы водорастворимые полимеры, вязкие полутвердые ЛФ и глазные капли, способные образовывать гель при контакте со слизистой оболочкой глаза [79-81]. Кроме того, применение наноносителей и мукоадгезивных систем, способствующих улучшению проникновения препарата, а также защите и регенерации эпителия глаза являются перспективными методами в данной области [82-86]

Несмотря на широкий выбор лекарственных препаратов(ЛП) для лечения офтальмологических заболеваний на современном рынке, эффективность доставки лекарственных веществ(ЛВ) остается актуальной проблемой, что связано со сложным анатомическим строением человеческого глаза и его природными защитными механизмами[87]. В

независимости от формы лекарственного препарата, биодоступность остается ограниченно-низкой, что связано с барьерной функцией роговицы и склеры глаза. Роговица глаза имеет покрытие, состоящее из трех слоев слезной пленки(липидной, водной и слизистой), которая вместе со слизистой оболочкой служит первичными препятствием для проникновения лекарственных веществ [88].

Существует несколько стратегий для улучшения биодоступности лекарственных систем. Одним из эффективных подходов является улечшение растворимости действующего вещества, что позволяетувеличить его концентрацию в ЛФ, снизить дренажные потери и уменьшить необходимую дозировку ЛП [89, 90]. Кроме того, исследуются вещества, способствующие усилению проникновения ЛП, например этилендиаминтетрауксусная кислота и ее аналоги, которые связывают ионы Ca^{2+} тем самым ослабляя межклеточные связи роговицы и повышают проницаемость тканей [91, 92]. Перспективным направлением в настоящее время являются оккулярные вставки, обеспечивающие пролонгированное высвобождение лекарства [93, 94]. Лечение заболеваний сетчатки глаза рассматривает целесообразным применение инвазивных методов: имплантаты, нацеленные на пролонгированную доставку лекарственного средства и снижающие частоту инъекций [95].

Swan [96] в своей работе впервые предложил использовать водорастворимые полимер с целью создания ЛФ, способных задерживаться на поверхности глаза. Вязкость офтальмологических растворов может быть повышена за счет использования производных целлюлозы, поли(винилового спирта), поли(винилпирролидона), карбомеров, природных полисахаридов и гиалуроновой кислоты [97, 98]. Примером успешного внедрения таких систем является препарат Тимол для лечения глаукомы, где, за счет использования геллана, удается сократить частоту приема в 4 раза по сравнению с традиционными каплями. Перспективным направлением можно считать гелеобразующие систему in situ, особенность которых заключается в способности перехода из жидкой формы в гель под действием физиологических факторов – pH, температуры и электролитов слезной жидкости. Кроме того, применение наночастиц с инкапсулированным препаратом способствует лучшему проникновению через барьеры глаза, обеспечивая удержание препарата в области роговицы глаза и конъюктивы и тем самым пролонгируя высвобождение действующего вещества.

1.5 Фракционирование биополимеров

Биополимер геллан, обладающий рядом преимуществ, также и обладет некоторыми недостатками, как например высокая молекулярная масса свыше ≈ 500 000 Дальтон , что является причиной низкой способности к растворимости в воде холодной или комнатной температуры, хорошей и

быстрой растворимостью только при повышении температуры ≈ 50 – 100 ºС, и повышенной вязкостью полученных растворов. В данной работе для устранения этих недостатков применено фракционирование коммерческого биополимера геллана.

Фракционирование – экспериментальное разделение полимеров на части (узкие фракции) более однородные по молекулярным массам, чем исходный образец полимера.

1.6 Модификация биополимеров

С целью повышения биодоступности и улучшения мукоадгезивных свойств данная работа включала этап модифицирования геллана.

Модификация полимера – направленное изменение свойств полимеров, заключающееся в преобразовании надмолекулярной структуры полимера и изменение химического состава и/или молекулярной массы полимера. Исследование было проведено с использованием модификации геллана с помощью полиоксазолина (ПОЗ).

2 Экспериментальная часть

2.1 Материалы

Геллан – природный полисахарид, открытие которого было осуществлено в 1977 году, производимый ферментативным путем с помощью бактерии *Sphingomonas* (иногда *Pseudomonas*) *elodea,* повторяющееся звено в макромолекулярной структуре состоит из остатков 4 полисахаридов: 1,3-β-D-глюкозы, 1,4-β-D-глюкуроновой кислоты, 1,4-β-D-глюкозы и 1,4-α-L -рамнозы (Рис. 2):

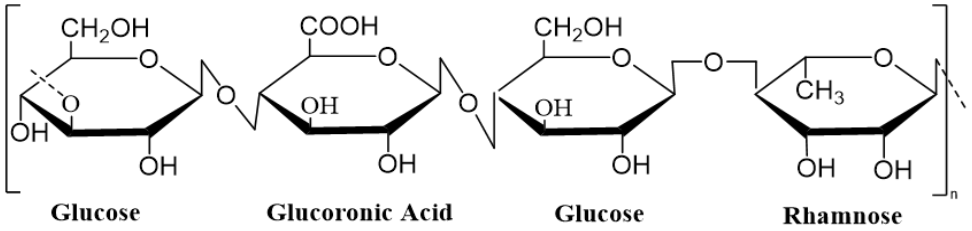

Рисунок 2 – Структура повторяющегося звена геллана

Коммерческий низкомолекулярный геллан был приобретен у “Zhejiang DSM Zhongken Biotechnology Co., Ltd.”, Китай.

Офлоксацин – это антибактериальное средство, относящееся к группе фторхинолонов, обладающее широким спектром действия. Офлоксацин является кристаллическим порошком бледно-желтого или ярко-желтого оттенков. Данное лекарственное средство применяется для лечения различных инфекционно-воспалительных заболеваний, вызванных микроорганизмами, чувствительными к L-энантиомеру-левофлаксоцину, который обусловливает антибактериальную активность. Офлоксацин – это надежный помощник в лечении инфекционно-воспалительных заболеваний, обусловленных ростом большинства грамотрицательных и некоторых грамположительных бактерий. Систематическое название офлоксацина – 9-фтор-2,3-дигидро-3-метил-10-(4-метил-1-пиперазинил)-7-оксо-7Н-пиридо(1,2,3,-d,e)-1,4-бензоксазин карбоновая кислота и структура изображена на рисунке 3.

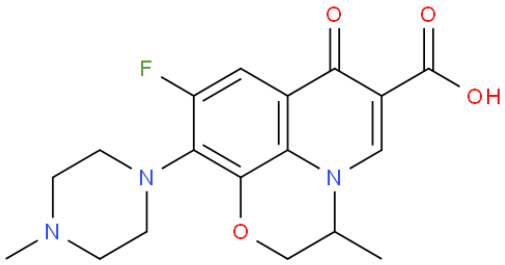

Рисунок 3 – Структурная формула офлоксацина

2-этил-2-оксазолин (EtOx, ≥99 %) M= 99,13г/моль – фирмы «Aldrich Chemical Co.» (США) марки «ч» был использован без дополнительной очистки. Мономер имел характеристики, совпадающие с литературными данными.

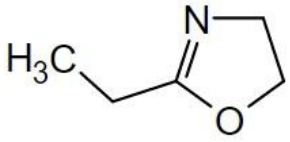

Рисунок 4 – Структурная формула 2-этил-2-оксазолина

Сульфолан – M=120,17 г/моль, ρ=1,26г/см^3, – фирмы «Aldrich Chemical Co.» (США) марки «ч» (99%) был использован без дополнительной очистки.

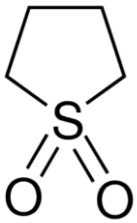

Рисунок 5 – Структурная формула сульфолана

Метилтрифторметансульфонат (MeOTf, 98%) - инициатор, продукт фирмы Sigma-Aldrich.

Метил-п-толуолсульфонат (MeOTs, 97%) - инициатор, продукт фирмы Sigma-Aldrich.

Растворители: *Диметилсульфоксид* (ДМСО, 99,99%, Fischer Scientific Oy) и *толуол* (≥99,9 %, Merck Mil lipore) перед использованием подвергался высушиванию на молекулярных ситах (3 Å, VWR). *Диэтиловый эфир* (безводный, J.T. Baker), и *тетрагидрофуран* (ТГФ, ≥99,9 %, Honeywell) были использованы для сушки геллана. Для очистки геллана применялись *ацетон* (≥99,8 %) и *изопропанол* (≥99,5 %, Fischer-Chemicals Oy) и хлорид тетраметиламмония (TMACl) (≥ 98%, Sigma-Aldrich).

В экспериментах с водными растворами использовалась деионизированная вода.

В синтезе также использовались гидрид натрия (NaH, 60% дисперсия в минеральном масле), диэтиловый эфир (безводный, J.T. Baker) и тетрагидрофуран (ТГФ, ≥99,9%, Honeywell), который применялся для сушки геллана. В экспериментах по ЯМР использовалась тяжеловодородная вода или оксид дейтерия(D_2O, 99% D, Euriso-Top). Диализные мембраны (с молекулярной массой 3,5 кДа и 12-14 кДа соответственно) были приобретены в Spectrum Laboratories. Для всех экспериментов

использовалась вода Milli-Q, полученную из аппарата Millipore, с удельным сопротивлением 18,2 МОМ/см при 298 К.

2.2 Методы исследования

ИК-Фурье спектры фракционированного и модифицированного геллана были записаны на приборе Cary 660 ATR-FTIR (Agilent, США).

ЯМР спектроскопия осуществлена на спектрометре Bruker BioSpin Avance III 500 MHz (частота 500 и 126 МГц соответственно) с использованием растворителя D_2O. Химические сдвиги измерены относительно сигналов остаточных протонов дейтерированного растворителя.

Спектры поглощения офлоксацина были сняты на УФ- и видимом спектрофотометре Specord 210 plus BU (Германия).

Измерения динамического рассеяния света (ДЛС), дзета-потенциала и значения изоэлектрической точки были выполнены с помощью Zetasizer Nano ZS90 (Malvern, Великобритания), оснащенного лазерным источником с длиной волны 633 нм при температуре 25°C.

Термогравиметрический анализ (ТГА) проведен с помощью LabSys Evo (Setaram, Франция), в диапазоне температур 25-700°C при скорости нагрева 10°C/мин.

Кинетика выхода лекарственных веществ была измерена с помощью диализной мембраны с размерами пор 14 кДа (Sigma-Aldrich).

Вязкость биополимера геллана измерялась вискозиметром Уббелоде. № 1с, K=0.03.

2.3 Методики исследования

2.3.1 Фракционирование геллана методом дробного осаждения

В дистиллированной воде был приготовлен 1% раствор коммерческого геллана растворением при 50 ^{0}C с постоянным перемешиванием в течение 24 часов. Полученный раствор затем подвергался центрифугированию с помощью лабораторной центрифуги Sigma 2K15C “B.Braun Biotech International” в течение 30 минут при 40°C со скоростью вращения 5000 об/мин. Прозрачная фракция – супернатант был собран и осажден в ацетоне (1:4 по объему). Образовавшийся осадок был собран отдельно и заново растворен, после чего также центрифугирован в течение 30 мин при 40°C со скоростью вращения 5000 об/мин. Дробное осаждение проводилось 4 раза, после чего остался нерастворимый осадок. Полученные 4 фракции супернатантов по отдельности были очищены осаждением в ацетоне (1:4 по объему), а затем очищенные фракции геллана отделялись от водно-

ацетоновой смеси вакуумной фильтрацией с использованием фильтровальной бумаги марки Whatman 541 и сушились в течение ~30 минут. Сухие образцы геллана дважды промывались изопропанолом, а после геллан растворялся в деионизированной воде и был подвержен диализу (12–14 кДа) в течение не менее 48 часов. После окончания диализа, образцы были высушены при помощи лиофильной сушки и собраны в виде сухих пушистых волокон белого цвета (рис.6).

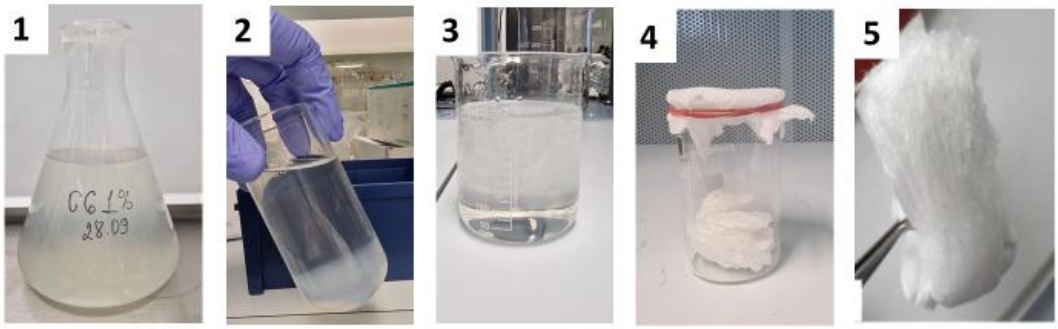

Рисунок 6 – Очистка коммерческого низкомолекулярного геллана методом дробного осаждения

2.3.2 Фракционирование методом ультразвуковой обработки

Для обработки образцов ультразвуком использовался ультразвуковой процессор UP400S (400 Вт, 24 кГц) “Hielscher Ultrasound Technology”. Ультразвуковую обработку водного раствора коммерческого низкомолекулярного геллана с начальной концентрацией 1 мас.% проводили при 50°C в течение 10, 20, 30, 60, 90 и 120 мин. Образцы, обработанные ультразвуком, центрифугировали с помощью лабораторной центрифуги Sigma 2K15C “B.Braun Biotech International”[6] при 50°C в течение 1 часа. Каждый раз отделенную жидкость осаждали изопропиловым спиртом, несколько раз подвергали диализу и подвергали сушке с помощью сублимационной сушилки FreeZone plus объемом 2,5 л “LABCONCO”.

2.3.3 Синтез поли (2-этил-2-оксазолина)

Стеклянная посуда, используемая при синтезе и дистилляции, перед использованием выдерживается в течение ночи в сушильном шкафу при температуре 90°C. Гидрид кальция используется для сушки 2-этил-2-оксазолина (EtO_X) и сульфолана. EtOx помещается в круглодонную колбу и добавляется CaH_2 до тех пор, пока смесь не приобретает молочный цвет. Сушильная трубка, заполненную гранулами хлорида кальция, подсоединяется к колбе, и смесь перемешивается до следующего дня. Для сульфолана сушка

идентична, но колба помещается в масляную ванну, установленную на 32°C, что выше точки замерзания сульфолана (28,4°C). На следующий день EtOx перегоняется при атмосферном давлении с использованием инертного газа – азота, а сульфолан при пониженном давлении.

В работе Loukotová et al. [99] был проведен синтез полимера, аналогичный описанному, но с некоторыми адаптациями. Соотношение мономера к инициатору составляло 50:1 для полимеризаций PEtOx с целью достижения молярной массы 5000 г/моль. В качестве инициатора использовался метилтрифторметансульфонат (MeOTf).

Для синтеза живых трансплантатов PEtOx процедура полимеризации начиналась с барботирования этилоксиэтанола (EtOx) в количестве 2 г (20,18 ммоль) и сульфолана (4 мл) азотом при температуре 35°C в течение 30 минут. Более высокая концентрация мономера приводила к формированию слишком вязких полимерных растворов, что оказывалось неэффективным. Раствор инициатора (примерно 100 мг/мл MeOTf) подготавливался в другой колбе (5 мл) и подвергался азотированию в течение 15 минут при 35°C. Затем раствор инициатора (0,66 мл) был переносен в реакционную смесь с помощью иглы. Смесь перемешивалась при умеренной скорости в течение 60 минут, после чего температура масляной ванны поднималась до 70°C. Перемешивание продолжалось около 24 часов в атмосфере азота. Образец PEtOx (Mn = 7960 г/моль) применялся для синтеза сополимеров геллан-PEtOx.

2.3.4 Модификация геллана с использованием полиоксазолина

Процесс модификации геллана полиоксозалином продемонстрирован на рисунке 7. Прививка гелановых цепей происходила в двух параллельных процессах, начиная с полимеризации EtOx. С помощью NaH происходила активировация геллана, образуя ионы алкоксида. Однако прививка может также происходить на карбоновых группах D-глюкуроната. В ходе прививки образуется новая ковалентная эфирная связь между цепью PEtOx и Геллан. Тестирование прививки осуществлялось при трех температурах. Прививка при 70°C привела к обширному разложению гелановой камеди. Синтез при температуре ниже 40°C способствует гелеобразованию, что неблагоприятно. Для указанных полимеров была выбрана оптимальная температура ≈ 50°C.

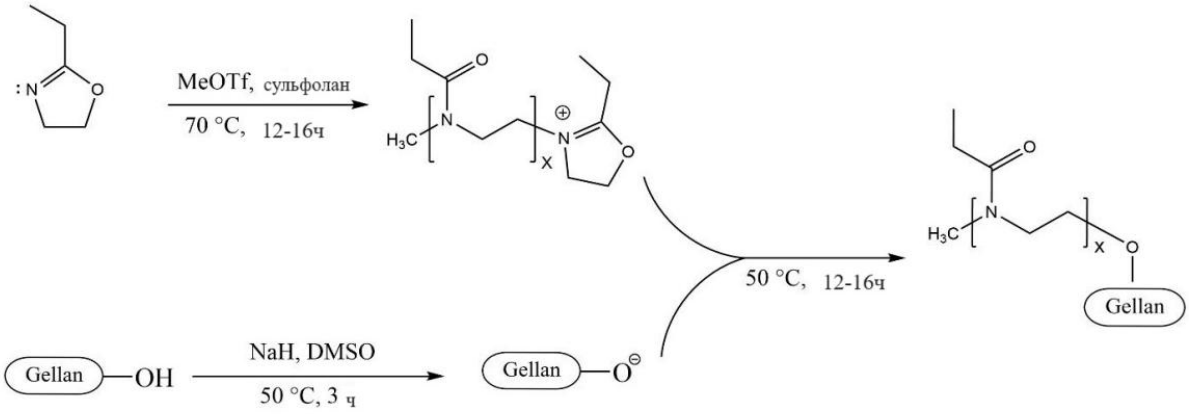

Рисунок 7 – Схематическое изображение синтеза сополимеров геллан-PEtOx

Гидрид натрия (340 мг, 8.4 ммоль) добавляли к 10 мг/мл раствору геллана в азеотропно высушенном ДМСО с использованием толуола (200 мг, 1,14 ммоль, что является усреднением четырех сахарных единиц, растворяли в 20 мл). Смесь перемешивали в течение 3 часов при 50°C. Иглу вводили через резиновую перегородку для высвобождения образовавшегося газообразного водорода. Затем предварительно определенное количество живых цепей PEtOx в сульфолане добавляли иглой к смеси геллан/ДМСО, и смесь перемешивали в течение ночи.

2.3.5 Моделирование слезной жидкости

Для приготовления раствора искусственной слезной жидкости (ИСЖ) использовались следующие реагенты [100]: 670 мг хлорида натрия (NaCl), 200 мг бикарбоната натрия ($NaHCO_3$), 8 мг дигидрата хлорида кальция ($CaCl_2 \cdot 2H_2O$), 100 мл деионизированной воды. Естественный водородный показатель pH слезной жидкости близок к нейтральному значение, поэтому исходный раствор ИСЖ был доведен до значения pH раствора 7,40. Кроме того температура раствора поддерживалась при 37 °C с помощью водяной бани на протяжении всех экспериментов по адгезии слизистой оболочки.

3. Результаты и обсуждение

3.1. Фракционирование коммерческого биополимера геллана с целью получения низкомолекулярных фракций

Коммерческий биополимер геллан – это природный полисахарид, высокая молекулярная масса которого является причиной слабой растворимости в воде, что приводит к получению мутных растворов с повышенной вязкостью. С целью получения низкомолекулярных фракций было проведено фракционирование двумя методами: дробного осаждения и ультразвуковой обработки.

Методом дробного осаждения было получено 4 фракции низкомолекулярного геллана и нерастворимый осадок. Согласно таблице 1, первая фракция GG-1 была выделена с преобладающей массой по сравнению с последующими фракциями.

Таблица 1 – Выход фракций геллана в процессе дробного осаждения

Фракция	Размер пор диализных мембран, кДа	Выход, мг
GG-1	12-14	30,2
GG-2	12-14	18,8
GG-3	12-14	14,8
GG-4	12-14	9,6
Нерастворимый осадок		19,8

Метод ультразвуковой обработки 1вес.% водного раствора коммерческого геллана проводилась при 50 °С в течение 5, 10, 30, 60 и 120 минут. Образцы, полученные фракционированием методом УЗ-обработки, были подвержены центрифугированию при 50 °С в течение 30 минут. Супернатант, полученный после каждого центрифугирования, был осажден изопропиловым спиртом, а затем был проведен диализ полученных образцов с использованием диализных мембран (размеры пор 12-14 кДа) в течение не менее 48 часов. После проведения диализа образцы были заморожены и высушены в лиофильной сушке. Полученные образцы имели вид сухих пушистых волокон белого цвета.

При применении метода обработки ультразвуком 1% водного раствора геллана была выявлено зависимость выхода полученных образцов низкомолекулярного гелана от длительности воздействия ультразвуком. Согласно таблице 2, с увеличением длительности воздействия, выход низкомолекулярных фракций также увеличивается.

Таблица 2 – Выход фракций геллана после методом ультразвуковой обработки

Фракция	Время ультразвуковой обработки, мин	Размер пор диализных мембран, кДа	Выход, %
1-GG	5	12-14	3,9
2-GG	10	12-14	2,4
3-GG	30	6-8	39,9
4-GG	60	3,5	24,1
5-GG	120	3,5	42,8

3.1.1 Определение молекулярных масс фракций геллана, полидисперсности и идентификация их структуры

Наличие карбоновых групп во фрагментах глюкороновой кислоты в фракционированных низкомолекулярных образцах геллана приводит к проявлению полиэлектролитных свойств, как например, зависимость ŋsp/C не может быть экстраполирована на нулевую концентрацию полиэлектролита для определения внутренней вязкости (рисунок 8).

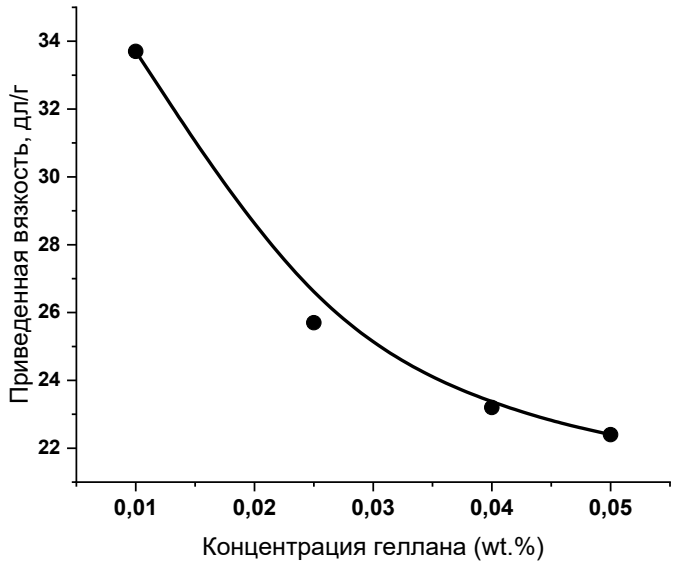

Рисунок 8 – Зависимость приведенной вязкости низкомолекулярного геллана в дистиллированном воде от концентрации полимера

Существует несколько способов решения данной проблемы:
1) при помощи эмпирического уравнения;

2) при помощи добавления низкомолекулярных солей с целью подавления полиэликтролитного эффекта.

Добавление низкомолекулярных солей приводит к гелеобразованию геллана, что является препятствием для измерения внутренней вязкости. На рисунке 9 изображена кривая из рисунка 8, которая была линеаризована с применением уравнения Фуосса [101]:

$$\frac{C}{\eta_{sp}} = \frac{1}{[\eta]} + k_{Fs}\frac{1}{[\eta]}c^{1/2}, \quad (1)$$

где C – концентрация раствора, г/мл;

η_{sp} – удельная вязкость, $см^3/г$;

k_{Fs} – коэффициент Фуосса.

Внутренняя вязкость геллана, определенная по уравнению Фуосса, равна 5680 $cm^3 \cdot g^{-1}$.

Вязкость различных фракций геллана была оценена с применением автоматизированного вискозиметра Micro-KPG Ubbelohde. Для проведения данных измерений были приготовлены растворы геллана различных концентраций (0.025 г/дл, 0.05 г/дл, 0.08 г/дл, 0.1 г/дл, 0.12 г/дл и 0.15 г/дл). В качестве растворителя использовался раствор триметиламмоний хлорида (TMACl) с концентрацией 0.025 М.

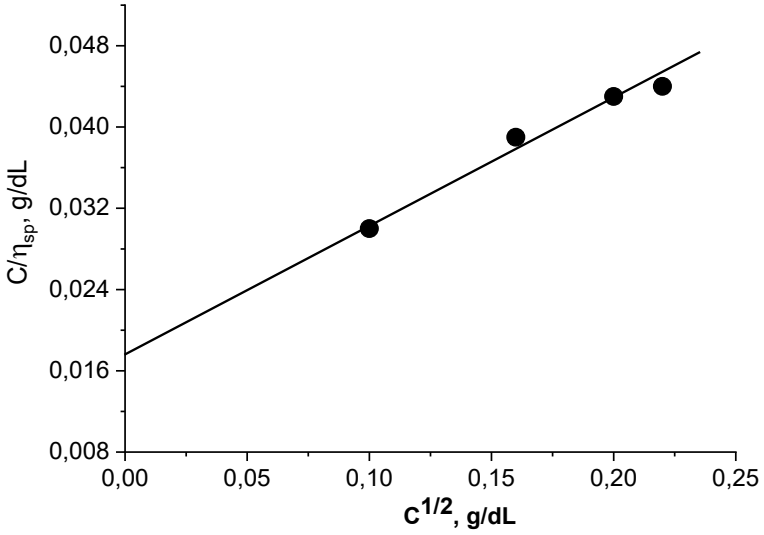

Рисунок 9 – Характеристическая вязкость низкомолекулярного геллана, определенная в дистиллированной воде по уравнению Фуосса

Приведенная вязкость образцов была измерена двумя методами: дробным растворением и ультразвуковой обработкой. На рисунках 10 и 11 соответственно представлены результаты. С целью получения характеристической вязкости [η], выполнена экстраполяция приведенной

вязкости η_{sp}/C к предельному значению при сосредоточении раствора, стремящемся к 0 ($C \rightarrow 0$).

В таблицах 4 и 5 представлены средние молекулярные массы фракций геллана (Mη) с применением уравнения Марка-Куна-Хоувинка [102]:

$$[\eta] = 7{,}48 \cdot 10^{-3} \cdot M_w^{0.91} \quad (2)$$

где [ŋ] – удельная вязкость, $см^3/г$;

$7{,}48 \cdot 10^{-3}$ – константа К, дЛ/г;

M_w – средневзвешенная молекулярная масса, $г/моль^{-1}$;

0,91 – показатель степени α, эмпирический параметр.

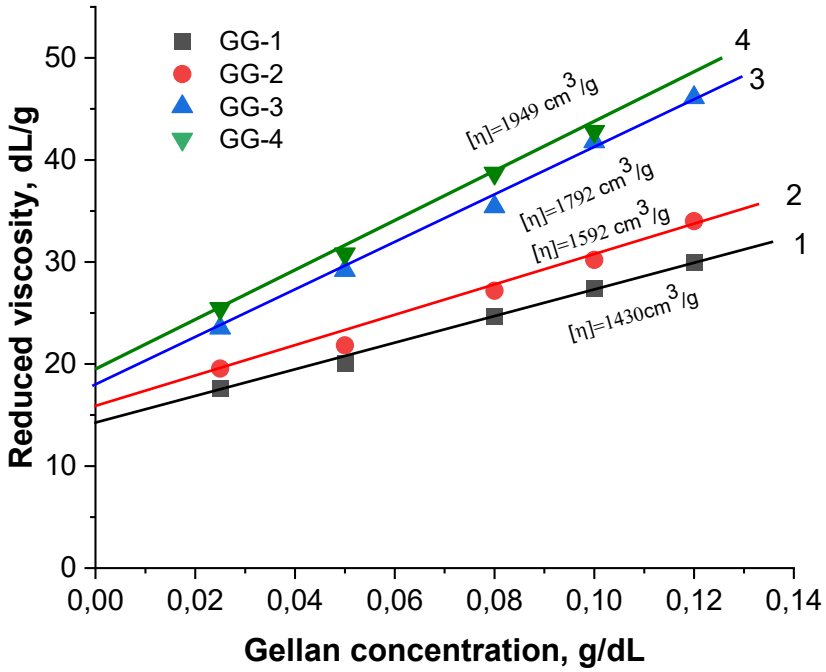

Рисунок 10 – Зависимость приведенной вязкости фракции GG от концентрации полимера, полученных методом фракционного растворения

Таблица 3 – Расчет молекулярной массы различных фракций геллана по уравнению Марка-Куна-Хаувинка по формуле $[\eta] = 7{,}48 \cdot 10^{-3} \cdot M_w^{0.91}$

Фракция	Характеристическая вязкость, [η], $см^3/г$	M_w, $г/моль^{-1}$
GG-1	1430	$6{,}43 \cdot 10^5$
GG-2	1592	$7{,}23 \cdot 10^5$
GG-3	1792	$8{,}23 \cdot 10^5$
GG-4	1949	$9{,}03 \cdot 10^5$

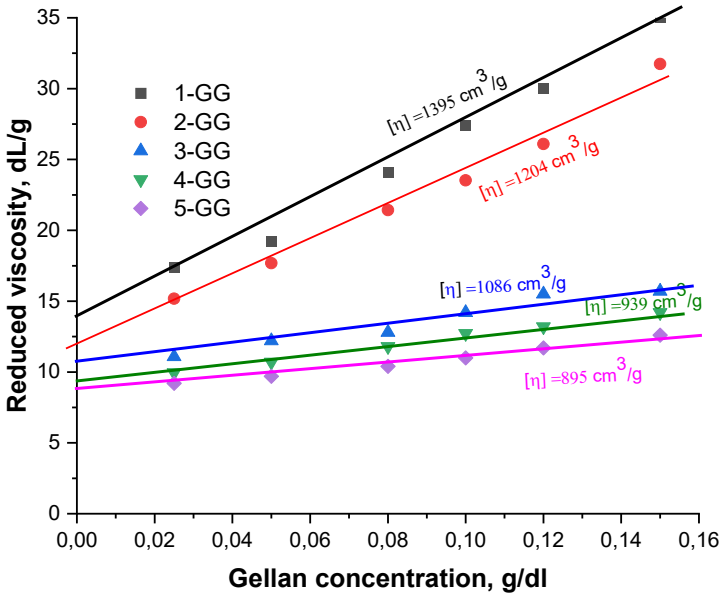

Рисунок 11 – Зависимость приведенной вязкости фракции GG от концентрации полимера после 5-,10-, 30-,60- и 120-минутной обработки ультразвуковым источником

Таблица 4 – Расчет молекулярной массы различных фракции геллана по уравнению Марка-Куна-Хаувинка по формуле $[\eta] = 7{,}48 \cdot 10^{-3} \cdot M_w^{0.91}$

Фракция	Время обработки УЗ, мин	Характеристическая вязкость, [η], $см^3/г$	M_w, $г/моль^{-1}$
1-GG	5	1395	$6{,}25 \cdot 10^5$
2-GG	10	1204	$5{,}32 \cdot 10^5$
3-GG	30	1086	$4{,}75 \cdot 10^5$
4-GG	60	939	$4{,}04 \cdot 10^5$
5-GG	120	895	$3{,}84 \cdot 10^5$

Фракционирование коммерческого геллана позволило получить девять фракций, средняя молекулярная масса которых находится впределать от 380 до 900 кДа. При помощи физико-химических методов была проведена идентификация структур образцов геллана.

Для проведения анализа методом ^{1}H ЯМР спектроскопии, была проведена пробоподготовка: взвешено по 5 мг каждого образца геллана, которые затем растворялись в 0,5 мл оксида дейтерия каждый при температуре 40-50 °С в печи в течение 1 суток.

Анализ методом ЯМР проводился при температуре 80 °С и было получено 32 скана. На рисунке 12 изображены полученные ^{1}H ЯМР спектры.

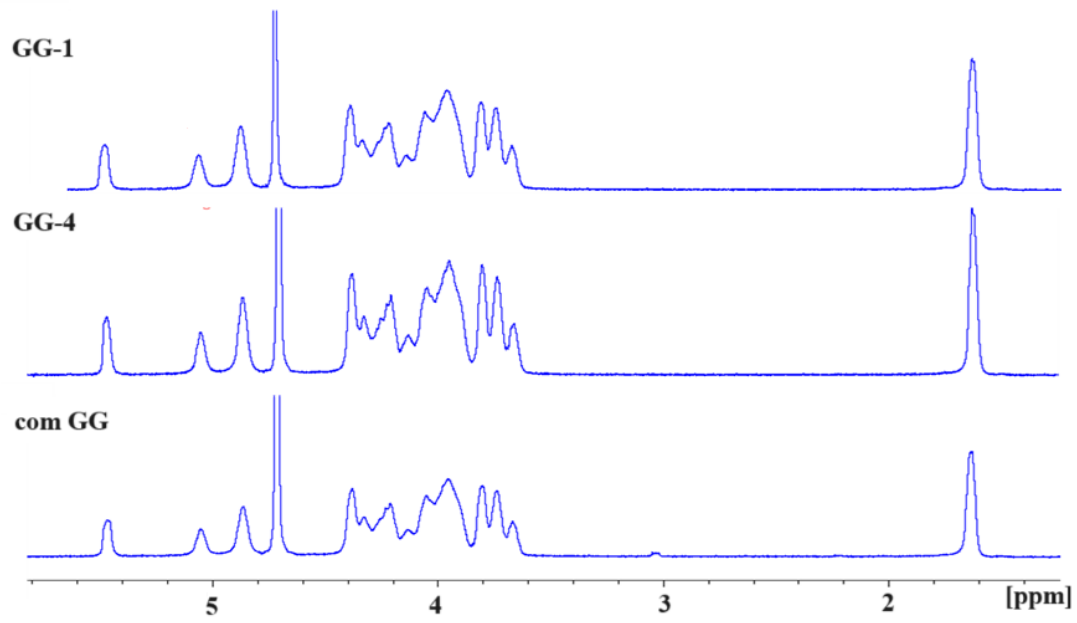

Рисунок 12 – Повторяющиеся мономерные звенья GG и спектры ^{1}H ЯМР фракции GG, полученные путем фракционного растворения коммерческого геллана

В цепочечной структуре фракций геллана, полученных методом ультразвуковой обработки в ^{1}H ЯМР спектрах изменений не замечено, что можно наблюдать по рисунку 13.

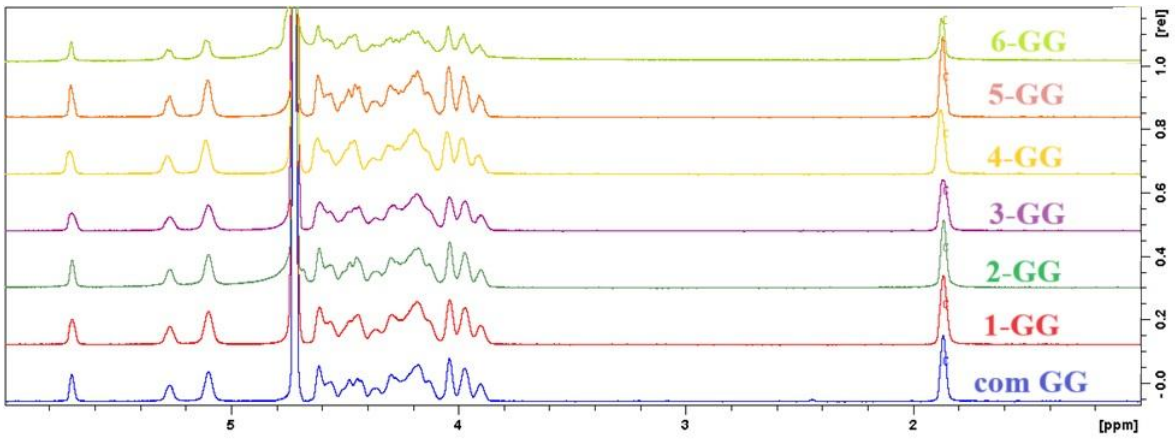

Рисунок 13 – Спектры 1H ЯМР фракции GG, полученных путем ультразвуковой обработки коммерческого геллана

Отчетливо видны пик C=O (175,2 ppm) глюкуроновой кислоты, метилольные пики (61,2 и 61,7 ppm) глюкозы и метильный пик (17,6 ppm) рамнозы.

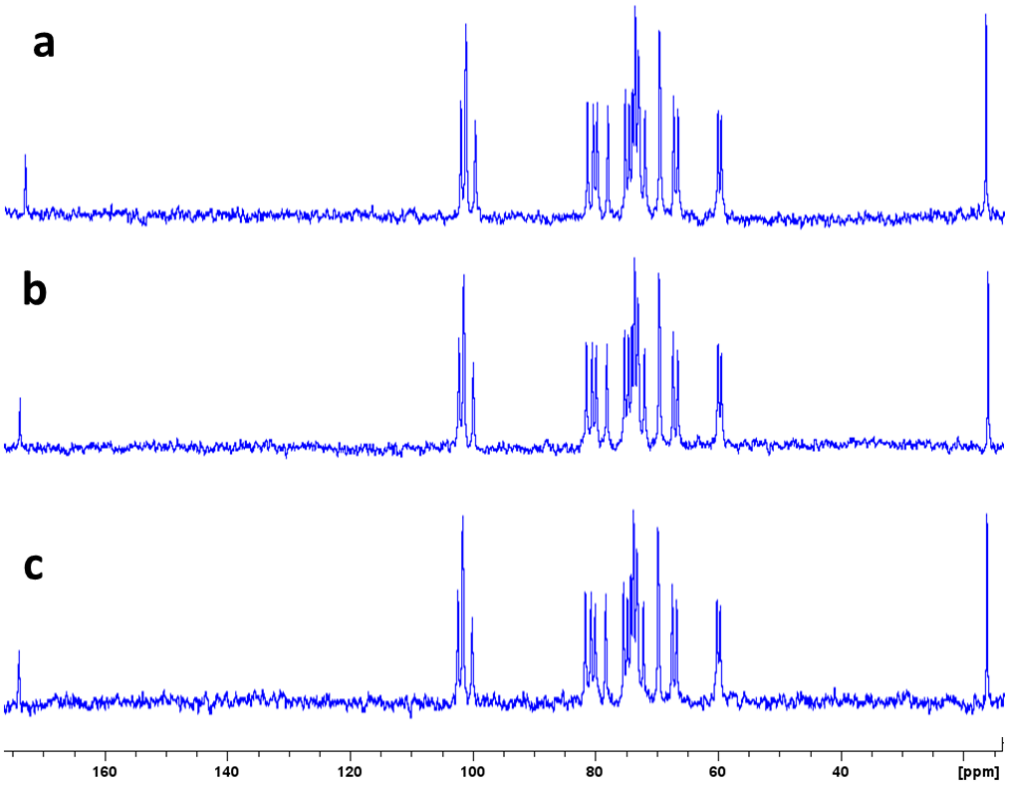

Рисунок 14 – ^{13}C ЯМР спектры различных фракции GG, полученных методом фракционного растворения a) GG-1, b) GG-4, c) коммерческий геллан.

ИК-спектры образцов коммерческого и низкомолекулярных фракций геллана изображены на рисунке 15.

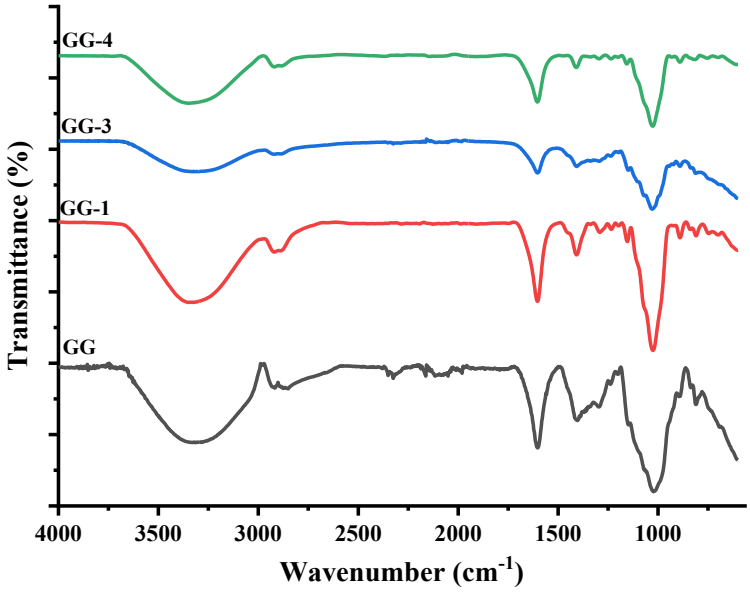

Рисунок 15 – ИК-спектры коммерческого геллана и фракций GG

В таблицу 5 внесены значения пиков ИК-спектров.

Таблица 5 – Значение пиков ИК спектра геллана

Пики, $см^{-1}$	Назначение
3370	O-H
2921	C-H
1604	COO^- валентная вариация карбоксилатной группы пик 1600 $см^{-1}$
1408	COO^- симметричные
1039	C-O полоса поглощения, появившаяся в диапазоне 1000-1200 $см^{-1}$, указывала на наличие связи β-(1→4)

Таблица 6 – Элементный анализ образцов коммерческого и очищенного геллана

Вещество	Содержание элементов (масс.%)			
	Азот	Углерод	Водород	Сера
Коммерческий геллан	0,05	36,31	5,60	0,00
Очищенный геллан	0,06	38,59	5,89	0,00

Применение метода ТГА с целью исследования структуры фракций геллана было проведено в диапазоне температур от комнатной (25 °C) до 700°C. Исследование проводилось на четырех фракциях, термограммы которых изображены на рисунке 16, все фракции проходят двухэтапный процесс деградации. Первый этап, характеризующийся потерей веса поглощенной воды, протекает в диапазоне температур от 25 до 100 °C. Это может быть связано с высвобождением влаги, которая была связана с гидратированными состояниями геллана. Второй этап деградации протекает в диапазоне температур 230-250 °C, что составляет около 50% от начального веса, отсюда следует, что разложение геллана происходит при относительно высоких температурах. При температуре 247 °C происходит самая быстрая потеря веса, что указывает на наиболее активный процесс разложения образца при этой температуре. По достижению 700 °C, потеря веса в общем составила 76%, что может демонстрировать значительную деградацию геллана при более высокой температуре. Таким образом, результаты термогравиметрического анализа продемонстрировали основные процессы разложения полимера, а также позволили идентифицировать структуру фракций геллана. Полученные данные могут быть эффекты в исследованиях свойств геллана и применении в различных отраслях промышленности, науки и медицины.

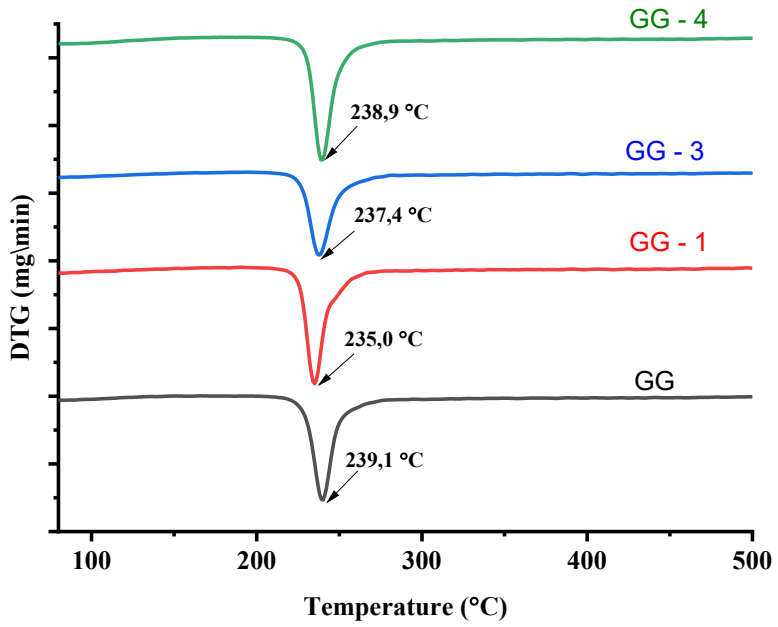

Рисунок 16 – ТГА-термограмма коммерческого геллана и фракций GG

Проведение анализов физико-химическими методами, такими как ИК-ЯМР- и УФ-спектроскопии, термоанализ и элементный анализ, не выявило значительных различий фракционированных образцов геллана от коммерческого высокомолекулярного геллана. Таким образом, не было никаких указаний на то, что геллан был не полностью деацетилирован и фракция была удалена во время очистки. Данный вывод также подтверждает элементный анализ: в обоих образцах содержится одинаковое содержание углерода и водорода. Отсюда следует, что наиболее вероятной причиной низкого выхода очистки являются двухвалентные катионы, незначительное количество этих катионов металлов связывает геллановые цепи в частицы, которые удаляются центрифугированием.

3.1.2 Определение среднегидродинамических размеров и дзета-потенциалов фракций геллана

Определение среднегидродинамических размеров коммерческого высокомолекулярного геллана и низкомолекулярных фракций, а также измерение дзета-потенциалов позволило установить, что среднегидродинамические размеры фракций геллана (рисунок 17) изменяются в зависимости от их концентрации и условий окружающей среды. Подробный анализ дзета-потенциалов (таблица 7) продемонстрировал различия в электрических свойствах поверхности образцов различных фракций, что говорит о том, что стабильность и потенциал вариабельны к агрегированию в растворимых системах.

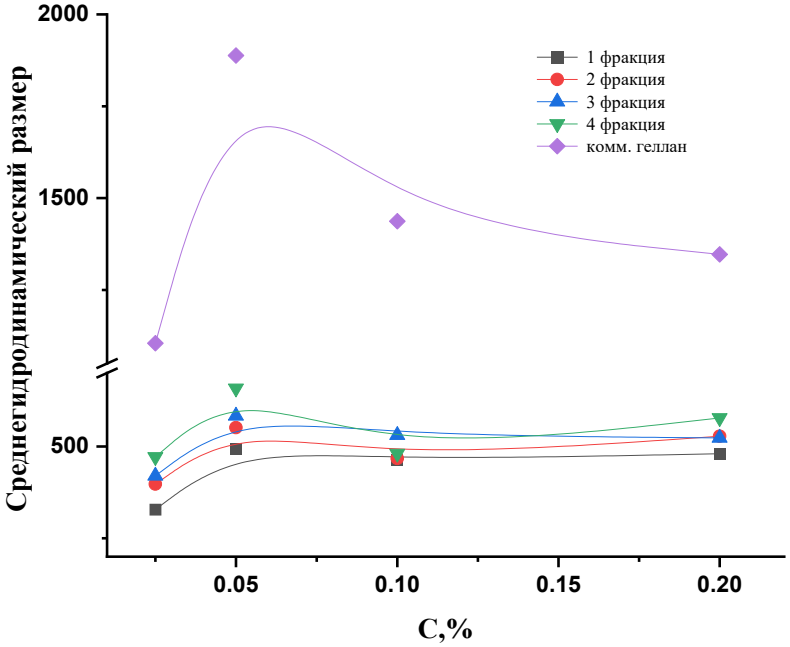

Рисунок 17 – Среднегидродинамические размеры геллана и его различных фракции в зависимости от концентрации низкомолекулярных солей

Таблица 7 – Дзета-потенциалы геллана и его различных фракций в зависимости от концентрации низкомолекулярных солей

Коммерческий геллан								
C, %	В воде			Δ	В слезной жидкости			Δ
0,2	-103	-89.1	-62	-84,7	-358	-411	-340	-370
0,1	-97.3	-125	-107	-110	-293	-462	-433	-396
0,05	-109	-80.6	-48.7	-79.4	-339	-441	-537	-439
0,025	0.373	0.321	-0.703	-0.003	-421	-654	-822	-632
1 фракция								
C, %	В воде			Δ	В слезной жидкости			Δ
0,2	-165	-156	-158	-159,67	-355	-525	-505	-461,6
0,1	-104	-115	-141	-120	-332	-461	-542	-445
0,05	-123	-128	-122	-124,33	-308	-440	-426	-391,3
2 фракция								
C, %	В воде			Δ	В слезной жидкости			Δ
0,2	-158	-125	-116	-133	-378	-509	-531	-472,6
0,1	-110	-120	-115	-115	-318	-443	-490	-417
0,05	-136	-143	-134	-137,6	-290	-450	-533	-424,3
3 фракция								
C, %	В воде			Δ	В слезной жидкости			Δ

Продолжение таблицы 7

0,2	-201	-219	-204	-208	-307	-511	-512	-443,3
0,1	-122	-128	-136	-128,67	-336	-343	-332	-337
0,05	-121	-101	-105	-109	-206	-336	-447	-329,6
4 фракция								
С, %	В воде			Δ	В слезной жидкости			Δ
0,2	-105	-119	-106	-110	-339	-440	-469	-416
0,1	-99,8	-105	-106	-103,6	-368	-493	-463	-441,3
0,05	-93,4	-71,5	-57,5	-74,13	-306	-551	-654	-503,6

3.2 Изучение гелеобразования геллана в зависимости от концентрации низкомолекулярных солей, pH среды, температуры

Для изучения взаимосвязи концентрации низкомолекулярных солей и степени гелеобразования фракций низкомолекулярного геллана была использована модельная слезная жидкость, состоящая из низкомолекулярных солей, растворенных в деионизированной воде (подробная методика описана в пункте 2.3.5). Концентрации геллана были выбраны в диапазоне 0,025-0,2%. Результаты гелеобразования в зависимости от концентрации проиллюстрированы на рисунках 18 и 19.

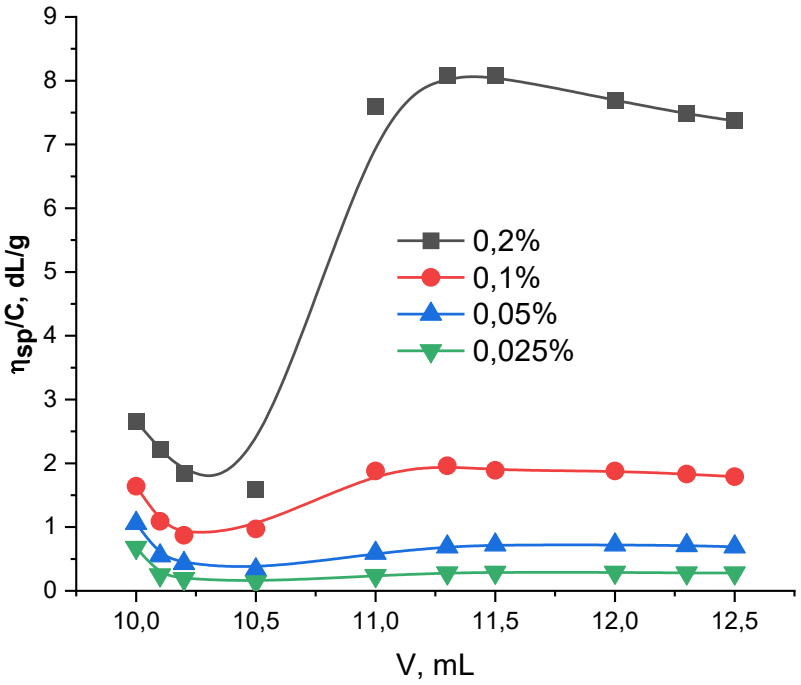

Рисунок 18 – Зависимость приведенной вязкости водного раствора 1 фракции геллана различной концентрации от объема, добавленной слезной жидкости при 25 °С

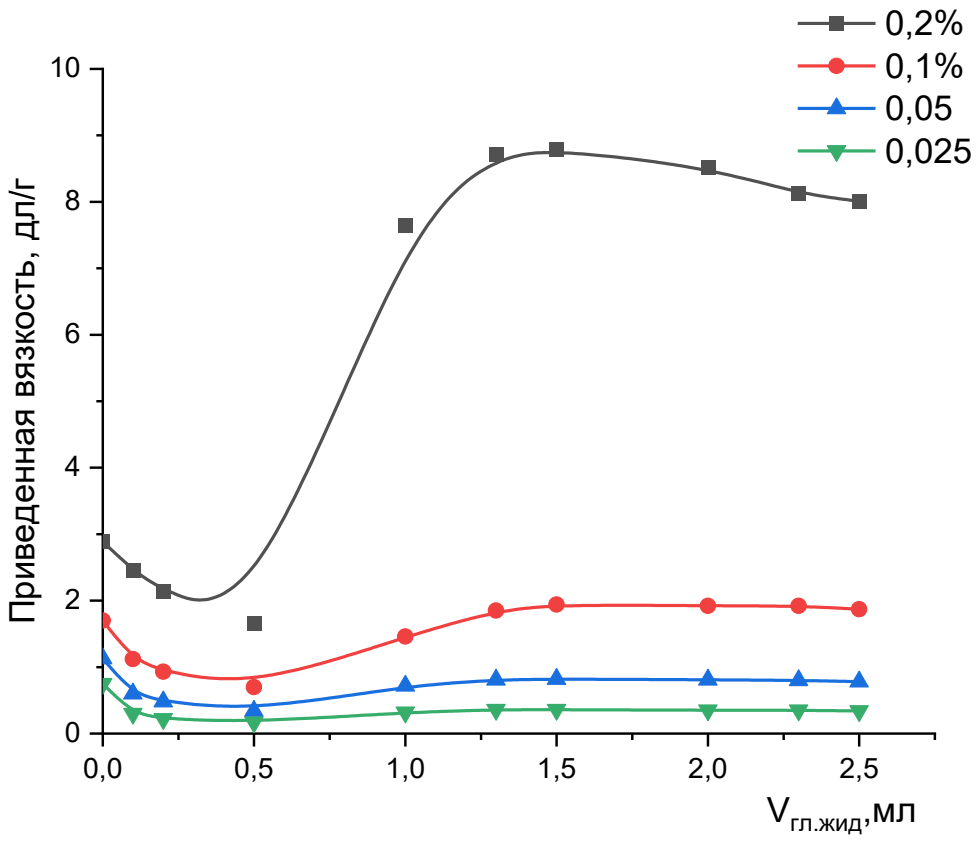

Рисунок 19 – Зависимость приведенной вязкости водного раствора 2 фракции геллана различной концентрации от объема, добавленной слезной жидкости при 25 °С

Полученные результаты позволили выбрать концентрацию геллана равную 0,2% для последующих исследований.

На рисунке 20 изображена зависимость вязкости 0,2% раствора геллана от молекулярной массы биополимера при увеличении ионной силы раствора. Замечено повышение вязкости раствора геллана при увеличении молекулярной массы биополимера, что является подтверждением золь-гель процесса. Кроме того, вязкость раствора биополимера геллана также имеет зависимость и увеличивается с усилением ионной силы. Ионная сила имеет влияние на межмолекулярное взаимодействие геллана, а также ее рост способствует усилению противостояния молекул геллана друг другу, что повышает вязкость раствора.

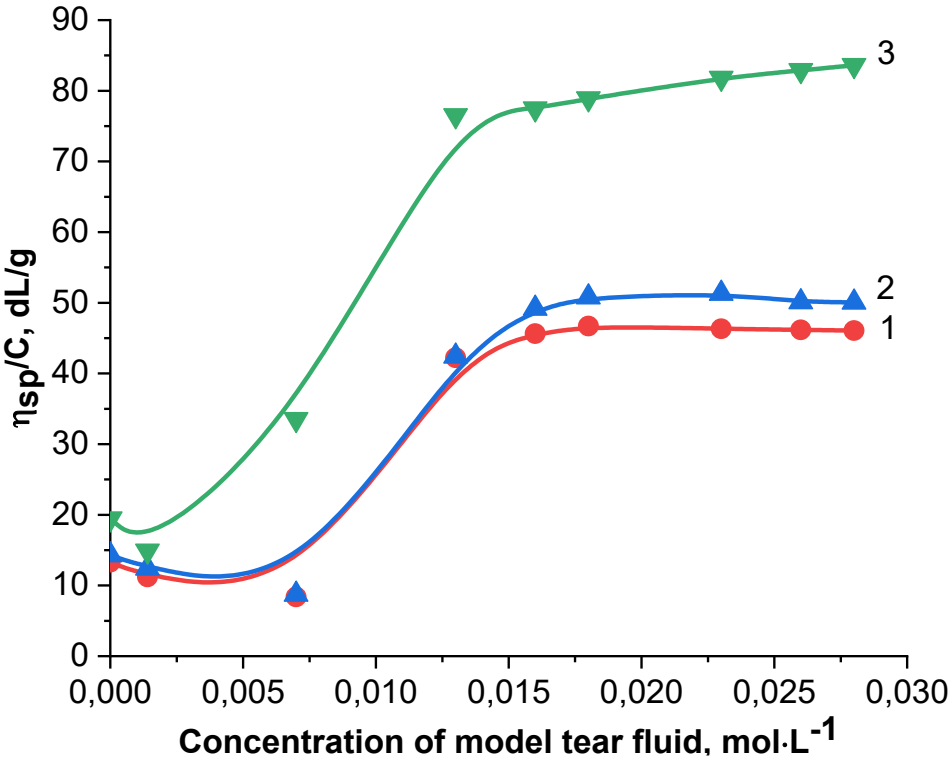

1) GG-1, 2) GG-2, 3) GG-4

Рисунок 20 – Зависимость приведенной вязкости 0,2% раствора фракции GG от ионной силы раствора, создаваемой слезной жидкостью при 25 °C

Была изучена взаимосвязь гелеобразования и температуры, результаты проиллюстрированы на рисунке 21. График показывает, что повышение температуры способствует постепенному снижению вязкости, что приводит к заключению: с повышением температуры геллан снижает способность к образованию геля и становится более текучим. Такое поведение свойственно биополимеру, что подтверждает график каждой фракции. Таким образом, можно сделать вывод, что геллан – это температурно-чувствительное вещество, вязкость которого снижается с повышением температуры.

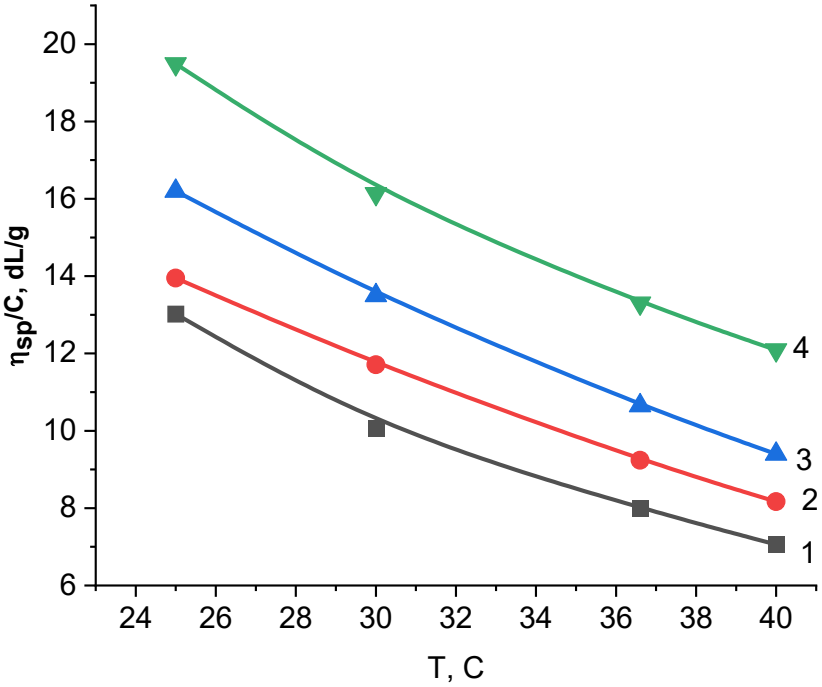

1- $M_w=3,84\cdot10^5$, 2- $M_w=6,43\cdot10^5$, 3- $M_w=7,23\cdot10^5$, 4- $M_w=9,03\cdot10^5$

Рисунок 21 – Изменение приведенной вязкости 0,2%-ного раствора фракции GG в зависимости от температуры

Проведение исследования позволило получить данные о четырех фракциях с различными молекулярными массами: фракция 1 с молекулярной массой $3,84\times10^5$, фракция 2 с молекулярной массой $6,43\times10^5$, фракция 3 с молекулярной массой $7,23\times10^5$, и фракция 4 с молекулярной массой $9,03\times10^5$. Применение динамического светорассеяния позволило установить, что с ростом молекулярной массы геллана увеличивается размер частиц, что указывает на то, что концентрация низкомолекулярных солей оказывает влияние на процесс гелеобразования геллана и его структуру. Чем выше концентрация низкомолекулярных солей, тем больше молекулярная масса геллана и соответственно размер его частиц.

Рисунок 22 демонстрирует взаимосвязь молекулярной массы геллана и размера его частиц: чем меньше молекулярная масса, тем меньше размер частиц. Данная взаимосвязь является благоприятно для матрицы глазных капель в связи с тем, что меньший размер частиц будет способствовать лучшему распределению и более стабильной дисперсии в растворе капель.

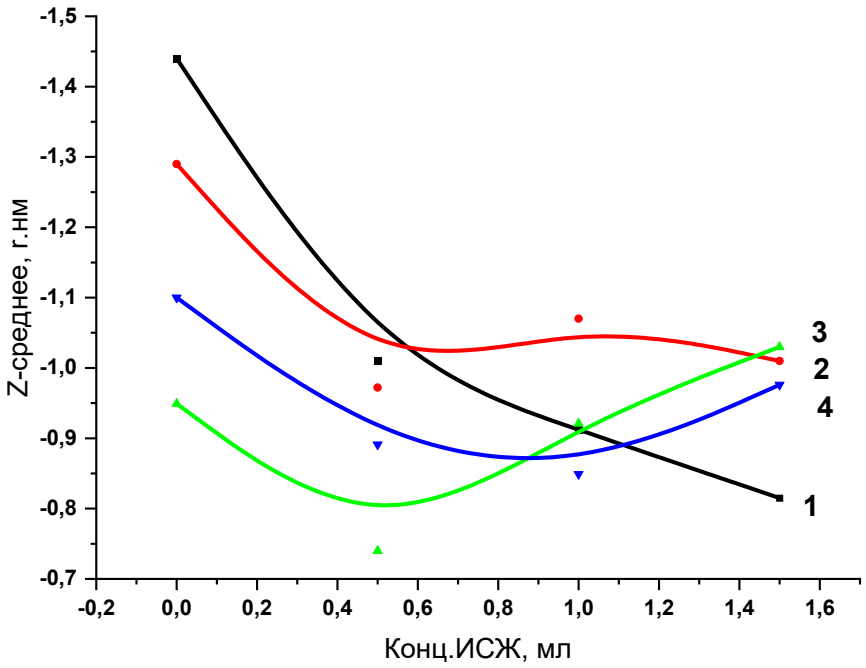

1- $M_w=3,84\cdot10^5$, 2- $M_w=6,43\cdot10^5$, 3- $M_w=7,23\cdot10^5$, 4- $M_w=9,03\cdot10^5$

Рисунок 22 – Изменение среднегидродинамических размеров 0,2%-ного раствора фракции GG в зависимости от ионной силы

На рисунке 23 изображены фотографии процесса гелеобразования фракций геллана. На фото а) раствор 0,5% геллана, добавленный в исходную среду, на фото б) перевернутые флаконы с образовавшемся гелем. Первые три фракции показали образование достаточно твердого геля, в то время как четвертая фракция образовала более слабый гель, непригодный для последующих исследований.

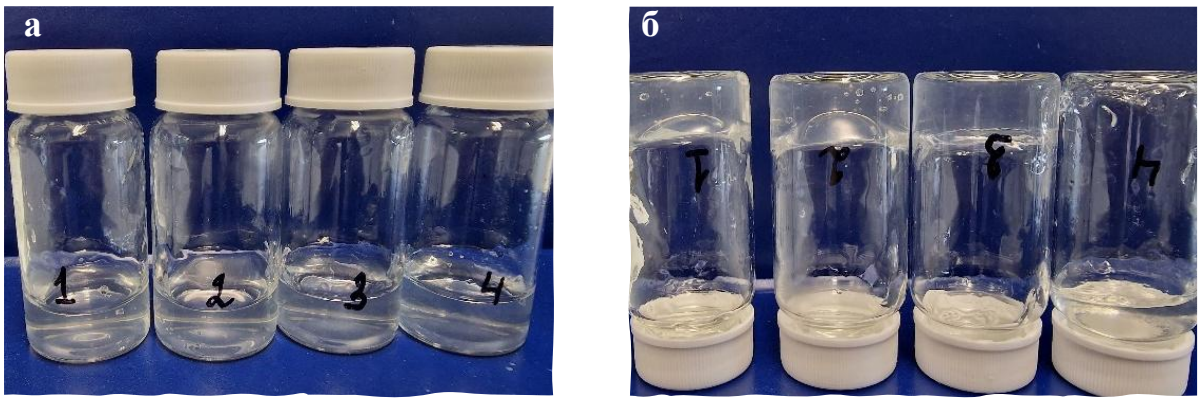

Рисунок 23 – Фотография гелеобразования геллана разных фракций при одинаковых условиях

3.3 Модификация геллана полиоксазолином и идентификация структуры

Следующим этапом было осуществление модификации геллана с помощью полиоксазолина (ПОЗ) с целью повышения проникновения лекарственных веществ и улучшения мукоадгезивных свойств. Полиоксазолин обладает множеством благоприятных свойств в области лекарственных средств, что обусловливает его ценность в различных отраслях медицины. ПОЗ применим как в качестве поглотителя токсинов, антибактериального средства [103], так и для улучшения растворимости и повышения стабильности лекарственных средств. Методика модификации описана в пункте 2.3.4.

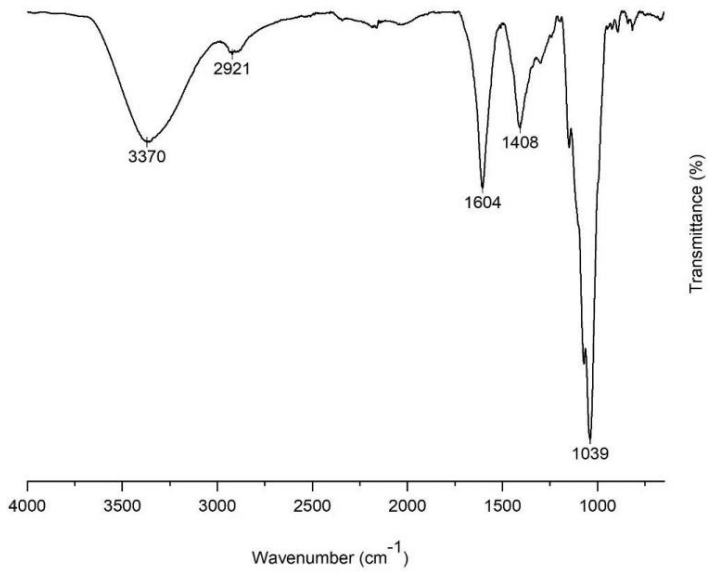

Рисунок 24 – ИК-спектр геллана

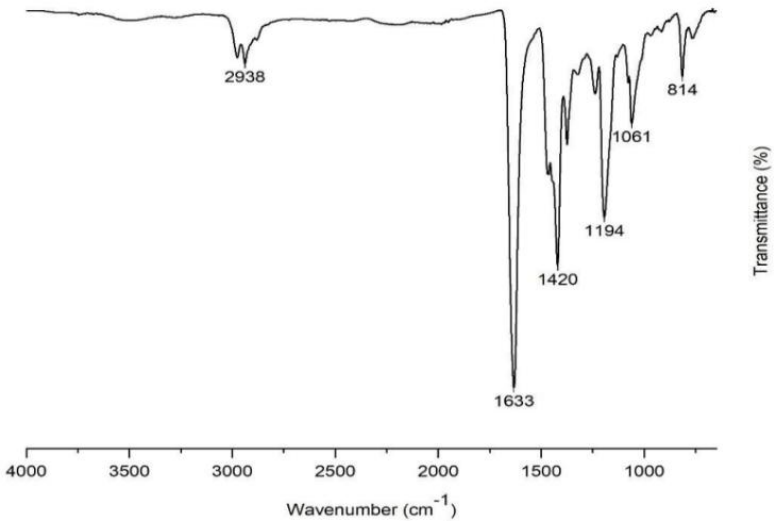

Рисунок 25 – ИК-спектр PEtOx

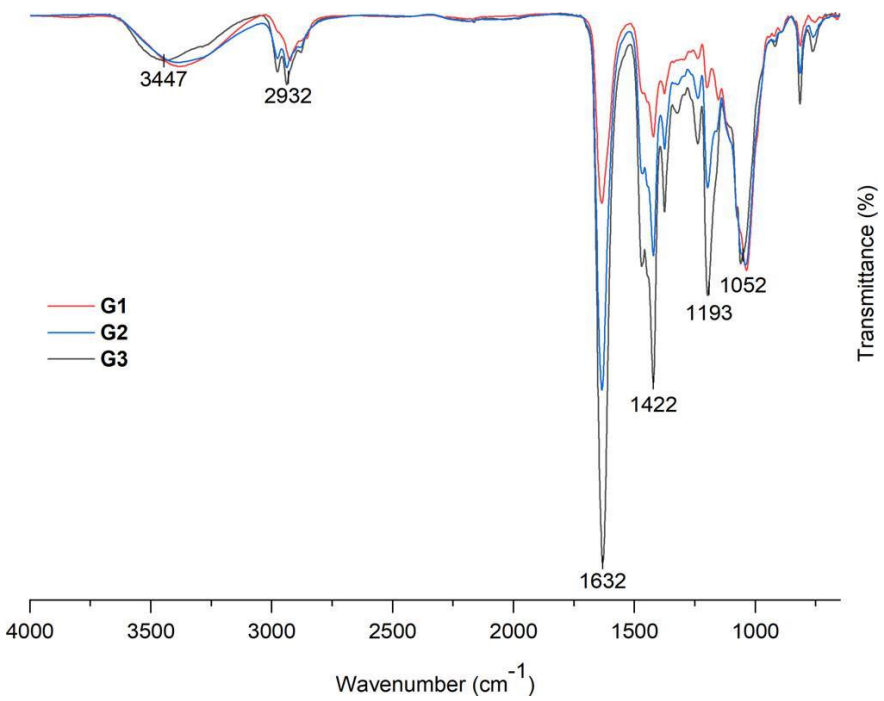

Рисунок 26 – ИК-спектр геллан- PEtOx

ИК-спектры сополимеров Геллан-PEtOx показаны на рисунке 26. На рисунках 24-25 показаны спектры чистого гомополимера Геллана и PEtOx. Полоса при 3447 см–1 соответствует Геллану и практически одинакова для всех сополимеров. Различная интенсивность пиков при 1632 и 1422 см–1 доказывает наличие PEtOx и демонстрирует тенденцию к снижению с уменьшением степени прививки. Пик при 1052 см–1 может быть суперпозицией двух вкладов: один исходит от Геллана (1039 см–1) и соответствует растяжению связи CO гидроксильной группы, тогда как другой исходит от PEtOx (1061 см–1) и соответствует третичному амиду. Интенсивность данного пика не меняется в зависимости от степени прививки из-за эквивалентного образования новых связей CH-O-CH2 между PEtOx и Геллан.

3.3.1 Иммобилизация офлоксацина в матрицу геллана и модифицированного полиоксазолином геллана и изучение кинетики выхода лекарственного препарата из матрицы геля

Иммобилизация офлоксацина осуществлялась соединением водного раствора офлоксацина с гелланом и происходило снижение электропроводности и показателя pH системы. Причиной данных изменений является образование ионных и водородных связей между этими двумя компонентами. Снижение электропроводности связано с тем, что молекулы офлоксацина связываются с полимером через водородные связи и это препятствует ионизации карбоновых групп. Однако, при достижении

определенного соотношения в комплексе и лекарственное вещество в избытке, то проводимость раствора увеличивается, в связи с избытком свободных ионов.

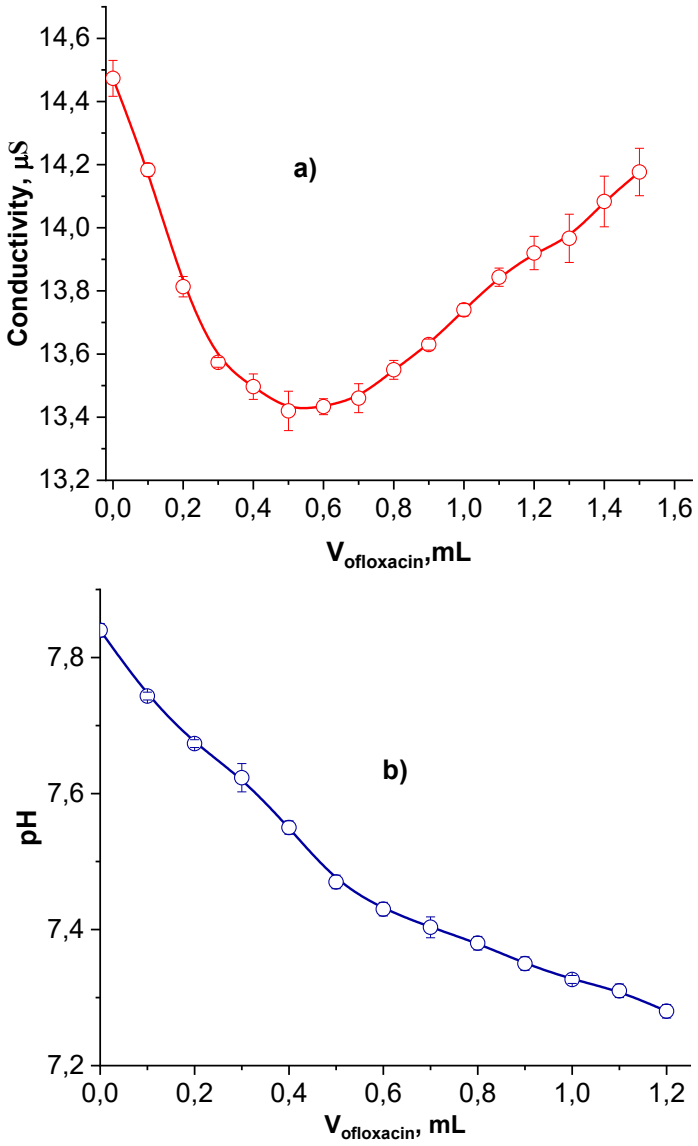

[Геллан] = 1·10-4 моль/л-1, [Офлоксацин] = 1·10-3 моль/л-1. Объем раствора геллана, используемого для титрования, составляет 10 мл.

Рисунок 27 – Кондуктометрические (а) и pH-метрические (б) кривые титрования геллана офлоксацином

Молярное соотношение геллан-офлоксацина, определенное по минимуму и изгибу кривых кондуктометрической и pH-метрической титрованием, примерно равно 2:1 моль/моль. Учитывая, что структура комплекса геллан-офлоксацина, определенная кондуктометрической и pH-метрической титрованием, близка к 2:1 моль/моль, ее можно представить, как показано на рисунке 28.

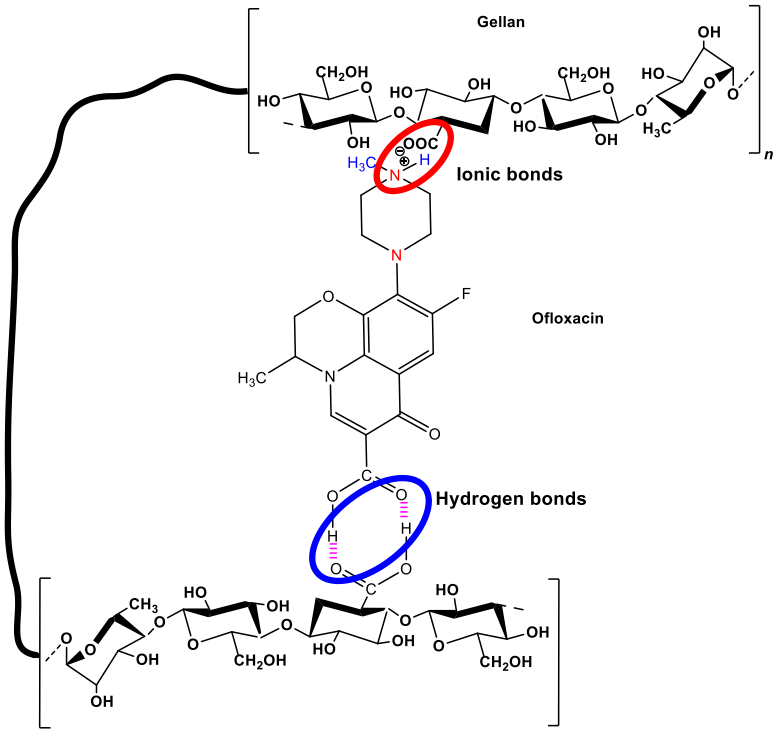

Рисунок 28 – Схематическое изображение внутримакромолекулярного комплекса геллан-офлоксацин состава 2:1 моль/моль

Важно отметить, что офлоксацин способен как к внутримолекулярному, так и к межмолекулярному комплексообразованию не только с гидроксильными, но и с карбоновыми группами геллана. Образование комплекса геллан-офлоксацин состава 2:1 моль/моль также подтверждается измерениями динамического света рассеяния.

В образовании комплекса с офлоксацином гидроксильные и карбоксильные группы геллана играют большую роль, образуя связи с соответствующими группами, способствуют формированию стабильного комплекса 2:1 моль/моль. (таблица 8).

Таблица 8 – Средний гидродинамический размер и дзета-потенциал геллана, офлоксацина и смеси геллан-офлоксацин различного состава

Состав геллан-офлоксацин, моль/моль	Средний гидродинамический размер, нм	Дзета-потенциал, мВ
4:1	336±5	– 42.9±2
2:1	**307±5**	**– 14.9±1**
1:1	315±5	– 40.4±2
Геллан	605±10	– 41.0±2

Минимальные значения среднего гидродинамического размера и дзета-потенциала комплекса геллан-офлоксацин подтверждают состав 2:1

моль/моль. Отрицательные заряды геллана, офлоксацина и сложных частиц обусловлены наличием карбоновых групп в структуре всех веществ. Минимальное значение дзета-потенциала (-14,9 мВ) в случае комплекса геллан-офлоксацин 2:1 моль/моль, вероятно, связано с частичной нейтрализацией карбоновых групп геллана аминогруппами офлоксацина и участием карбоновых групп геллана и офлоксацина в образовании водородные связи, как схематично показано на рисунке 28. Образование комплекса геллан-офлоксацин приводит к двукратному сокращению макромолекул геллана из-за внутримолекулярного и межмолекулярного образования мостиков.

На рисунке 29 продемонстрированы ИК-спектры геллана, офлоксацина и комплекса геллан-офлоксацин (2:1 моль/моль) вместе с идентификацией некоторых характерных полос (таблица 9).

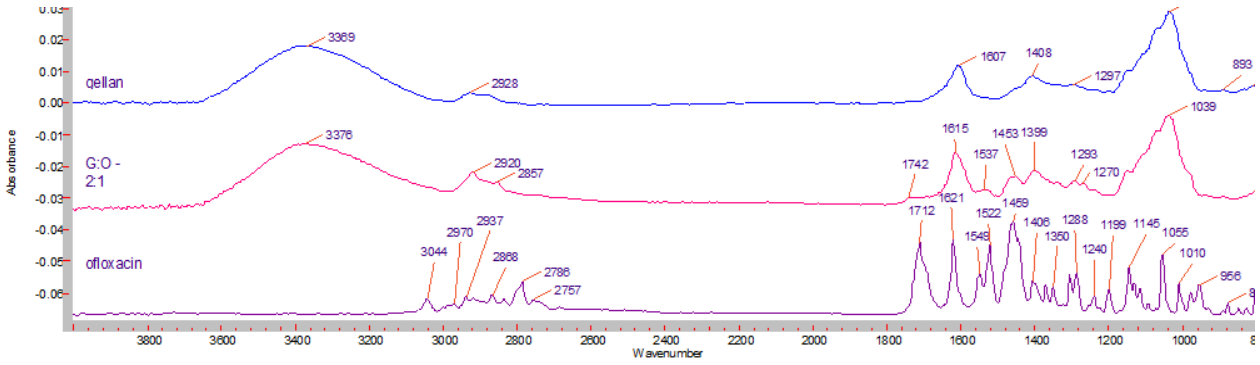

Рисунок 29 – ИК-спектры сухого геллана (1), офлоксацина (2) и комплекса геллан-офлоксацин (3) состава 2:1 моль/моль

Таблица 9 – Идентификация характеристических полос геллана, офлоксацина и комплекса геллан-офлоксацина (2:1 моль/моль)

Волновое число, $см^{-1}$			
Геллан	Офлоксацин	Комплекс Геллан-офлоксацин (2:1 моль/моль)	Назначения диапазонов
3369	-	3376	OH
2928	3044-2786	2920, 2857	CH
-	1712	-	C=O растяжение групп COOH
1607	1621	1615	COO^- симметричные
-	1549, 1522	1537	C-N
	1459	1453	C-C в бензольном кольце
1408	1406	1399	CH деформация
1037		1039	C-O-C

ИК-спектры показывают, что в комплексе геллан-офлоксацин

происходит образование водородных связей между карбоновыми группами офлоксацина и гидроксильными или карбоновыми группами геллана. Образование данных водородных связей приводит к исчезновению интенсивного пика при 1712 $см^{-1}$, который наблюдается в спектре офлоксацина. При 1549 и 1522 $см^{-1}$ наблюдаются колебания C-N при растяжении офлоксацина, которые смещаются до 1537 $см^{-1}$, что является подтверждением участия аминогрупп офлоксацина в образовании ионных связей.

Таким образом, ИК-спектры демонстрируют, что в комплексе геллан-офлоксацин образуются водородные связи между карбоновыми группами офлоксацина и гидроксильными или карбоновыми группами геллана, а аминогруппы офлоксацина участвуют в образовании ионных связей.

На рисунке 30 изображены кривые термогравиметрического анализа геллана, офлоксацина и комплекса геллан-офлоксацин. В диапазоне температур 200-300 °C происходит разложение геллана. При 249 °C наблюдается наиболее резкая потеря веса, что подтверждают литературные данные [6], в которых описано термическоме разложение офлоксацина при 243 ^{0}C. Согласно ИК-спектрам комплекса геллан-офлоксацин (2:1 моль/моль) пики разложения отдельных компонентов (геллана и офлоксацина) полностью исчезают, демонстрируя потерю массы комплекса при 338 и 379 ^{0}C, что связано с образованием комплекса геллан-офлоксацин в качестве единственного соединения.

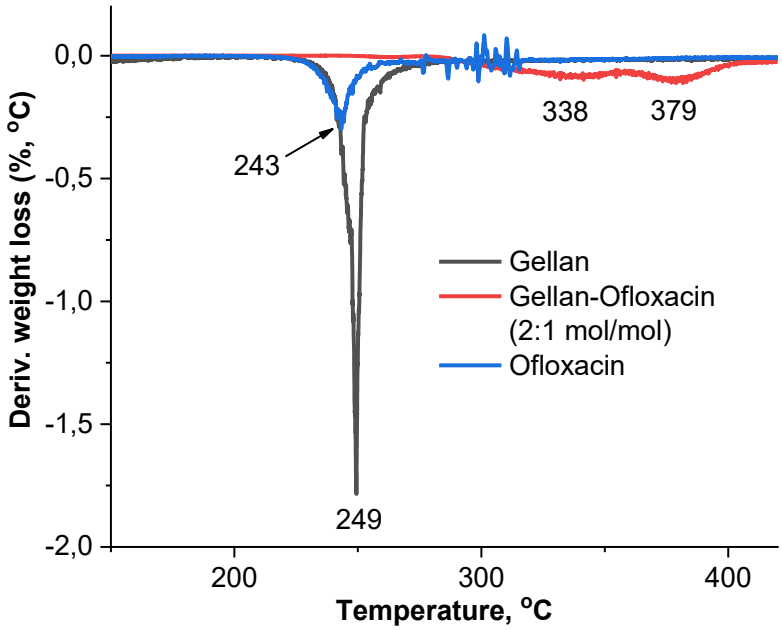

Рисунок 30 – Кривые ТГА геллана, офлоксацина и комплекса геллан-офлоксацин (2:1 моль/моль)

С помощью УФ-видимой спектроскопии была оценена кинетика высвобождения офлоксацина из тонких пленок геллан-офлоксацина,

стабилизированных добавлением 0,3% вес. $CaCl_2$. Оценка кинетики проводилась путем определения временно зависимого спектра поглощения офлоксацина при λ = 289 нм в дистиллированной воде и фосфатном буфере при комнатной температуре (рис. 31).

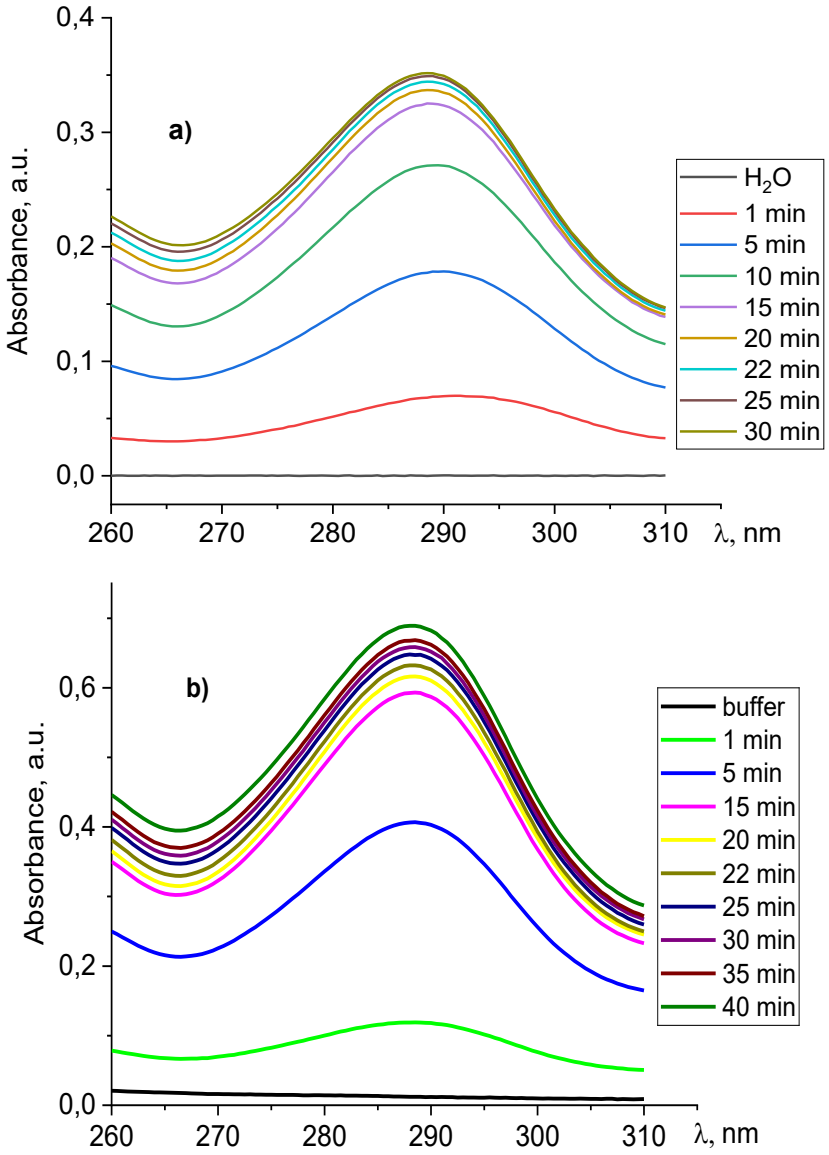

Рисунок 31 – Зависящая от времени абсорбция офлоксацина из тонких пленок геллан-офлоксацин (2:1 моль/моль), загущенных добавлением 0,3 мас.% CaCl2 в дистиллированную воду (а) и фосфатный буфер (б) при комнатной температуре

Рисунки 31 и 32 демонстрируют различия кинетики высвобождения офлоксацина в дистиллированной воде и фосфатном буфере. В течение 30-40 минут высвобождение офлоксацина в фосфатном буфере происходит в 2 раза быстрее по сравнению с дистиллированной водой, что связано с присутствием неорганических ионов в буферном растворе, которые уменьшают прочность ионных связей между полимером и лекарственным

веществом. Расчет кинетики высвобождения осуществлен с использованием модели Ритгера-Пеппаса [71], выраженной как:

$$A_t/A_\infty = kt^n, \quad (3)$$

где A_t – поглощение офлоксацина в момент времени t, мг;

A_∞ – поглощение офлоксацина в бесконечный момент времени t_∞, мг;

k – структурно-геометрическая константа гелеобразующей пленки;

n – показатель высвобождения, представляющий механизм высвобождения.

Результат расчета соответствует нериксовой диффузии (n = 0,59) в дистиллированной воде и транспорту по случаю II (n = 0,95) в фосфатном буфере. Данное исследование показало, что накопленное высвобождение офлоксацина из гель-пленок на основе геллана в дистиллированную воду и буферный раствор составляет соответственно 36,0% и 97,3%. В случае дистиллированной воды высвобождение офлоксацина может быть влиянием гидратации и отекания геллановой пленки, проникновения воды в гелевую матрицу и пассивной диффузии офлоксацина из гелевой матрицы. Более быстрое высвобождение офлоксацина в буферном растворе можно объяснить разрушением ионных связей, образованных между карбоксильными группами геллана и аминогруппами офлоксацина, ионными видами раствора, что сопровождается усиленной диффузией офлоксацина из гелевой матрицы.

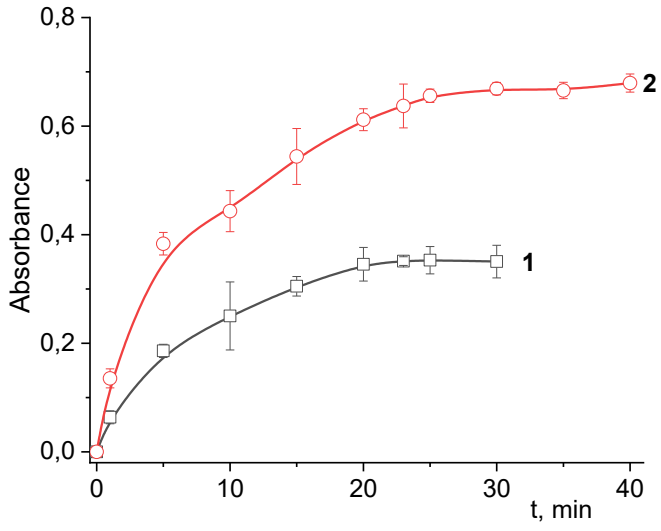

Рисунок 32 – Кинетика высвобождения офлоксацина из тонких пленок геллан-офлоксацин, загущенных добавлением 0,3 мас.% CaCl2, в дистиллированную воду (1) фосфатный буфер (2) при комнатной температуре

Водорастворимый комплекс геллан-офлоксацина в соотношении 2:1 моль/моль стабилизируется как ионными, так и водородными связями, образованными карбоксильными, гидроксильными и аминогруппами двух взаимодействующих компонентов. Образование комплекса подтверждается при помощи кондуктометрического и потенциометрического титрования, динамического светорассеяния и измерения дзета-потенциала, а также Фурье-трансформацией ИК-спектра и термогравиметрическим анализом. Комплекс геллан-офлоксацина образует гель при добавлении 0,3 масс. % CaCl2 и образует тонкие гель-пленки. Кинетика высвобождения офлоксацина из комплекса геллан-офлоксацина описывается моделью Ритгера-Пеппаса ($A_t/A_\infty = kt^n$) и соответствует неламинарной диффузии (n = 0,59) в дистиллированной воде и случаю II транспорта (n = 0,95) в буферном растворе фосфата. Кумулятивное высвобождение офлоксацина из гель-пленок геллан-офлоксацина составило 97,3% в буферном растворе фосфата в течение 40 минут и 36,0% в дистиллированной воде в течение 30 минут. Для оценки эффективности системы геллан-офлоксацина в качестве устойчивой системы доставки лекарств необходимо провести эксперименты, как in vitro, так и *in vivo*, в слезных жидкостях при различных температурах и значениях pH среды.

Кинетика высвобождения офлоксацина из тонких пленок геллан-офлоксацин, загущенных добавлением 0,3 мас.% $CaCl_2$, оценена с помощью УФ-видимой спектроскопии путем определения зависящих от времени спектров поглощения офлоксацина при λ = 289 нм в дистиллированной воде при комнатной температуре (рис. 33).

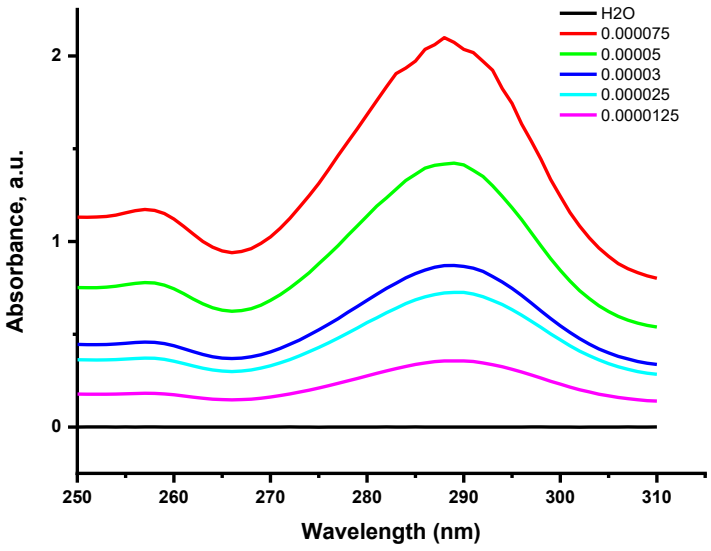

Рисунок 33 – Зависимость высвобождения офлоксацина из тонких пленок геллан-офлоксацин (2:1 моль/моль), загущенных добавлением 0,3 мас.% $CaCl_2$ в дистиллированную воду при температуре 25±1°C от времени

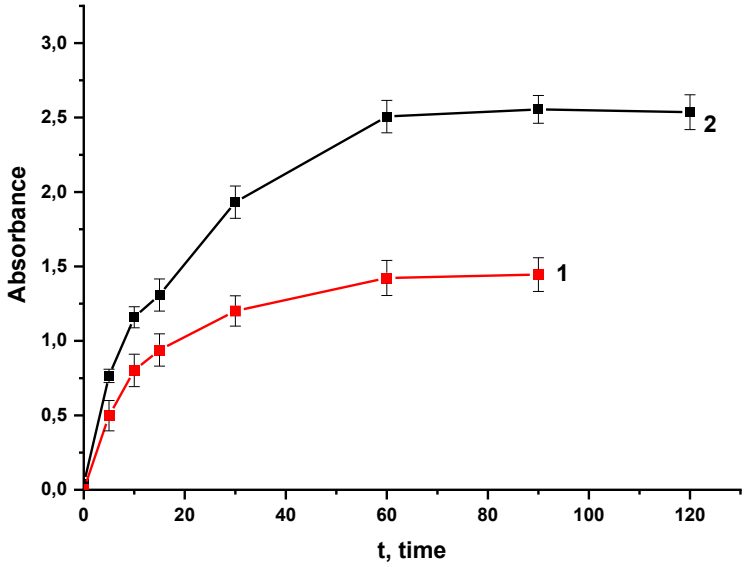

Рисунок 34 – Кинетика высвобождения офлоксацина из тонких пленок геллан-офлоксацин, загущенных добавлением 0,3 мас.% CaCl2, в дистиллированную воду (1) и фосфатный буфер (2) при 25±1°C

Кинетика высвобождения офлоксацина из тонких пленок геллан-офлоксацин (2:1 моль/моль) в дистиллированную воду и фосфатный буфер различна (рисунок 32). В течение 30-40 мин высвобождение офлоксацина в фосфатном буфере происходит в 2 раза быстрее по сравнению с высвобождением в дистиллированной воде, что связано с присутствием в буферном растворе неорганических ионов, которые снижают прочность ионных связей полимер-лекарственное средство. Расчет кинетики высвобождения с использованием модели Ритгера-Пеппаса [104] выраженное как At /A∞ = ktn соответствует не Фикианской (non-Fickian) диффузии (n = 0,59) в дистиллированной воде и перенос в случае II (n = 0,95) в фосфатном буфере.

Процентное высвобождение офлоксацина в дистиллированную воду и фосфатный буфер через 60 мин составило ≈ 10±1% и ≈ 21±0,5% соответственно (рис. 34). Кумулятивное высвобождение офлоксацина из пленок геллан-офлоксацин, рассчитанное по методике [105], равно 40±2% и 85±2% в дистиллированную воду и буферный раствор соответственно. В случае дистиллированной воды на высвобождение офлоксацина могут влиять гидратация и набухание геллановой пленки, проникновение воды в гелевую матрицу, приводящее к пассивной диффузии офлоксацина из гелевой матрицы. Более быстрое высвобождение офлоксацина в буферный раствор объясняли разрушением ионных связей, образующихся между карбоксильными группами геллана и аминогруппами офлоксацина, ионными частицами раствора, что сопровождается усиленной диффузией офлоксацина

из гелевой матрицы.

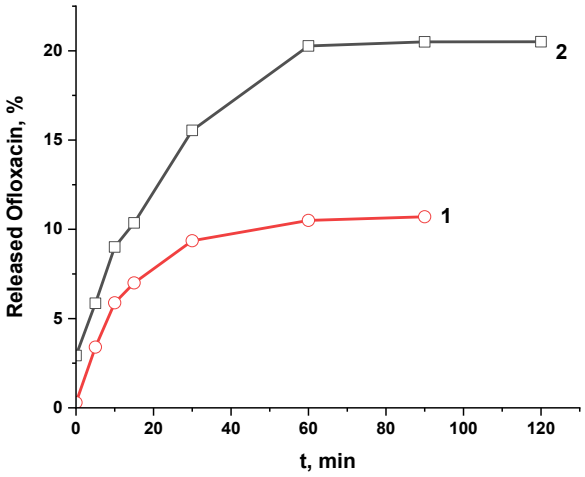

Рисунок 35 – Процентное содержание высвободившегося офлоксацина в дистиллированной воде (1) и фосфатном буфере (2) из тонких пленок геллан-офлоксацин, загущенных добавлением 0,3 мас.% CaCl2 при 25±1°C

ЗАКЛЮЧЕНИЕ

В заключении можно отметить, что уникальное свойство золь-гель перехода биополимера геллана нашло широкое применение в пищевой, а также других отраслях промышленности, науки, биотехнологии и др. Кроме того данное свойство в сочетании с превосходной биосовместимостью полимера позволяет применять геллан в медицине и фармацевтической разработке, при условии изменения некоторых физико-химических свойств методами фракционирования и модификации.

Фракционирование коммерческого биополимера геллана было осуществлено двумя методами: методом дробного осаждения и методом ультразвуковой обработки. Данные методы позволили значительно снизить молекулярную массу LAG и не вызывали структурных изменений. Очищенный коммерческий геллан обладает полиэлектролитными свойствами благодаря наличию карбоновых групп глюкуроновой кислоты. Идентификация структур низкомолекулярный фракций осуществлялась методами ^{1}H и ^{13}C ЯМР спектроскопии, ИК спектроскопии и термогравиметрии. Применение уравнения Фуосса позволило определить характерную вязкость очищенного коммерческого геллана в водном растворе.

Кроме того, изучено влияние модельной слезной жидкости на вязкостные характеристики геллана. Показано, что оптимальное загущение водного раствора геллана наступает при концентрации ИСЖ 0.016-0.017 моль·л$^{-1}$.

Осуществлена модификация геллана с помощью полиоксазолина и подтверждена привязка сополимеров Геллан-PEtOx при помощи ИК-спектроскопии.

В ходе исследования было показано, что комплекс геллан-офлоксацин, стабилизированный ионными и водородными связями, образуется при соотношении 2:1 моль/моль и обладает хорошей стабильностью. Кинетика высвобождения офлоксацина из комплекса различается в дистиллированной воде и фосфатном буфере: в буфере высвобождение происходит быстрее, что связано с разрушением ионных связей, а в воде процесс замедляется за счет гидратации и набухания геллановой пленки. Кумулятивное высвобождение офлоксацина из пленок геллан-офлоксацина составило 36% в воде и 97,3% в буфере, что подтверждает эффективность системы как потенциальной платформы для доставки лекарств.

Результаты проведенной работы были опубликованы в междунароных рецензируемых статьях (Приложение А).

ПЕРЕЧЕНЬ СОКРАЩЕНИЙ

ГК	– гиалуроновая кислота
ЛВ	– лекарственное вещество
ЛФ	– лекарственная форма
ЛС	– лекарственное средство
ЛП	– лекарственный препарат
ДЛС	– динамическое лазерное светорассеяние
ИСЖ	– модельная слезная жидкость
КМЦ	– карбоксиметилцеллюлоза
СДЛ	– система доставки лекарств
ТГА	– термогравиметрический анализ
УЗ	– ультразвук
ЯМР	– ядерный магнитный резонанс
ИК	– инфракрасное (излучение)
GG	– gellan gum
EtOx	– 2-Этил-2-оксазолин
PEtOx	– поли(2-этил-2- оксазолин)

СПИСОК ИСПОЛЬЗОВАННОЙ ЛИТЕРАТУРЫ

1 Giavasis I., Harvey L.M., McNeil B. Gellan Gum // Critical Reviews in Biotechnology. – 2000. –Vol. 2, № 3. – P. 177-211. – DOI: 10.1080/07388550008984169.

2 Osmałek T., Froelich A., Tasarek S. Application of gellan gum in pharmacy and medicine // International Journal of Pharmaceutics. – 2014. – Vol. 466, № 1-2. – P. 328-340. – DOI: 10.1016/j.ijpharm.2014.03.038.

3 Gussenov I., Kudaibergenov S.E. Permeability reduction by gellan gum solutions // Journal of Petroleum Science and Engineering. – 2021. – Vol. 208 – Art. 109546. – DOI: 10.1016/j.petrol.2021.109546.

4 Morris E.R., Nishinari K., Rinaudo M. (2012). Gelation of gellan – A review // Food Hydrocolloids. – 2012. – Vol. 28, № 2. – P. 373-411. – DOI: 10.1016/j.foodhyd.2012.01.004.

5 Tatykhanova G.S., Aseyev V., Vamvakaki M., Khutoryanskiy V.V., Kudaibergenov S.E. Ophthalmic drug delivery system based on the complex of gellan and ofloxacin // Chemical Bulletin of Kazakh National University. – 2022. – Vol. 2. – P. 4-12. – DOI: /10.15328/cb1239.

6 Lavikainen J., Dauletbekova M., Toleutay G., Kaliva M., Chatzinikolaidou M., Kudaibergenov S.E., Tenkovtsev A., Khutoryanskiy V.V., Vamvakaki M., Aseyev V. Poly(2-ethyl-2-oxazoline) grafted gellan gum for potential application in transmucosal drug delivery // Polymers for Advanced Technologies. – 2021. – Vol. 32, № 7. – P. 2770-2780. – DOI: 10.1002/pat.5298.

7 Dreveton E., Monot F., Lecourtier J., Ballerini D., Choplin L. Influence of fermentation hydrodynamics on gellan gum physico-chemical characteristics // Journal of Fermentation and Bioengineering. – 1996. – Vol. 82, № 3. – P. 272–276. – DOI: 10.1016/0922-338x(96)88819-2.

8 Jansson P. E., Lindberg B., and Sandford P. A. Structural studies of gellan gum, an extracellular polysaccharide elaborated by Pseudomonas elodea // Carbohydrate Research. – 1983 – Vol.124 – P.135-139. – DOI: 10.1016/0008-6215(83)88361-x.

9 O'Neill M. A., Selvendran R. R., and Morris V. J. Structure of the acidic extracellular gelling polysaccharide produced by Pseudomonas elodea // Carbohydrate Research. – 1983. – Vol. 124. – P. 123-133. – DOI: 10.1016/0008-6215(83)88360-8.

10 Kudaibergenov S., Shimei Xu., Tatykhanova G., Kudaibergenova G. Gellan Gum Immobilized Anticancer Drugs and Gold Nanoparticles in Nanomedicine // Academic Journal of Polymer Science. – 2019. – Vol.2, № 3. – Art. 555588.

11 Chandrasekaran R., Radha A., Thailambal V.G. Roles of potassium ions, acetyl and L-glyceril groups in native gellan double helix: An X-ray study // Carbohydrate Research. – 1992. – Vol. 224. – P. 1-17.

12 Kang K.S., Veeder G.T., Mirrasoul P.J., Kaneko T., Cottrell I.M. Agar-like polysaccharide produced by a pseudomonas species: production and basic

properties // Applied and Environmental Microbiology. – 1981. – Vol. 43. – P. 1086-1091.

13 Jansson P.E., Lindberg B., Sandford P.A. Structural studies of gellan gum an extracellular polysaccharide elaborated by Pseudomonas elodea // Carbohydrate Research. – 1983. – Vol. 124. – P. 135-139.

14 Morris E., R., Katsuyoshi N., Rinaudo M. Gelation of gellan // Food Hydrocolloids. – 2012. – Vol. 28. – P. 373-411.

15 Fukada H., Takahashi K., Kitamura S., Yuguchi Y., Urakawa H., Kajiwara K. Termodynamics and structural aspect of the gelling process in the gellan gum/metal salt aqueous solutions // Journal of Thermal Analyss Calorimetry. – 2002. – Vol. 70. – P. 797-806.

16 Jennifer F., Robin H., Fotios S., Ian T. Self- structuring foods based on acid-sensitive low and high acyl mixed gellan systems to impact on satiety // Food Hydrocolloids. – 2014. – Vol. 35. – P. 522-530.

17 Mariella D., Pasquale D., Vittorio C. Solution and gelling properties of gellan benzyl esters // Macromolecules. – 1999. – Vol. 32. – P. 7109-7115.

18 Matsukawa S., Huang Z., Watanabe T. Structural change of polymer chains of gellan monitored by circular dichroism // Progress in Colloid and Polymer Science. – 1999. – Vol. 114. – P. 92-97.

19 Miyoshi E., Nishinari K. Non-Newtonian flow behavior of gellan gum aqueous solutions // Progress in Colloid and Polymer Science. – 1999. – Vol. 277. – P. 727−734.

20 Tuan-Chew T., Wan-Teck F., Min-Tze L., Azhar M. (2014) Comparative assessment of rheological properties of gelatin or gellan in maize starch – egg white composite gels // Journal of King Saud University– Science. – 2014. – Vol. 4. – P. 311-322. – DOI: 10.1016/j.jksus.2014.02.001.

21 Kudaibergenov S., Adilov Zh., Nuraje N., Sagindykov A., Tatykhanova G., Ibragimov R., Gusenov I. Laboratory test for enhanced oil recovery with gellan // International Journal of Biology and Chemistry. – 2012. – Vol. 4. – P. 58-68.

22 Ibragimov R., Gusenov I., Tatykhanova G., Adilov Zh., Nurxat Nuraje, Kudaibergenov S. Study of gellan for polymer flooding // Journal of Dispersion Science and Technology. – 2013. – Vol. 34. – P. 1-8. – DOI: 10.1080/01932691.2012.742766.

23 Gussenov I.Sh., Ibragimov R.Sh., Kudaibergenov S.E., Abilkhairov D.T., Kudaibergenov D.N. Application of polymer gellan for injectivity profile leveling // SPE Annual Caspian Conference and Exhibition: Processing of the Conference, 12–14 November 2014, Astana, Kazakhstan. – P. 1-7. – DOI: 10.2118/172299-MS.

24 Kudaibergenov S., Nuraje N., Adilov Zh., Abilkhairov D., Ibragimov R., Gusenov I., Sagindykov A. Plugging behavior of gellan in porous saline media // Journal of Applied Polymer Science. – 2015. – Vol. 132. – Art. 41256. – DOI: 10.1002/app.41256.

25 Kudaibergenov S.E., Gussenov I.Sh., Zhappasbayev B.Zh., Shakhvorostov A.V. Application of polymer flooding technology for enhanced oil recovery // Chemical Bulletin of Kazakh National University. – 2015. – Vol. 4, № 80. – P. 74-80. – DOI: 10.15328/cb644.

26 Nurakhmetova Zh., Gussenov I.Sh., Tatykhanova G.S., Kudaibergenov S.E. Behavior of gellan in aqueous-salt solutions and oilfield saline water // Chemical Bulletin of Kazakh National University. – 2015. – Vol. 3, № 79. – P. 35-40. – DOI: 10.15328/cb640.

27 Kudaibergenov S.E., Tatykhanova G.S., Sigitov V.B., Nurakhmetova Z.A., Blagikh E.V. Gussenov I.Sh., Seilkhanov T.M. Physico-chemical and rheological properties of gellan in aqueous-salt solutions and oilfield saline water // Macromol Symp. – 2016. – Vol. 363. – P. 20-35. – DOI: 10.1002/masy.201500139.

28 Gussenov I., Zhappasbayev B., Kudaibergenov S. Permeability reduction of heterogeneous oil reservoirs by brine-triggered gellan gel // Journal of Nanoscience and Nanotechnology. – 2017. – Vol. 17. – P. 9198-9201. – DOI: 10.1166/jnn.2017.14295.

29 Nurakhmetova Zh., Gussenov I., Aseyev V., Sigitov V., Kudaibergenov S. Application of sol-gel transition of gellan and xanthan for enhanced oil recovery and as drilling fluids // Journal of Chemical Technology and Metallurgy. – 2018. – Vol. 53. – P. 68-78.

30 Morris E.R., Nishinari K. Gellan gum and its food applications // Food Hydrocolloids. – 2025. – Vol. 123. – Art. 106789.

31 Bajaj I.B., Survase S.A., Saudagar P.S., Singhal R.S. Gellan gum: Fermentative production, downstream processing and applications // Food Technology and Biotechnology. – 2007. – Vol. 45, № 4. – P. 341-354.

32 Oomoto K., Uno T., Asai T. Gelation of gellan // Food Hydrocolloids. – 1999. – Vol. 13, № 3. – P. 247–258.

33 Tamaki H., Tanaka Y., Matsuzawa H. et al. Armatimonas rosea gen. nov., sp. nov., a novel member of the phylum Armatimonadetes // Frontiers in Microbiology. – 2005. – Vol. 6. – Art. 698. – DOI: 10.3389/fmicb.2015.00698.

34 Shandera V.X., Tindall B.J. Use of a gellan-based, sodium-deficient medium to determine the requirement for Na^+ in Vibrio species // Canadian Journal of Microbiology. – 1993. – Vol. 39, № 8. – P. 782-785. – DOI: 10.1139/m93-118.

35 Kawaguchi T., et al. Evaluation of gellan gum as an alternative gelling agent in PCR-compatible microbiological media // Journal of Microbiological Methods. – 2001. – Vol. 45, № 3. – P. 241–249.

36 Padhye A.A., Springer D.J., Marr, K. A. Rapid identification of Aspergillus species from agar cultures using polymerase chain reaction // Journal of Clinical Microbiology. – 2003. – Vol. 41, № 7. – P. 3111–3115.

37 Yasuda M., Orikasa Y., Hashidoko Y., Tada M., Osaki M., Tahara S. A simple method for isolation of nitrogen-fixing bacteria from plant roots using gellan gum as a gelling agent // Bioscience, Biotechnology, and Biochemistry. – 2006. – Vol. 70, № 8. – P. 1936–1939. – DOI: 10.1271/bbb.60096.

38 Lee K.Y., Mooney D.J. Hydrogels for tissue engineering // Chemical Reviews. – 2001. – Vol. 101, № 7. – P. 1869–1879. – DOI: 10.1021/cr000108x.

39 Abu Bakar A.J., Mat Amin K.A. Progress and opportunities in gellan gum and collagen as wound healing materials // Science, Engineering and Health Studies. – 2024. – Vol. 18. – Art. 240100004. – DOI: 10.69598/sehs.18.24010004.

40 Oliveira J.T., Santos T.C., Martins L., Picciochi R., Marques A.P., Castro A.G., Neves N.M., Mano J.F., Reis R.L. Gellan gum injectable hydrogels for cartilage tissue engineering applications: in vitro studies and preliminary in vivo evaluation // Tissue Engineering Part A. – 2010. – Vol. 16, № 1. – P. 343–353. – DOI: 10.1089/ten.TEA.2009.0117.

41 Gussenov I.Sh., Berzhanova R.Zh., Mukasheva T.D., Tatykhanova G.S., Imanbayev B.A., Sagyndykov M.S., Kudaibergenov S.E. Investigation of gellan gum potential for enhanced oil recovery // Gels. – 2023. – Vol. 9, № 11. – P. 858. – DOI: 10.3390/gels9110858.

42 Nurakhmetova Zh., Gussenov I., Tatykhanova G., Kudaibergenov S. Behavior of gellan in aqueous salt solutions and formation waters // Chemical Bulletin of Kazakh National University. – 2015. – Vol. 79, № 3. – P. 34–40. – DOI: 10.15328/cb640.

43 Osmalek T., Froelich A., Tasarek S. Application of gellan gum in pharmacy and medicine // International Journal of Pharmaceutics. – 2014. – Vol. 466. – P. 328-340. – DOI: 10.1016/j.ijpharm.2014.03.038.

44 Gan L., Gan Y., Zhu X., Zhu J. Novel microemulsion in situ electrolyte-triggered system for ophthalmic delivery of lipophilic cyclosporine A: In vitro and in vivo results // International Journal of Pharmaceutics. – 2009. – Vol. 365. – P. 143-149. – DOI: 10.1016/j.ijpharm.2008.08.004.

45 Silva-Correa J., Zavan B., Vindigni V., Silva T.H., Oliveira J.M., Abatangelo G., Reis R.L. Biocompatibility evaluation of ionic- and photo-crosslinked methacryalted gellan gum hydrogels: In vivo and in vitro study // Advanced Healthcare Materials. – 2013. – Vol. 2. – P. 568-575. – DOI: 10.1002/adhm.201200256.

46 Gong Y., Wang C., Lai R.C., Su K., Zhang K., Wang D-A. An improved injectable polysaccharide hydrogel: Modified gellan gum for long-term cartilage regeneration in vitro // Journal of Materials Chemistry. – 2009. – Vol. 19. – P. 1968-1977. – DOI: 10.1039/B818090C.

47 Oliveira J.T., Gardel L.S. Rada T., Martins L., Gomes M.E., Reis R.L. Injectable gellan gum hydrogels with autologous cells for the treatment of rabbit articular cartilage defects // Journal of Orthopaedic Research. – 2010. – Vol. 28. – P. 1193-1199. – DOI: 10.1002/jor.21114.

48 Coutinho D.F., Sant S., Shin H., Oliveira J.T., Gomes M.E., Neves N.M., Khademhosseini A., Reis R.L. Modified gellan gum hydrogels with tunable physical and mechanical properties // Biomaterials. – 2010. – Vol. 31. – P. 7494-7502. – DOI: 10.1016/j.biomaterials.2010.06.035.

49 Silva-Correa J., Oliveira J.M., Caridade S.G., Oliveira J.T., Sousa R.A., Mano J.F., Reis R.I. Gellan gum-based hydrogels for intervertebral disc

tissue engineering applications // Journal of Tissue Engineering and Regenerative Medicine. – 2011. – Vol. 5. – P. e97–e107.

50 Tsaryk R., Silva-Correia J., Oliveira J.M., Unger R.E. Landes C., Brochhausen C., Chanaati S., Reis R.L., Kirkpatrick C.J. Biological performance of cell-encapsulated methacrylated gellan gum-based hydrogels for nucleus pulposes regeneration // Journal of Tissue Engineering and Regenerative Medicine. – 2017. – Vol. 11, № 3 – P. 637-648. – DOI: 10.1002/term.

51 Silva-Correa J., Miranda-Goncalves V., Salgado A.J., Sousa N., Oliveira J.M., Reis R.L. Angiogenic potential of gellan-gum-based hydrogels for application nucleus pulposes regeneration: In vivo study // Tissue Engineering. Part A. – 2012. – Vol. 18. – P. 1203-1212. – DOI: 10.1089/ten.tea.2011.0632.

52 Wagner A.M., Spencer D.S., Peppas N.A. Advanced architectures in the design of responsive polymers for cancer nanomedicine // Journal of Applied Polymer Science. – 2018. – Vol. 135. – Art. 46154. – DOI: 10.1002/app46154.

53 Shan J., Tenhu H. Recent advances in polymer protected gold nanoparticles: Synthesis, properties and applications // Chemical Communications. – 2007. – Vol. 44. – P. 4580-4598. – DOI: 10.1039/B707740H.

54 Dhar S., Mali V., Bodhankar S., Shiras A., Prasad B.L.V., Pokharkar V. Biocompatible gellan gum-reduced gold nanoparticles: cellular uptake and subacute oral toxicity studies // Journal of Applied Toxicology. – 2011. – Vol. 31. – P. 411-420. – DOI: 10.1002/jat.1595.

55 Dhar S., Reddy E.M., Pokharkar V., Prasad B.L.V. Natural gum reduced/stabilized gold nanoparticles for drug delivery formulations // Chemistry - A European Journal. – 2008. – Vol. 14. – P.10244-10250. – DOI: 10.1002/chem.200801093.

56 Dhar S., Reddy E.M., Prabhune A., Pokharkar V., Shiras A., Prasad B.L.V. Cytotoxicity of sophorolipid-gellan gum-gold nanoparticle conjugates and their doxorubicin loaded derivatives towards human glioma stem cell lines // Nanoscale. – 2011. – Vol. 3. – P. 575-580. – DOI: 10.1039/C0NR00598C.

57 Dhar S., Murawala P., Shiras A., Pokharkar V., Prasad B.L.V. Gellan gum capped silver nanoparticle dispersions and hydrogels: cytotoxicity and in vivo diffusion studies // Nanoscale. – 2012. – Vol. 4. – P. 563- 567. – DOI: 10.1039/C1NR10957J.

58 Huang X.H., Jain P.K. El-Sayed I.H., El-Sayed M.A. Plasmonic photothermal therapy (PPTT) using gold nanoparticles // Lasers in Medical Science. – 2008. – Vol. 23. – P. 217-228. – DOI: 10.1007/s10103-007-0470-x.

59 Huang X., Neretina S., El-Sayed M.A. Gold nanorods: From synthesis and properties to biological and biomedical applications // Advanced Materials – 2009. – Vol. 21. – P. 4880-4910. – DOI: 10.1002/adma.200802789.

60 Huang X.H., Jain P.K. El-Sayed I.H., El-Sayed M.A. Gold nanoparticles: interesting optical properties and recent applications in cancer diagnostic and therapy // Nanomedicine. – 2007. – Vol. 2. – P. 681-693. – DOI: 10.2217/17435889.2.5.681.

61 Lim W.Q., Gao Z. Plasmonic nanoparticles in biomedicine // Nano Today. – 2016. – Vol. 11. – P. 168-188. – DOI: 10.1016/j.nanotod.2016.02.002.

62 Jabeen F., Najam-ul-Haq M., Javeed R., Huck C.W., Bonn G.K. Au-nanomaterials as a superior choice for near-infrared photothermal therapy // Molecules. – 2014. – Vol. 19. – P. 20580-20593. – DOI: 10.3390/molecules191220580.

63 Day E.S., Thompson P.A., Zhang L., Lewinski N.A., Drezek R.A., Blaney S.M., West J.L. Nanoshell-mediated photothermal therapy improves survival in a murine glioma model // Journal of Neuro-Oncology – 2011. – Vol. 104. – P. 55- 63. – DOI: 10.1007/s11060-010-0470-8.

64 Mackey M.A., Ali M.R.K., Austin L.A., Near R.D., El-Sayed M.A. The most effective gold nanorod size for plasmonic photothermal therapy: Theory and in vivo experiments // The Journal of Physical Chemistry B. – 2014. – Vol. 118. – P. 1319-1326. – DOI: 10.1021/jp409298f.

65 Huang X., Neretina S., El-Sayed M.A. Gold nanorods: From synthesis and properties to biological and biomedical applications // Advanced Materials – 2009. – Vol. 21. – P. 4880-4910. – DOI: 10.1002/adma.200802789.

66 Viera S., Vial S., Maia F., Carvalho M., Reis R.L., Granja P.L., Oliveira J.M. Gellan gum-coated gold nanorods: an intracellular nanosystem for bone tissue engineering // RSC Advances. – 2015. – Vol. 5. – P. 77996-78005. – DOI: 10.1039/C5RA13556G.

67 Nikoobakht B., El-Syed M.A. Preparation and growth mechanism of gold nanorods (NRs) using seed-mediated growth method // Chemistry of Materials. – 2003. – Vol. 15. – P. 1957-1962. – DOI: 10.1021/cm020732l.

68 Pautke C., Schieker M., Tischer T., Kolk A., Neth P., Mutschler W., Milz S. Characterization of osteosarcoma cell lines MG-63, Saos-2 and U-2 OS in comparison to human osteoblasts. Anticancer Research. – 2004. – Vol. 24, №6. – P. 3743-3748.

69 Sivakumar B., Aswathy R.G., Sreejith R., Nagaoka Y., Iwai S., Suzuki M., Fukuda T., Hasumura Y., Yoshida Y., Maekawa T., Sakthikumar D.N. Bacterial exopolysaccharide based magnetic nanoparticles: a versatile nanotool for cancer cell imaging, targeted drug delivery and synergistic effect of drug and hyperthermia mediated cancer therapy // Journal of Biomedical Nanotechnology. – 2014. – Vol. 10. – P. 885-899. – DOI: 10.1166/jbn.2014.1820.

70 Ayala-Orozco C., Urban C., Knight M.W., Urban A.S., Neumann O., Bishnoi S.W., Mukherjee S., Goodman A.M., Charron H., Mitchell T.) Au nanomatryoshkas as efficient near-infrared photothermal transducers for cancer treatment: Benchmarking against nanoshells // ACS Nano. – 2014. – Vol. 8. – P. 6372-6381. – DOI: 10.1021/nn501871d.

71 Singh S.R., Carreiro S.T., Chu J., Niesman M.R., Collette W.W., Younis H.S., Sartnurak S., Gukasyan H.J. L-Carnosine: multifunctional dipeptide buffer for sustained-duration topical ophthalmic formulations // Journal of Pharmacy and Pharmacology. – 2009. – Vol. 61, №6. – P. 733-742. – DOI: 10.1211/jpp.61.06.0005.

72 Rozier A., Mazuel C., Grove J., Plazonnet B., Gelrite: a novel, ion-activated, in situ gelling polymer for ophthalmic vehicles - effect on bioavailability of timolol // International Journal of Pharmaceutics. – 1989. – Vol. 57. – P. 163-168. – DOI: 10.1016/0378-5173(89)90305-0.

73 Arthur Sh. H., Laurence J., Barrish A., et al. Plasma timolol concentrations of timolol maleate: Timolol gel-forming solution (TIMOPTIC-XE(R)) once daily versus timolol maleate ophthalmic solution twice daily // Documental Ophthalmologica. – 2001. – Vol.103, № 1. – P. 73-79. – DOI: 10.1023/A:1017962731813.

74 Kesavan K., Nath G., Pandit J. K. Preparation and in vitro antibacterial evaluation of gatifloxacin mucoadhesive gellan system // Daru-journal of Pharmaceutical Sciences. – 2010. – Vol. 18, № 4. – P. 237-246.

75 Liu Y., Liu J., Zhang X., et al. In situ gelling Gelrite/Alginate Formulations as Vehicles for ophthalmic drug delivery // AAPS PharmSciTech. – 2010. – Vol. 11, № 2. – P. 610-620. – DOI: 10.1208/s12249-010-9413-0.

76 Ahmed T. S., Ahmed E. M., Ibrahim T. M., et al. Promising ion-sensitive in situ ocular nanoemulsion gels of terbinafine hydrochloride: Design, in vitro characterization and *in vivo* estimation of the ocular irritation and drug pharmacokinetics in the aqueous humor of rabbits // International Journal of Pharmaceutics. – 2012. – Vol. 443, № 1-2. – P. 293-305. – DOI: 10.1016/j.ijpharm.2012.12.049.

77 Urtti A., Salminen L., Miinakainen O. Systemic absorption of ocular pilocarpine is modified by polymer matrices // International Journal of Pharmaceutics. – 1985. – Vol. 23. – P. 147-161. – DOI: 10.1016/0378-5173(85)90005-5.

78 Prausdnitz M.R., Noonan J.S. Permeability of cornea, sclera, and conjunctiva: a literature analysis for drug delivery to the eye // Journal of Pharmaceutical Science. – 1998. – Vol. 87, №12. – P. 1479-1488. – DOI: 10.1021/js9802594.

79 Ludwig A., van Ooteghem M. Influence of viscolysers on the residence of ophthalmic solutions evaluated by slit lamp fluorophotometry // S.T.P. Pharma Science. – 1992. – Vol. 2. – P. 81-87.

80 Al Khateb K., Ozhmukhametova E.K., Elvira K. Mussin M.N., Seilkhanov S.K., Rakhypbekov T.K., Lau W.M., Khutoryanskiy V.V. In situ gelling systems based on Pluronic F127/Pluronic F68 formulations for ocular drug delivery // International Journal of Pharmaceutics. – 2016. – Vol. 502, № 1-2. – P. 70-79. – DOI: 10.1016/j.ijpharm.2016.02.027.

81 Agibayeva L.E., Kaldybekov D.B., Porfiryeva N.N., Garipova V.R., Mangazbayeva R.A., Moustafine R.I., Semina I.I., Mun G.A., Kudaibergenov S.E., Khutoryanskiy V.V. Gellan gum and its methacrylated derivatives as in situ gelling mucoadhesive formulations of pilocarpine: In vitro and in vivo studies // International Journal of Pharmaceutics. – 2020. – Vol. 577. – P. 119093. – DOI: 10.1016/j.ijpharm.2020.119093.

82 Hui H.-W., Robinson J.R. Ocular drug delivery of progesterone using a bioadhesive polymer // International Journal of Pharmaceutics. – 1985. – Vol. 26. – P. 203-213. – DOI: 10.1016/0378-5173(85)90230-3.

83 Robinson J.R. Ocular drug delivery. Mechanism(s) of corneal transport and mucoadhesive delivery systems // S.T.P. Pharma Science. – 1989. – Vol. 5. – P. 839-846.

84 Le Bourlais C.A., Treupel-Acar L., Rhodes C.T., Sado P.A., Leverge R. New ophthalmic drug delivery systems // Drug Development and Industrial Pharmacy. – 2008. – Vol. 21. – P. 19-59. – DOI: 10.3109/03639049509048095

85 Calonge M. The treatment of dry eye // Survey of Ophthalmology. – 2001. – Vol. 45. – P. S227-S239. – DOI: 10.1016/S0039-6257(00)00205-8.

86 Greaves J.L., Wilson C.G. Treatment of diseases of the eye with mucoadhesive delivery systems // Advanced Drug Delivery Reviews. – 1993. – Vol. 11. – P. 349–383. – DOI: 10.1016/0169-409X(93)90016-W

87 Lee V.H.L., Robinson J.R. Review: topical ocular drug delivery: recent developments and future challenges // Journal of Ocular Pharmacology and Therapeutics. – 1986. – Vol. 2. – P. 67-108. – DOI: 10.1089/jop.1986.2.67.

88 Moiseev R.V., Morrison P.W.J., Steele F., Khutoryanskiy V.V. Penetration Enhancers in Ocular Drug Delivery // Pharmaceutics. – 2019. – Vol. 11. – P. 321. – DOI: 10.3390/pharmaceutics11070321.

89 Morrison P. W. J., Porfiryeva N. N., Chahal S., Salakhov I.A., Lacourt Ch., Semina I.I., Moustafine R. I., Khutoryanskiy V.V. Crown Ethers: Novel Permeability Enhancers for Ocular Drug Delivery // Molecular Pharmaceutics. – 2017. – Vol. 14. – P. 3528-3538. – DOI: 10.1021/acs.molpharmaceut.7b00556.

90 Washington N., Washington C., Wilson C.G. Ocular drug delivery. In: Physiological Pharmaceutics: Barriers to Drug Absorption. 2nd ed. – FL, USA: CRC Press, 2001. – P. 249–270.

91 Morrison P.W.J., Khutoryanskiy V.V. Enhancement in corneal permeability of riboflavin using calcium sequestering compounds // International Journal of Pharmaceutics. – 2014. – Vol. 472, № 1-2. – P. 56-64. – DOI: 10.1016/j.ijpharm.2014.06.007.

92 Liu R., Liu Z., Zhang C., Zhang B. Gelucire44/14 as a novel absorption enhancer for drugs with different hydrophobicities: in vitro and in vivo improvement on transcorneal permeation // Journal of Pharmaceutical Sciences. – 2011. – Vol. 100, № 8. – P. 3186–3195.

93 Kumari A., Sharma P.K., Garg V.K., Garg G. Ocular inserts – advancement in therapy of eye diseases // Journal of Advanced Pharmaceutical Technology & Research. – 2010. – Vol. 1, № 3. – P. 291-296. – DOI: 10.4103/0110-5558.72419.

94 del Amo E.M., Urtti A. Current and future ophthalmic drug-delivery systems: a shift to the posterior segment // Drug Discovery Today. – 2008. – Vol. 13, № 3–4. – P. 135-143. – DOI: 10.1016/j.drudis.2007.11.002

95 Thrimawithana T.R., Young S., Bunt C.R., Green C., Alany R.G. Drug delivery to the posterior segment of the eye // Drug Discovery Today. – 2011. – Vol. 16, № 5-6. – P. 270-277. – DOI: 10.1016/j.drudis.2010.12.004.

96 Swan K.C. Use of methyl cellulose in ophthalmology // Archives of Ophthalmology. – 1945. – Vol. 33. – P. 378-380. – DOI: 10.1001/archopht.1945.00890170054004.

97 Kaur I.P., Smitha R. Penetration enhancers and ocular bioadhesives: two new avenues for ophthalmic drug delivery // Drug Development and Industrial Pharmacy. – 2002. – Vol. 28, № 4. – P. 353-369. – DOI: 10.1081/DDC-120002997.

98 Shahwal V.K., Dr. Dubey B.K., Bhoumick M., Upadhyay A. Ocular drug delivery: an overview // International Journal of Biomedical Research. – 2011. – Vol. 2, № 5. – P. 167-187.

99 Loukotová L., Konefał R., Venclíková K., et al. Hybrid thermoresponsive graft constructs of fungal polysaccharide β-glucan: Physico-chemical and immunomodulatory properties // European Polymer Journal. – 2018. – Vol. 106. – P. 118-127. – DOI: 10.1016/j.eurpolymj.2018.07.004.

100 Lin H.R., Sung K.C. Carbopol/pluronic phase change solutions for ophthalmic drug delivery // Journal of Controlled Release. – 2000. – Vol. 69. – P. 379-388. – https://doi.org/10.1016/S0168-3659(00)00329-1.

101 Fuoss R. M. Errata: Viscosity function for polyelectrolytes // Journal of Polymer Science. – 1949. – Vol. 3, № 4. – P. 603-604. – DOI: 10.1002/pol.1949.120040111.

102 Dreveton E., Monot F., Lecourtier J., Ballerini D., Choplin L. Influence of fermentation hydrodynamics on gellan gum physic-chemical characteristics // Journal of Fermentation and Bioengineering. – 1996. – Vol. 82, № 3. – P. 272-276. – DOI: 10.1016/0922-338X(96)88819-2.

103 Waschinski J.Ch., Joerg C. Tiller. Poly(oxazoline)s with Telechelic Antimicrobial Functions // Biomacromolecules. – 2005. – Vol. 6, № 1. – P. 235-243. – DOI: 10.1021/bm049553i.

104 Ritger P.L., Peppas N.A. A simple equation for description of solute release I. Fickian and non-fickian release from non-swellable devices in the form of slabs, spheres, cylinders or discs // Journal of Controlled Release. – 1987. – Vol. 5. – P. 23-36. – DOI: 10.1016/0168-3659(87)90034-4.

105 Madan M., Bajaj A., Lewis S., Udupa N., Baig J.A. In situ forming polymeric drug delivery systems // Indian Journal of Pharmaceutical Science & Research. – 2009. – Vol. 71, № 3. – P. 242-251. – DOI: 10.4103/0250-474X.56015.

Приложение А

Список опубликованных работ

1. Tatykhanova G.S., Tuleyeva R.N., Nurakhmetova Z.A., Gizatullina N.N., Krasnoshtanov V.K., Kaldybekov D.B., Aseyev V.O., Khutoryanskiy V.V., Kudaibergenov S.E. Polymer-Protected Gold Nanoparticles for Photothermal Treatment of Ehrlich Adenocarcinoma: In Vitro and In Vivo Studies // Macromolecular Chemistry and Physics. 2024. Early View. Article 2400128. DOI: 10.1002/macp.202400128. Q2
2. Tatykhanova G.S., Gizatullina N.N., Kudaibergenova G.M., Berzhanova R.Zh., Mukasheva T.D., Kudaibergenov S.E. Comparative Study of Gellan Gum Derived from Domestic Raw Materials of Kazakhstan and Commercial Gellan // Macromolecular Symposia. 2024. Vol. 413, Issue 4. Article 2400004. DOI: 10.1002/masy.202400004. Q3
3. Tatykhanova G.S., Hirvonen S.-P., Bardadym Y.V., Gizatullina N.N., Saulimbay M.A. Fractionation and Characterization of Commercial Low Acyl Gellan Gum // Macromolecular Symposia. 2024. Vol. 413, Issue 4. Article 2400001. DOI: 10.1002/masy.202400001. Q3
4. Tatykhanova G.S., Tuleyeva R.N., Gizatullina N.N., Kaldybekov D.B., Bardadym Y.V., Aseyev V.O., Kudaibergenov S.E. Characterization of Biocompatible Gellan Gum Fractions for Prolonged Retention in Ocular Drug Delivery Systems // Polymers for Advanced Technologies. 2024. Vol. 35, Issue 11. Article e6635. DOI: 10.1002/pat.6635. Q2
5. Tuleyeva R.N., Tatykhanova G.S., Gizatullina N.N., Kaldybekov D.B., Bardadym Y.V., Aseyev V.O., Kudaibergenov S.E. Preparation and Characterization of Amphoteric Polysaccharides Derived from Chitosan and Gellan Gum // Polymers for Advanced Technologies. 2024. Vol. 35, Issue 12. Article e70033. DOI: 10.1002/pat.70033. Q2
6. Kudaibergenov S.E., Tatykhanova G.S., Gizatullina N.N., Tuleyeva R.N., Kaldybekov D.B., Gussenov I.Sh., Berzhanova R.Zh., Mukasheva T.D., Vamvakaki M., Aseyev V.O., Khutoryanskiy V.V. Anionic Polysaccharide – Gellan as a Perspective Polymer for Potential Application in Medicine and Oil Recovery: A Mini-Review // Uzbekistan Journal of Polymers. 2023. Vol. 2, No. 2. P. 39-56. DOI: http://uzpolymerjournal.com/articles/article.php?id=230205.

RESEARCH ARTICLE

Macromolecular Chemistry and Physics
www.mcp-journal.de

Polymer-Protected Gold Nanoparticles for Photothermal Treatment of Ehrlich Adenocarcinoma: In Vitro and In Vivo Studies

Gulnur S. Tatykhanova, Rysgul N. Tuleyeva, Zhanara A. Nurakhmetova, Nargiz N. Gizatullina, Vladimir K. Krasnoshtanov, Daulet B. Kaldybekov, Vladimir O. Aseyev, Vitaliy V. Khutoryanskiy, and Sarkyt E. Kudaibergenov**

Photothermal therapy (PTT) is recognized as an effective tool for the treatment of cancer and it has attracted considerable attention of scientists. In this work, gold nanospheres (AuNSs) and gold nanorods (AuNRs) stabilized using poly(*N*-vinylpyrrolidone) (PVP), pristine gellan gum (PGG), and poly(2-ethyl-2-oxazoline)-grafted gellan gum (GG-*g*-PEtOx) are synthesized and evaluated as PTT agents in Ehrlich cancer cells. The physicochemical characteristics of these AuNSs and AuNRs, including their surface plasmon resonance absorption spectra, size, zeta potential, and aspect ratio are studied using UV–vis-spectroscopy, dynamic light scattering, zeta potential, transmission electron microscopy, and optical microscopy techniques. The polymer-protected AuNSs exhibit light-to-heat conversion, raising the temperature from 37 to 43 °C when irradiated using a visible light source. In the case of AuNSs, considerable damage to Ehrlich cancer cells is observed following irradiation and 40 days of examination. However, with regard to AuNSs, the damage to Ehrlich cancer cells is slightly lower than observed in AuNRs. In vivo experiments demonstrate that laser irradiation of tumors in mice after injecting AuNSs leads to a statistically significant decrease in tumor size as compared to those not irradiated and the control samples.

1. Introduction

Cancer is a multifaceted disease characterized by uncontrolled growth and spread of abnormal cells in the body and is one of the leading causes of human morbidity and mortality worldwide.[1–4] Unfortunately, due to the heterogeneous nature of cancer, which poses a significant public health challenge, there are currently no fully inclusive approaches to effectively treat this condition.[5] The primary modalities currently employed for cancer treatment include chemotherapy, radiation therapy, immunotherapy, and surgery. These methods have become widely used in clinical practice for decades. However, cancer patients undergoing these therapies often experience significant adverse effects.[6] For this reason, the majority of studies in cancer therapy are focused on the development of alternative therapies that can complement or even substitute the existing therapies. The goal is to improve their efficacy and minimize any potential side effects that they may have on patients. These methods ideally should selectively eliminate cancerous cells only, without damaging healthy cells.[7,8] Among the advanced phototherapy methods for treating cancer, photothermal therapy (PTT) offers a great advantage due to its noninvasive nature and selective therapeutic potential for different cancers. PTT has several advantages including the ability to externally irradiate tumors, which means the therapy can be applied from outside the body. PTT is also associated with limited complications, meaning it has a lower risk of side effects compared to other cancer

G. S. Tatykhanova, R. N. Tuleyeva, Z. A. Nurakhmetova, N. N. Gizatullina, D. B. Kaldybekov, S. E. Kudaibergenov
Institute of Polymer Materials and Technology
Almaty 050019, Kazakhstan
E-mail: gulnur-ts81@yandex.kz; skudai@mail.ru
G. S. Tatykhanova
Satbayev University
Almaty 050013, Kazakhstan
R. N. Tuleyeva, D. B. Kaldybekov
Department of Chemistry and Chemical Technology
Al-Farabi Kazakh National University
Almaty 050040, Kazakhstan
V. K. Krasnoshtanov
Kazakh Research Institute of Oncology and Radiology
Almaty 050022, Kazakhstan
V. O. Aseyev
Department of Chemistry
University of Helsinki
Helsinki 00014, Finland
D. B. Kaldybekov, V. V. Khutoryanskiy
Reading School of Pharmacy
University of Reading
Whiteknights, Reading RG6 6DX, UK
The ORCID identification number(s) for the author(s) of this article can be found under https://doi.org/10.1002/macp.202400128

DOI: 10.1002/macp.202400128

therapies. Additionally, PTT offers enhanced selectivity, meaning it can specifically target cancer cells while minimizing the damage to normal cells. Another benefit of PTT is a relatively quick patient recovery, implying that they may experience a faster recuperation period after undergoing PTT. In phototherapy, certain wavelengths of light within the visible and near-infrared (NIR) resonance bands are utilized to heat photothermal agents such as nanoparticles. This leads to a localized increase in the temperature of specific tissues resulting in the elimination of malignant cells in those tissues. The higher sensitivity of cancer cells to temperature elevation results in their increased susceptibility to the effects of heat compared to normal cells. Moreover, an exposure to an external laser with adjustable dosing facilitates the selective eradication of various types of cancer cells while minimizing the damage to the surrounding healthy tissues.[9–14]

Gold nanoparticles (AuNPs) are considered to be the foremost photothermal agents used in PTT treatment. These nanoparticles have an important attribute such as a high light-to-heat conversion efficiency, which makes them particularly effective in converting light energy into heat. In PTT, visible and NIR laser lights are employed to activate and stimulate AuNPs, which cause the nanoparticles to resonate and generate heat, thus enabling localized heating of the targeted tumor tissues. The application of AuNPs as photothermal agents provides enhanced therapeutic outcomes due to the possibility of their direct injection into the tumor, while minimizing nonspecific distribution in the body. Furthermore, these nanoparticles can be safely eliminated from the body after completing the therapy.[15–17]

AuNPs exhibit distinctive physicochemical properties such as a possibility for localized surface plasmon resonance (LSPR). The LSPR phenomenon facilitates interactions between incident light and the electrons in the conduction band on the surface of AuNPs.[18–20] The optical properties of AuNPs are dependent on their dimensions. The LSPR properties can be altered by modifying the shape and size of AuNPs. This enables the use of different wavelengths of light, including those in the NIR and visible spectra for achieving localized heating effects.[21–24] Therefore, the ability to tune the LSPR properties of AuNPs through size and shape manipulation offers flexibility in designing AuNPs for specific applications that require interaction with different wavelengths of light. Visible light has limited penetration ability into biological tissues compared to NIR light. This property makes visible light more suitable for certain medical procedures that require higher precision.[25–28]

Small spherical gold nanoparticles are easy to produce.[12] They are less toxic than particles of large size and show improved photoconversion capability that may result from the irradiation with the visible light using standard surgical green lasers. In particular, the efficiency of light-to-heat conversion (photoconversion at 530 nm) of 14 nm gold nanospheres (AuNSs) irradiated in the visible region and its application to selectively obliterate cancer cells using breast cancer as a model was shown. Thus, the AuNSs with diameters ranging from 10 to 30 nm were considered nontoxic due to such properties, as stability, cellular uptake efficiency, and favourable clearance mechanism. They were recognized as ideal photothermal agents for biomedical applications[29,30] and demonstrated a characteristic LSPR band around 520 nm, i.e., in the visible region of the spectrum, with an efficient light-to-heat conversion.[26,31] As such, AuNSs, as photothermal agents, are an efficient way to induce precise heating leading to less damage to surrounding tissues, while destroying malignant thermosensitive cells.[25,32]

Many synthetic and natural polymers can function as both reducing and capping agents to form AuNPs.[33,34] According to literature, the efficacy of PTT with regard to the antitumor activity of AuNSs and gold nanorods (AuNRs), among other noble and transition metal nanoparticles stabilized with natural and/or synthetic polymers, has been studied with respect to melanoma,[35] 4T1 and HeLa cells,[36] 4T1 murine breast tumor cells,[37] U87 MG human glioblastoma cell,[38] and transplanted liver tumor.[39]

In the present work, AuNSs and AuNRs stabilized using poly(*N*-vinylpyrrolidone) (PVP), pristine gellan gum (PGG), and poly(2-ethyl-2-oxazoline)-grafted gellan gum (GG-*g*-PEtOx) were prepared and characterized for their size and morphology using dynamic light scattering (DLS) and transmission electron microscopy (TEM). Coating and stabilization of AuNPs and AuNRs by biocompatible, nontoxic, and biodegradable polymers, such as poly(*N*-vinylpyrrolidone) and gellan, allow us to preserve the colloidal gold nanoparticles in aqueous solution for an extended period and to prepare effective photothermal agent for the treatment of cancer cells.[40–48] Polymer-protected gold nanoparticles were produced through one-pot and growth seeding methods in aqueous solutions. These particles were observed to exhibit temperature-dependent changes and high stability over a period of 36 days, thus making them suitable for application in photothermal therapy. The protocols have been developed herein for the evaluation of the photothermal conversion ability of AuNSs and AuNRs when irradiated using visible and NIR laser light sources. The potential use of AuNSs and AuNRs in PTT treatment was tested both in vitro and in vivo against Ehrlich cancer cells. Ehrlich ascites carcinoma is a well-established murine model used for studying breast cancer.[49,50] It represents hyperdiploid and an undifferentiated carcinoma with 100% malignancy, short life span, high transplantable capability, and rapid proliferation. Since 2010, there has been an increase in the number of publications mentioning Ehrlich tumours. This is due to the systematic alterations induced by the tumors, the sensitivity of the tumor cells to chemotherapies and the antitumor potential of synthetic and natural products.

It is known[51] that malignant cells require large amounts of monosaccharide uptake in order to sustain their accelerated growth and division in comparison to that of healthy cells. We hypothesize that gellan gum composed of tetrasaccharide repeating units (1,3-β-D-glucose, 1,4-β-D-glucuronic acid, 1,4-β-D-glucose, and 1,4-α-L-rhamnose) may function as a "food" for cancer cells to support their accelerated growth. It is supposed that the cancer cells, feeding on tetrasaccharides, consume them and thereby "bare" gold nanoparticles that have been stabilized by the polysaccharide—gellan. Gold nanoparticles lacking a protective shell consisting of gellan will be forced to adsorb on cancer cells in order to minimize the free energy of the nanoparticles. Irradiation of these gold nanoparticles, attached to the cancerous cells, with appropriate laser light can induce local heating due to the LSPR and hyperthermia causing apoptosis of the cancer cells. In addition, GG-*g*-PEtOx could act as a bioadhesive[52] or a mucus-penetrating polymer.[53] Therefore, coating or conjugating gold particles with these polymers could facilitate the adhesion of gold nanoparticles to the mucosal

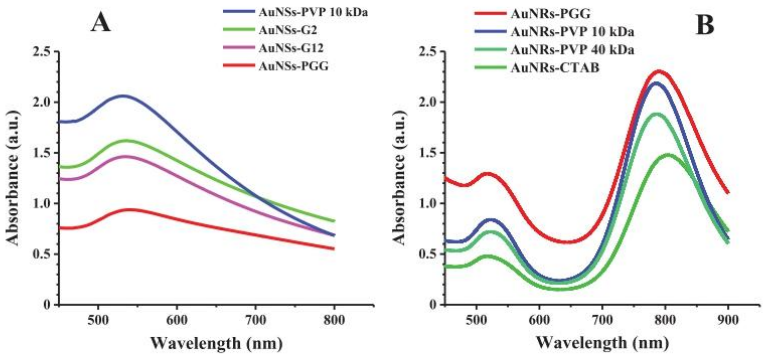

Figure 1. Representative surface plasmon resonance (SPR) absorption bands of A) spherical and B) rod-shaped gold nanoparticles stabilized using different amounts of polymers and a surfactant. Pristine gellan gum (PGG, 0.5%); G2 and G12 are poly(2-ethyl-2-oxazoline)-grafted gellan gums with different grafting densities (each at 2%); poly(*N*-vinylpyrrolidone) (PVP) with M_n = 10 and 40 kDa (4%), and cetyltrimethylammonium bromide (CTAB, 0.2 M). All spectra were recorded at 25 °C.

surface of tumors or their penetration into tumors. This process may prolong the efficacy of PTT by ensuring better localization of gold nanoparticles within the tumor tissue.

2. Results and Discussion

2.1. Physicochemical Characterization of Nanoparticles

Poly(*N*-vinylpyrrolidone) with M_n = 10 and 40 kDa, PGG, and poly(2-ethyl-2-oxazoline)-grafted gellan gums (abbreviated as G2, G3, and G12) were used as polymeric stabilizing agents of the AuNSs and AuNRs. It was expected that the surface modification of AuNPs with polymers can facilitate their cellular uptake. This enhancement is attributed to the affinity of both natural and synthetic polymers to cellular membranes.[54,55]

UV–vis spectroscopy is an effective method for confirming the formation and stabilization of aqueous dispersions of AuNSs and AuNRs. In general, AuNSs possess a single absorption band in the visible (500–550 nm) spectral region, which is known as a surface plasmon resonance (SPR). AuNRs exhibit two major absorption bands corresponding to the transverse and longitudinal SPR bands in the visible (≈520 nm) and the near-infrared regions, respectively.[56,57] The SPR spectrum is dependent on both the size and shape of gold nanoparticles. In this study, the adsorption spectra of polymer-coated AuNSs and AuNRs dispersions were recorded (**Figure 1**). The spectra confirmed a distinctive SPR band for AuNSs in the visible (≈530 nm) region (Figure 1A), while two characteristic surface plasmon bands corresponding to the transverse (≈520 nm, a weaker band in the visible region) and longitudinal (≈780 nm in NIR region) bands were observed for gold nanorods (Figure 1B).[54,57,58]

Controlling the size of AuNPs is a critical factor in the synthesis of colloidal gold and their application in PTT. Many studies have demonstrated that the interaction between gold nanoparticles and polymers significantly influences the size, stability, and size distributions of the particles.[59,60] Producing monodisperse polymer-coated AuNPs with smaller sizes in aqueous media can lead to improved biocompatibility, reduced cytotoxicity, and enhanced catalytic properties.

The average hydrodynamic size and zeta potential values of the spherical and rod-shaped AuNPs synthesized and stabilized with optimally selected concentrations of synthetic and natural polymers are summarized in **Tables 1** and **2**, respectively. During the dialysis, the pH of aqueous solution of AuNPs decreased from 12 to 8 confirming that most of the low-molecular-weight impurities are washed out. The mean diameter and zeta potential values of AuNSs were measured by DLS before and after dialysis against deionized water. It was observed that after dialysis, the size of AuNSs decreased by 2–3 times (Table 1). Overall, most of the spherical gold nanoparticles were polydisperse. The size distributions (before and after dialysis) of spherical gold nanoparticles stabilized with different polymers determined with DLS are shown in Figure S2 (Supporting Information).

In order to estimate the nanoparticles surface charge, the zeta potential values of the different AuNPs were measured. It appears that the zeta potential values of AuNPs significantly decreased following the dialysis, resulting in a further reduction of negative charges. The average zeta potential values of AuNSs were between −42 and −10 mV depending on the polymers used and dialysis (Table 1).

AuNRs stabilized using PGG displayed a negative zeta potential (−30 ± 3 mV) value due to the presence of carboxylic groups in the macromolecular chains of the polysaccharide (Table 2). Initially, the surface of AuNRs stabilized using PVP 10 and 40 kDa was positively charged, perhaps due to the presence of some excessive counterions of cetyltrimethylammonium bromide (CTAB); however, after dialysis, AuNR's zeta potential decreased down to −7 and −6 mV.

The TEM images (**Figure 2**) further confirmed the DLS results regarding the size of AuNPs, and both AuNSs and AuNRs were uniformly distributed. For instance, AuNSs in all batches displayed particles with sizes less than 40 nm in diameter. AuNSs stabilized with G2 (GG-g-PEtOx) demonstrated even smaller size with 10 ± 1 nm. The aspect ratio, i.e., length/width, for the gold

Table 1. Size and zeta potential values of polymer-protected AuNSs determined by DLS (G2, G3, and G12: poly(2-ethyl-2-oxazoline)-grafted gellan gums with different grafting densities; PDI: polydispersity index; PGG: pristine gellan gum; PVP: poly(*N*-vinylpyrrolidone). Data are expressed as mean ± standard deviation values ($n = 3$)).

Type of polymer	Concentration of polymer [% w/v]	Mean diameter [nm]				Zeta potential [mV]	
		Before dialysis	PDI	After dialysis	PDI	Before dialysis	After dialysis
PVP 10 kDa	4.0	42 ± 2	0.353	15 ± 1	0.309	−13 ± 2	−19 ± 2
PVP 40 kDa	4.0	47 ± 2	0.225	16 ± 2	0.238	−7 ± 2	−10 ± 3
PGG	0.5	88 ± 2	0.300	37 ± 2	0.415	−32 ± 2	−42 ± 3
G12	2.0	38 ± 1	0.513	13 ± 1	0.795	−21 ± 2	−33 ± 2
G3	2.0	22 ± 1	0.587	17 ± 1	0.671	−20 ± 2	−40 ± 2
G2	2.0	39 ± 1	0.496	11 ± 1	0.496	−18 ± 2	−39 ± 2

Table 2. Aspect ratio (measured using TEM) and zeta potential values of AuNRs synthesized and stabilized using PGG, G2, and PVPs (CTAB: cetyltrimethylammonium bromide; PGG: pristine gellan gum; PVP: poly(*N*-vinylpyrrolidone); n/a: not applicable. Data are presented as mean ± standard deviation ($n = 3$)).

Type of polymer	Concentration of polymer [% w/v]	Average length [nm]	Average width [nm]	Aspect ratio	ζ-potential [mV]
CTAB	n/a	42 ± 4	14 ± 2	3 ± 1	54 ± 11
PGG	0.5	34 ± 3	9 ± 2	4 ± 1	−30 ± 3
G2	2.0	53 ± 5	18 ± 3	3 ± 1	− 17 ± 2
PVP 10 kDa	4.0	44 ± 13	15 ± 3	3 ± 1	−7 ± 1
PVP 40 kDa	4.0	55 ± 2	16 ± 1	4 ± 1	−6 ± 2

nanorods stabilized using PVP 10 kDa was ≈3–4 in average (44 ± 13 nm lengthwise by 15 ± 3 nm in width) and the microphotographs are displayed in Figure 2 (also see Figure S3 in the Supporting Information).

2.1.1. Study of Photothermal Effects of AuNPs

The photothermal effect (i.e., light-to-heat conversion) of AuNSs was studied on porcine stomach tissues as an ex vivo tissue model. The temperature change in tissue samples was measured with an IR thermometer upon irradiation using a 530 nm visible light laser. Visible light was chosen for the current study to avoid unwanted heat stimulation, as it is generally not strongly absorbed by the bulk tissue (Figure 1A). **Figure 3** shows the temperature changes in porcine stomach tissue samples with and without injection of polymer-stabilized AuNSs' dispersion as a function of irradiation time. The highest temperature recorded was 43.5 ± 0.2 °C for AuNSs–PVP 40 kDa dispersion without tissue sample when exposed to irradiation for 60 min. For the tissue sample containing AuNSs–PVP 40 kDa; PGG and G2 (GG-g-PEtOx), the maximum temperature reached up to 41.1 ± 0.2, 41.0 ± 0.2, and 40.7 ± 0.2 °C, respectively, whereas the tissue sample without AuNSs was heated up to 39.0 ± 0.2 °C during 60 min of irradiation. These results clearly indicate that photothermal heating was induced by AuNSs in the tissue samples when exposed to the visible light source.

As seen from Figure 3, aqueous dispersion of AuNSs stabilized by PVP 40 kDa without tissue sample shows higher heating temperature upon irradiation compared to tissue-containing samples at identical conditions. Exact explanation of this phenomenon is complicated because the light-to-heat conversion depends on many parameters, in particular incident laser power, light wavelength, irradiation time, concentration, and size and shape of AuNPs.[61] In our opinion, overall increase in the temperature may be due to a collective heating effect of many nanoparticles within the excitation volume.[62] Our results are consistent with the data of the authors[63] indicating that the cancerous tissues can be overheated above the physiological level (typically 39–45 °C). In our case, the heating reaches up to ≈40–43 °C ($\Delta T \approx$ 3–6 °C). The temperature profiles of colloidal AuNPs' solutions (not stabilized by polymers) with different particle sizes were studied.[64] The temperature of the AuNPs solution increased exponentially upon laser illumination ($\lambda = 532$ nm), reached the equilibrium after ≈1200 s, and then returned to the ambient value after discontinuing irradiation. Upon irradiation the system is averagely heated up to 31.5 °C ($\Delta T \approx 6.5$ °C). Our observations are in good agreement with these results. The photothermal properties of gold nanoparticles, in addition to laser power, light wavelength, irradiation time, concentration, and size and shape, depend on various experimental factors, such as stirring, data recording and analysis, and the effective mass of the system. Moreover, in the presence of natural tissue, other molecules adsorb 530 nm light (e.g., hemoglobin and myoglobin), which makes the irradiation less effective. However, 530 nm light corresponds to the maximum of SPR and makes the photothermal phenomenon more effective. However, the 530 nm light is the most appropriate for laboratory tests and basic studies; it is less suitable for work with natural tissues. Short wavelengths are often adsorbed by natural molecules, e.g., hemoglobin and myoglobin have absorbance maxima about this value. This decreases the effectiveness of the photothermal treatment, and one has to

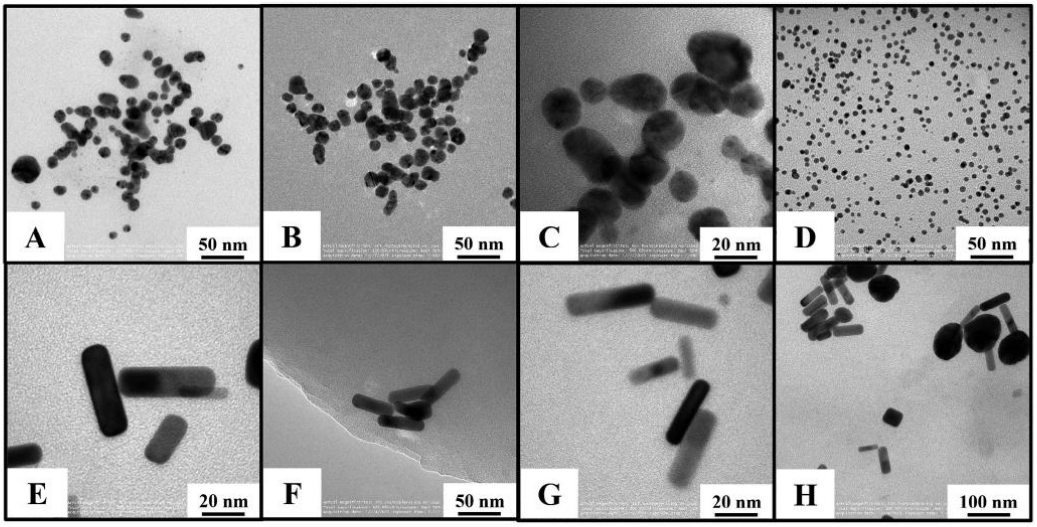

Figure 2. TEM images of AuNSs and AuNRs stabilized using A,E) poly(*N*-vinylpyrrolidone) with M_n = 10 kDa; B,F) poly(*N*-vinylpyrrolidone) with M_n 40 kDa; C,G) pristine gellan gum; D) G2–poly(2-ethyl-2-oxazoline)-grafted gellan gum (for spherical AuNPs), and H) cetyltrimethylammonium bromide without polymer (for AuNRs).

work with the light of longer wavelengths. In our case, we used 780 nm light, which guaranteed that the studied photothermal effect originates from the light absorbance.

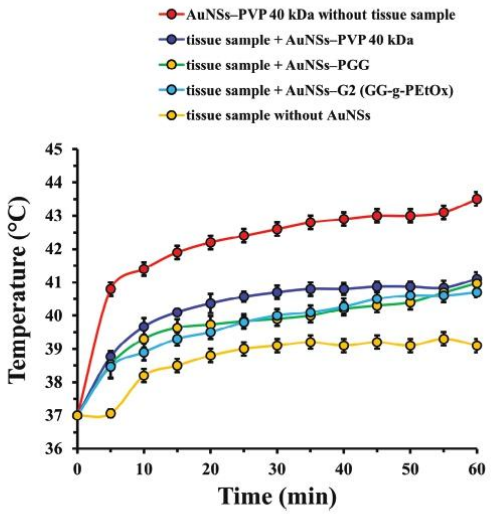

Figure 3. Time-dependent heating curves for AuNSs upon irradiation using a 530 nm visible light source. AuNSs: gold nanospheres; PGG: pristine gellan gum; G2: poly(2-ethyl-2-oxazoline)-grafted gellan gum; PVP 40 kDa: poly(*N*-vinylpyrrolidone) with M_n = 40 kDa.

2.1.2. Efficacy of PTT Treatment in Ehrlich Cancer Cells

Ehrlich cancer cells were used to investigate the efficacy of AuNP-based PTT treatment under the visible light irradiation. Ehrlich tumor is a well-established murine tumor model frequently employed in many cancer researches, both solid and ascitic forms. Classified as a carcinoma, it originates in the epithelial tissue of the skin or lining of internal organs. This tumor was initially derived from a spontaneous mammary adenocarcinoma in a mouse and has since been propagated in various strains of mice. Ehrlich tumor cells exhibit rapid proliferation and are characterized by their ability to induce ascites fluid accumulation in the peritoneal cavity when injected intraperitoneally. This tumor model is commonly employed to study tumor biology, tumor immunology, anticancer drug screening, and evaluating therapeutic interventions. Such attributes as high growth rate, good reproducibility, metastatic potential, and relative stability in morphological and biological characteristics were the reason to use Ehrlich cancer cells in this study.[65–69] In order to assess the potential effect of bio–nano interactions, in vitro experiments were performed using a Hanks' balanced salt solution (HBSS) buffer solution. First, Ehrlich cancer cells were dispersed in a buffer solution at a ratio of 1:9. Then, 1 mL of the suspension of extracted Ehrlich cancer cells was mixed with 1 mL of either polymer-stabilized AuNPs or AuNRs for 5 min. The suspension was irradiated with visible (530 nm) and NIR (780 nm) laser lights for 60 min at intensities of 10 and 90 mW, respectively. Micro-photographs of the cells were then acquired from randomly selected ten points in a Goryaev chamber and Ehrlich tumor cells in the visible area of the microscope were counted (**Figure 4**). Interestingly, the number of cells was considerably reduced in the presence of AuNSs

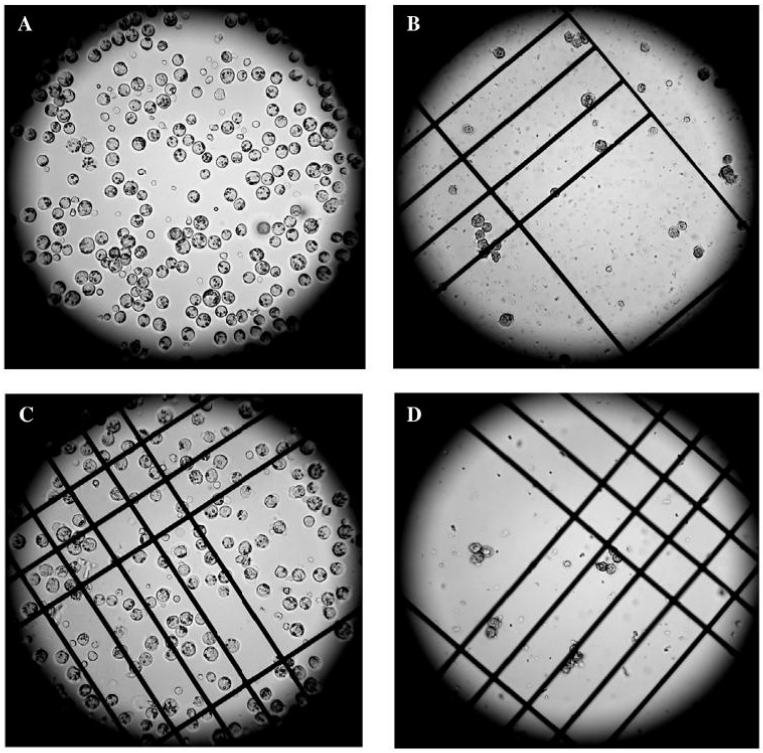

Figure 4. Micro-photographs of a suspension of Ehrlich cancer cells irradiated with visible (530 nm) light: A) before irradiation and without AuNSs; B) in the presence of AuNSs–PVP 40 kDa with no irradiation (in 40 days). C,D) After irradiation and in 40 days: C) without AuNSs, D) in the presence of AuNS–PVP 40 kDa. PVP 40 kDa: poly(*N*-vinylpyrrolidone) with $M_n = 40$ kDa.

stabilized with PVP 40 kDa even without irradiation after 40 days of examination (Figure 4B). An explanation of this phenomenon requires further experiments. No significant cell damage was observed in control experiments without AuNSs, indicating that the membranes were intact and that the cells have not been affected very much during 60 min of laser irradiation. However, due to an increase in the temperature of the medium up to 39 °C, when the samples were irradiated with either a visible or NIR light source for 60 min and further inspection during the experimental period, there was some reduction in the number of cells recorded in 40 days. As such there was no statistically significant difference between the numbers recorded in control samples with and without irradiation.

Irradiating cancer cells using visible light at 530 nm in the presence of spherical AuNPs stabilized with polymers and without yielded good results. **Figure 5** displays the reduction in the number of cancer cells counted from micro-photographs taken from randomly selected ten points (numerical values are shown in Table S1 in the Supporting Information). For instance, the number of cancer cells counted after 30–40 days decreased by 10–40 times in comparison with the control samples ($p < 0.0001$). It should be noted that the number of cells in the presence of AuNSs stabilized with polymers was reduced even without irradiation. Probably the gold nanoparticles retard the growth of cancer cells; however, irradiation enhances this process. The true mechanism of this phenomenon is not well understood and will be clarified in subsequent experiments.

Experimental results showing the effects of irradiation on the cancer cells using NIR light at 780 nm in the presence of AuNRs stabilized with polymers and control samples are illustrated in **Figure 6** (numerical values are presented in Table S2 in the Supporting Information). The results are presented after 40 days of examination. The number of damaged cancer cells following irradiation increased markedly after 30–40 days of inspection; particularly, there was a statistically significant difference between the numbers recorded for polymer-stabilized AuNRs and control samples without gold nanorods ($p < 0.0001$). At the same time, no statistically significant difference was observed between the samples of AuNRs stabilized with polymers followed by irradiation and in 40 days of observation, demonstrating a similar PTT effect. Numerous studies have shown that gold nanorods with an appropriate dimension (28 × 8 nm) are the most effective for PTT compared to other types of gold nanoparticles, such as nanospheres and nanoshells.[9,70] Despite the AuNRs having

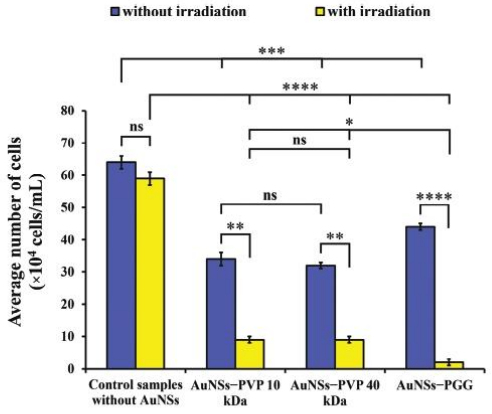

Figure 5. Number of cancer cells in control samples and in the presence of polymer-stabilized AuNSs when exposed to the visible light source at 530 nm and without irradiation. The results are presented after 40 days of examination. Data are expressed as mean ± standard error of the mean (SEM) of triplicate with $n = 10$ measurements in each. Statistically significant differences are given as **** = $p < 0.0001$; *** = $p < 0.001$; ** = $p < 0.01$; and * = $p < 0.05$; ns denotes no significance. AuNSs: spherical gold nanoparticles; PGG: pristine gellan gum; PVP 10 and 40 kDa: poly(*N*-vinylpyrrolidone) with M_n = 10 and 40 kDa, respectively.

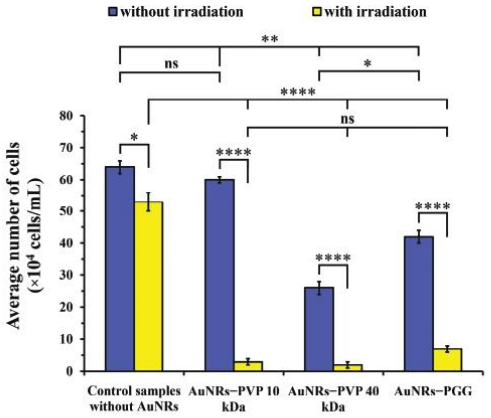

Figure 6. Number of cancer cells in control samples and in the presence of polymer-stabilized AuNRs when exposed to NIR light irradiation at 780 nm and without irradiation. The results are presented after 40 days of examination. Data are expressed as mean ± SEM of triplicate with $n = 10$ measurements in each. Statistically significant differences are shown as **** = $p < 0.0001$; ** = $p < 0.01$; * = $p < 0.05$; ns denotes no significance. AuNRs: gold nanorods; PGG: pristine gellan gum; PVP 10 and 40 kDa: poly(*N*-vinylpyrrolidone) with M_n = 10 and 40 kDa, respectively.

slightly larger dimensions in size, as reported in the present work (Table 2), overall, polymer-coated AuNRs demonstrated good efficacy in PTT treatment in vitro and showed a comparable PTT effect as to spherical AuNPs.

In our experiments, the photothermal conversion efficiency of AuNPs irradiated with 530 and 780 nm laser sources was not evaluated. As seen from Figure 1, for polymer-stabilized AuNSs and AuNRs, the adsorption maximums are in the range of 535 ± 5 nm and close to ≈800 nm. The physiotherapeutic Lasmik laser apparatus used for irradiation had only two laser sources with wavelengths of 530 and 780 nm. In case of AuNSs, the absorption band at $\lambda \approx 535 \pm 5$ nm more or less corresponds to the laser light at 530 nm. But the adsorption peaks of AuNRs at $\lambda \approx 800$ nm considerably deviate from the laser light at 780 nm. Probably this is the reason of lower efficiency of AuNRs in light-to-heat conversion compared to AuNSs. The photothermal conversion efficiency of different shapes of AuNPs under laser irradiation has been reported.[71–74] In particular, the photothermal conversion efficiency of AuNSs and AuNRs was evaluated at different irradiation intensities of NIR broadband (754–816 nm) and NIR laser (808 nm) irradiation.[75] It was shown that the photothermal conversion efficiency of AuNSs and AuNRs is comparable. But the spherical gold nanoparticles might be preferable for hyperthermia applications with a higher accumulation rate within the tumor sites.

2.1.3. In Vivo Study of the Photothermal Effect of AuNPs

As the in vitro experiments demonstrated successful photothermal destruction of cancer cells in the presence of polymer-stabilized AuNSs under irradiation with visible light, subsequent in vivo studies were conducted to evaluate the therapeutic efficacy of this approach further. Tumor development was induced by injecting cancer cells into the left flanks of CD-1 mice subcutaneously (see Figure S4A in the Supporting Information), after which the tumors were allowed to grow for a period of 10 days. This is consistent with the results of the authors[68] because the death of the animal with Ehrlich ascites carcinoma occurs between 10 and 14 days after cell inoculation depending on I) the concentration of inoculated cells, II) the amount of fluid in the peritoneal cavity, which causes abdominal pressure and compression of the organs, and III) the number of passages, in which repeated transplantation increases malignancy and tumor proliferation. Before each exposure, the linear dimensions of the tumors in animals were measured using a caliper (see Figure S4B in the Supporting Information). The volumes of the tumors were then calculated using the following equation

$$V = \frac{4}{3}\pi R^3 \quad (1)$$

where R is the radius of the tumor, and π has a value equal to 3.14.

Laser irradiation of tumor-bearing mice injected with AuNSs stabilized with PVP 40 kDa demonstrated a remarkable PTT effect (**Figure 7**). This result shows that further tumor growth is successfully inhibited by AuNSs–PVP injection in combination with a visible light laser irradiation.

Three days following the last exposure (see Figure S4C in the Supporting Information), the animals were humanely sacrificed, and the tumors were removed and weighed (**Figure 8**; Figure S4D, Supporting Information). The average tumor weight in the control group was 1.00 ± 0.30 g; in group 2 with AuNSs–PVP

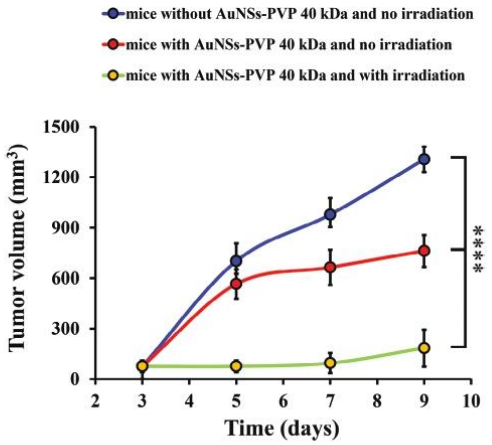

Figure 7. Tumor growth in each treatment group as monitored for 9 days. Data are expressed as mean ± standard deviation (SD) values ($n = 5$). Statistically significant difference is represented as **** = $p < 0.0001$. PVP 40 kDa: poly(*N*-vinylpyrrolidone) with $M_n = 40$ kDa.

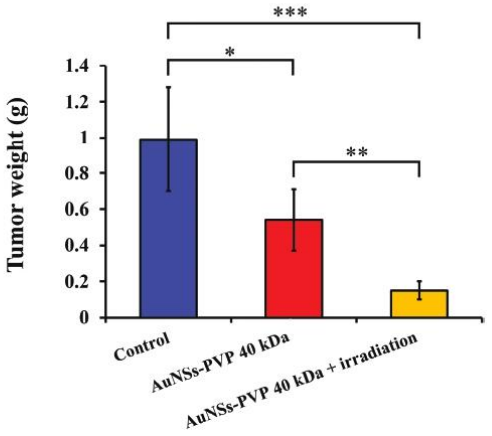

Figure 8. Tumor weight in different groups of animals measured when the animals were sacrificed. Data are produced as mean ± SD ($n = 5$). Statistically significant differences are represented as *** = $p < 0.001$; ** = $p < 0.01$; * = $p < 0.05$. PVP 40 kDa: poly(*N*-vinylpyrrolidone) with M_n = 40 kDa.

40 kDa it was 0.54 ± 0.20 g; and in group 3 with AuNSs–PVP 40 kDa and irradiation it was 0.15 ± 0.04 g. Figure 8 shows the comparison between tumor weight in different groups of animals measured when the animals were sacrificed.

The tumor growth inhibition coefficient (TGIC) was calculated using the following equation

$$\mathrm{TGIC} = \frac{V_k - V_0}{V_k} \times 100\% \quad (2)$$

Table 3. Inhibition of tumor growth with intratumoral injection of AuNSs–PVP (40 kDa) before and after irradiation at $\lambda = 633$ nm (PVP 40 kDa: poly(*N*-vinylpyrrolidone) with $M_n = 40$ kDa).

Samples	Inhibition [%]			
	Tumor volume			Tumor weight
	3 days	5 days	7 days	9 days
AuNSs–PVP 40 kDa without irradiation	19 ± 10	32 ± 12	42 ± 5	43 ± 23
AuNSs–PVP 40 kDa with irradiation	86 ± 8	90 ± 4	90 ± 6	85 ± 3

where V_k is the volume (or weight) of the tumor in the control group of animals, and V_0 is the volume (or weight) of the tumor in each experimental group of animals.

The comparison of the sizes of tumors from different groups of mice was performed and the results are summarized in **Table 3**. The visual inspection of tumor sizes is depicted in Figure S5 (Supporting Information). Samples with AuNSs–PVP 40 kDa and without irradiation exhibited a reduced tumor growth after 3 days by 19 ± 10%, which was an effect that gradually increased after 7 days, reaching 42 ± 5%. Samples with AuNSs–PVP 40 kDa and with irradiation showed a greater effect with up to 90 ± 6% reduction in the tumor size after 7 days. In 9 days, TGIC calculated using the tumor weight in samples with AuNSs–PVP 40 kDa and without irradiation was 43 ± 23%, and in samples with AuNSs–PVP 40 kDa plus irradiation reached 85 ± 3%. Based on these results, it can be concluded that the spherical AuNSs stabilized using PVP 40 kDa could be considered as suitable candidates to inhibit Ehrlich tumor growth and could potentially be used in PTT treatment.

3. Conclusion

Spherical and rod-like gold nanoparticles protected with poly(*N*-vinylpyrrolidone), pristine gellan gum, and poly(2-ethyl-2-oxazoline)-grafted gellan gum were prepared and characterized in this study. The gold nanoparticles exhibited the presence of characteristic SPR bands. The nanoparticles were analyzed for their applicability as PTT agents with respect to Ehrlich cancer cells when exposed to the visible light source. Following the dialysis, the average hydrodynamic size of AuNPs reduced by ≈2–3 times and the zeta potential decreased by ≈1.5–2 times, indicating that the AuNPs are suitable for PTT. Experiments with ex vivo porcine stomach tissues containing AuNSs were performed to determine the photothermal effect of nanoparticles when exposed to the visible light source. In the course of laser irradiation of the tissue at 530 nm, the highest temperature recorded was 43 ± 0.5 °C for AuNSs stabilized using PVP 40 kDa. In vitro experiments demonstrated a similar PTT effect for Ehrlich cancer cells containing polymer-protected AuNPs upon irradiation both at 530 and 780 nm. After 40 days of examination, the number of Ehrlich cancer cells decreased by 10–40 times in comparison with the control samples. In vivo experiments in mice revealed that injection of AuNSs–PVP 40 kDa followed by irradiation with visible light considerably decreased the size of tumors, indicating that polymer-stabilized gold nanoparticles could potentially

be used in the PTT treatment of Ehrlich tumors. The AuNPs developed and stabilized with polymers in this work might potentially be considered as a platform for the PTT treatment of not only Ehrlich tumors, but also other type of carcinoma. In near perspectives our study may be related to light-to-heat conversion efficiency evaluation of AuNSs and AuNRs, toxicological experiments, study the bioadhesive properties polymer-protected AuNPs to improve the adhesion to cancer cell, modification of the surface of AuNPs with poly(ethylene glycol) to enhance the cellular uptake, conjugation of AuNPs with the anticancer drug doxorubicin, etc. In future perspectives the "green" synthesis using the natural substances (for instance, bacterium, fungi, and plants) may contribute to reducing and stabilizing agents for the synthesis of AuNPs and enhance their medical properties such as antimicrobial and anticancer activity.

4. Experimental Section

Materials: A standard aqueous solution of tetrachloroauric acid ($HAuCl_4$) with a concentration of 100 mg mL^{-1}, CTAB (99%), sodium borohydride ($NaBH_4$, 98.5%), ascorbic acid, PVP with $M_n = 10$ and 40 kDa, and HBSS buffer were purchased from Sigma–Aldrich (Germany). Gellan gum with M_w = 500 kDa was purchased from Zhejiang DSM Zhongken Biotechnology Co., Ltd. (China). Poly(2-ethyl-2-oxazoline)-grafted gellan gum was kindly provided by the authors.[70] Depending on the grafting density, the GG-g-PEtOx samples were abbreviated as G2, G3, and G12. Grafting density was given as the number of repeating units, where each gellan gum consists of four sugar units, per one PEtOx grafted chain. Thus, on average, every 12th repeating unit (equivalent to 12 × 4 sugar units) in G12 copolymer contains one PEtOx grafted chain. Potassium hydroxide, silver nitrate, and all other chemicals were of analytical grade and used as received.

Synthesis of AuNSs and AuNRs: Spherical AuNPs (or AuNSs) stabilized by PVP, PGG, and GG-g-PEtOx were prepared using a "one-pot" synthetic method as described previously.[56] Briefly, a mixture consisting of polymer solutions with different concentrations (either 4% PVP; 0.5% PGG; or 2% of each G12, G3, and G2), 5 mL of $HAuCl_4$ (100 mg mL^{-1}), and 4 mL of 0.5 M KOH was combined, agitated, and heated up to 100 °C for 3–5 min in an Anton Paar Monowave 50 microwave reactor (Graz, Austria) equipped with a temperature and time controller. Consequently, tinted solutions, varying in color from yellow to dark red or purple, were produced due to the formation of AuNSs. The initial solution with pH 12 decreased down to pH 8 following the dialysis (cellulose membrane with a molecular weight cut-off 12–14 kDa) against deionized water.

In order to prepare AuNRs, the seed-mediated growth technique was employed.[56] Initially, a solution comprising 5 mL of 0.2 M CTAB was combined with 5 mL of 0.5 mM $HAuCl_4$ and stirred. Subsequently, 0.6 mL of cold 0.01 M $NaBH_4$ was introduced, resulting in the formation of a brownish-yellow solution containing AuNSs. Concurrently, a mixture composed of CTAB (0.2 M; 30 mL), $AgNO_3$ (4 mM; 1.5 mL), and $HAuCl_4$ (1 mM; 30 mL) was gently mixed, and 78.8 M (0.42 mL) ascorbic acid was added. Ascorbic acid was acting as a mild reducing agent, causing the color of the growth solution to change from dark yellow to colorless. Finally, the first seed solution (72 µL) was added to the second growth solution, and the mixture was allowed to incubate at 30 °C overnight. Consequently, a crimson solution containing AuNRs was generated. To eliminate byproducts and CTAB from the AuNRs, the solution underwent centrifugation at 10 650 rpm for 30 min using an Eppendorf 5810R centrifuge (Tuttlingen, Germany). The resulting precipitate was re-dispersed by adding 3 mL of deionized water and centrifuged again at 10 650 rpm for 15 min. After undergoing washing procedure thrice, the AuNRs were re-dispersed and stabilized in 5 mL of designated polymer solutions and then dialyzed using a cellulose membrane (molecular weight cut-off 12–14 kDa) against deionized water.

Characterization: Absorption spectra of AuNSs and AuNRs were recorded using a Specord 210 plus BU UV/Vis-spectrophotometer (Jena, Germany). The mean hydrodynamic size of gold nanoparticles in solution, their polydispersity index (PDI) and zeta potential values were determined using DLS and electrophoretic measurements with a Malvern Zetasizer Nano ZS90 (Malvern Instruments, UK) at 25 °C. Gold nanoparticles were imaged using a JEOL JEM-1400Plus (JOEL Ltd., Japan) transmission electron microscope operated at an acceleration voltage of 120 kV. TEM grids were prepared by placing 10 µL of the diluted sample solutions on a carbon-coated copper grid and evaporating the solution at room temperature completely. The concentrations of AuNS and AuNR solutions stabilized with the polymers were quantified using an Agilent 7500 ICP-MS inductively coupled plasma mass spectrometer (Agilent Technologies, USA).

Study of Ex Vivo Photothermal Effect of AuNSs Induced by Visible Light Irradiation: The porcine stomach tissue was used as an ex vivo tissue model to study ex vivo photothermal effect of AuNSs when exposed to irradiation. Porcine stomach tissues were received from Altyn-Orda Abattoirs (Almaty, Kazakhstan) immediately after animal slaughter, carefully packed, transported to the laboratory in cold plastic containers, and used within 24 h of retrieval. Tissue samples (cut into ≈3 × 3 cm) were placed in Petri dishes, and with the help of a marker pen, an area to be exposed to irradiation was highlighted. Using a sterile syringe, 0.5 mL of polymer-coated AuNSs' dispersion was injected interstitially in the porcine stomach tissue. The concentration of AuNSs in the colloidal solution was determined to be ≈45 µg mL^{-1}. Irradiation of AuNSs was carried out using a physiotherapeutic Lasmik laser apparatus (Lazmik Ltd., Russia) (Figure S1A, Supporting Information). Matrix light-emitting diode (LED) heads operated at 530 and 780 nm wavelengths were used. Experiments with irradiation were performed within an incubator at 37 °C with a relative humidity of 80% (Figure S1B, Supporting Information). The temperature was measured every 5 min using a VT04 visual infrared thermometer (Fluke VT02 Visual IR Thermometer, Everett, WA, USA). The irradiation was carried out for 60 min. All experiments were performed in triplicate and the mean ± SD values were calculated.

Irradiation of Ehrlich Cancer cells: Ehrlich cells were received from the cell culture collection of the Kazakh Research Institute of Oncology and Radiology (Almaty, Kazakhstan). The ascites' form of a transplanted Ehrlich tumor strain was used to study the photothermal effect of AuNPs on cancer cells. The tumor cells were transplanted intraperitoneally into CD-1 mice. The material was extracted on the 10th day after transplantation. The concentration of cells was determined to be 100 million mL^{-1}. In this experiment, a suspension of biomaterial was prepared from 1 mL suspension of Ehrlich tumor cells, and 9 mL of HBSS buffer solution (Hanks culture medium). Next, 1 mL of the suspension was aspirated and then mixed with 1 mL of either AuNPs (≈45 µg mL^{-1}) or AuNRs (≈179 µg mL^{-1}) solutions. The resulting mixture was subsequently irradiated for 60 min using matrix LED heads operated at λ = 530 and 780 nm. The cover glass was placed on the grid of a Goryaev chamber. Then, 5–10 µL of cell suspension was transferred to the edge of the cover glass in the chamber. Afterward, micro-photographs of the cells were taken at 40× magnification using a Nikon Eclipse LV150N microscope (Tokyo, Japan), equipped with a Motic digital camera, and the cells were counted in Goryaev chamber manually before and after irradiation. The average number of cells in one square of grids and in 1 mL of suspension was calculated, considering the area of the square. The cells were maintained in an incubator at 37 °C and in the dark throughout the experimental period. In order to evaluate the long-term photothermal effect of polymer-coated AuNSs on Ehrlich cancer cells, the cells' death was observed over a 40 day period. All measurements were conducted in triplicate and the mean ± SEM (n = 10) values were calculated and then evaluated statistically.

Study of In Vivo Photothermal Effect of AuNSs Induced by Visible Light Irradiation: All animal experiments were conducted in compliance with the protocol approved by the local ethical committee (LEC) at the Kazakh Research Institute of Oncology and Radiology (Protocol No.5-2021, 10 December 2021).

For the in vivo experiments, 18 CD-1 male mice of 23–25 g weight and 60 days of age were selected. Tumor cell transplantation into the animals

was accomplished through subcutaneous injection of 5×10^6 tumor cells. The experiments commenced 10 days later when the tumors reached a size of about 4–5 mm in diameter. However, throughout the experiment, some mice developed purulence and so the other three mice were excluded from the experiment due to this condition. The mice were divided into three groups: group 1 consisted of five control animals, with no AuNSs solution injected and no exposure to irradiation; group 2 included five animals with AuNSs' solution injected, but no irradiation treatment; and group 3 involved five animals with AuNSs solution injected and with irradiation treatment.

Prior to commencing each experiment, hair from the surface of the skin covering the tumor was removed, then intratumoral injection of 50 µL of AuNSs–PVP (40 kDa) was administered. The concentration of AuNSs in the suspension was ≈45 µg mL^{-1}. After 25 min, the tumor node was subjected to a daily laser exposure for 30 min over a period of 7 days. Taking into account 10 days of inoculation and 7 days of laser exposure the total experimental time duration was 17 days. According to the protocols reported in ref. [76], the experiment associated with an increase in the tumor weight was conducted for 20 days until the animals were sacrificed. A Polyaron LG-75 helium–neon laser at a wavelength of 633 nm and an emissive power of 25 mW (Kyiv, Ukraine) was used in the experiments. Throughout the experiment, the tumor size was measured daily using a caliper. Following the internationally recognized guidelines established by the Council for International Organizations of Medical Sciences (CIOMS) for biomedical research involving animals, the mice were euthanized prior to surgical removal of tumor tissues. The tumors were extracted from the peritoneum by dissection with a subsequent weighing on the ninth day.

Statistical Analysis: The data were presented as mean values ± SD and/or SEM and assessed for significance using a one-way and two-way analysis of variance (ANOVA) followed by Bonferroni posthoc test, where $p < 0.05$ was considered as the statistical significance difference (GraphPad Prism software, version 7.0; San Diego, CA, USA).

Supporting Information

Supporting Information is available from the Wiley Online Library or from the author.

Acknowledgements

This research was funded by the Science Committee of the Ministry of Education and Science of the Republic of Kazakhstan (Grant No. AP13067773) and was supported by the Horizon 2020 research and innovation program of the European Union Maria Sklodowska-Curie (Grant agreement 823883-NanoPol-MSCA-RISE-2018).

Conflict of Interest

The authors declare no conflict of interest.

Data Availability Statement

Research data are not shared.

Keywords

Ehrlich cancer cells, gold nanoparticles, gold nanorods, gold nanospheres, photothermal therapy (PTT), surface plasmon resonance (SPR)

Received: April 23, 2024
Published online:

[1] J. Peng, X. Liang, L. Calderon, *Medicine* **2019**, *98*, e15311.
[2] Z. Yang, Z. Sun, Y. Ren, X. Chen, W. Zhang, X. Zhu, Z. Mao, J. Shen, S. Nie, *Mol. Med. Rep.* **2019**, *20*, 5.
[3] *World Cancer Report: Cancer Research for Cancer Prevention* (Eds: C. P. Wild, E. Weiderpass, B. W. Stewart), International Agency for Research on Cancer, Lyon, France **2020**, ISBN 978-92-832-0447-3.
[4] H. S. Han, K. Y. Choi, *Biomedicines* **2021**, *9*, 305.
[5] J. B. Vines, J.-H. Yoon, N.-E. Ryu, D.-J. Lim, H. Park, *Front. Chem.* **2019**, *7*, 167.
[6] P. E. Costantini, M. Di Giosia, L. Ulfo, A. Petrosino, R. Saporetti, C. Fimognari, P. P. Pompa, A. Danielli, E. Turrini, L. Boselli, M. Calvaresi, *Nanomaterials* **2021**, *11*, 1608.
[7] N. Zhao, Y. Pan, Z. Cheng, H. Liu, *J. Innov. Opt. Health Sci.* **2016**, *9*, 1630004.
[8] J. Lee, Y. H. Lee, C. B. Jeong, J. S. Choi, K. S. Chang, M. Yoon, *J. Nanobiotechnol.* **2018**, *16*, 104.
[9] M. A. Mackey, M. R. K. Ali, L. A. Austin, R. D. Near, M. A. El-Sayed, *J. Phys. Chem. B* **2014**, *118*, 1319.
[10] I. Fratoddi, I. Venditti, C. Cametti, M. Russo, *J. Mater. Chem. B* **2014**, *2*, 4204.
[11] D. Jaque, M. Maestro, L. del Rosal, B. Haro-Gonzalez, P. Benayas, A. Plaza, J. L. M. Rodríguez, E. García Solé, *Nanoscale* **2014**, *6*, 9494.
[12] R. Mendes, P. Pedrosa, J. C. Lima, A. R. Fernandes, P. Baptista, *Sci. Rep.* **2017**, *7*, 10872.
[13] S. Wang, G. Lu, in *Noble and Precious Metals—Properties, Nanoscale Effects and Applications* (Eds. M. S. Seehra, A. D. Bristow) IntechOpen, London **2017**, pp. 291–309.
[14] H. S. Kim, D. Y. Lee, *Polymers* **2018**, *10*, 961.
[15] Y.-C. Yeh, B. Creran, V. M. Rotello, *Nanoscale* **2012**, *4*, 1871.
[16] M. R. K. Ali, I. M. Ibrahim, H. R. Ali, S. A. Selim, M. A. El-Sayed, *Int. J. Nanomed.* **2016**, *11*, 4849.
[17] R. S. Riley, E. S. Day, *WIREs Nanomed. Nanobiotechnol.* **2017**, *9*, e1449.
[18] W. Cai, T. Gao, H. Hong, J. Sun, *Nanotechnol. Sci. Appl.* **2008**, *1*, 17.
[19] C. Ayala-Orozco, C. Urban, M. W. Knight, A. S. Urban, O. Neumann, S. W. Bishnoi, S. Mukherjee, A. M. Goodman, H. Charron, T. Mitchell, M. Shea, R. Roy, S. Nanda, R. Schiff, N. J. Halas, A. Joshi, *ACS Nano* **2014**, *8*, 6372.
[20] C. Yao, L. Zhang, J. Wang, Y. He, J. Xin, S. Wang, H. Xu, Z. Zhang, *J. Nanomater.* **2016**, *2016*, 5497136.
[21] D. Peer, J. M. Karp, S. Hong, O. C. Farokhzad, R. Margalit, R. Langer, *Nat. Nanotechnol.* **2007**, *2*, 751.
[22] F. Jabeen, M. Najam-ul-Haq, R. Javeed, C. W. Huck, G. K. Bonn, *Molecules* **2014**, *19*, 20580.
[23] J. Wang, R. Bai, R. Yang, J. Liu, J. Tang, Y. Liu, J. Li, Z. Chai, C. Chen, *Metallomics* **2015**, *7*, 516.
[24] P. Singh, S. Pandit, V. R. S. S. Mokkapati, A. Garg, V. Ravikumar, I. Mijakovic, *Int. J. Mol. Sci.* **2018**, *19*, 1979.
[25] X. Huang, M. A. El-Sayed, *J. Adv. Res.* **2010**, *1*, 13.
[26] S. Jain, D. G. Hirst, J. M. O'Sullivan, *Br. J. Radiol.* **2012**, *85*, 101.
[27] R. M. Cabral, P. Baptista, *Nano Life* **2013**, *3*, 1330001.
[28] V. Guerrero-Florez, S. C. Mendez-Sanchez, O. A. Patrón-Soberano, V. Rodríguez-González, D. Blach, O. Martínez, *J. Mater. Chem. B* **2020**, *8*, 2862.
[29] J. Conde, M. Larguinho, A. Cordeiro, L. R. Raposo, P. M. Costa, S. Santos, M. S. Diniz, A. R. Fernandes, P. V. Baptista, *Nanotoxicology* **2014**, *8*, 521.
[30] J. Conde, J. Rosa, P. Baptista, *Protoc. Exch.* **2013**, https://doi.org/10.1038/PROTEX.2013.088.
[31] Z. Qin, Y. Wang, J. Randrianalisoa, V. Raeesi, W. C. W. Chan, W. Lipiński, J. C. Bischof, *Sci. Rep.* **2016**, *6*, 29836.
[32] R. M. Cabral, P. V. Baptista, *Expert Rev. Mol. Diagn.* **2014**, *14*, 1041.
[33] F. Dumur, A. Guerlin, E. Dumas, D. Bertin, D. Gigmes, C. R. Mayer, *Gold Bull.* **2011**, *44*, 119.

[34] C. S. Yah, *Biomed. Res.* **2013**, *24*, 400.
[35] Y. Zhang, X. Zhan, J. Xiong, S. Peng, W. Huang, R. Joshi, Y. Cai, Y. Liu, R. Li, K. Yuan, N. Zhou, W. Min, *Sci. Rep.* **2018**, *8*, 8720.
[36] Y. Liu, K. Ai, J. Liu, M. Deng, Y. He, L. Lu, *Adv. Mater.* **2013**, *25*, 1353.
[37] W. Li, P. Rong, K. Yang, P. Huang, K. Sun, X. Chen, *Biomaterials* **2015**, *45*, 18.
[38] R. Amatya, S. Hwang, T. Park, K. A. Min, M. C. Shin, *Pharmaceutics* **2021**, *13*, 871.
[39] A. B. Bucharskaya, G. N. Maslyakova, G. A. Afanasyeva, G. S. Terentyuk, N. A. Navolokin, O. V. Zlobina, D. S. Chumakov, A. N. Bashkatov, E. A. Genina, N. G. Khlebtsov, B. N. Khlebtsov, V. V. Tuchin, *J. Innov. Opt. Health Sci.* **2015**, *8*, 1541004.
[40] S. Dhar, E. Maheswara Reddy, A. Shiras, V. Pokharkar, B. L. V. Prasad, *Chem. - Eur. J.* **2008**, *14*, 10244.
[41] S. Dhar, V. Mali, S. Bodhankar, A. Shiras, B. L. V. Prasad, V. Pokharkar, *J. Appl. Toxicol.* **2011**, *31*, 411.
[42] S. Dhar, E. M. Reddy, A. Prabhune, V. Pokharkar, A. Shiras, B. L. V. Prasad, *Nanoscale* **2011**, *3*, 575.
[43] G. D'Arrigo, C. Di Meo, E. Gaucci, S. Chichiarelli, T. Coviello, D. Capitani, F. Alhaique, P. Matricardi, *Soft Matter* **2012**, *8*, 11557.
[44] G. D'Arrigo, G. Navarro, C. Di Meo, P. Matricardi, V. Torchilin, *Eur. J. Pharm. Biopharm.* **2014**, *87*, 208.
[45] C. A. Reis, C. F. Rodrigues, A. F. Moreira, T. A. Jacinto, P. Ferreira, I. J. Correia, *Mater. Sci. Eng., C* **2019**, *98*, 960.
[46] S. E. Kudaibergenov, S. Xu, G. S. Tatykhanova, G. M. Kudaibergenova, *Acad. J. Polym. Sci.* **2019**, *2*, 555588.
[47] K. Soleimani, H. Derakhshankhah, M. Jaymand, H. Samadian, *Carbohydr. Polym.* **2021**, *254*, 117422.
[48] E. Nurgaziyeva, S. Kudaibergenov, G. Mun, V. Khutoryanskiy, *Chem. Bull. Kazakh Natl. Univ.* **2021**, *100*, 12.
[49] N. D. Agsish, S. Fedoroff, *Can. J. Genet. Cytol.* **1968**, *10*, 723.
[50] N. K. Badr El-Din, S. M. Shabana, B. A. Abdulmajeed, M. Ghoneum, *BMC Complementary Med. Ther.* **2020**, *20*, 127.
[51] E. Niemelä, D. Desai, Y. Nkizinkiko, J. E. Eriksson, J. M. Rosenholm, *Eur. J. Pharm. Biopharm.* **2015**, *96*, 11.
[52] L. E. Agibayeva, D. B. Kaldybekov, N. N. Porfiryeva, V. R. Garipova, R. A. Mangazbayeva, R. I. Moustafine, I. I. Semina, G. A. Mun, S. E. Kudaibergenov, V. V. Khutoryanskiy, *Int. J. Pharm.* **2020**, *577*, 119093.
[53] T. M. M. Ways, S. K. Filippov, S. Maji, M. Glassner, M. Cegłowski, R. Hoogenboom, S. King, W. M. Lau, V. V. Khutoryanskiy, *J. Colloid Interface Sci.* **2022**, *626*, 251.
[54] J. Shan, H. Tenhu, *Chem. Commun.* **2007**, *44*, 4580.
[55] X. Li, J. Guo, J. Asong, M. A. Wolfert, G. J. Boons, *J. Am. Chem. Soc.* **2011**, *133*, 11147.
[56] Z. A. Nurakhmetova, A. N. Azhkeyeva, I. A. Klassen, G. S. Tatykhanova, *Polymers* **2020**, *12*, 2625.
[57] J. M. Bingham, K. A. Willets, N. C. Shah, D. Q. Andrews, R. P. Van Duyne, *J. Phys. Chem. C* **2009**, *113*, 16839.
[58] H. Chen, X. Kou, Z. Yang, W. Ni, J. Wang, *Langmuir* **2008**, *24*, 5233.
[59] R. Shenhar, T. B. Norsten, V. M. Rotello, *Adv. Mater.* **2005**, *17*, 657.
[60] M. Sengani, A. M. Grumezescu, V. D. Rajeswari, *OpenNano* **2017**, *2*, 37.
[61] D. K. Roper, W. Ahn, M. Hoepfner, *J. Phys. Chem. C.* **2007**, *111*, 3636.
[62] H. H. Richardson, M. T. Carlson, P. J. Tandler, P. Hernandez, A. O. Govorov, *Nano Lett.* **2009**, *9*, 1139.
[63] J. Van der Zee, Z. Vujaskovic, M. Kondo, T. Sugahara, *Int. J. Hyperthermia* **2008**, *24*, 111.
[64] K. Jiang, D. A. Smith, A. Pinchuk, *J. Phys. Chem. C* **2013**, *117*, 27073.
[65] H. M. Patt, R. L. Straube, N. Y. Ann, *Acad. Sci.* **1956**, *63*, 728.
[66] N. I. Ryzhova, V. P. Deryagina, L. A. Savluchinskaya, *Int. J. Appl. Fundam. Res.* **2019**, *4*, 220.
[67] M. A. Abd Eldaim, E. Tousson, E. T. I. El Sayed, A. Abd Elmaksoud, A. A. S. Ahmed, *Environ. Sci. Pollut. Res.* **2021**, *28*, 21835.
[68] D. R. Radulski, M. C. Stipp, C. M. Galindo, A. Acco, *Transl. Breast Cancer Res.* **2023**, *4*, 22.
[69] W. Q. Lim, Z. Gao, *Nano Today* **2016**, *11*, 168.
[70] J. Lavikainen, M. Dauletbekova, G. Toleutay, M. Kaliva, M. Chatzinikolaidou, S. E. Kudaibergenov, A. Tenkovtsev, V. V. Khutoryanskiy, M. Vamvakaki, V. Aseyev, *Polym. Adv. Technol.* **2021**, *32*, 2770.
[71] A. T. Diallo, M. Tlemçani, M. Khan, J. Spadavecchia, *Part. Part. Syst. Charact.* **2020**, *37*, 2000255.
[72] K. Ma, Y. Li, Z. Wang, Y. Chen, X. Zhang, C. Chen, H. Yu, J. Huang, Z. Yang, X. Wang, Z. Wang, *ACS Appl. Mater. Interfaces* **2019**, *11*, 29630.
[73] J. Zhou, Y. Jiang, S. Hou, P. K. Upputuri, D. Wu, J. Li, P. Wang, X. Zhen, M. Pramanik, K. Pu, H. Duan, *ACS Nano* **2018**, *12*, 2643.
[74] M. Alrahili, R. Peroor, V. Savchuk, K. McNear, A. Pinchuk, *J. Phys. Chem. C* **2020**, *124*, 4755.
[75] R. Vikas Kumar, S. Sanjeev, *Beilstein J. Nanotechnol.* **2023**, *14*, 205.
[76] H. Aljohani, A. E. Khodier, M. M. Al-Gayyar, *Cureus* **2023**, *15*, e39789.

RESEARCH ARTICLE

Macromolecular Symposia

www.ms-journal.de

Comparative Study of Gellan Gum Derived from Domestic Raw Materials of Kazakhstan and Commercial Gellan

Gulnur S. Tatykhanova, Nargiz N. Gizatullina, Gulnar M. Kudaibergenova, Ramza Zh. Berzhanova, Togzhan D. Mukasheva, and Sarkyt E. Kudaibergenov*

Gellan gum prepared from the domestic raw materials of Kazakhstan is studied by methods of ^{1}H NMR spectroscopy, FTIR, GPC, TGA, and compared with characteristics of commercial gellan gum. Fermentation on glucose-fructose syrup of Zharkent and Burunday corn starch plants (Kazakhstan) by *Sphingomonas paucimobilis* ATCC 31461 produces a biomass containing a high acyl gellan gum (HAG). The average molecular weights, M_w, M_n, M_z, and polydispersity index (PDI) of HAG are determined by GPC. Low acyl gellan (LAG) is obtained by treatment of HAG with alkaline solution. It is shown that the spectral and thermal characteristics of HAG and LAG produced from the glucose-fructose syrup and commercial gellan gum are similar.

1. Introduction

Gellan gum is extracellular polysaccharide industrially produced by bacterium *Sphingomonas paucimobilis*.[1,2] It is widely applied as gelling, thickening, and stabilizing agent in food industry, biotechnology, medicine, pharmacy, and oil recovery.[3–6] Gellan is composed of glucose (60%), glucuronic acid (20%), and rhamnose (20%) linked in a linear tetrasaccharide repeating unit.[1,2] There are two types of gellan gum differentiated on the basis of degree of deacetylation: high acyl (HAG) and low acyl (LAG) gellan gum (Figure S1, Supporting Information).[7] The conformational (coil-helix) and phase (sol–gel) behavior of gellan depends on polymer concentration, pH, temperature, and the presence of monovalent or divalent cations.[8] In this regard gellan belongs to stimuli-responsive polymer. A new strategy of gellan production was developed[9] searching the low-cost sources and media,[10] as well as optimizing the fermentative reaction condition.[7,11] The use of low-cost substrates such as glucose-fructose syrup of Zharkent and Burunday corn starch plants (Almaty region, Kazakhstan) can help to boost their market competitiveness. In this communication, the process of gellan production from domestic raw materials of Kazakhstan using *S. paucimobilis* ATCC 31461 is described.

G. S. Tatykhanova
Satbayev University
Satpayev str. 22, Almaty 050013, Kazakhstan
E-mail: gulnur-ts81@yandex.kz

G. S. Tatykhanova, N. N. Gizatullina, G. M. Kudaibergenova, S. E. Kudaibergenov
Institute of Polymer Materials and Technology
"Atyrau 1", Almaty 050019, Kazakhstan

R. Z. Berzhanova, T. D. Mukasheva
al-Farabi Kazakh National University
al-Farabi Ave. 71, Almaty 050040, Kazakhstan

The ORCID identification number(s) for the author(s) of this article can be found under https://doi.org/10.1002/masy.202400004

DOI: 10.1002/masy.202400004

2. Results and Discussion

Fermentation on glucose-fructose syrup by *S. paucimobilis* in the media of "БС" and "CP1" produces the biomasses containing HAG (**Figure 1**).

After thermal treatment of biomass at 90–95 °C during 10–15 min according to Kang et al.[12] the samples showed the following dynamic viscosities: 22 000 mPa s (No. 1), 18 800 mPa s (No. 2), 3600 mPa s (No. 5), and 3900 mPa s (No. 6). Further the samples No. 3, 4, 6, 7 were deacetylated by addition of 1.0 M NaOH at 80 °C for 10 min and the pH was adjusted to 7.0 using 1.0 M HCl. Cell mass from the broth was separated by centrifugation at 8000 rpm for 30 min at 4 °C. The ice-cold three volumes of isopropyl alcohol were then added into supernatant to precipitate the deacetylated gellan. The precipitated LAG was dried to constant mass in hot air oven at 80 °C for 12 h. FTIR spectra of commercial HAG purchased from "Xinjiang Fufeng Biotechnologies Co., Ltd.," China, and Kazakhstan HAG separated from the fermentation broth are compared in **Figure 2**. In all cases the appearance of intensive bands at 1724–1727 cm^{-1} is specific for acyl groups of HAG.

In deacylated gellan gum, or LAG, the intensive peaks at 1724–1726 cm^{-1} disappear that confirms the elimination of acyl groups from HAG (**Figure 3**). The commercial and Kazakhstan LAG contains the bands at 3340, 1406, 2921, 1622, and 1037 cm^{-1} that belong to stretching and bending OH, stretching CH, C = O, and C—O—C bonds, respectively. ^{1}H NMR spectra of LAG coincide well with literature data[13] and show the characteristic peaks of CH of rhamnose (5.27 ppm), CH of glucuronic acid (5.09 ppm), and CH_3 of rhamnose (1.86 ppm) (**Figures 4 and 5**). ^{13}C NMR spectra of commercial LAG and Kazakhstan LAG are shown in Figure S2, Supporting Information.

The weight average (M_w), number average (M_n), M_z molecular weights, and polydispersity index (PDI) of Kazakhstan HAG are presented in **Table 1**. The value of PDI close to 1 indicates on narrow distribution of molecular mass of HAG.

Thermogravimetric curves of commercial HAG and Kazakhstan HAG were compared (Figure S3, Supporting

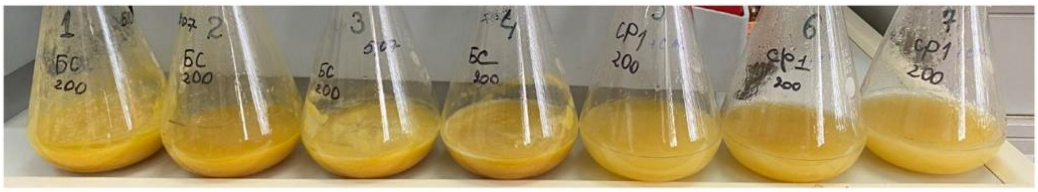

Figure 1. Biomasses obtained upon fermentation of glucose-fructose syrup by *S. paucimobilis* in the media of "БС" (No. 1–4) and "CP1" (No. 5–7).

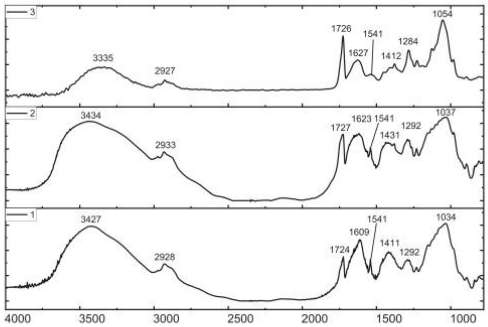

Figure 2. FTIR spectra of self-purified (1), technical (2) HAG produced by Xinjiang Fufeng Biotechnologies Co., Ltd. and Kazakhstan HAG (3) obtained by fermentation of glucose-fructose syrup.

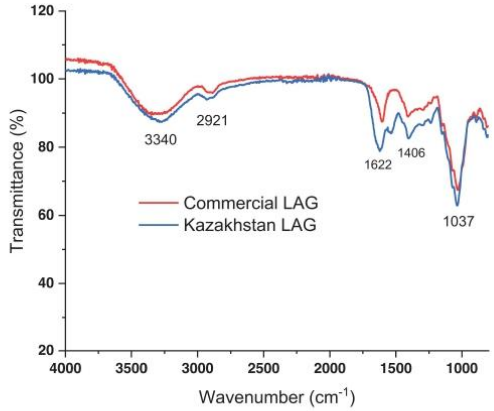

Figure 3. FTIR spectra of commercial LAG purchased from Xinjiang Fufeng Biotechnologies Co., Ltd. and Kazakhstan LAG obtained by deacylation of Kazakhstan HAG.

Table 1. Average molecular weight and PDI of Kazakhstan HAG.

Polymer	Molecular weights [Da]			PDI (M_w/ M_n)
HAG	M_w	M_n	M_z	
	343 500	333 000	360 000	1.03

Information). The decomposition temperature of both samples lies in the region of 250 °C and completely coincides. Aqueous solutions 0.25% and 0.5% Kazakhstan LAG showed an excellent gelation property upon addition of salts (NaCl and $CaCl_2$) in the range of concentration 0.01–1.0 M (Figure S4, Supporting Information).

3. Conclusion

By fermentation on glucose-fructose syrup of Zharkent and Burunday corn starch plants by *S. paucimobilis*, the high and low acyl gellan gums were produced. They were characterized by various physico-chemical methods and compared with commercial gellan produced in China. In perspective the developed technology of gellan production from the domestic raw materials of Kazakhstan may be scaled up and used in food industry and oil recovery.

4. Experimental Section

Materials: Glucose-fructose syrups were commercial products of Zharkent and Burunday corn starch plants (Almaty region, Republic of Kazakshtan). *S. paucimobilis* ATCC 31461 was used in this study. Commercial high acyl (HAG) and low acyl gellan (LAG) were purchased from "Xinjiang Fufeng Biotechnologies Co., Ltd.," China. Isopropanol (≥99.5%, Fischer-Chemicals Oy) was used for precipitation of HAG and LAG. Deuterated water (D_2O, 99% D, Euriso-Top) was used in NMR experiments. "БС" medium contained glucose (2%), yeast extract (0.3%), peptone (0.5%), pH = 7.0,[14] and "CP1" medium contained glucose (10%), peptone (0.2%), K_2HPO_4 (0.2%), NaCl (0.2%), $MgSO_4$ (0.04%), $FeSO_4$ (0.001%).

Methods: FTIR spectra were obtained with the help of a Cary 660 ATR-FTIR instrument (Agilent, USA). ^1H and ^{13}C NMR spectra were recorded on a Bruker Avance III 500 spectrometer. Thermogravimetric analysis (TGA) was carried out using a LabSys Evo (Setaram, France) under a nitrogen atmosphere in a temperature range of 25–500 °C, with a heating rate of 10 °C min^{-1}. The dynamic viscosity of the biomass was measured with a Brookfield rotational viscometer (Brookfield AMETEK DV2TLV, USA). Gel permeable chromatography (GPC) was carried out on a Viscotek GPC/SEC (UK).

Fermentation of Glucose-Fructose Syrup: The production of gellan gum by *S. paucimobilis* from ATCC 31461 was performed on a 50 L stirred bioreactor (ФС-50, Russia) with 30 L working volume.

Supporting Information

Supporting Information is available from the Wiley Online Library or from the author.

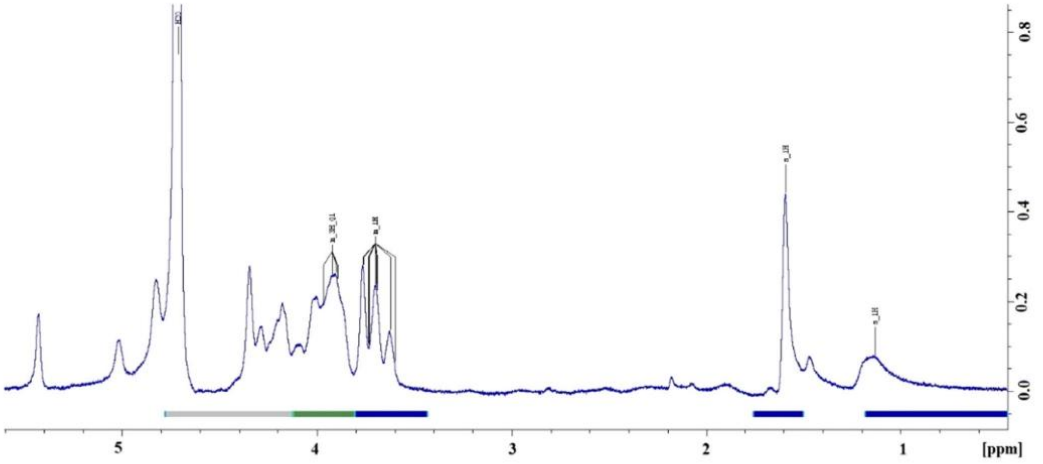

Figure 4. ^{1}H NMR spectrum of commercial LAG in D_2O at 60 °C. C = 10 mg·mL^{-1}.

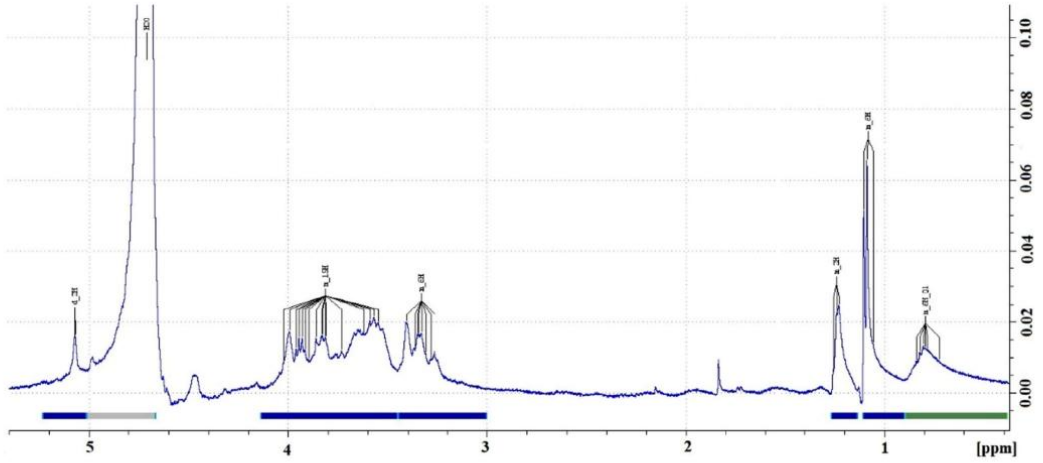

Figure 5. ^{1}H NMR spectrum of Kazakhstan LAG in D_2O at 60 °C. C = 10 mg·mL^{-1}.

Acknowledgements

This work was financially supported by Science Committee of the Ministry of Science and High Education of the Republic of Kazakhstan (Grant No. AP14871512). G.S.T, G.M.K., and S.E.K. thank the Horizon 2020 research and innovation program of the European Union Maria Sklodowska-Curie (grant agreement 823883-NanoPol-MSCA-RISE-2018) for financial support. All authors contributed equally to this work.

Conflict of Interest

The authors declare no conflict of interest.

Data Availability Statement

The data that supports the findings of this study are available in the supplementary material of this article.

Keywords

average molecular weights, fermentation, glucose-fructose syrup, high acyl gellan (HAG), low acyl gellan (LAG), spectral and thermal characteristics, *S. paucimobilis*

Received: January 3, 2024

[1] I. Giavasis, L. M. Harvey, B. McNeil, *Crit. Rev. Biotechnol.* **2000**, *20*, 177.
[2] I. B. Bajaj, S. A. Survase, P. S. Saudagar, R. S. Singhal, *Food Technol. Biotechnol.* **2007**, *45*, 341.
[3] T. Osmalek, A. Froelich, S. Tasarek, *Int. J. Pharm.* **2014**, *466*, 328.
[4] Z. Feketshane, S. Alven, B. A. Aderibigbe, *Polymers* **2022**, *14*, 4098.
[5] I. Gussenov, N. Nuraje, S. Kudaibergenov, *Energy Rep.* **2019**, *5*, 733.
[6] Y. Li, L. Xu, H. Gong, B. Ding, M. Dong, Y. Li, *Energy Fuels* **2017**, *31*, 3960.
[7] I. B. Bajaj, P. S. Saudagar, R. S. Singhal, A. Pandey, *J. Biosci. Bioeng.* **2006**, *102*, 150.
[8] E. R. Morris, N. Nishinari, M. Rinaudo, *Food Hydrocolloids* **2012**, *28*, 373.
[9] G. Zhu, L. Sheng, Q. Tong, *Carbohydr. Polym.* **2013**, *98*, 829.
[10] A. Vanderhoff, W. R. Gibbons, N. Bauer, T. P. West, *J. Biotech. Res.* **2010**, *2*, 67.
[11] I. Giavasis, L. M. Harvey, B. McNeil, *Enzyme Microb. Technol.* **2006**, *38*, 101.
[12] K. S. Kang, G. T. Veeder, P. J. Mirrasoul, T. Kaneko, L. W. Cottrell, *Appl. Environ. Microbiol.* **1982**, *43*, 1086.
[13] Z. h. A. Nurakhmetova, I. S. h. Gussenov, G. S. Tatykhanova, S. E. Kudaibergenov, *Chem. Bull. Kazakh Natl. Univ.* **2015**, *3*, 35.
[14] B. Manna, A. Gambhir, P. Ghosh, *Lett. Appl. Microbiol.* **1996**, *23*, 141.

RESEARCH ARTICLE

Macromolecular Symposia

www.ms-journal.de

Fractionation and Characterization of Commercial Low Acyl Gellan Gum

Gulnur S. Tatykhanova, Sami-Pekka Hirvonen, Yuliia V. Bardadym, Nargiz N. Gizatullina, and Moldir A. Saulimbay*

Commercial low acyl gellan (LAG) is purified by the fractional dissolution method. An aqueous solution of purified commercial LAG exhibits polyelectrolyte character due to its high molar mass and carboxylic groups in glucuronic acid fragments. The empirical Fuoss equation determines the intrinsic viscosity of purified LAG in salt-less water. Fractionation of commercial LAG is carried out by ultrasound treatment. LAG fractions are characterized by ^{1}H NMR and FTIR spectroscopy. The intrinsic viscosities of ultrasonically treated LAG samples are measured in 0.025 M of tetramethylammonium chloride (TMACl). The molecular weights of LAG fractions are determined by the Mark–Kuhn–Houwink equation.

1. Introduction

Gellan gum attracts much attention of researchers due to wide application in biotechnology, medicine, and oil recovery.[1–3] The repeating monomeric units of gellan gum consist of the following residues: 1,3-β-D-glucose, 1,4-β-D-glucuronic acid, 1,4-β-D-glucose, and 1,4-α-L-rhamnose.[4] The drug-loaded gellan can be used in pharmaceuticals as oral, buccal, nasal, ophthalmic, vaginal, and other forms.[2] Earlier,[5] we have developed ophthalmic drug delivery system based on the complex of gellan with an antimicrobial drug – ofloxacin. It was found that the gelation of gellan in response to simulated tear fluid is suitable for ophthalmic formulations in conditions of in vitro as a thickening component resisting ocular drainage and prolonging the drug retention time.[6] However, extremely high molecular weight of pristine gellan[7] in the range of $(5–10)\cdot10^5$ restricts a wide application of gellan as drug delivery system. This communication is devoted to lowering of the molecular weights of commercial gellan gum by using the ultrasound treatment.

G. S. Tatykhanova, N. N. Gizatullina, M. A. Saulimbay
Satbayev University
Almaty 050012, Kazakhstan
E-mail: gulnur-ts81@yandex.kz
G. S. Tatykhanova, N. N. Gizatullina
Institute of Polymer Materials and Technology
Almaty 050019, Kazakhstan
S.-P. Hirvonen, Y. V. Bardadym
Department of Chemistry
University of Helsinki
Helsinki P.O. Box 55, FIN-00014 HY, Finland

The ORCID identification number(s) for the author(s) of this article can be found under https://doi.org/10.1002/masy.202400001

DOI: 10.1002/masy.202400001

2. Results and Discussion

2.1. Characterization of Purified Commercial LAG in Aqueous Solution

The purified low acyl gellan (LAG) due to presence of carboxylic groups in glucuronic acid fragments exhibits polyelectrolyte behavior, e.g., the dependence of η_{sp}/C cannot be extrapolated to zero polyelectrolyte concentration for intrinsic viscosity determination (Supporting Information Figure S1). Usually, this problem can be solved in two ways: 1) by means of empirical equation; 2) by addition of low-molecular weight salts to suppress the polyelectrolyte effect. However, addition of low-molecular-weight salts causes the gelation of LAG and restricts the intrinsic viscosity measurement. As seen from Supporting Information Figure S2, the curve in Supporting Information Figure S1 was linearized applying the Fuoss equation[8]: $\frac{C}{\eta_{sp}} = \frac{1}{[\eta]} + k_{Fs}\frac{1}{[\eta]}c^{1/2}$, where k_{Fs} is Fuoss coefficient. The intrinsic viscosity of LAG determined by Fuoss equation was equal to 5680 $cm^3\ g^{-1}$.

2.2. Characterization of Ultrasonically Treated LAG

The reduced viscosities of ultrasonically treated LAG samples were measured in aqueous solution containing 0.025 M tetramethylammonium chloride (TMACl) (**Figure 1**). Extrapolation of the reduced viscosity η_{sp}/C to $C \to 0$ gives the intrinsic viscosity $[\eta]$. The viscosity average molecular weights (M_η) of LAG fractions calculated according to Mark–Kuhn–Houwink equation[7] $[\eta] = 7.48\cdot10^{-3}\cdot M_w^{0.91}$ are shown in **Table 1**.

It is seen that the ultrasonic treatment of LAG leads to gradually decreasing of both $[\eta]$ and M_η. It is probably connected with cleavage of glycosidic linkages and degradation of LAG.[9] Proton NMR and FTIR spectra of LAG after 10 and 120 min ultrasound treatment are shown in **Figures 2**, **3**. The results show that both ^{1}H NMR and FTIR spectra of samples are the same confirming the absence of structural changes. ^{1}H NMR spectra of LAG contain CH groups of rhamnose (δ 5.27 ppm), CH groups of glucuronic acid (δ 5.09 ppm), and CH_3 groups of rhamnose (δ 1.86 ppm).[6,10]

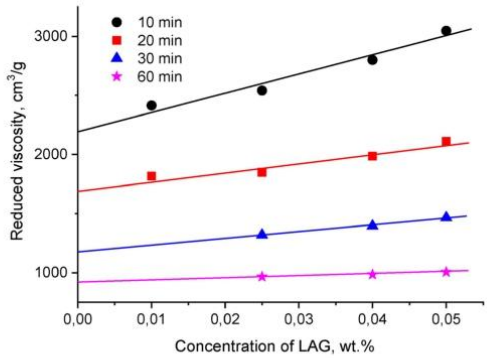

Figure 1. Concentration dependence of the reduced viscosity of low acyl gellan (LAG) after 10, 20, 30, and 60 min treatment by ultrasonic source.

Table 1. The intrinsic viscosity and M_η of low acyl gellan (LAG) fractions.

Ultrasonic treatment [min]	Intrinsic viscosity [$cm^3\ g^{-1}$]	$M_\eta \cdot 10^{-5}$ [Da]
10	2200	10.0
20	1690	7.63
30	1180	5.12
60	920	3.92

In FTIR spectra, the bands at 3568–3513 and 1419–1412 cm^{-1} correspond to stretching and bending vibrations of OH groups. The peaks at 2935–2920 and 2886–2870 cm^{-1} are due to the stretching CH bonds. The sharp peaks at 1612–1610 and 1042–1041 cm^{-1} belong to asymmetric COO^- stretching and COC stretching bonds, respectively.

3. Conclusion

Ultrasound treatment significantly decreases the molecular weight of LAG but does not cause the structural changes. The purified commercial LAG reveals a polyelectrolyte character due to presence of carboxylic groups of glucuronic acid. Application of Fuoss equation allows to determine the intrinsic viscosity of purified commercial LAG in aqueous solution.

4. Experimental Section

Materials: Commercial LAG was purchased from "Zhejiang DSM Zhongken Biotechnology Co., Ltd.," China. Acetone (purity was ≥99.8%), isopropyl alcohol (purity was ≥99.5%), and TMACl (purity was ≥98%) were the products of "Fisher Chemicals Oy" and "Sigma–Aldrich." Deuterated water (D_2O) (purity was 99.96%) was purchased from "Eurisotop." Dialysis membranes (molecular weight cut off 3.5 kDa and 12–14 kDa) were purchased from Spectrum laboratories.

Methods: The ultrasonic processor UP400S (400 Watts, 24 kHz) "Hielscher Ultrasound Technology" was used for sonication of samples. Separation of insoluble gellan fractions was performed by Sigma laboratory centrifuge 2K15C "B.Braun Biotech International".[6] The samples were freeze dried by FreeZone plus 2.5 L "LABCONCO" freeze dryer. ^1H NMR spectra were registered on 500 MHz "Bruker" spectrometer. FTIR spectra of samples were registered on "PerkinElmer" spectrophotometer. The viscosity of solutions was measured using the system PVS 1 "LAUDA," Micro-KPG Ubbelohde auto.

Purification of Commercial LAG: Purification of commercial LAG was carried out as described previously.[6] Briefly, the turbid solution/dispersion of 1 wt.% LAG was centrifuged for 30 min at 40 °C with a

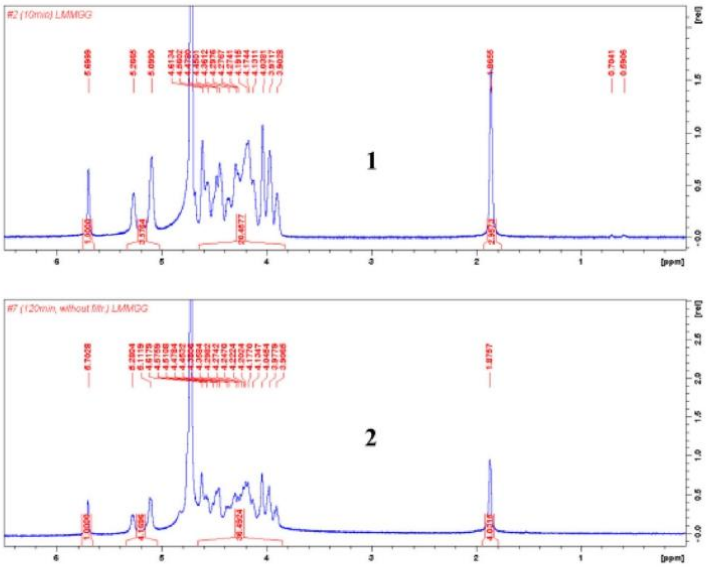

Figure 2. ^1H NMR spectra of low acyl gellan (LAG) after 10 (1) and 120 (2) min ultrasound treatment.

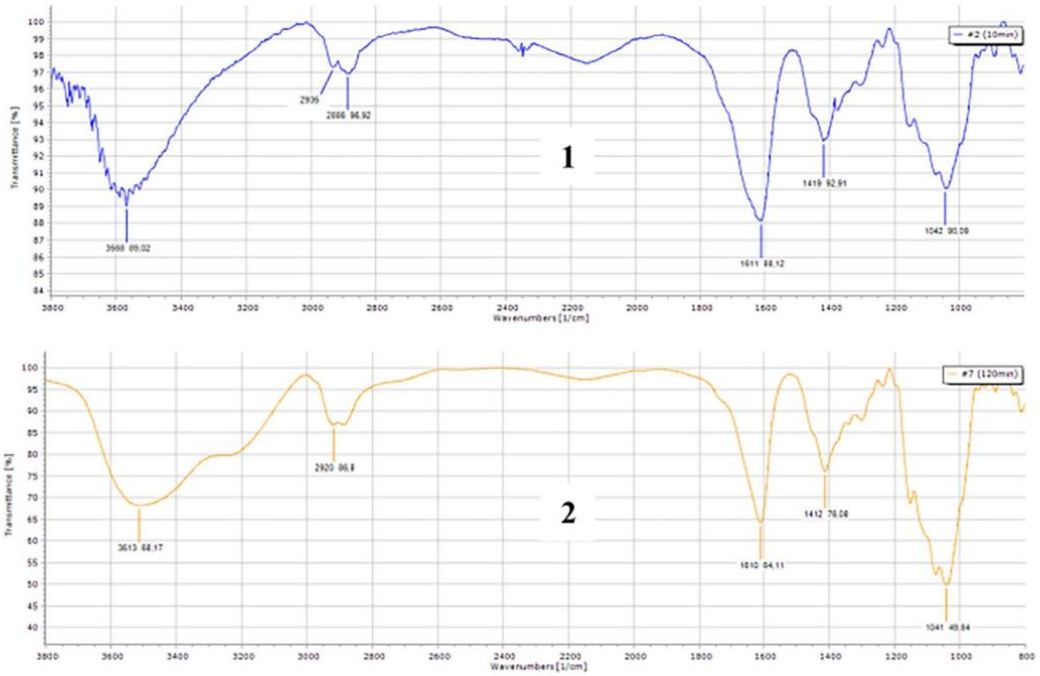

Figure 3. FTIR spectra of low acyl gellan (LAG) after 10 (1) and 120 (2) min ultrasound treatment.

spinning rate of 5000 rpm. The clear supernatant fraction was collected, precipitated in acetone (1:4 v/v), filtrated and dried. Then, the LAG was again redissolved in deionized water and dialyzed against deionized water (cut off 12–14 kDa) for at least 24 h. The product was freeze-dried and collected as dry fluffy white fibers.

Sonication of Commercial LAG: The ultrasonic treatment of aqueous solution of commercial LAG with initial concentration 1 wt.% was carried out at 50 °C during 10, 20, 30, 60, 90, and 120 min. Ultrasonically treated samples were centrifuged at 50 °C during 1 h. Every time the separated supernatant was precipitated by isopropyl alcohol, dialyzed several times, and freeze-dried.

Supporting Information

Supporting Information is available from the Wiley Online Library or from the author.

Acknowledgements

This work was financially supported by Science Committee of the Ministry of Science and High Education of the Republic of Kazakhstan (Grant No. AP13067773). Authors thank the Horizon 2020 research and innovation program of the European Union Maria Sklodowska-Curie (grant agreement 823883-NanoPol-MSCA-RISE-2018) for financial support. All authors contributed equally to this work.

Conflict of Interest

The authors declare no conflict of interest.

Data Availability Statement

The data that supports the findings of this study are available in the supplementary material of this article.

Keywords

commercial low acyl gellan gum, Fuoss equation, intrinsic viscosity, Mark–Kuhn–Houwink equation, purification, reduced viscosity, ultrasound treatment, viscosity average molecular weights

Received: January 2, 2024

[1] I. Giavasis, L. M. Harvey, Mc. B. Neil, *Crit. Rev. Biotechnol.* **2000**, *20*, 177.
[2] T. Osmalek, A. Froelich, S. Tasarek, *Int. J. Pharm.* **2014**, *466*, 328.
[3] I. Gussenov, S. E. Kudaibergenov, *J. Petrol. Sci. Eng.* **2021**, *208*, 109546.
[4] E. R. Morris, N. Nishinari, M. Rinaudo, *Food Hydrocoll.* **2012**, *28*, 373.
[5] G. Tatykhanova, V. Aseyev, M. Vamvakaki, V. Khutoryanskiy, S. Kudaibergenov, *Chem. Bull. Kaz. Nat. Univ.* **2022**, *105*, 4.
[6] J. Lavikainen, M. Dauletbekova, G. Toleutay, M. Kaliva, M. Chatzinikolaidou, S. Kudaibergenov, A. Tenkovtsev, V. Khutoryanskiy, M. Vamvakaki, V. Aseyev, *Polym. Adv. Technol.* **2021**, *32*, 2770.

[7] E. Dreveton, F. Monot, J. Lecourtier, D. Ballerini, L. Choplin, *J. Ferment. Bioeng.* **1996**, *82*, 272.
[8] R. M. Fuoss, *J. Polym. Sci.* **1948**, *3*, 603.
[9] R. M. Fuoss, *J. Polym. Sci.* **1949**, *4*, 96.
[10] Y. Gong, C. Wang, R. C. Lai, K. Su, F. Zhang, D. Wang, *J. Mater. Chem.* **2009**, *19*, 1968.
[11] Z. H. A. Nurakhmetova, I. S. H. Gussenov, G. S. Tatykhanova, S. E. Kudaibergenov, *Chem. Bull. Kaz. Nat. Univ.* **2015**, *3*, 35.

Polymers for Advanced Technologies

WILEY

polymers advanced technologies

RESEARCH ARTICLE

Characterization of Biocompatible Gellan Gum Fractions for Prolonged Retention in Ocular Drug Delivery Systems

Gulnur S. Tatykhanova[1,2] | Rysgul N. Tuleyeva[2,3] | Nargiz N. Gizatullina[1,2] | Daulet B. Kaldybekov[2,3] | Yuliia V. Bardadym[4] | Vladimir O. Aseyev[4] | Sarkyt E. Kudaibergenov[2]

[1]Laboratory of Engineering Profile, Satbayev University, Almaty, Kazakhstan | [2]Institute of Polymer Materials and Technology, Almaty, Kazakhstan | [3]Department of Chemistry and Chemical Technology, Al-Farabi Kazakh National University, Almaty, Kazakhstan | [4]Department of Chemistry, University of Helsinki, Helsinki, Finland

Correspondence: Gulnur S. Tatykhanova (gulnur-ts81@yandex.kz) | Sarkyt E. Kudaibergenov (skudai@mail.ru)

Received: 20 August 2024 | **Revised:** 25 October 2024 | **Accepted:** 25 October 2024

Funding: This work was supported by Horizon 2020, 823883-H2020-MSCA-RISE-2018. Ministry of Science and Higher Education of the Republic of Kazakhstan, AP13067773.

Keywords: commercial low acyl gellan gum | fractional dissolution | intrinsic viscosity | Mark-Kuhn-Houwink equation | reduced viscosity | ultrasound treatment | viscosity average molecular weight

ABSTRACT

Gellan gum (GG) emerges as a promising candidate for developing polymeric carriers with extended retention on the ocular surface, aiming to enhance the efficacy of topical ocular drug delivery systems. This study undertakes the purification of commercial GG through fractional dissolution and ultrasonic treatment, producing fractions characterized by ^{1}H, ^{13}C NMR, FTIR spectroscopy and thermogravimetric analysis. The intrinsic viscosity of GG samples was measured in a 0.025 M tetramethylammonium chloride solution and their molecular weights were calculated via the Mark-Kuhn-Houwink equation. Methodological choices regarding synthetic procedures, solvents and reagents were guided by considerations of biocompatibility, aligning with the end goal of drug delivery applications. The study further explores the mucoadhesive potential of GG fractions with varying molecular weights for ocular drug delivery, utilizing an in vitro flow-through technique with fluorescent detection on freshly excised bovine corneal mucosa surfaces. The findings under-score the viability of GG formulations in enhancing ocular drug retention and pave the way for future applications in topical ocular therapeutics.

1 | Introduction

In the realm of ocular health, the treatment of various eye conditions often hinges on the application of eye drops. However, a significant challenge arises as less than 5% of the applied dose typically reaches the intraocular tissues when administered via conventional eye drops. This is related to the rapid loss of the instilled solution (continuous production of tear fluid, blinking reflex, nasolacrimal drainage) and poor permeability of ocular membranes [1]. Addressing this concern becomes crucial and one promising avenue lies in enhancing the lipophilic character of drugs to substantially improve ocular absorption. The quest for precision in drug delivery has become a focal point in modern medicine, prompting the pharmaceutical industry to prioritize the development and implementation of innovative drug delivery systems. Notably, approximately 25% of global drug sales now comprise medications equipped with enhanced delivery systems [2–4]. There were many methods and improvements in ocular drug delivery developed over the last decades exploring more effective treatments for different ocular diseases. Nevertheless, this field of medicine remains one of the most challenging.

Abbreviations: FITC-dextran, fluorescein isothiocyanate-labeled dextran; GG, Gellan gum; NaFI, fluorescein sodium salt; STF, simulated tear fluid

In the pursuit of enhancing the efficacy of ocular drug delivery, extending the contact time between the drug and the eye's internal structures emerges as a pivotal strategy. The significance of prolonged contact lies not only in its simplicity but also in its potential to increase the bioavailability of ophthalmic drugs. This becomes particularly crucial when considering the convenience and benefits associated with a single daily intake for the patient [5].

Various approaches have been explored to achieve this goal, each presenting its own set of advantages and drawbacks. One notable strategy involves the utilization of water-soluble biopolymers [6, 7] and nanomaterials [8, 9], aiming to extend the contact time and potentially enhance the amount of drug penetration. On the other hand, viscous semi-solid preparations such as sprayable fluid gels, nanoparticles and films have also been considered [10–13]. While these preparations can offer prolonged contact, they may induce side effects such as stickiness, blurred vision and reflex blinking due to the thickness of the formulation, thereby causing discomfort or irritation to the eye [14, 15].

Ophthalmic gels can be divided into two categories: (1) gel eye drops and (2) in situ gels [16]. The first exist as viscous solutions before application to the eye and are normally used for dry eyes as a tear substitute [17]. In situ gels are applied as drops and undergo thickening and/or gelation after administration [18]. There are numerous gel-based materials for ophthalmic drug delivery [19] and approaches to prolong the duration of ocular drug residence time of ophthalmic formulations, including the use of in situ gelling systems [20, 21]. The most important is the fact that the sol–gel phase transition of GG occurs immediately after administration, before dilution by the tear fluid and drainage can take place. The weak gels formed in dilute tear fluid can be easily destroyed by shearing [22]. Following instillation, these systems exhibit a phase transition in response to variations in temperature, pH and ionic strength [6, 23–26]. Additionally, corneal and conjunctival surfaces are covered with a thin layer of mucus that hydrates and lubricates the ocular surfaces as well as protects them from pathogens [27]. Thus, mucoadhesive polymers are also commonly employed to enhance retention time.

The ocular bioavailability of eye drops could be substantially improved when water-soluble mucoadhesive polymers are used as a part of the formulation. The mucoadhesive properties of gellan and its modified derivatives were reviewed in [28]. Adhesiveness of gellan and its retention on mucosal tissues depend on several mechanisms of action, such as those favoring ionic interactions that promote strong hydrogen bonding with hydroxyl, carboxyl and amino groups; polymers with high molecular weight (generally > 100 kDa) [29]; chain flexibility (able to interpenetrate into the mucus and form chain entanglements); and the rheological properties, etc. [30] The mucoadhesive properties of gellan and its modified derivatives are mostly based on the combination of several mentioned mechanisms. Following administration to the eye, the gellan gum (GG) is expected to form an ultrathin transparent film on the mucus membrane, therefore enhancing ocular retention and precorneal drug loss. This, in its turn, can lead to more efficient drug release absorption.

Exploring alternative methods, in situ gelation systems present a promising avenue where droplets, initially in liquid form during storage, but transform into a viscoelastic gel upon contact with the eye's surface, thereby resulting in improved patient compliance and reduced administration frequency. This approach aims to mitigate the discomfort associated with prolonged use of semi-solid preparations. Additionally, modern nanotechnology introduces a novel dimension to the field, offering nanocarriers as a means to increase both the contact time and penetration ability of ocular drugs [13, 25, 31–34].

Authors [35, 36] proposed to use an aqueous solution of GG as in situ gelling drug delivery system because it easily undergoes a sol–gel transition in the presence of sodium, potassium and calcium ions containing in lacrimal fluid. In particular, an ion-activated ketotifen ophthalmic delivery system was developed by using deacetylated GG [37]. Gellan gum with concentrations of 0.2% and 0.6% showed a considerable increase in viscosity after mixing with artificial tear fluid. In vitro release showed that ketotifen release from in situ gels was moderate with no bursting effects. In situ gelling properties of low acyl GG were enhanced when tear fluid monovalent cations—sodium and potassium were displaced by calcium gluconate [38]. Rheological properties of gellan gels formed through the addition of calcium chloride to gellan solutions were studied by authors [39, 40].

The unique rheological properties and gelling abilities of GG have made it a popular choice for pharmaceutical formulations, contributing to the stability and performance of various drugs. However, for ophthalmological purposes, commercial GG cannot be used directly due to its high molecular weight, broad molecular weight distribution, polydispersity and poor solubility in distilled and deionized water, producing a cloudy solution. For example, the high molecular weight GG needs a stressed heating process to be dispersed and water (90°C for 30 min) [41]. Moreover, even at relatively low concentrations (0.5%–1% w/v), it forms too viscous aqueous dispersions, which quickly undergo gelation and lose fluidity as a consequence of temperature lowering. These factors limit its use in preparing a clear eye drop solution for ophthalmology, necessitating the selection of appropriate GG excipients. In this regard, we have purified and fractionated commercial GG using fractional dissolution and ultrasound treatment, differing from the purification method suggested by authors [42, 43]. As we explore the proposed strategy aimed at extending contact time and enhancing the delivery of ophthalmic drugs, in this communication we highlight its potential benefit and application in the field of ocular drug delivery.

2 | Materials and Methods

2.1 | Materials

Gellan gum (GG) was purchased from Zhejiang DSM Zhongken Biotechnology Co. Ltd. (China) ($M_n = 10^6$ g/moL estimated by viscosity). Acetone (≥ 99.8%) and isopropanol (≥ 99.5%, Fischer-Chemicals Oy) were used in the purification of GG. Deuterium oxide (D_2O, 99% D, Euriso-Top) were used in NMR experiments. Dialysis membranes (molecular weight cut off 3.5 kDa and 12–14 kDa) were purchased from Spectrum Laboratories. Milli-Q water with a resistivity of 18.2 MΩ cm at 298 K was used for all experiments. Sodium bicarbonate,

fluorescein isothiocyanate-labeled dextran (FITC-dextran), fluorescein sodium salt (NaFl) was purchased from Sigma-Aldrich (Gillingham, UK). Calcium chloride dihydrate, sodium chloride were purchased from Fisher Scientific (Loughborough, UK). Deionized water was used throughout the experiments involving aqueous solutions.

2.2 | Characterization

2.2.1 | ^{1}H and ^{13}C NMR Spectroscopy

Solutions of GG and its fractions (10 mg/mL) were prepared in D_2O. ^{1}H and ^{13}C NMR spectra of samples were recorded using a Bruker 500 MHz NMR spectrometer (Bruker, UK) at 60°C. Bruker's TopSpin 3.6.2 software was used for analysis of spectra.

2.2.2 | FTIR Spectroscopy

FTIR spectra of GG and its fractions were registered on PerkinElmer Spectrum One FT-IR spectrometer (PerkinElmer, USA) using an iD5 attenuated total reflectance (ATR) accessory equipped with a diamond crystal. Samples were scanned from 4000 to 650 cm^{-1}. The spectra were plotted and analyzed using the OriginLab 2021 software.

2.2.3 | Thermogravimetric Analysis (TGA)

Thermogravimetric analysis was performed using a LABSYS evo TGA instrument. Samples (3–5 mg) were heated from 25°C to 800°C with a heating rate of 10°C/min in a nitrogen atmosphere. Thermograms were plotted and analyzed using the OriginLab 2021 software.

2.2.4 | Elemental Analysis

Elemental analysis was used to compare the composition of the pristine (commercial GG) and purified GG fractions (Table S3). Elemental composition was determined using a HANAU Elementar Analysensysteme GmbH (Germany), using the vario MICRO cube with sulfanilamide as a standard. Three samples (~2 mg of dry polymer per measurement) were studied and the results were averaged.

2.2.5 | Viscometric and Rheological Measurements

The reduced viscosity of GG solutions was measured using the system PVS 1 "LAUDA", Micro-KPG Ubbelohde auto, Nr. 1c, $K = 0.03$.

Rheological measurements of GG samples with and without STF were performed using a Rotational Rheometer RheolabQC (Anton Paar, Austria) at 34°C ± 0.5°C across shear rates ranging from 1 to 100 s^{-1} and a Brookfield DV rotary viscometer (Brookfield, USA) at 34°C ± 0.5°C across shear stress ranging from 0.01 to 1.6 s^{-1}.

2.2.6 | Other Stages of Sample Preparation

The ultrasonic processor UP400S (400 W, 24 kHz) "Hielscher Ultrasound Technology" was used for sonicating the samples. Separation of insoluble gellan fractions was performed by Sigma laboratory centrifuge 2K15C "B.Braun Biotech International". The samples were freeze dried using a FreeZone plus 2.5 L "LABCONCO" freeze dryer.

Simulated tear fluid (STF) containing 6.78 g NaCl; 0.084 g $CaCl_2{\cdot}2H_2O$; 1.38 g KCl and 2.18 g $NaHCO_3$ was prepared in 1000 mL of distilled and deionized water according to [44].

2.2.7 | Ex Vivo Retention Studies on Bovine Corneal Tissues

Whole intact bovine eyeballs with eyelids were received from P.C. Turner Abattoirs (Farnborough, UK) immediately after slaughter of the animals, packed and transported to the laboratory in insulated plastic containers. These tissues were visually assessed in terms of any damage and corneal opacification present. The corneal tissues were carefully excised using disposable sharp blades, avoiding contact with their surfaces and then used for evaluating the retention properties of the formulations using the methodology previously developed by the Khutoryanskiy research group [24, 31, 45, 46]. Each corneal tissue was pre-rinsed with 1 mL of STF, mounted on a microscope glass slide with the testing surface facing upward, placed in Petri dishes and then stored at 4°C in a refrigerator. All tissues were used within 12 h of retrieval.

STF solution used to wash a mucosal surface was prepared as described in a previous report [47]. Briefly, sodium chloride (670 mg), sodium bicarbonate (200 mg) and calcium chloride dihydrate (8 mg) were dissolved in 100 mL of deionized water. The pH of the STF solution was adjusted to 7.40 due to the natural tear pH being around a neutral value and the solution was maintained at 37°C throughout mucoadhesion experiments using a water bath.

Experiments were conducted with the corneal tissues maintained at 37°C and 100% relative humidity in an incubator to mimic physiological conditions. Each cornea, already mounted on a glass slide, was placed on a substrate, fixed at an angle of 20° and prewarmed for 1 min within the incubator before starting each ex vivo mucoadhesion experiment. Next, prewarmed aliquots (200 μL) from 0.3% (w/v) GG formulations prepared in deionized water containing 1 mg/mL fluorescein sodium salt (NaFl); two controls of NaFl (1 mg/mL) and FITC-dextran (0.3% w/v) solutions were applied onto the corneal surface and were then repeatedly irrigated with STF (pH 7.40) at a constant flow rate of 100 μL/min using a syringe pump for 30 min (total washing time). The flow rate selection was intentionally set higher than the physiological secretion rate of tear fluid (~1–2 μL/min in human eyes) for practical reasons [48]. This adjustment was made to expedite the experiments and ensure they could be conducted within a reasonable timeframe. The fluorescence images of corneas were acquired at predetermined time intervals after each washing cycle using a Leica MZ10F stereomicroscope (Leica Microsystems, UK) fitted with the GFP filter (blue,

$\lambda_{emission}$ = 520 nm) and Leica DFC3000G digital camera at 1.0× magnification, with 30 ms of exposure time and a 1.0× gain. These images were then analyzed using ImageJ software (version 1.54g, 2023, NIH, USA.) by measuring the pixel intensity after each washing with STF. The pixel intensity of the blank tissues (i.e., the background microscopy image of each corneal surface before administering a fluorescent test material) was subtracted from each measurement. Data were normalized and converted into % mucosal retention values.

All retention tests were performed in triplicate for each formulation, the mean ± standard deviation values were calculated and then evaluated statistically.

2.3 | Statistical Analysis

Statistical analysis of data from mucoadhesion studies was performed using GraphPad Prism software (version 8.0; San Diego, CA, USA.). Data were compared and assessed for significance using a two-tailed Student's *t*-test and a one-way analysis of variance (ANOVA) with Bonferroni post hoc test, where $p \leq 0.05$ was considered the statistically significant criterion.

3 | Results and Discussion

3.1 | Characterization of Purified Commercial GG in Aqueous Solution

The purified GG, due to the presence of carboxylic groups in glucuronic acid fragments, displays polyelectrolyte behavior. As a result, the dependence of η_{sp}/C cannot be extrapolated to zero polymer concentration for determining the intrinsic viscosity [η] (Figure S1). Typically, this issue can be addressed in two ways: (1) using an empirical Fuoss equation, or (2) adding low-molecular-weight salt to suppress the polyelectrolyte effect.

As shown in Figure S2, the curve in Figure S1 was linearized using the Fuoss equation [49, 50]:

$$\frac{C}{\eta_{sp}} = \frac{1}{[\eta]} + k_{Fs}\frac{1}{[\eta]}c^{\frac{1}{2}} \quad (1)$$

where η_{sp}—specific viscosity, which is determined as $(\eta - \eta_s)/\eta_s$, where η is the viscosity of the polymer solution and η_s is the viscosity of the solvent; [η]–is the intrinsic viscosity, which is determined by extrapolation of η_{sp}/C–C → 0; k_{Fs} is the Fuoss coefficient; C—is the concentration of the polymer in the solution.

The intrinsic viscosity of GG, determined using the Fuoss equation, was found to be 5680 $cm^3 g^{-1}$.

3.2 | Fractionation and Determination of the Molecular Weights of GG

The extremely high molecular weight of commercial low acyl GG in the range of (0.5–1) ≈10^6 limits the widespread use of GG as an eye drops of a drug delivery system. A 1.0% w/v GG solution is poorly soluble in water; it forms a fraction of soluble chains and a dispersed fraction of swollen gellan particles. To reduce the molecular weights and to improve the solubility in water, the fractionation of GG was carried out by two methods: Fractional dissolution and ultrasonic treatment. Using the method of fractional dissolution, we obtained reduced molecular weights of GG (Figure 1). Here GG-1, GG-2, GG-3, GG-4 refer to GG fractions isolated by the fractional dissolution method.

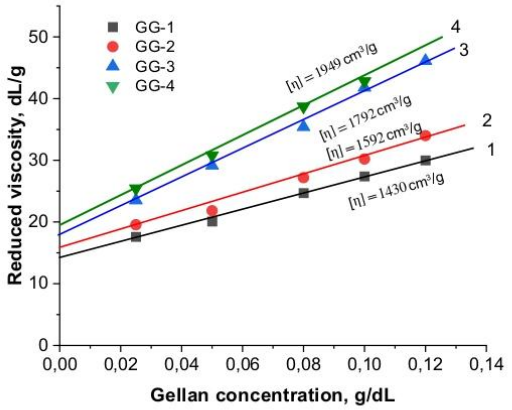

FIGURE 1 | Concentration dependences of the reduced viscosities of GG fractions obtained by fractional dissolution.

At first, GG (1.0% w/v) was dissolved for 24 h in deionized water at 50°C. The turbid solution/dispersion was centrifuged for 30 min at 40°C with a rotation speed of 5000 rpm. The upper transparent fraction of the liquid was collected and precipitated in acetone (1:4 by volume). Then the separated precipitate was dissolved again in deionized water and the process was repeated 4 times. The stages of cleaning commercial GG can be viewed in Figure S3. GG was separated from the water-acetone mixture by vacuum filtration using Whatman 541 filter paper and dried for 30 min. Then it was dissolved in deionized water and subjected to dialysis against deionized water (cut off 12–14 kDa) for at least 24 h (Table S1). The product was freeze-dried and collected in the form of dry fluffy white fibers. The intrinsic viscosities of GG fractions, found from the extrapolation of η_{sp}/C to C → 0, are shown in Figures 1 and 2.

Chains scissoring of commercial GG was carried out using ultrasound treatment to obtain GG fractions of lower molecular weights. 1.0% w/v GG samples ultrasonically treated at 50°C during 5, 10, 30, 60 and 120 min were centrifuged at 50°C for 1 h (Table S2). Every time the separated supernatant was precipitated in isopropanol, dialyzed and freeze-dried. The intrinsic viscosities of ultrasonically treated GG samples were measured in an aqueous solution containing 0.025 M tetramethylammonium chloride (Figure 2). Here 1-GG, 2-GG, 3-GG, 4-GG, 5-GG are GG fractions obtained by ultrasonic treatment during 5, 10, 30, 60 and 120 min.

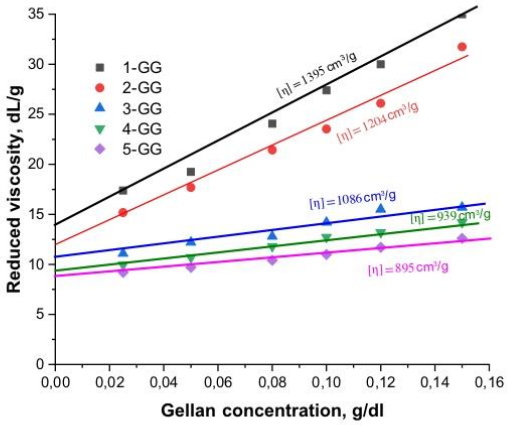

FIGURE 2 | Concentration dependences of the reduced viscosities of GG after 5-, 10-, 30-, 60- and 120-min treatment by ultrasonic source.

TABLE 1 | The intrinsic viscosities and M_η of GG fractions obtained by fractional dissolution.

Fractions	Intrinsic viscosity, $cm^3 g^{-1}$	$M_\eta \cdot 10^{-5}$, dalton
GG-1	1430	6.43
GG-2	1592	7.23
GG-3	1792	8.23
GG-4	1949	9.03

TABLE 2 | The intrinsic viscosities and M_η of GG fractions obtained by ultrasonic treatment.

Fractions	Ultrasonic treatment, min	Intrinsic viscosity, $cm^3 g^{-1}$	$M_\eta \cdot 10^{-5}$, dalton
1-GG	5	1395	6.25
2-GG	10	1204	5.32
3-GG	30	1086	4.75
4-GG	60	939	4.04
5-GG	120	895	3.84

The viscosity average molecular weights (M_η) of GG fractions calculated according to Mark-Kuhn-Houwink equation in 0.025M tetramethylammonium chloride $[\eta] = 7.48 \cdot 10^{-3} M_w^{0.91}$ [51] are summarized in Tables 1 and 2. It is revealed that the ultrasonic treatment of GG leads to gradual decrease of both [η] and M_η. It could be associated with cleavage of glycosidic linkages and degradation of GG [52]. In contrast, in fractional dissolution, the low molecular weight fractions are separated at the beginning and at the end, fractions with high molecular weights remain.

3.3 | Spectroscopic Characterization of Commercial Gellan and GG Fractions

FTIR and NMR spectroscopy revealed no significant differences between the purified and pristine GG. Thus, there was no indication that GG was not completely deacetylated and the fraction was removed during purification. This conclusion is also confirmed by elemental analysis, which shows the same carbon and hydrogen content in samples.

^1H, ^{13}C NMR and FTIR spectra GG fractions obtained by fractional dissolution and ultrasound treatment are shown in Figures 3–6. The results show no significant differences between the samples, confirming the absence of structural changes in the course of fractionation. The spectra of GG obtained at 60°C showed the presence of four characteristic peaks corresponding to: —CH of rhamnose (δ 5.27 ppm), —CH of glucuronic acid (δ 5.11 ppm), —CH of glucose (δ 4.88 ppm) and —CH3 of rhamnose (δ 1.86 ppm).

The ^{13}C NMR spectra of commercial gellan and GG fractional dissolution are shown in Figure 5. Although the detailed signal assignment has not been made at the present stage, the carbonyl peak (δ 175.2 ppm) for glucuronic acid ring, methylol peaks (δ 61.2 and δ 61.7 ppm) for glucose rings and the methyl peak (δ 17.6 ppm) for the rhamnose ring are clearly seen. Thus, ^{13}C NMR spectroscopy showed clear and well-distinguishable peaks, each of which can be correlated with specific functional groups in the polysaccharide composition.

(a) GG-1, (b) GG-4, (c) commercial gellan.

Figure 6 displays the FTIR spectra of GG and its fractions obtained by fractional dissolution. Absorption peaks observed at 3370 and 1408 cm^{-1} are associated with OH vibrational modes. The peak at 2921 cm^{-1} corresponds to C-H stretching vibrations. The peaks at 1604 and 1039 cm^{-1} are attributed to the stretching vibrations of C═O and C—O bonds, respectively.

Thermograms of commercial and GG fractions are presented in Figure 7. It can be observed that the thermal properties of the GG samples are similar, but an increase in molecular weight slightly raises the decomposition temperature.

3.4 | Viscosity and Rheology of GG Fractions in STF

The reduced viscosities of GG fractions were measured in STF, which was adjusted according to [44] (Figure 8). The viscosity of GG significantly increases upon addition of STF. The optimal concentration of STF that leads to effective viscosification of the GG fractions is approximately 0.016–0.018 mol L^{-1}, as further increases in salt concentration result in the viscosity leveling off. Moreover, the viscosification of the aqueous solution of GG increases in the order: GG-4>>GG-2>GG-1 and is more pronounced in high molecular weight fractions. This approach may be important for regulation of retaining time of drug in eye.

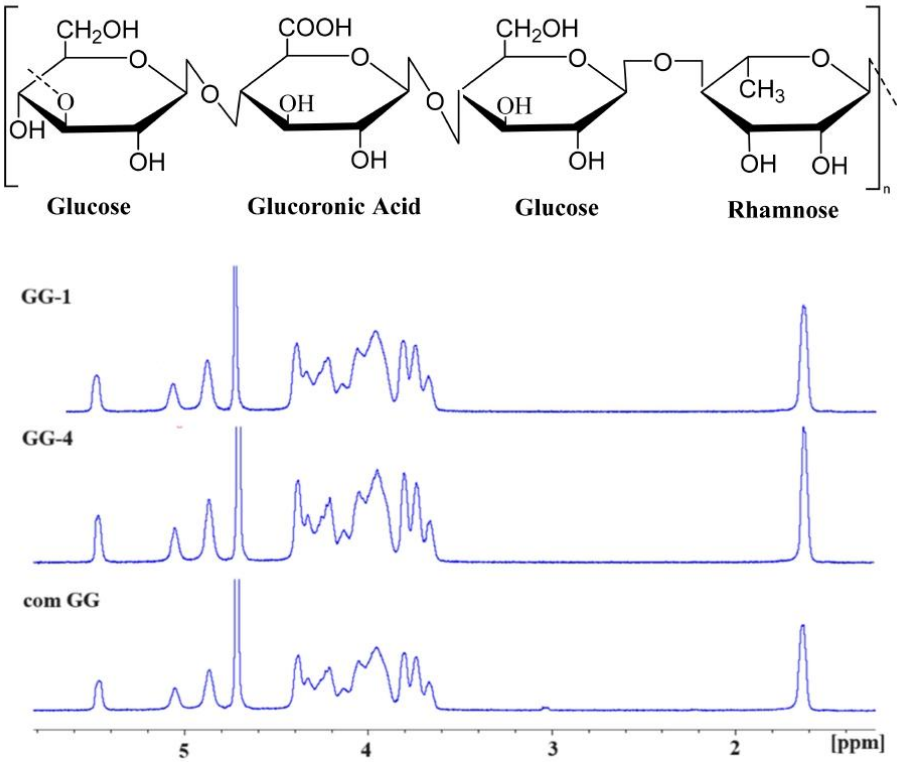

FIGURE 3 | Repeating monomeric units of GG and ^{1}H NMR spectra of GG fractions obtained by fractional dissolution of commercial gellan.

The influence of shear rate on the viscosity of GG may help evaluate the effect of eye blinking on the retention time of eye drops. The dynamic viscosity of 0.2 wt.% aqueous solutions of commercial GG ($M_w \sim 10^6$ Da, product supplier information) and the GG-1 fraction with $M_\eta = 6{,}43 \cdot 10^5$, as a function of shear rate, is shown in Figures 9 and 10. In situ gels were prepared by adding 3 mL of STF to 20 mL of GG solution. In this case, the concentration of STF, expressed as the total ionic strength (μ), corresponds to 0.018 mol·L^{-1}, which aligns well with the effective viscosification of the GG fractions shown in Figure 8. In all experiments, the temperature was maintained at 34°C ± 0.5°C to simulate real in vivo conditions.

All samples exhibit a shear-thinning viscosity profile and demonstrate pseudoplastic behavior [37]. As a general trend, viscosity decreases as shear rate increases. It is obvious that molecular weight and molecular weight distribution influence the rheological behavior of GG solutions. In the high molecular weight commercial GG sample, the chains in aqueous solutions adopt a helical conformation and the chains are highly extended due to electrostatic repulsion from the charged groups on the side chains. In the case of GG-1, although a double helix forms, but the molecular weight may be lower to stabilize it, leading to continuous rearrangement of the microstructures during shear for the low molar mass GG. Additionally, reducing the molecular weight of GG is advantageous for obtaining more easily processable samples, as they can be dispersed in water at relatively high concentrations without forming overly viscous solutions [41].

In the presence of STF, the dynamic viscosities of both commercial GG and the GG-1 fraction are higher than without STF. The extremely high dynamic viscosity of commercial GG with STF is attributed to cation-mediated aggregation of macromolecules, leading to the formation of entangled gel network. In contrast, the addition of STF to the lower molecular weight GG-1 solution allows for fine-tuning of the viscosity, which likely enhances the retention time of the formulated eye drops when applied [33].

3.5 | Mucoadhesion Studies, Particularly Retention on Ex Vivo Bovine Corneal Tissues

Effective tear drainage and blinking result in a 10-fold reduction in drug concentration when the drug solution is administered, allowing the drug to reach the ocular tissue for only a very short time [53]. Patients respond better to in situ gelling systems, which are administered as solutions that instantly form gels upon contact with the ocular surface. Some studies have demonstrated the advantages of these systems, including reduced nasolacrimal drainage, sustained and prolonged drug release and

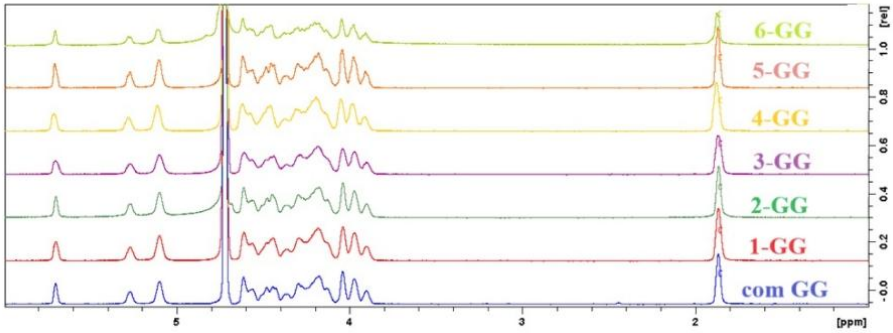

FIGURE 4 | ^{1}H NMR spectra of GG fractions obtained by ultrasonic treatment of commercial gellan.

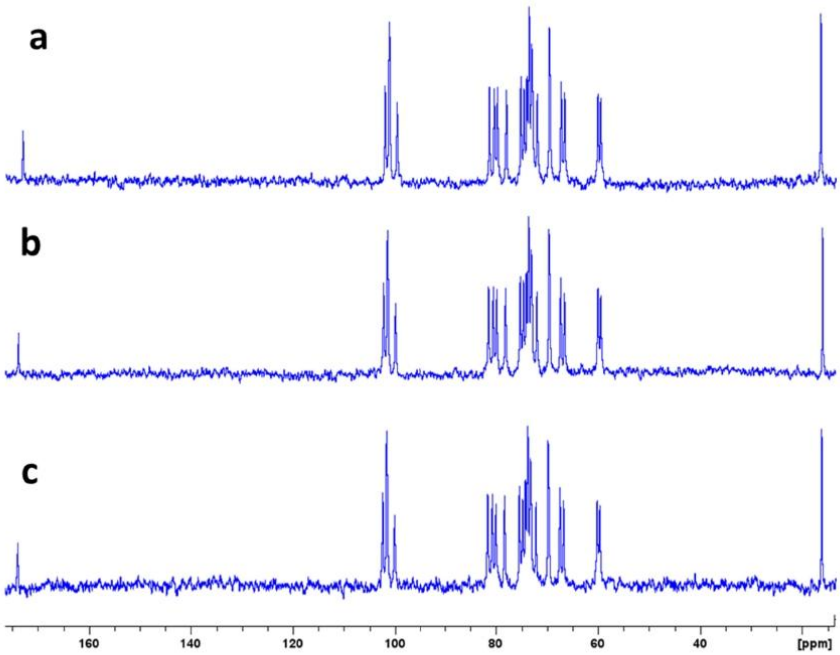

FIGURE 5 | ^{13}C NMR spectra of different fractions of GG obtained by fractional dissolution.

enhanced bioavailability resulting from an extended precorneal residence time [54, 55].

The potential use of GG fractions (with different molecular weights) in ocular drug delivery formulations was examined by assessing mucoadhesion on freshly excised bovine corneal tissues using a well-established in vitro flow-through technique with fluorescent detection. These formulations were prepared with NaFl (1 mg/mL), which serves as a fluorescent marker that facilitates easy detection and measurement of mucosal retention levels. The method has been extensively used to evaluate the retention properties of various test materials on different mucosal surfaces, including ocular tissues [24, 45, 56–58]. The effectiveness of this technique was validated against other established methodologies used to assess mucoadhesive properties [54].

Figure 11 displays the exemplar fluorescence microphotographs of the retention of fractionated GG formulations, as well as solutions of NaFl (1 mg/mL) and 0.3% (w/v) FITC-dextran (both used as non-mucoadhesive controls) on ex vivo bovine cornea taken after washing with varying volumes of STF (pH 7.40; flow rate 100 μL/min) over 30 min. The fluorescent images were then analyzed with ImageJ software and fluorescence intensity values were normalized and converted to 100% retention values (Figure 12). During mucoadhesion

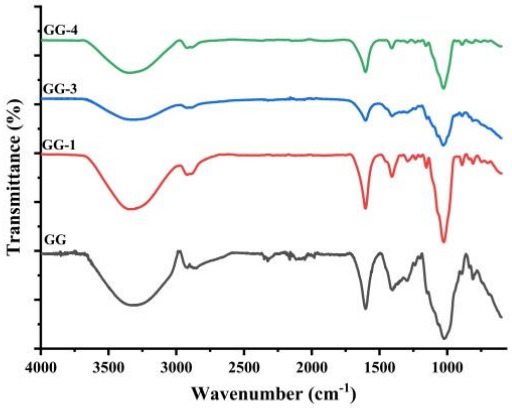

FIGURE 6 | FTIR spectra of commercial and GG fractions.

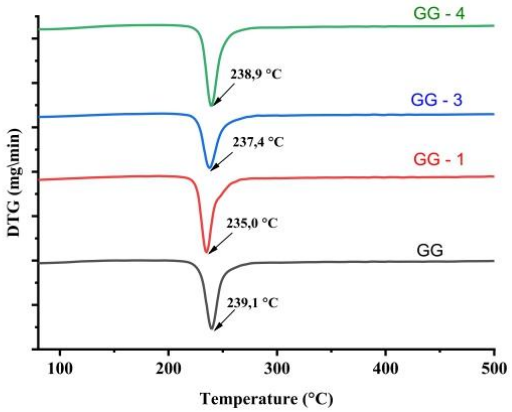

FIGURE 7 | TGA curves of commercial gellan and GG fractions.

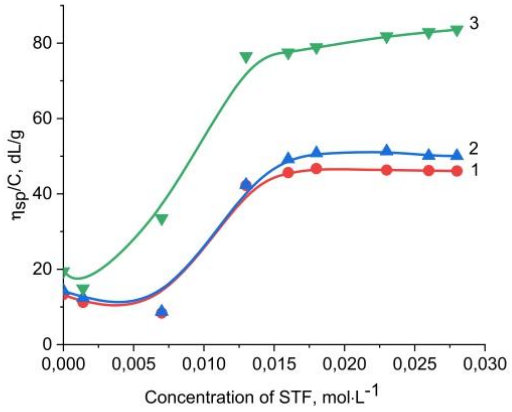

FIGURE 8 | The dependence of the reduced viscosity of 0.2wt.% solutions of GG fractions on the concentration of STF at 25°C. (1) GG-1, (2) GG-2, (3) GG-4.

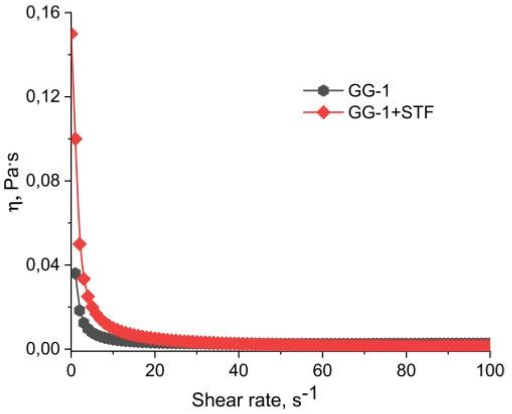

FIGURE 9 | Dependence of the viscosity 0.2wt.% aqueous solution of GG-1 and GG-1 + STF on shear rate at 34°C ± 1°C.

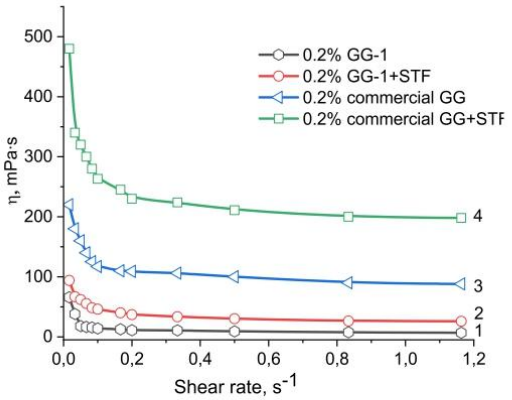

FIGURE 10 | Changing of the dynamic viscosity of GG-1 fraction (curves 1,2) and commercial gellan (curves 3,4) on shear rate in absence (curves 1,3) and presence (2,4) of STF.

experiments conducted at 37°C and 100% relative humidity within the incubator, all GG formulations formed in situ gels and the percentage of their retention on the cornea was estimated.

Analyzing the images, it was revealed that all GG formulations exhibited similar retention abilities on freshly isolated bovine corneas, as values were not significantly different from each other ($p > 0.05$). After washing with varying volumes of STF solution approximately 30% of GG retained on the surface of bovine corneal tissues during 30 min. However, all GG samples exhibited superior retention ($p < 0.001$) compared to solutions of NaFl (served as a negative non-mucoadhesive control) and FITC-dextran (served as a non-gel-forming polymer control). According to the findings, the increased mucoadhesive performance of the GG formulations until the end of washing cycles is likely attributed to the fact that the samples form a thin layer of viscous physical gels (polymer chain entanglements) upon

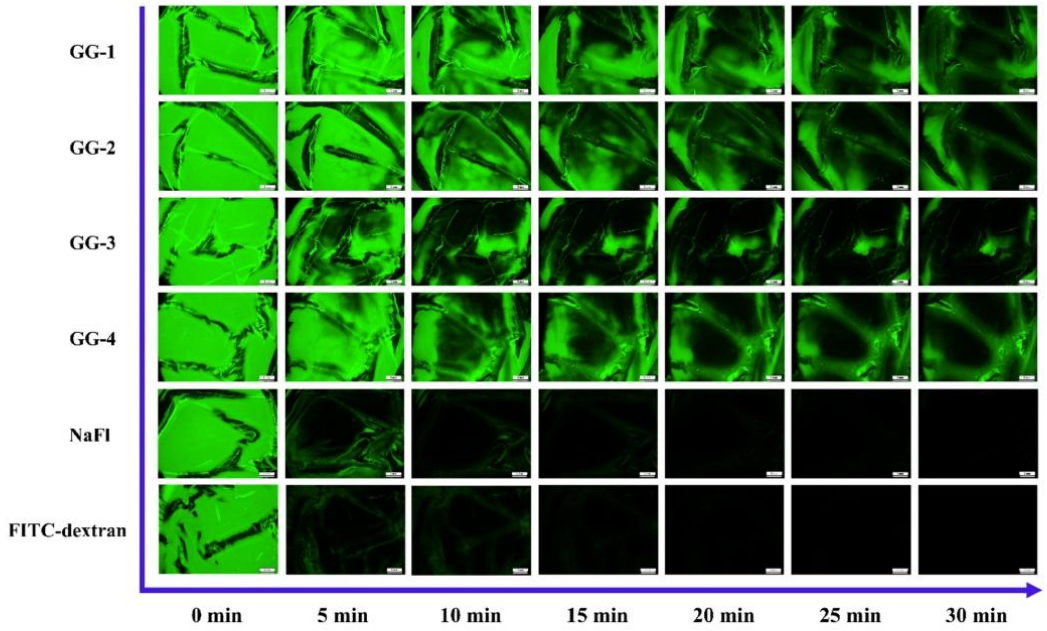

FIGURE 11 | Selected exemplar fluorescence microphotographs showing mucosal retention of 0.3% (w/v) solutions of fractionated GG formulations (with different $M\eta$) containing 1 mg/mL fluorescein sodium salt (NaFl); as well as free 1 mg/mL NaFl and 0.3% (w/v) FITC-dextran (both served as non-mucoadhesive controls), on freshly isolated bovine corneal tissues after washing with varying volumes of STF solution (pH 7.40; flow rate 100 μL/min). Fluorescence microscope parameters: Magnification—1.00×; exposure time—30 ms; gain—1.0×. Scale bars correspond to 2 mm.

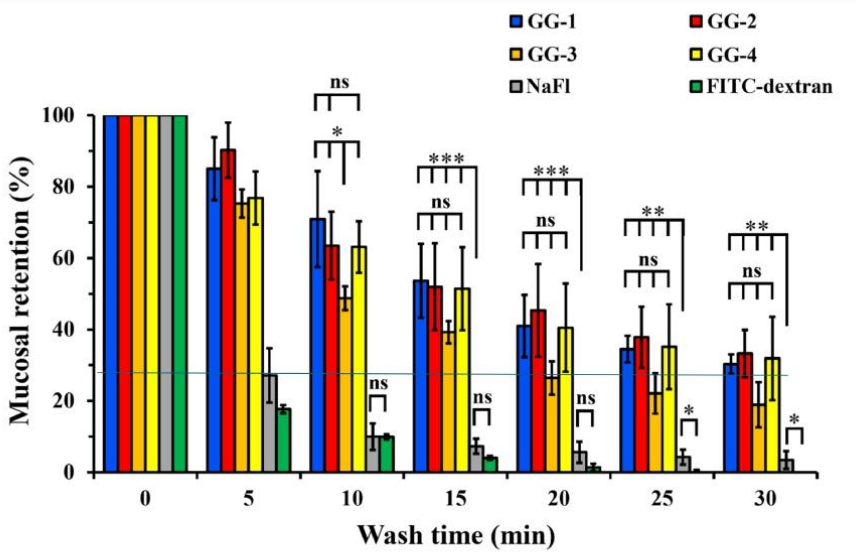

FIGURE 12 | Percentage mucosal retention of 0.3% (w/v) solutions of fractionated GG formulations (with different M_η) containing 1 mg/mL fluorescein sodium (NaFl); as well as fluorescein NaFl and 0.3% (w/v) FITC-dextran (both served as non-mucoadhesive controls) on ex vivo bovine corneas after washing with varying volumes of STF (pH 7.40; flow rate 100 μL/min). The corneal retention was assessed using a wash-off in vitro assay over 30 min. Data are expressed as mean ± standard deviation values ($n = 3$). Statistically significant differences are represented as ***—$p < 0.001$; **—$p < 0.01$; *—$p < 0.05$; ns—denotes no significance.

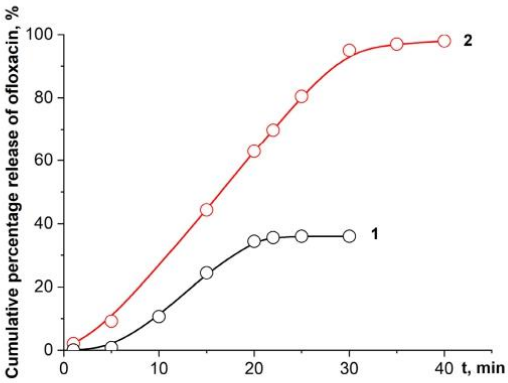

FIGURE 13 | Cumulative percentage release of ofloxacin from commercial gellan-ofloxacin thin films gelled by the addition of 0.027 mol L^{-1} $CaCl_2$ into distilled water (1) and phosphate buffer (2) at 25°C ± 1°C. Reproduced from [13].

interaction with salt ions in the STF solution. Additionally, NaFl and FITC-dextran solutions showed significantly lower retention capability, with > 90% of them being washed out from the corneal surface.

3.6 | Release of Ofloxacin From GG Matrix

Previously [13] we have studied the cumulative release of antimicrobial drug–ofloxacin from the commercial gellan-ofloxacin films gelled by the addition of 0.027 mol L^{-1} $CaCl_2$ into distilled water and phosphate buffer at 25°C ± 1°C (Figure 13).

The in vitro release profiles indicate that ofloxacin releases from the GG thin films in a sustained fashion. During 30 min the amount of cumulative ofloxacin release from the commercial gellan-ofloxacin films was 96% ± 2% in phosphate buffer and 36% ± 2% in distilled water.

Comparison of the cumulative release of ofloxacin (36% ± 2%) from the GG matrix into distilled water over 30 min with the mucosal retention time of GG on bovine corneal tissues, which also lasts 30 min, suggests that in this study the developed eye drops can retain ocular drug residence for 30 min. This duration is sufficient to prolong the effect of ophthalmic formulations. It is proposed that tear fluids containing sodium, potassium and calcium ions can, on the one hand, enhance the viscosification of fractionated GG due to entanglements of macromolecular chains and, on the other hand, accelerate the release of the ocular drug by breaking the ionic bonds formed between the carboxyate groups of gellan and the protonated amine groups of ofloxacin [13].

4 | Conclusions

This study offers a comprehensive approach to the purification and characterization of GG for potential use in drug delivery systems, specifically for topical ocular applications. By employing two distinct fractionation techniques—fractional dissolution and ultrasonic processing—we successfully isolated nine fractions of commercial GG, with molecular weights ranging from $3.8{\cdot}10^5$ to $9.0{\cdot}10^5$ Da. The structural integrity of these GG fractions was confirmed through various analytical methods, including ^1H and ^{13}C NMR spectroscopy, FTIR spectroscopy and thermogravimetric analysis. Additionally, we assessed the effect of model tear fluid on the viscosity and rheological characteristics of GG fractions, determining that optimal thickening of aqueous GG occurs at a tear fluid concentration of approximately 0.016–0.018 mol·L^{-1}. Mucoadhesion experiments showed that all tested GG formulations had similar retention abilities on freshly isolated bovine corneas.

In conclusion, we have optimized a formulation for eye drops involving gellan based on the sol–gel transition mediated by tear fluid. This highlights a promising method for the development of effective ocular drug delivery systems, leveraging the unique properties of GG to enhance drug retention and bioavailability on the ocular surface. The strong correlation between cumulative drug release and mucosal retention time suggests that the developed eye drops could be recommended for further clinical trials in ophthalmological settings.

Acknowledgments

This research was funded by the Science Committee of the Ministry of Science and Higher Education of the Republic of Kazakhstan (Grant No. AP13067773) and was supported by the Horizon 2020 research and innovation program of the European Union Maria Sklodowska-Curie (grant agreement 823883-H2020-MSCA-RISE-2018).

Conflicts of Interest

The authors declare no conflicts of interest.

Data Availability Statement

The data that supports the findings of this study are available in the Supporting Information of this article.

References

1. T. Järvinen and K. Järvinen, "Prodrugs for Improved Ocular Drug Delivery," *Advanced Drug Delivery Reviews* 19 (1996): 203–224.

2. M. C. Hacker and H. A. Nawaz, "Multi-Functional Macromers for Hydrogel Design in Biomedical and Regenerative Medicine," *International Journal of Molecular Sciences* 16 (2015): 27677–27706.

3. L. Gan, Y. Gan, X. Zhu, and J. Zhu, "Novel Microemulsion In Situ Electrolyte-Triggered System for Ophthalmic Delivery of Lipophilic Cyclosporine A: In Vitro and In Vivo Results," *International Journal of Pharmaceutics* 365 (2009): 143–149.

4. R. Venkatalakshmi, Y. Sudhakar, C. Madhu, and M. Varma, "Buccal Drug Delivery System Using Adhesive Polymeric Patches," *International Journal of Pharmaceutical Sciences and Research* 3, no. 1 (2012): 35–41.

5. A. Ludwig and M. V. Ooteghem, "Influence of Viscolysers on the Residence of Ophthalmic Solutions Evaluated by Slit Lamp Fluorophotometry," *S.T.P. Pharma. Science* 2 (1992): 81–87.

6. F. Abedini, M. Ebrahimi, A. H. Roozbehani, A. J. Domb, and H. Hosseinkhan, "Overview on Natural Hydrophilic Polysaccharide Polymers in Drug Delivery," *Polymers for Advanced Technologies* 29 (2018): 2564–2573.

7. F. Mottaghitalab, M. Farokhi, M. A. Shokrgozar, F. Atyabi, and H. Hosseinkhani, "Silk Fibrin Nanoparticles as Novel Drug Delivery Systems," *Journal of Controlled Release* 206 (2015): 161–176.

8. H. Hosseinkhani, *Nanomaterials in Advanced Medicine* (Weinheim, Germany: Wiley-VCH Verlag GmbH, 2019), 222.

9. H. Hosseinkhani, *Biomedical Engineering: Materials, Technology, and Applications* (Weinheim, Germany: Wiley-VCH GmbH, 2022), 320.

10. M. H. Mahdi, B. R. Conway, and A. M. Smith, "Development of Mucoadhesive Sprayable Gellan Gum Fluid Gels," *International Journal of Pharmaceutics* 488 (2015): 12–19.

11. G. D' Oria, X. Zeng, H. J. Limbach, C. Hartmann, L. Ahrn, and D. Z. Gunes, "Effect of Stirring Speed on Low Acyl Gellan Gum Fluid Gels' Rheology, Particle Morphology and Physical Ageing," *Food Hydrocolloids* 149 (2024): 109614.

12. Z. Arabpour, M. Salehi, S. An, et al., "Exploring Hydrogel Nanoparticle Systems for Enhanced Ocular Drug Delivery," *Gels* 10 (2024): 589.

13. G. Tatykhanova, V. Aseyev, M. Vamvakaki, V. Khutoryanskiy, and S. Kudaibergenov, "Ophthalmic Drug Delivery System Based on the Complex of Gellan and Ofloxacin," *Chemical Bulletin of Kazakh National University* 2 (2022): 4–12.

14. O. Dudinski, B. C. Finnin, and B. L. Reed, "Acceptability of Thickened Eye Drops to Human Subjects," *Current Therapeutic Research* 33 (1983): 322–337.

15. M. B. Sintzel, S. F. Bernatchez, C. Tabatabay, and R. Gurny, "Biomaterials in Ophthalmic Drug Delivery," *European Journal of Pharmaceutics and Biopharmaceutics* 42 (1996): 358–374.

16. M. Dubald, S. Bourgeois, V. Andrieuand, and H. Fessi, "Ophthalmic Drug Delivery Systems for Antibiotherapy. A Review," *Pharmaceutics* 10 (2018): 10.

17. I. P. Kaur and M. Kanwar, "Ocular Preparations: The Formulation Approach," *Drug Development and Industrial Pharmacy* 28 (2002): 473–493.

18. G. Rajoria and A. Gupta, "In Situ Gelling System: A Novel Approach for Ocular Drug Delivery," *American Journal of Pharm Tech Research* 2 (2012): 25–53.

19. R. R. Cassano, M. L. Di Gioia, and S. S. Trombino, "Gel-Based Materials for Ophthalmic Drug Delivery," *Gels* 7 (2021): 130.

20. A. Majeed and N. A. Khan, "Ocular In Situ Gel: An Overview," *Journal of Drug Delivery and Therapeutics* 9 (2019): 337–347.

21. I. S. Kurniawansyah, T. Rusdiana, H. A. Wahab, and A. Subarnas, "In Situ Ophthalmic Gel With Ion Activated System," *International Journal of Applied Pharmaceutics* 11, no. 4 (2019): 15–18.

22. M. Paulsson, H. Hagerstrom, and K. Edsman, "Rheological Studies of the Gelation of Deacetylated Gellan Gum (Gelrite) in Physiological Conditions," *European Journal of Pharmaceutical Sciences* 9 (1999): 99–105.

23. V. V. Khutoryanskiy, "Mucoadhesive Materials and Drug Delivery Systems," in *Mucoadhesive Materials and Drug Delivery Systems* (Chichester, UK: John Wiley & Sons, Ltd, 2014).

24. V. V. Khutoryanskiy, "Advances in Mucoadhesion and Mucoadhesive Polymers," *Macromolecular Bioscience* 11 (2011): 748–764.

25. K. Al Khateb, E. K. Ozhmukhametova, M. N. Mussin, et al., "In Situ Gelling Systems Based on Pluronic F127/Pluronic F68 Formulations for Ocular Drug Delivery," *International Journal of Pharmaceutics* 502, no. 1–2 (2016): 70–79.

26. P. Gadzi'nski, A. Froelich, B. Jadach, et al., "Ionotropic Gelation and Chemical Crosslinking as Methods for Fabrication of Modified-Release Gellan Gum-Based Drug Delivery Systems," *Pharmaceutics* 15 (2023): 108.

27. I. K. Gipson, "Distribution of Mucins at the Ocular Surface," *Experimental Eye Research* 78, no. 3 (2004): 379–388.

28. G. Tatykhanova, V. Aseyev, and S. Kudaibergenov, "Mucoadhesive Properties of Gellan and Its Modified Derivatives," *Reviews and Advances in Chemistry* 10, no. 2–3 (2020): 140–157.

29. J. W. Lee, J. H. Park, and J. R. Robinson, "Bioadhesive-Based Dosage Forms: The Next Generation," *Journal of Pharmaceutical Sciences* 89, no. 7 (2000): 850–866.

30. A. Ludwig, "The Use of Mucoadhesive Polymers in Ocular Drug Delivery," *Advanced Drug Delivery Reviews* 57 (2005): 1595–1639.

31. L. E. Agibayeva, D. B. Kaldybekov, N. N. Porfiryeva, et al., "Gellan Gum and Its Methacrylated Derivatives as In Situ Gelling Mucoadhesive Formulations of Pilocarpine: In Vitro and In Vivo Studies," *International Journal of Pharmaceutics* 577 (2020): 119093.

32. I. B. Bajaj, S. A. Survase, P. S. Saudagar, and R. S. Singhal, "Gellan Gum: Fermentative Production, Downstream Processing and Applications," *Food Technology and Biotechnology* 45 (2007): 341–354.

33. P. Khare, M. M. Chogale, P. Kakade, and V. B. Patravale, "Gellan Gum–Based In Situ Gelling Ophthalmic Nanosuspension of Posaconazole," *Drug Delivery and Translational Research* 12 (2022): 2920–2935.

34. A. J. Domb, G. Ghorbanali Sharifzadeh, V. Nahum, and H. Hosseinkhani, "Safety Evaluation of Nanotechnology Products," *Pharmaceutics* 13 (2021): 1615.

35. J. F. Bradbeer, R. Hancocks, F. Spyropoulos, and I. T. Norton, "Low Acyl Gellan Gum Fluid Gel Formation and Their Subsequent Response With Acid to Impact on Satiety," *Food Hydrocolloids* 43 (2015): 501–509.

36. S. Sharma and S. Bhattacharya, "Flow Behaviour of Gellan Sol With Selected Cations," *Journal of Food Science and Technology* 52, no. 2 (2015): 1233–1237.

37. L. Zhu, J. Ao, and L. P. Peiling, "A Novel In Situ Gel Base of Deacetylase Gellan Gum for Sustained Ophthalmic Drug Delivery of Ketotifen: In Vitro and In Vivo Evaluation," *Drug Design, Development and Therapy* 9 (2015): 3943–3949.

38. K. Reed, A. Li, B. Wilson, and T. Assamoi, "Enhancement of Ocular In Situ Gelling Properties of Low Acyl Gellan Gum by Use of Ion Exchange," *Journal of Ocular Pharmacology and Therapeutics* 32, no. 9 (2016): 1–9.

39. E. N. Ambebila, E. Santamaría, A. Maestro, J. M. Gutiérrez, and C. González, "Gellan Hydrogels: Preparation, Rheological Characterization and Application in Encapsulation of Curcumin," *Food Biophysics* 14 (2019): 154–163.

40. M. Jelkmann, C. Leichner, S. Zaichik, F. Laffleur, and A. Bernkop-Schnürch, "A Gellan Gum Derivative as In Situ Gelling Cationic Polymer for Nasal Drug Delivery," *International Journal of Biological Macromolecules* 158 (2020): 1037–1046.

41. C. Fiorica, G. Biscari, F. S. Palumbo, G. Pitarresi, A. Martorana, and G. Giammona, "Physicochemical and Rheological Characterization of Different Low Molecular Weight Gellan Gum Products and Derived Ionotropic Crosslinked Hydrogels," *Gels* 7 (2021): 62.

42. L. W. Doner, "Rapid Purification of Commercial Gellan Gum to Highly Soluble and Gellable Monovalent Cation Salts," *Carbohydrate Polymers* 32 (1997): 245–247.

43. D. M. Kirchmajer, B. Steinhoff, H. Warren, R. Clark, and M. Panhuis, "Enhanced Gelation Properties of Purified Gellan Gum," *Carbohydrate Research* 388 (2014): 125–129.

44. M. Moshirfar, K. Pierson, K. Hanamaikai, L. Santiago-Caban, V. Muthappan, and S. F. Passi, "Artificial Tears Potpourri: A Literature Review," *Clinical Ophthalmology* 8 (2014): 1419–1433.

45. G. S. Irmukhametova, G. A. Mun, and V. V. Khutoryanskiy, "Thiolated Mucoadhesive and PEGylated Nonmucoadhesive Organosilica Nanoparticles From 3-Mercaptopropyltrimethoxysilane," *Langmuir* 27 (2011): 9551–9556.

46. R. V. Moiseev, F. Steele, and V. V. Khutoryanskiy, "Polyaphron Formulations Stabilised With Different Water-Soluble Polymers for Ocular Drug Delivery," *Pharmaceutics* 14 (2022): 926.

47. H. R. Lin and K. C. Sung, "Carbopol/Pluronic Phase Change Solutions for Ophthalmic Drug Delivery," *Journal of Controlled Release* 69 (2000): 379–388.

48. N. J. Van Haeringen, "Clinical Biochemistry of Tears," *Survey of Ophthalmology* 26 (1981): 84–96.

49. R. M. Fuoss, "Viscosity Function for Polyelectrolytes," *Journal of Polymer Science* 3 (1948): 603–604.

50. R. M. Fuoss, "Errata: Viscosity Function for Polyelectrolytes," *Journal of Polymer Science* 4, no. 4 (1949): 96.

51. E. Dreveton, F. Monot, J. Lecourtier, D. Ballerini, and L. Choplin, "Influence of Fermentation Hydrodynamics on Gellan Gum Physic-Chemical Characteristics," *Journal of Fermentation and Bioengineering* 82, no. 3 (1996): 272–276.

52. Y. Gong, C. Wang, R. C. Lai, K. Su, F. Zhang, and D. Wang, "An Improved Injectable Polysaccharide Hydrogel: Modified Gellan Gum for Long-Term Cartilage Regeneration In Vitro," *Journal of Materials Chemistry* 19, no. 14 (2009): 1968–1977.

53. A. Tuwar, N. Mahajan, S. Gondkar, and R. Bachhav, "An Overview of Ophthalmic In-Situ Gel," *World Journal of Pharmaceutical Research* 12, no. 12 (2023): 421–433.

54. P. L. Destruel, N. Zeng, M. Maury, N. Mignet, and V. Boudy, "In Vitro and In Vivo Evaluation of In Situ Gelling Systems for Sustained Topical Ophthalmic Delivery: State of the Art and Beyond," *Drug Discovery Today* 22, no. 4 (2017): 638–651.

55. T. R. Thrimawithana, I. D. Rupenthal, S. A. Young, and R. G. Alany, "Environment Sensitive Polymers for Ophthalmic Drug Delivery," *Journal of Drug Delivery Science and Technology* 22 (2012): 117–124.

56. P. Tonglairoum, R. P. Brannigan, P. Opanasopit, and V. V. Khutoryanskiy, "Maleimide-Bearing Nanogels as Novel Mucoadhesive Materials for Drug Delivery," *Journal of Materials Chemistry B* 4 (2016): 6581–6587.

57. R. V. Moiseev, D. B. Kaldybekov, S. K. Filippov, A. Radulescu, and V. V. Khutoryanskiy, "Maleimide-Decorated PEGylated Mucoadhesive Liposomes for Ocular Drug Delivery," *Langmuir* 38 (2022): 13870–13879.

58. M. Davidovich-Pinhas and H. Bianco-Peled, "Methods to Study Mucoadhesive Dosage Forms," in *Mucoadhesive Materials and Drug Delivery Systems*, ed. V. V. Khutoryanskiy (Chichester, UK: John Wiley & Sons Ltd., 2014), 175–196.

Supporting Information

Additional supporting information can be found online in the Supporting Information section.

Polymers for Advanced Technologies

WILEY

polymers advanced technologies

RESEARCH ARTICLE

Preparation and Characterization of Amphoteric Polysaccharides Derived From Chitosan and Gellan Gum

Rysgul N. Tuleyeva[1,2] | Gulnur S. Tatykhanova[1,3] | Nargiz N. Gizatullina[1,3] | Daulet B. Kaldybekov[1,2] | Yuliia V. Bardadym[4] | Vladimir O. Aseyev[4] | Sarkyt E. Kudaibergenov[1]

[1]Institute of Polymer Materials and Technology, Almaty, Kazakhstan | [2]Department of Chemistry and Chemical Technology, Al-Farabi Kazakh National University, Almaty, Kazakhstan | [3]Satbayev University, Almaty, Kazakhstan | [4]Department of Chemistry, University of Helsinki, Helsinki, Finland

Correspondence: Rysgul N. Tuleyeva (risgul_93@mail.ru) | Sarkyt E. Kudaibergenov (skudai@mail.ru)

Received: 30 September 2024 | **Revised:** 30 November 2024 | **Accepted:** 3 December 2024

Funding: This work was supported by Horison 2020, 823883-H2020-MSCA-RISE-2018. Ministry of Science and Higher Education of the Republic of Kazakhstan, AP13067773.

Keywords: carboxymethylated chitosan | degree of quaternization | electrophoretic mobility | isoelectric point | polyampholyte gellan gum | rod-like gold nanoparticles | spherical gold nanoparticles

ABSTRACT

Polysaccharides such as chitosan (Ch) and gellan gum (GG) were chemically modified to produce water–soluble amphoteric polyelectrolytes. These derivatives were synthesized via carboxymethylation and quaternization reactions and characterized using techniques including ^{1}H NMR, FTIR spectroscopies, elemental analysis, potentiometric titration, and thermogravimetric analysis (TGA). The degree of quaternization of gellan gum (QGG) with trimethylammonium groups was determined to be ~38% as by ^{1}H NMR spectroscopy; ~35% based on potentiometric titration, and ~39% according to elemental analysis. Similarly, the degree of carboxymethylation of chitosan (CMCh) was calculated as ~37% according to ^{1}H NMR data, while back potentiometric titration provided a value of ~35%. The modified polysaccharides exhibited distinct isoelectric points (pH_{IEP}) as determined through electrophoretic mobility measurements and conventional viscometric analysis. The data collected from both techniques were in good agreement indicating $pH_{IEP} = 2.0–2.5$ for the modified gellan gum and $pH_{IEP} = 7.0$ for the modified chitosan. Amphoteric Ch and GG were used to stabilize spherical (AuNSs) and rod-like (AuNRs) gold nanoparticles, synthesized using "one-pot" and seed-growth methods, respectively. Dynamic light scattering (DLS) and transmission electron microscopy (TEM) confirmed particle binding to the modified polymers. The average diameters of AuNSs stabilized with QGG and CMCh were ~45 and 85 nm, respectively, whereas AuNRs stabilized by QGG and CMCh exhibited dimensions of ~50–55 nm (length) and ~12–14 nm (width). These findings suggest that amphoteric QGG and CMCh-stabilized AuNSs and AuNRs could potentially be used as effective photothermal agents for treating Ehrlich cancer cells, as previously reported by our research group (Macromolecular Chemistry and Physics, 2024, 2400128).

1 | Introduction

Recent advancements have highlighted the potential role of polysaccharide-based materials as stabilizers for gold nanoparticles (AuNPs), improving biocompatibility and therapeutic efficacy while minimizing toxicity [1–5]. The integration of nanotechnology has transformed biomedical engineering, enabling the development of polymeric nanoparticles for diverse applications, including cancer therapy [6], photothermal treatment [2, 5], and gene-silencing technologies [3, 7]. Chitosan has been extensively used in gene therapy and siRNA delivery, providing protection against enzymatic degradation and facilitating cellular uptake [1, 7]. Similarly, gellan gum has been employed in controlled drug release and as a stabilizer for AuNPs, demonstrating

enhanced cytotoxicity against cancer cells and excellent in vivo biocompatibility [2, 5]. Recently [8] it was shown that the gellan gum is a promising candidate for developing polymeric carriers with extended retention on the ocular surface, aiming to enhance the efficacy of topical ocular drug delivery systems.

Advanced polymeric systems have addressed many limitations of conventional therapies. For instance, surface-functionalized AuNPs, demonstrate remarkable efficiency by selectively targeting cancerous tissues, reducing side effects, and allowing precise heat generation under external stimuli during photothermal therapy. Additionally, gellan-based hydrogels have exhibited significant potential in tissue engineering, gene transfer, and anticancer treatments, showcasing their multifunctional application. Other natural polysaccharides, such as alginate, dextran, and chitosan, further contribute to the stability and delivery efficiency of nanocarriers, extending their applications to regenerative medicine and diagnostic imaging [3, 9–12].

Chitosan (Ch) and gellan gum (GG) are classified as polybases and polyacids, respectively, due to the presence of primary amine in Ch and carboxylic groups in GG within their macromolecular chains. These polysaccharides can be chemically modified into amphoteric polyelectrolytes. Chitosan can be modified into amphoteric forms by introducing carboxylic (or sulfo-) groups, while gellan gum can acquire amphoteric properties through the incorporation of amine (or ammonium) groups [13–24]. For instance, the conjugation of strong anionic sulfonate groups to chitosan (Ch), such as in *N*-(3-sulfopropyl) chitosan salt, is achieved by reacting Ch with 1,3-propane sultone in aqueous medium [25]. Similarly, GG is quaternized by grafting *N*-(3-chloro-2-hydroxypropyl)-trimethylammonium chloride onto the primary hydroxyl groups of gellan through nucleophilic substitution, a process conducted under alkaline conditions [16]. These modifications confer amphoteric properties to the polysaccharides, enhancing their water solubility, biocompatibility, and biodegradability. Amphoteric polysaccharides based on Ch and GG have attracted significant attention for their potential applications as bioactive materials in fields such as drug delivery, antibiofouling coatings, self-healing materials, and bio- and hemocompatible artificial organs [26, 27]. Their dual charge (positive and negative) characteristics enable interactions with diverse molecules, making these biopolymers highly versatile for biomedical and industrial applications.

Various sorption experiments have been conducted using materials including carboxymethyl chitosan based polyampholyte superabsorbents [20, 21], magnetically recyclable macroporous chitosan-*g*-poly(acrylic acid) hydrogels [28] and cryogels functionalized with aminopolycarboxylic acids. These studies were performed under both batch and fixed-bed column conditions to evaluate their efficacy in removing heavy metal ion from solutions [29]. Furthermore, carboxyethyl chitosan polyampholyte was employed in molecular dynamics (MD) simulations to investigate the structural changes of the polyampholyte in aqueous solutions. The simulations investigated how pH, temperature, and ionic strength influence the polyampholyte's structure, offering valuable molecular-level insights [19].

Chitosan and gellan gum are capable of forming interpolyelectrolyte complexes both with each other [30–32] and with other polyacids and polybases [22, 33]. Both Ch [34–38] and GG [4, 39–44] are capable of stabilizing the gold nanoparticles (AuNPs) and demonstrate potential in the treatment of Ehrlich cancer cells [5]. Recent reviews [2] have highlighted progress in designing anticancer drug delivery systems involving gellan gum, while advancements [45] include developing pH- and thermo-responsive injectable carboxymethyl chitosan hydrogels containing nanodrugs for combined chemotherapy and photothermal tumor therapy.

Despite these advancements, a review of the literature reveals that the solution properties of amphoteric derivatives of chitosan and gellan gum remain insufficiently explored. Few studies have addressed their role in stabilizing gold nanoparticles (GG) [46–48]. Nevertheless, amphoteric polysaccharides based on Ch and GG hold significant potential as platforms for advanced material development. Their ability to form stable, biocompatible hydrogels and complexes and the potential for chemical modification, make them as valuable candidates for designing next-generation biomedical devices and therapies. These polysaccharides could find applications ranging from drug delivery to photothermal cancer treatments, with future research focusing on optimization to broaden their application and improve their effectiveness.

In the present study, chitosan and gellan gum were functionalized to produce amphoteric derivatives. These modified polysaccharides were characterized using various techniques, including ^{1}H NMR, FTIR spectroscopies, thermogravimetric analysis (TGA), elemental analysis, potentiometric and conductimetric titrations, and viscosity measurements. Spherical (AuNSs) and rod-like (AuNRs) gold nanoparticles were synthesized via "one-pot" and seed-growth methods in aqueous media and stabilized with polyampholyte chitosan and gellan gum. The nanoparticles were subsequently characterized for their size and morphology. The application of biocompatible and nontoxic amphoteric polysaccharides for coating and stabilizing AuNSs and AuNRs is expected to enhance the stability of colloidal gold nanoparticles in aqueous solutions. This approach holds promise for developing effective photothermal agents for cancer therapy.

2 | Materials and Methods

2.1 | Materials

Chitosan (Ch; commercial low molecular weight, M_n 65,200 Da determined using a GPC), monochloroacetic acid (99%), 2-Propanol (99.9%) and (3-chloro-2-hydroxypropyl) trimethyl-ammonium chloride (CHPTMAC) were purchased from Sigma-Aldrich (Gillingham, UK). Before use, Ch was dissolved in 0.1 M HCl, stirred overnight, vacuum filtered through a PTFE membrane disc filter with Ø 47 mm and 1 μm pore size to remove insoluble residual chitin particles. Ch solution was then purified by dialysis against distilled water and lyophilized. Gellan gum (GG) was purchased from Zhejiang DSM Zhongken Biotechnology Co. Ltd. (China). GG was purified and fractionated by ultrasonic treatment as described in our previous report [8, 49]. The viscosity-average molecular weight (M_v) of GG was determined using the Mark-Kuhn-Houwink equation in 0.025 M tetramethyl-ammonium

chloride $[\eta] = 7.48 \times 10^{-3}\ M_w^{0.91}$ [50] and yielded M_v 6.43×10^5 Da. Deuterium oxide (D_2O, 99.9% D, Eurisotop, France) and deuterated trifluoroacetic acid (99.5 atom % D, Sigma-Aldrich, USA) were used in NMR experiments. A standard aqueous solution of tetrachloroauric acid ($HAuCl_4$) with a concentration of 100 mg/mL, cetyltrimethylammonium bromide (CTAB, 99%), sodium borohydride ($NaBH_4$, 98.5%) and ascorbic acid were purchased from Sigma–Aldrich (Germany). Dialysis tubing with a molecular weight cut-off of 12–14 kDa was purchased from Sigma–Aldrich (USA). Distilled water was used in all experiments involving aqueous solutions.

2.2 | Synthesis of Carboxymethylated Chitosan (CMCh)

Chitosan was first pre-treated by immersing 2 g of the sample in 50 mL of 40% NaOH solution overnight to produce alkalized chitosan [51]. The pre-treated chitosan was then filtered and subsequently dissolved in 25 mL of 50% isopropanol with continuous stirring for 30 min. Separately, 5 g of monochloroacetic acid was dissolved in 5 mL of 50% isopropanol, and this solution was added dropwise to the chitosan solution. The reaction mixture was stirred at room temperature for 10 h, followed by dialysis for 2–3 days against distilled water, and then frozen for 24 h. The resulting product CMCh was lyophilized, collected as a powder and stored in a dry place until further use.

2.3 | Synthesis of Quaternized Gellan Gum (QGG)

In order to synthesize quaternized gellan gum (QGG), 0.5 g of fractionated gellan was dispersed in 100 mL of distilled water with stirring for 2 h to ensure complete dissolution. A solution of CHPTMAC in 50 mL of 1 M NaOH was then added dropwise to the gellan gum solution at 50°C, maintaining a QGG/CHPTMAC molar ratio of 1:10 [16]. The reaction mixture was kept at 50°C overnight. To stop the quaternization reaction, 37% HCl was added to adjust the pH to 5.5. The resulting product was purified by dialysis using a cellulose membrane against distilled water until a neutral pH was achieved, ensuring the removal of unreacted compounds. Finally, the purified QGG was freeze-dried and stored in a dry place until further use.

2.4 | Synthesis of AuNSs and AuNRs

Spherical gold nanoparticles (AuNSs) stabilized with gellan gum (GG) and quaternized gellan gum (QGG) were synthesized using a "one-pot" approach, as described [5]. Briefly, a mixture containing polymer solutions, 5 mL of $HAuCl_4$ (100 mg/mL), and 4 mL of 0.5 M KOH were combined, stirred, and heated up to 100°C for 3–5 min in an Anton Paar Monowave 50 microwave reactor (Graz, Austria) equipped with temperature and time controllers. The reaction produced solutions that changed color from yellow to dark red or purple, indicating the successful formation of AuNSs. The pH of the initial solution, which was 12, reduced to pH 8 following the dialysis against deionized water.

Chitosan-gold nanoparticles were synthesized following the procedure described by Huang, Yuan, and Yang [52]. Initially, 20 mg of chitosan was dissolved in 10 mL of 1% acetic acid to yield a 2 mg/mL solution. The mixture was vortexed until fully dissolved and then stored overnight. Subsequently, 2 mL of this solution was filtered through a 0.22 μm polyethersulfone (PES) syringe filter and mixed with 1 mL of 10 mM $HAuCl_4$ solution under vigorous stirring for 30 min. A freshly prepared 0.4 mL of cold 100 mM $NaBH_4$ (used as a reducing agent) was then gradually added, resulting in a rapid color change from yellow to wine-red, indicating the formation of gold nanoparticles. The reaction was allowed to continue with stirring for an additional 2 h to complete the process. Chitosan-gold nanoparticles were purified using the dialysis against deionized water (5 L; water changed 8 times).

In order to synthesize gold nanorods (AuNRs), the seed-mediated growth method was employed [4, 5]. Initially, a solution consisting of 5 mL of 0.2 M CTAB was mixed with 5 mL of 0.5 mM $HAuCl_4$ and stirred. Subsequently, 0.6 mL of chilled 0.01 M $NaBH_4$ was added, producing a brownish-yellow solution that contained gold nanoseeds. In parallel, another solution composed of CTAB (0.2 M; 30 mL), $AgNO_3$ (4 mM; 1.5 mL), and $HAuCl_4$ (1 mM; 30 mL) was gently mixed, and 0.42 mL (78.8 mM) ascorbic acid was introduced. Ascorbic acid served as a mild reducing agent, causing the color of the growth solution to change from dark yellow to colorless. Finally, the initial seed solution (72 μL) was added to the growth solution, and the mixture was allowed to incubate at 30°C overnight. Consequently, a crimson solution containing gold nanorods (AuNRs) was generated. To remove by-products and excess CTAB, the solution underwent centrifugation at 10,650 rpm for 30 min using an Eppendorf 5810R centrifuge (Tuttlingen, Germany). The resulting precipitate was then re-dispersed in 3 mL of deionized water and centrifuged again at 10,650 rpm for 15 min. After repeating the washing cycle three times, the AuNRs were re-dispersed and stabilized in 5 mL of the designated polymer solutions and then dialyzed against deionized water using a cellulose membrane.

2.5 | Characterization

2.5.1 | Nuclear Magnetic Resonance (^{1}H NMR) Spectroscopy

^{1}H NMR spectra of the samples were recorded using a 500 MHz Bruker Avance III NMR spectrometer (Bruker UK Ltd., Coventry, UK). The samples were prepared at 10 mg/mL. GG and QGG samples were dissolved in D_2O, while Ch and CMCh samples were dissolved in D_2O by adding a few drops of deuterated trifluoroacetic acid (TFA-d, 99%).

2.5.2 | Fourier Transform Infrared (FTIR) Spectroscopy

FTIR spectra of the samples were recorded using an IRTracer-100 Shimadzu FTIR spectrometer (Kyoto, Japan). The spectra were collected from an average of 16 scans between 4000 and 500 cm^{-1}, employing the absorbance mode with a spectral resolution of 4 cm^{-1}. The spectra were plotted and analyzed using Origin 2022 (version 9.9.0.225) software (OriginLab Corporation, MA, USA).

2.5.3 | Potentiometric Titration

Potentiometric titration of chlorine ions from QGG – $[N^+(CH_3)_3Cl^-]$ groups was performed with $AgNO_3$ solution using an automatic titrator Metrohm 905 Titrando (Metrohm AG, Herisau, Switzerland). A total of 10 mg of QGG was dissolved in 20 mL distilled water and 0.1 M $AgNO_3$ aqueous solution was added dropwise into QGG solution with 0.01 mL increment. The degree of quaternization (DQ) was calculated using the following equation:

$$\mathrm{DQ} = \frac{n_{\text{quaternary ammonium groups}}}{n_{\text{polymer repeating units}}}. \quad (1)$$

$$n_{\text{quaternary ammonium groups}} = C_{AgNO_3} \times V_{AgNO_3}.$$

$$n_{\text{polymer repeating units}} = \frac{m_{\text{polymer}}}{M_{\text{repeating unit}}},$$

where, C is a concentration of $AgNO_3$ (mol/L), V is a volume of $AgNO_3$ (L), m is a mass of quaternized gellan gum used (g), and M is a molecular weight of the repeating unit of gellan gum (g/mol).

2.5.4 | Elemental Analysis

Elemental analysis was conducted to determine the composition of the modified gellan gum in comparison to GG. The measurements were performed using a Vario MICRO cube instrument (Elementar Analysensysteme GmbH, Hanau, Germany), with sulfanilamide as the calibration standard. Three samples, each approximately 2 mg of dry polymer, were analyzed and the mean average values were reported.

2.5.5 | Thermogravimetric Analysis (TGA)

Thermogravimetric analysis (TGA) was performed using a NETZSCH STA 449 F3 Jupiter instrument (Selb, Germany). Samples (8–10 mg) were heated from 25°C to 600°C at a heating rate of 10°C/min in a nitrogen atmosphere. Thermograms were plotted and analyzed using Origin 2022 software.

2.5.6 | Determination of the Isoelectric Point (IEP) by Electrophoretic and Viscometric Measurements

The isoelectric points of CMCh and QGG were determined using a conventional viscometric technique and electrophoretic mobility analysis using a Zetasizer Nano-ZS90 instrument (Malvern Instruments, Malvern, UK), by varying pH levels of the solutions. All measurements were conducted in triplicate at 25°C. Briefly, 0.05 g of QGG was prepared in 10 mL of deionized water at room temperature and stirred until complete dissolution. Simultaneously, 0.05 g of CMCh was dissolved in 10 mL of 0.03 M HCl. The specific viscosity measurements were carried out using an Ostwald-type capillary viscometer (capillary diameter of 0.86 mm) and calculated as the ratio of flow time (t) to that of water (t_0):

$$\eta_{sp} = \frac{t - t_0}{t_0}. \quad (2)$$

The isoelectric point ($IEP_{viscometry}$) for each sample was determined by measuring the pH at which the polymer solution reached its lowest viscosity, indicating that the net charge of the macromolecules is close to zero at that specific pH.

In electrophoretic mobility experiments, a refractive index of 1.33 and an absorbance of 0.01 were used for all measurements in zeta-potential mode at 25°C. Viscosity (0.8872 cP) and refractive index (1.33) of water served as dispersant parameters. Each sample was analyzed five times, and the results were processed using the Smoluchowski model (Fκa = 1.50) to calculate the mean electrophoretic mobility ± standard deviation values. The electrophoretic mobility versus pH curve was generated for each test sample and the point at which the curve intersects zero mobility was considered as an IEP_{EM} [53].

2.5.7 | Dynamic Light Scattering (DLS)

Dynamic light scattering (DLS) measurements were performed using a Zetasizer NanoZS90 instrument (Malvern Instruments, Malvern, UK). All solutions were filtered through 0.45 μm PES syringe filters. The reported values are intensity-weighted diameters, calculated as averages of repetitive measurements at 25°C. Similar refractive index and absorbance values were used as in the electrophoretic mobility measurements mentioned above.

2.5.8 | Transmission Electron Microscope (TEM)

The morphology of the particles was examined using a Hitachi S-4800 FESEM (Tokyo, Japan). For TEM imaging, dilute dispersions (5 μL) were placed on carbon-coated copper grids with a mesh size of 200 square micrometers and air dried prior to imaging.

3 | Results and Discussion

3.1 | Synthesis and Characterization

Following purification by dialysis and lyophilization, modified polymers were then characterized using ^{1}H NMR spectroscopy.

The ^{1}H NMR spectra of both Ch and CMCh recorded in CCl_3COOH/D_2O showed a distinct methyl characteristic peak at 2.01 ppm from – NHCO**CH_3** methyl protons, as well as a singlet at 3.12 ppm (H2) and multiplets from 3.50 to 3.90 ppm (H3–H6) corresponding to the methine protons in polysaccharide ring (Figure 1). Additionally, new signals appeared at 3.30; 4.10 and 4.24–4.30 ppm in CMCh, which were attributed to the protons of the – O – **CH_2** – COO^- group substituted at the C2 amino group; the C6 and C3 hydroxyl groups of Ch, respectively. These findings are in good agreement with previous observations [54]. The signal at 4.10 ppm was significantly stronger, while that at 3.30 ppm was lower, suggesting that carboxymethylation occurred mainly at the

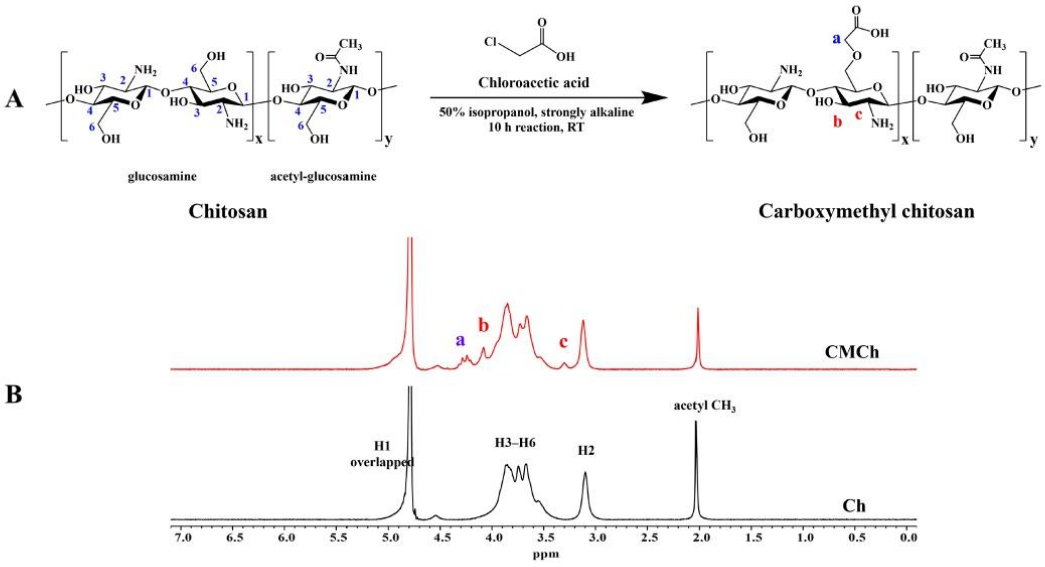

FIGURE 1 | Synthesis and characterization of carboxymethyl chitosan (CMCh). (A) Schematic illustration of the carboxymethylation reaction. Please note that the schematic structure shows only one possibility of a chloroacetic acid reaction with the hydroxyl groups (which are the reactive sides) at C6 in the polysaccharide backbone. In reality, it could also react with any primary amino (C2) and/or hydroxyl (C3) groups present in chitosan and (B) ^{1}H NMR spectra of chitosan (Ch) and carboxymethyl chitosan (CMCh) recorded in CCl_3COOH/D_2O.

C3 and C6 hydroxyl (or O-carboxymethylation), but much less at the amino C2 groups, that is, *N*-carboxymethylation. Perhaps this depends on different reaction conditions that favor obtaining either O-carboxymethyl or *N*-carboxymethyl chitosan [51, 55]. Nevertheless, the chitosan backbone allows carboxymethylation at three potential locations: C6-O-, C3-O-, and C2-N-. Based on ^{1}H NMR analysis, it was observed that the carboxymethylation preferentially occurs at hydroxyl groups, specifically favoring the C6-O- site when the reaction temperature exceeds 20°C. As such, the synthesized CMCh includes both amino (C2-N site) and carboxymethyl (C6-O site) functional groups [14]. The degree of substitution (DS%) was calculated by integrating the corresponding peaks and using the following equation:

$$DS\% = \left\{ \frac{\frac{I_{\text{C3 and C6–substituted } (-O-CH_2-COOH)}}{4} + \frac{I_{\text{C2–substituted } (-N-CH_2-COOH)}}{2}}{I_{C2,H}} \right\} \times 100, \quad (3)$$

where, $I_{\text{C3 and C6–substituted } (-O-CH_2-COOH)}$ are the integral of the signals of methylene protons from C3 and C6 substituted $-O-\mathbf{CH_2}-COOH$ moieties, while $I_{C2,H}$ is the integral of the signal corresponding to the methine protons in the polysaccharide's glucosamine unit. Figures S1 and S2 display the ^{1}H NMR spectra of modified chitosan with corresponding peak integrals as well as the monomer, respectively.

In ^{1}H NMR spectrum of gellan gum, distinct signals can be observed: the peak at 1.30 ppm corresponds to the methyl protons of the rhamnose unit, while the peak at 4.53 ppm is assigned to the hydrogen bonded to C1 of glucose II. Additionally, the peak at 5.15 ppm is associated with the hydrogen attached to C1 of the rhamnose unit. The solvent peak (D_2O) is assigned at 4.80 ppm and chemical shifts of all protons of the tetrasaccharide repeating unit formed by glucose I, glucuronic acid, glucose II, and rhamnose can be observed in the range between 3.34 and 4.25 ppm (Figure 2). In the ^{1}H NMR spectrum of QGG, a new peak at 3.22 ppm is identified, which corresponds to the vibrations of three pairs of protons from $-\left[N^+(\mathbf{CH_3})_3\right]$ group. The degree of quaternization (DQ%) for QGG was quantified by integrating the corresponding peaks and using the following equation:

$$DQ\% = \left\{ \frac{I_{-N(CH_3)_3}}{I_{CH_3\ (\text{rhamnose})}} \times \frac{3}{9} \right\} \times 100, \quad (4)$$

where, $I_{-N(CH_3)_3}$ represents the integral of the signal corresponding to the methyl protons of newly substituted cationic *N,N,N*-trimethyl moiety observed at 3.22 ppm, while $I_{CH_3\ (\text{rhamnose})}$ refers to the integral of the signal associated with the methyl protons of the rhamnose unit that appeared at 1.30 ppm. Figures S3 and S4 depict the ^{1}H NMR spectra of modified gellan gum with corresponding peak integrals and the monomer, respectively.

The FTIR spectra of chitosan and CMCh are illustrated in Figure 3A. In the FTIR spectrum of chitosan, strong characteristic peaks corresponding to the amino groups were observed at approximately 3328 (O—H stretch and N—H stretch), 1651 cm^{-1} (C═O stretching, amide I), and 1375 cm^{-1}.

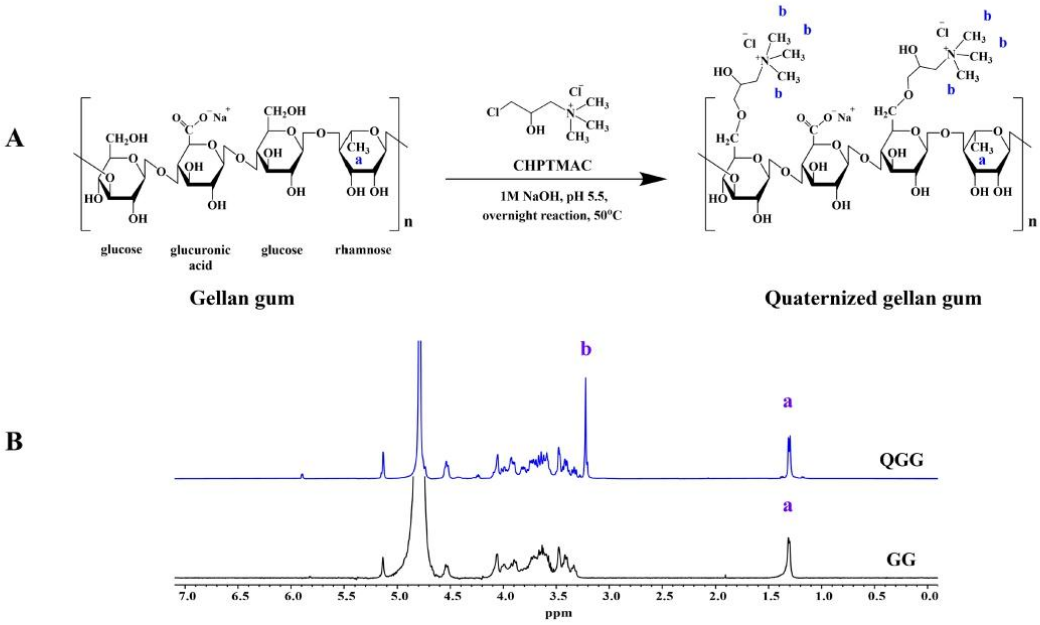

FIGURE 2 | Synthesis and characterization of quaternized gellan gum (QGG). (A) Schematic illustration of the quaternization reaction. Please note that the schematic structure illustrates only one possibility of (3-chloro-2-hydroxypropyl)trimethyl-ammonium chloride (CHPTMAC) reaction with $-CH_2-OH$ groups of gellan gum. In reality, it could react with any hydroxyl groups present in gellan gum and (B) ^1H NMR spectra of gellan gum (GG) and quaternized gellan gum (QGG) recorded in D_2O at 60°C.

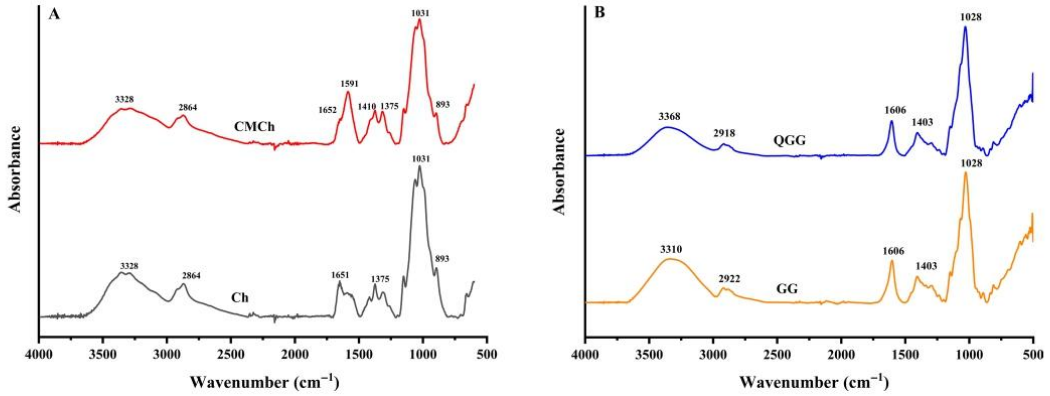

FIGURE 3 | The FTIR spectra of (A) chitosan (Ch) and carboxymethyl chitosan (CMCh); and (B) gellan gum (GG) and quaternized gellan gum (QGG).

Additionally, peaks associated with the polysaccharide structure were identified at 1153 cm^{-1} (C—H stretching) and 1031 cm^{-1} (C—O stretching) [56]. In the CMCh spectrum, the broad band observed at 3328 cm^{-1} is attributed to the vibrational stretching of the O—H bonds and the symmetric stretching vibration of C═O bonds within —COOH groups, which both overlapped in that region. This peak, along with the peak at 1591 cm^{-1}, which originates from the symmetric stretching vibration of the $-COO^-$ group, substantiates the incorporation of carboxymethyl groups onto the chitosan backbone. Additionally, two bands at 1652 and 1410 cm^{-1}, assigned to NH_3^+, suggest that carboxymethylation has occurred at the OH positions. The peaks observed at 1375 and 1309 cm^{-1} correspond to the symmetric angular deformation of C—H bonds and the C—N stretching vibration (amide III), respectively. The peak at 2864 cm^{-1} is attributed to the C—H stretching vibration, while the stretching vibration of the C—O bonds in the $-OCH_2COOH$ group accounts for the peak at

1260 cm^{-1}. Peaks in the range between 1031 and 893 cm^{-1} are attributed to the vibrations of C—O and C—O—C bonds, along with other bonds constituting the polysaccharide chain [57]. Thus, analysis of FTIR spectra confirms the successful introduction of carboxymethyl groups onto the chitosan backbone.

The modification of gellan gum was further confirmed using FTIR spectroscopy (Figure 3B). FTIR analysis of spectra clearly revealed key absorbance peaks: the spectrum of pristine gellan gum displays a broad band (3000–3600 cm^{-1}) with a maximum peak at 3310 cm^{-1} corresponding to O—H stretching vibrations, and a band at 2922 cm^{-1}, which is attributed to asymmetric and symmetric C—H stretching vibrations in CH— and CH_2— groups. Additionally, peaks at 1606 and 1403 cm^{-1} are assigned to the asymmetric and symmetric vibrations of the $-COO^-$ group, respectively. The peak at 1028 cm^{-1} indicates the characteristic vibration of the C—O—C bond within the rhamnose ring or the β-(1–4) glycosidic linkage [58, 59], with the additional C—O bond from the incorporated cationic hydroxypropyl group overlapping in the 1000–1150 cm^{-1} region and an increase in peak intensity. A characteristic absorption band (symmetric bending) typical for C—H of the methyl groups in the quaternary ammonium should appear at ~1450–1480 cm^{-1} in modified gellan gum spectrum; however, in our case, it was overlapped by the broader signals of the $-COO^-$ group [60]. Nevertheless, the incorporation of the cationic moiety caused shifts in the hydroxyl bands of gellan gum to higher frequencies (3368 cm^{-1}). Overall, similar infrared spectra were acquired for QGG and GG, suggesting the limitations of FTIR spectroscopy in confirming the effectiveness of gellan gum derivatization. However, elemental analysis confirmed the presence of amine groups in QGG.

TABLE 1 | Elemental analysis of gellan gum (GG) and quaternized gellan gum (QGG).

	Element content (wt.%)			
Biopolymer	**Nitrogen**	**Carbon**	**Hydrogen**	**Sulfur**
GG	0.05	36.31	5.60	0.00
QGG	1.14	38.07	6.67	0.00

Abbreviations: GG: gellan gum; QGG: quaternized gellan gum.

TABLE 2 | Degree of quaternization of GG and carboxymethylation of chitosan (CMCh).

Method	**^{1}H NMR**	**Elemental analysis**	**Potentiometric titration**
QGG (%)	38	38.87	34.55
CMCh (%)	37	—	35.20

Abbreviations: CMCh: carboxymethylated chitosan; QGG: quaternized gellan gum.

The results of the elemental analysis for both GG and QGG are displayed in Table 1. The analysis reveals a trace amount of nitrogen (0.05 wt.%) in pristine GG is likely attributed to the residual cell proteins or nutrients from the fermentation process [61]. In contrast, the nitrogen content in modified gellan gum is notably significant. This increase substantiates the successful grafting of quaternary ammonium groups onto the gellan gum backbone. The degree of quaternization (DQ) determined according to Equation (1) is 34.55%.

Table 2 summarizes the degrees of modification for QGG and carboxymethylated chitosan (CMCh), as determined by ^{1}H NMR spectroscopy, elemental analysis, and potentiometric titration. The data indicate that all methods yield results that are in satisfactory agreement. Degrees of substitution calculated based on analysis of ^{1}H NMR spectra of modified polymers are in good agreement with the values reported in the literature [16, 62].

Figure 4A presents the thermogravimetric analysis (TGA) thermograms of chitosan and CMCh. The TGA curve for chitosan displays two distinct stages of weight loss within the temperature range of 28°C–490°C. The initial weight loss, occurring between 28°C and 124°C, is attributed to the evaporation of absorbed water, accounting for ~5% (0.5 mg) of the total weight. The primary degradation of chitosan commences at 250°C and concludes around 490°C, resulting in a total weight loss of about

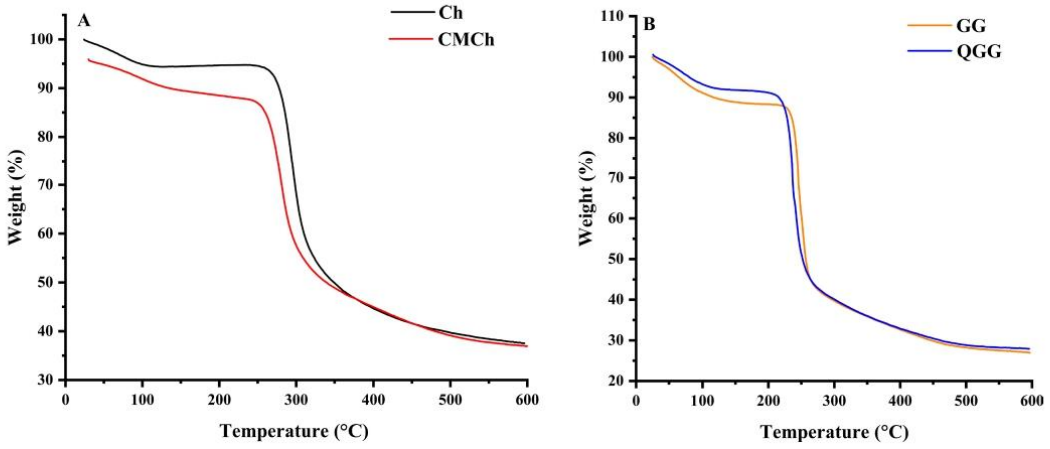

FIGURE 4 | Thermogravimetric analysis of Ch, CMCh (A), GG and QGG (B).

55% (5.5 mg). In the case of CMCh, the TGA curve similarly exhibits two distinct stages of weight loss (Figure 4A). The initial stage, occurring between 40°C and 159°C, is likely due to the loss of adsorbed water with 9% weight loss (1.0 mg). The subsequent stage of decomposition, spanning from 232°C to 447°C, corresponds to thermal degradation and results in a weight loss of approximately 54% (5.9 mg). These results suggest a slight reduction in the thermal stability of CMCh compared to pure chitosan. Similar results were reported for other chitosan derivatives [63, 64].

Figure 4B shows the TGA results for both gellan gum and quaternized gellan gum. All samples exhibit a weight loss within the temperature range from room temperature up to ~100°C resulting in evaporation of absorbed or bound water with around 11% (1.08 mg). The initial degradation temperature and the temperature at which the main degradation phase occurs are slightly lower for the modified gellan gum compared to unmodified gellan gum, shifting from 247°C to 237°C with a total weight loss of 58.53% (5.07 mg). This observation is in good agreement with the findings reported for similar quaternized polysaccharides [65, 66].

3.2 | The Isoelectric Points (IEP) of Polymers

CMCh and QGG possess both carboxylic and amino groups, which enable them to exhibit anionic, cationic, or quasi-electroneutral properties depending on the pH of the solution. In acidic and basic environments, the macromolecules of CMCh and QGG are either positively or negatively charged. At the isoelectric point (IEP), these polymers achieve a quasi-electroneutral state due to the balanced compensation of opposing charges. At this point, the polyampholyte chains adopt their most compact conformation, resulting in a minimum in solution viscosity [67].

In this study, the IEPs or isoelectric pH values (pH_{IEP}) of both CMCh and QGG macromolecules were determined using electrophoretic mobility measurements and by analyzing changes in solution viscosity as a function of pH. Aqueous solutions (0.5% w/v) of CMCh and QGG were titrated by adding drops of 0.03 M HCl or 0.02 M NaOH, and the resulting pH changes were recorded using a pH meter. The IEPs of the samples were estimated by determining the pH at which the electrophoretic mobility curve intersected zero (Figure 5) or at which the polyampholyte solution reached a minimum specific viscosity (Figure 6). It was observed that the IEP_{EM} of CMCh and QGG are pH 7.0 and pH 2.0, respectively (Figure 5). The IEP determined by viscometric technique for CMCh is pH 7.0 (Figure 6A), which is in good agreement with the value obtained through electrophoretic mobility measurement. The $IEP_{viscometry}$ of QGG was found to be pH ~2.50 (Figure 6B). This discrepancy is likely attributed to the measurement accuracy of each technique. It should be noted that the pH-dependent electrophoretic mobility of GG remains negative across the entire pH range due to the presence of only carboxylic groups. In contrast, chitosan (Ch), which contains amine groups, exhibits a zero crossing of electrophoretic mobility at pH ~8.60, remaining negative at higher pH levels (Figure 5). This behavior of Ch has been previously explained in literature [68] by the

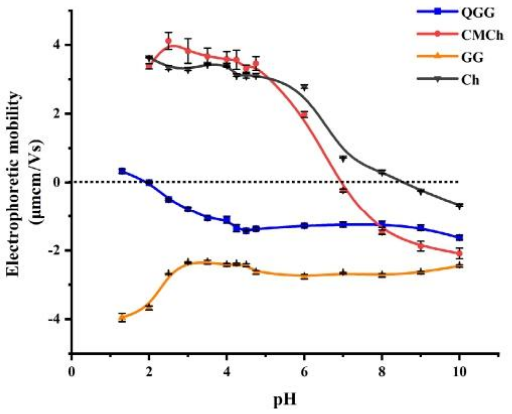

FIGURE 5 | Electrophoretic mobility of GG, QGG, Ch, and CMCh as a function of solution pH.

fact that the protonated $-NH_2$ groups are significantly compensated by the accumulation of counterions in the diffusive part of the electric double layer in line with Manning theory [69] and experimental studies on poly(*N,N*-dimethyl-*N,N*-diallylammonium chloride) [70] and poly-L-lysine [71]. Our findings are consistent with the explanations provided by the studies observed in [68].

The observed difference in the isoelectric points (IEP) between quaternized gellan gum (pH ~2.0–2.5) and carboxymethyl chitosan (pH ~7.0) can be explained by the varying ratios of acidic and basic groups in each modified polysaccharide. QGG, with approximately 62% carboxylic groups, exhibits an IEP at a lower pH. In contrast, CMCh has a greater proportion of amine groups (~63%), resulting in a higher IEP. This behavior is consistent with established findings that the IEP of polyampholytes shifts to lower pH as the content of acidic groups increases, and to higher pH with more basic groups present in the macromolecular chain [72, 73].

As anticipated, the difference between the IEP values determined by electrophoretic mobility and viscometry likely arises from the fundamental principles underlying each technique. Electrophoretic mobility, or electrophoresis, is generally more precise for IEP determination as it directly measures the net charge of the macromolecule. For instance, in a quasi-neutral state, the polyampholyte macromolecule does not migrate toward either electrode under an applied electric field, allowing for an accurate determination of zero charge. In contrast, the viscometric method observes changes in solution viscosity, that is, changes in the hydrodynamic volume, which vary with the macromolecular conformation. Nonetheless, both techniques place the IEP of QGG between pH 2.0 and 2.5, demonstrating good overall agreement.

The relationship between the hydrodynamic size of polyampholytes and pH is depicted in Figure 6. For CMCh, the minimum hydrodynamic size of macromolecules is observed at pH 7.0, which is in good agreement with the results obtained

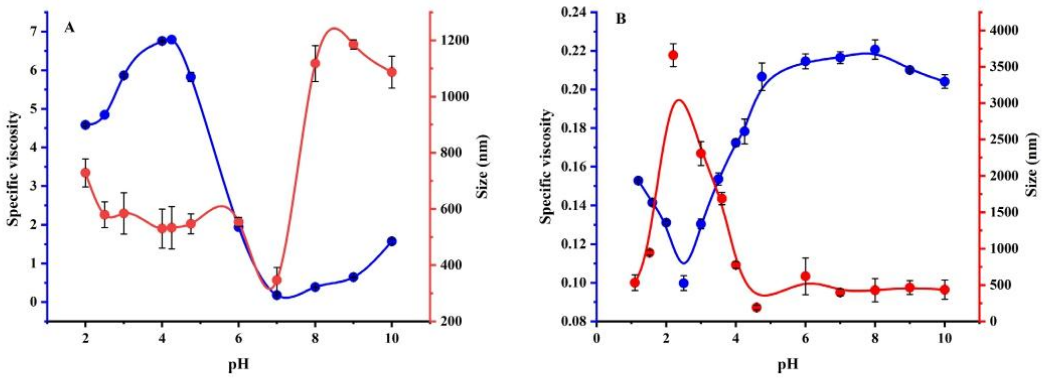

FIGURE 6 | Determination of the IEP and hydrodynamic size of CMCh (A) and QGG (B) by viscometric and DLS techniques.

TABLE 3 | Size and zeta-potential values of polymer-protected AuNSs determined by DLS at pH 6.50–7.0.

Type of polymer	Concentration of polymer (% w/v)	Mean diameter (nm)	PDI	Zeta-potential (mV)
Ch	0.2	99 ± 2	0.442	42 ± 2
CMCh	0.2	85 ± 1	0.414	40 ± 1
GG	0.5	170 ± 2	0.402	−15 ± 1
QGG	0.5	45 ± 2	0.318	−25 ± 2

Note: Data are expressed as mean ± standard deviation values of five measurements ($n = 5$).
Abbreviations: Ch: chitosan; CMCh: O-carboxymethyl chitosan; GG: gellan gum; PDI: polydispersity index; QGG: quaternized gellan gum.

from electrophoretic and viscosity measurements. At an IEP, the polyampholyte chains reach their compact conformation due to electrostatic attractions between oppositely charged functional groups [73]. Deviations from the IEP lead to changes in the overall charge of the polyampholyte, causing it to become either positively or negatively charged. This results in increased electrostatic repulsion between uniformly charged groups and, consequently, an expansion of macromolecular chains. In contrast, for QGG the average hydrodynamic size of the macromolecules sharply increases near the IEP. This phenomenon is likely attributed to the aggregation of high molecular weight QGG (~10^5 Da) around the IEP due to intra-macromolecular complexation of the polyampholytes [74] and no precipitation of polymer from the solution was detected.

3.3 | Stabilization of Gold Nanoparticles (AuNPs) by Amphoteric Gellan Gum and Chitosan

A water-soluble amphoteric chitosan derivative, 6-O-carboxylmethyl chitosan, which possesses a nearly equivalent number of cationic and anionic functional groups, was used as a pH-sensitive template for the reversible assembly of gold nanoparticles (AuNPs) [46, 47]. Aggregation of AuNPs was observed at extreme pH values of 2.0 and 12.0, resulting in aggregates with markedly different morphologies. TEM microphotographs at pH 9.60 reveal that the average diameter of the spherical nanoparticles is ~5 nm. At pH 12.0, the AuNPs aggregate into needle-like structures, with particle–particle distances within these aggregates measuring less than 3 nm. Conversely, at pH 2.0, the gold nanoparticles form larger, more densely packed aggregates. The morphology of these aggregates is more regular, with a length of 360 nm and a width of 150 nm, displaying symmetrical angles at the cluster ends. Depending on the pH level, the color of the colloidal dispersions changes from purple at pH 2.0 to pink at pH 9.60, and pale purple at pH 12.0. The reversibility of these changes upon pH alteration was confirmed by a shift in the plasmon resonance UV-absorption band, which moved from 526 nm (at pH 2.0) to 510 nm (at pH 9.60), and then to 515 nm (at pH 12.0).

The chemical modification of chitosan with phthalimide moieties results in the synthesis of two water-soluble bisphthalimides (BPIs), specifically, *N,N′*-(*1*,3-phenylene)bis(phthalimide-5-carboxylic acid) (BPI-1) and *N,N′*-(1,4-phenylene)bis(phthalimide-5-carboxylic acid) (BPI-2). These bisphthalimides, with relatively low molecular weights, are effective in the green synthesis of gold nanoparticles (AuNPs) [48]. ^{1}H NMR, FTIR, UV/Vis spectroscopy analyses and TEM imaging demonstrate that the BPIs can reduce gold ions and stabilize AuNPs in colloidal solutions. Consequently, the AuNPs exhibited a quasi-spherical shape, with average diameters of 3 nm for BPI-1 and 12 nm for BPI-2. The reaction to produce AuNPs was most rapid with the polyampholyte derivative of chitosan, completing in 5 min, which is attributed to the high number of oxidizable groups present in the polymer structure and its high molecular weight. The average size of AuNPs stabilized with this polyampholyte was 10 nm. Thus, polyampholyte derivatives of chitosan can effectively stabilize gold nanoparticles across a broad pH range, producing quasi-spherical particles with average diameters of 3, 5, 10,

TABLE 4 | Aspect ratio (measured using TEM) and zeta-potential values of AuNRs synthesized and stabilized using Ch, CMCh, GG, and QGG at pH 6.50–7.0.

Type of polymer	Concentration of polymer (% w/v)	Average length (nm)	Average width (nm)	Aspect ratio	Zeta-potential (mV)
Ch	0.5	55 ± 4	14 ± 2	4 ± 1	70 ± 1
CMCh	0.5	54 ± 3	14 ± 1	4 ± 1	17 ± 2
GG	0.5	50 ± 6	13 ± 3	4 ± 1	−31 ± 2
QGG	0.5	51 ± 3	12 ± 2	4 ± 1	−25 ± 2

Note: Data are presented as mean ± standard deviation of five measurements ($n = 5$).
Abbreviations: Ch: chitosan; CMCh: O-carboxymethyl chitosan; GG: gellan gum; QGG: quaternized gellan gum.

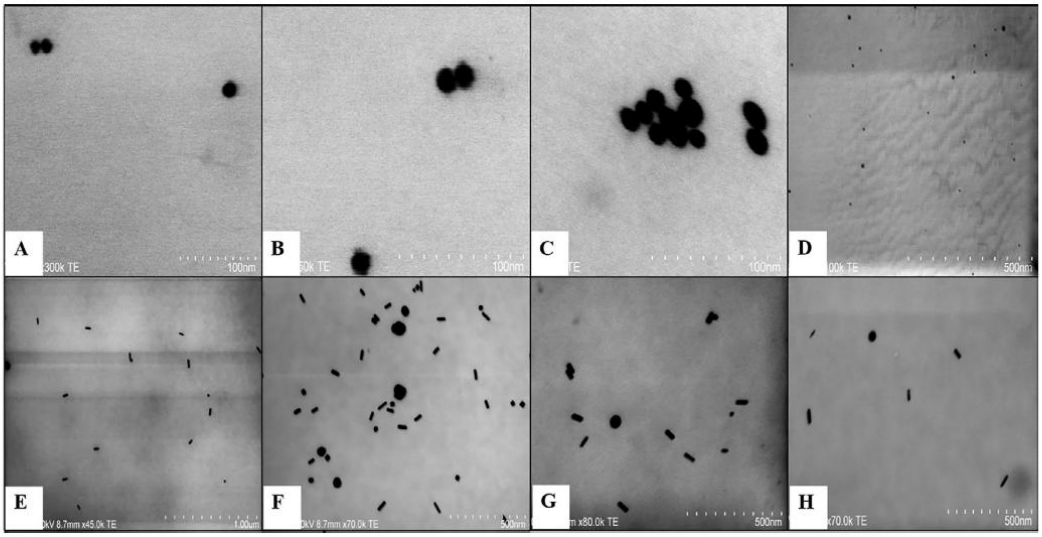

FIGURE 7 | TEM microphotographs of AuNSs and AuNRs stabilized using Ch (A and E), CMCh (B and F), GG (C and G), and QGG (D and H).

and 12 nm, as well as rod-like aggregates measuring 360 nm in length and 150 nm in width (aspect ratio of 2.4).

In this study, spherical and rod-shaped gold nanoparticles were synthesized and subsequently stabilized by QGG and CMCh. Their average hydrodynamic sizes and zeta-potential values of are summarized in Tables 3 and 4. The mean size and zeta-potential values of the spherical gold nanoparticles (AuNSs) were measured using dynamic light scattering (DLS). Generally, all spherical gold nanoparticles exhibited polydispersity. To evaluate the surface charge of the nanoparticles, the zeta-potential values of the various AuNPs were determined, as detailed in Table 3. Figure 7 displays the representative TEM microphotographs for AuNSs and AuNRs stabilized by Ch, GG, CMCh, and QGG. For the gold nanorods (AuNRs) the aspect ratio, that is, length/width, was ≈4 ± 1.

In summary, the AuNPs stabilized by amphoteric polysaccharides described in this study may serve as a potential platform for the effective photothermal therapy of Ehrlich cancer cells. This prospective application extends our previous research [5].

4 | Conclusion

Amphoteric polysaccharides derived from chitosan and gellan gum were synthesized using a procedure involving monochloroacetic acid and (3-chloro-2-hydroxypropyl) trimethylammonium chloride as modification agents. The resulting polysaccharides, namely carboxymethylated chitosan (CMCh) and quaternized gellan gum (QGG), were characterized using various physicochemical techniques. The degree of quaternization for QGG and the degree of carboxymethylation for CMCh were determined to be ~38% and ~37%, respectively. Both QGG and CMCh demonstrated polyampholytic behavior in aqueous solutions, with isoelectric points (IEPs) observed at pH 7.0 for CMCh and pH 2.0–2.5 for QGG. Spherical (AuNSs) and rod-like (AuNRs) gold nanoparticles were synthesized in the presence of these polysaccharaides through "one-pot" and seed-growth methods, respectively. Dynamic light scattering (DLS) and transmission electron microscopy (TEM) analyses revealed that the average diameter of AuNSs stabilized with modified polymers (QGG and CMCh) were determined to be ~45 and~85 nm, respectively, whereas the average dimensions of AuNRs stabilized by QGG

and CMCh were ~50–55 (length) as well as ~12–14 (width). Future research will aim to evaluate the light-to-heat conversion efficiency of these gold nanoparticles stabilized by amphoteric polysaccharides. Additionally, toxicological assessments and mucoadhesive studies will be conducted to optimize the anticancer efficacy of the developed nanoparticle systems.

Acknowledgments

This research was funded by the Science Committee of the Ministry of Science and High Education of the Republic of Kazakhstan (Grant No. AP13067773) and was supported by the Horizon 2020 research and innovation program of the European Union Maria Skłodowska-Curie (grant agreement 823883-NanoPol-MSCA-RISE-2018). The authors are grateful to ALD center Finland research infrastructure (University of Helsinki) for their help with transmission electron microscope. Yuliia Bardadym is thankful to the Academy of Finland (No. 353886 and 359456 for Ukrainian researchers) for her financial support.

Conflicts of Interest

The authors declare no conflicts of interest.

Data Availability Statement

The data that support the findings of this study are available from the corresponding author upon reasonable request.

References

1. F. Abedini, M. Ebrahimi, A. H. Roozbehani, A. J. Domb, and H. Hosseinkhani, "Overview on Natural Hydrophilic Polysaccharide Polymers in Drug Delivery," *Polymers for Advanced Technologies* 29 (2018): 2564–2573.

2. S. E. Kudaibergenov, S. Xu, G. S. Tatykhanova, and G. M. Kudaibergenova, "Gellan Gum Immobilized Anticancer Drugs and Gold Nanoparticles in Nanomedicine," *Academic Journal of Polymer Science* 2 (2019): 555588.

3. H. Hosseinkhani, *Nanomaterials in Advanced Medicine* (Weinheim: Verlag GmbH & Co. KGaA, 2019).

4. Z. A. Nurakhmetova, A. N. Azhkeyeva, I. A. Klassen, and G. S. Tatykhanova, "Synthesis and Stabilization of Gold Nanoparticles Using Water-Soluble Synthetic and Natural Polymers," *Polymers (Basel)* 12 (2020): 1–15.

5. G. S. Tatykhanova, R. N. Tuleyeva, Z. A. Nurakhmetova, et al., "Polymer-Protected Gold Nanoparticles for Photothermal Treatment of Ehrlich Adenocarcinoma: In Vitro and in Vivo Studies," *Macromolecular Chemistry and Physics* (2024): 2400128, https://doi.org/10.1002/macp.202400128.

6. D. B. Kaldybekov, S. K. Filippov, A. Radulescu, and V. V. Khutoryanskiy, "Maleimide-Functionalised PLGA-PEG Nanoparticles as Mucoadhesive Carriers for Intravesical Drug Delivery," *European Journal of Pharmaceutics and Biopharmaceutics* 143 (2019): 24–34.

7. H. Hosseinkhani and A. J. Domb, "Biodegradable Polymers in Gene-Silencing Technology," *Polymers for Advanced Technologies* 30 (2019): 2647–2655.

8. G. S. Tatykhanova, R. N. Tuleyeva, N. N. Gizatullina, et al., "Characterization of Biocompatible Gellan Gum Fractions for Prolonged Retention in Ocular Drug Delivery Systems," *Polymers for Advanced Technologies* 35 (2024): e6635.

9. W. He, H. Hosseinkhani, R. Mohammadinejad, et al., "Polymeric Nanoparticles for Therapy and Imaging," *Polymers for Advanced Technologies* 25 (2014): 1216–1225.

10. M. Ghadiri, E. Vasheghani-Farahani, F. Atyabi, F. Kobarfard, F. Mohamadyar-Toupkanlou, and H. Hosseinkhani, "Transferrin-Conjugated Magnetic Dextran-Spermine Nanoparticles for Targeted Drug Transport Across Blood-Brain Barrier," *Journal of Biomedial Materials Research Part A* 105 (2017): 2851–2864.

11. A. J. Domb, G. Sharifzadeh, V. Nahum, and H. Hosseinkhani, "Safety Evaluation of Nanotechnology Products," *Pharmaceutics* 13 (2021): 1615.

12. H. Hosseinkhani, *Biomedical Engineering: Materials, Technology, and Applications* (Weinheim: Wiley-VCH GmbH, 2022).

13. M. R. Bazt, E. E. Skorikova, L. S. Vikhoreva, and L. S. Galbraikh, "Dilute Solution Properties of Carboxymethyl Ester of Chitosan," *Vysokomolekulyarnyye soyedineniya. Seriya A* 32 (1990): 805–809.

14. X. G. Chen and H. J. Park, "Chemical Characteristics of O-Carboxymethyl Chitosans Related to the Preparation Conditions," *Carbohydrate Polymers* 53 (2003): 355–359.

15. S. Dimassi, N. Tabary, F. Chai, N. Blanchemain, and B. Martel, "Sulfonated and Sulfated Chitosan Derivatives for Biomedical Applications: A Review," *Carbohydrate Polymers* 202 (2018): 382–396.

16. O. Novac, G. Lisa, L. Profire, C. Tuchilus, and M. I. Popa, "Antibacterial Quaternized Gellan Gum Based Particles for Controlled Release of Ciprofloxacin With Potential Dermal Applications," *Materials Science and Engineering: C* 35 (2014): 291–299.

17. L. Chen, Z. Tian, and Y. Du, "Synthesis and pH Sensitivity of Carboxymethyl Chitosan-Based Polyampholyte Hydrogels for Protein Carrier Matrices," *Biomaterials* 25 (2004): 3725–3732.

18. U. Jančiauskaite, Č. Višnevskij, K. Radzevičius, and R. Makuška, "Polyampholytes From Natural Building Blocks: Synthesis and Properties of Chitosan-o-Alginate Copolymers," *Chemija* 20 (2009): 128–135.

19. Q. Yin, G. Zhou, Y. Y. Liu, Q. J. Yin, J. H. Luo, and B. Jiang, "Molecular Dynamic Simulation of Carboxyethyl Chitosan: Effect of Temperature, Salt Concentration and pH," *Journal of Theoretical and Computational Chemistry* 9 (2010): 167–176.

20. C. Yu, Y. F. Liu, H. L. Tang, and H. M. Tan, "Study of Carboxymethyl Chitosan-Based Polyampholyte Superabsorbent Polymer (Part II): Investigating the State of Water in CMCTS-g-(PAA-Co-PTMAAC) Hydrogel," *Iranian Polymer Journal* 19 (2010): 417–425.

21. C. Yu, L. Yun-fei, T. Huan-lin, and T. Hui-min, "Study of Carboxymethyl Chitosan Based Polyampholyte Superabsorbent Polymer I. Optimization of Synthesis Conditions and pH Sensitive Property Study of Carboxymethyl Chitosan-g-Poly(Acrylic Acid-Co-Dimethyldiallylammonium Chloride) Superabsorbent Polymer," *Carbohydrate Polymers* 81 (2010): 365–371.

22. N. Dhar, S. P. Akhlaghi, and K. C. Tam, "Biodegradable and Biocompatible Polyampholyte Microgels Derived From Chitosan, Carboxymethyl Cellulose and Modified Methyl Cellulose," *Carbohydrate Polymers* 87 (2012): 101–109.

23. B. Cheng, B. Pei, Z. Wang, and Q. Hu, "Advances in Chitosan-Based Superabsorbent Hydrogels," *RSC Advances* 7 (2017): 42036–42046.

24. H. Kono, I. Oeda, and T. Nakamura, "The Preparation, Swelling Characteristics, and Albumin Adsorption and Release Behaviors of a Novel Chitosan-Based Polyampholyte Hydrogel," *Reactive and Functional Polymers* 73 (2013): 97–107.

25. A. Heydari, M. Darroudi, and I. Lacik, "Efficient N-Sulfopropylation of Chitosan With 1,3-Propane Sultone in Aqueous Solutions: Neutral pH as the Key Condition," *Reaction Chemistry & Engineering* 6 (2021): 2146–2158.

26. M. Lin, H. Liu, J. Deng, et al., "Carboxymethyl Chitosan as a Polyampholyte Mediating Intrafibrillar Mineralization of Collagen via Collagen/ACP Self-Assembly," *Journal of Materials Science and Technology* 35 (2019): 1894–1905.

27. S. Ouerghemmi, S. Dimassi, N. Tabary, et al., "Synthesis and Characterization of Polyampholytic Aryl-Sulfonated Chitosans and Their In Vitro Anticoagulant Activity," *Carbohydrate Polymers* 196 (2018): 8–17.

28. Y. Zhu, Y. Zheng, F. Wang, and A. Wang, "Fabrication of Magnetic Macroporous Chitosan-g-Poly (Acrylic Acid) Hydrogel for Removal of Cd2+ and Pb2+," *International Journal of Biological Macromolecules* 93 (2016): 483–492.

29. M. V. Dinu, I. Humelnicu, C. A. Ghiorghita, and D. Humelnicu, "Aminopolycarboxylic Acids-Functionalized Chitosan-Based Composite Cryogels as Valuable Heavy Metal Ions Sorbents: Fixed-Bed Column Studies and Theoretical Analysis," *Gels* 8 (2022): 221.

30. H. Yamamoto, K. Ohkawa, E. Nakamura, K. Miyamoto, and T. Komai, "Preparation of Polyion Complex Capsule and Fiber of Chitosan and Gellan-Sulfate at Aqueous Interface," *Bulletin of the Chemical Society of Japan* 76 (2003): 2053–2057.

31. D. F. Coutinho, S. Sant, M. Shakiba, et al., "Microfabricated Photocrosslinkable Polyelectrolyte-Complex of Chitosan and Methacrylated Gellan Gum," *Journal of Materials Chemistry* 22 (2012): 17262–17271.

32. S. Vasiliu, S. Racovita, M. Popa, L. Ochiuz, and C. A. Peptu, "Chitosan-Based Polyelectrolyte Complex Hydrogels for Biomedical Applications BT—Cellulose-Based Superabsorbent Hydrogels," in *Cellulose-Based Superabsorbent Hydrogels. Polymers and Polymeric Composites: A Reference Series*, ed. M. I. H. Mondal (Cham: Springer International Publishing, 2019), 1695–1725.

33. H. Wang, W. Li, Y. Lu, and Z. Wang, "Studies on Chitosan and Poly(Acrylic Acid) Interpolymer Complex. I. Preparation, Structure, pH-Sensitivity, and Salt Sensitivity of Complex-Forming Poly (Acrylic Acid): Chitosan Semi-Interpenetrating Polymer Network," *Journal of Applied Polymer Science* 65 (1997): 1445–1450.

34. H. Huang and X. Yang, "Synthesis of Chitosan-Stabilized Gold Nanoparticles in the Absence/Presence of Tripolyphosphate," *Biomacromolecules* 5 (2004): 2340–2346.

35. H. N. Guan, "Synthesis of Chitosan-Stabilized Gold Nanorod Using Tripolyphosphate," *Advances in Materials Research* 652–654 (2013): 250–253.

36. M. S. P. Boyles, T. Kristl, A. Andosch, et al., "Chitosan Functionalisation of Gold Nanoparticles Encourages Particle Uptake and Induces Cytotoxicity and Pro-Inflammatory Conditions in Phagocytic Cells, as Well as Enhancing Particle Interactions With Serum Components," *Journal of Nanobiotechnology* 13 (2015): 84.

37. A. Franconetti, J. M. Carnerero, R. Prado-Gotor, F. Cabrera-Escribano, and C. Jaime, "Chitosan as a Capping Agent: Insights on the Stabilization of Gold Nanoparticles," *Carbohydrate Polymers* 207 (2019): 806–814.

38. A. H. Hashem, A. M. Shehabeldine, O. M. Ali, and S. S. Salem, "Synthesis of Chitosan-Based Gold Nanoparticles: Antimicrobial and Wound-Healing Activities," *Polymers (Basel)* 14 (2022): 2293.

39. S. Dhar, E. Maheswara Reddy, A. Shiras, V. Pokharkar, and B. L. V. Prasad, "Natural Gum Reduced/Stabilized Gold Nanoparticles for Drug Delivery Formulations," *Chemistry* 14 (2008): 10244–10250.

40. S. Dhar, V. Mali, S. Bodhankar, A. Shiras, B. L. V. Prasad, and V. Pokharkar, "Biocompatible Gellan Gum-Reduced Gold Nanoparticles: Cellular Uptake and Subacute Oral Toxicity Studies," *Journal of Applied Toxicology* 31 (2011): 411–420.

41. S. Dhar, E. M. Reddy, A. Prabhune, V. Pokharkar, A. Shiras, and B. L. V. Prasad, "Cytotoxicity of Sophorolipid-Gellan Gum-Gold Nanoparticle Conjugates and Their Doxorubicin Loaded Derivatives Towards Human Glioma and Human Glioma Stem Cell Lines," *Nanoscale* 3 (2011): 575–580.

42. S. Dhar, P. Murawala, A. Shiras, V. Pokharkar, and B. L. V. Prasad, "Gellan Gum Capped Silver Nanoparticle Dispersions and Hydrogels: Cytotoxicity and In Vitro Diffusion Studies," *Nanoscale* 4 (2012): 563–567.

43. G. D'Arrigo, G. Navarro, C. Di Meo, P. Matricardi, and V. Torchilin, "Gellan Gum Nanohydrogel Containing Anti-Inflammatory and Anti-Cancer Drugs: A Multi-Drug Delivery System for a Combination Therapy in Cancer Treatment," *European Journal of Pharmaceutics and Biopharmaceutics* 87 (2014): 208–216.

44. S. Vieira, S. Vial, F. R. Maia, et al., "Gellan Gum-Coated Gold Nanorods: An Intracellular Nanosystem for Bone Tissue Engineering," *RSC Advances* 5 (2015): 77996–78005.

45. J. Song, Y. Zhang, X. Yang, Y. Li, X. Wang, and R. Tang, "pH/Temperature Dual-Sensitive Hydrogel Based on Carboxymethyl Chitosan and a Pluronic for Combined Chemo-Photothermal Therapy," *ACS Applied Polymer Materials* 6 (2024): 9960–9973.

46. Y. Ding, X. H. Xia, and H. S. Zhai, "Reversible Assembly and Disassembly of Gold Nanoparticles Directed by a Zwitterionic Polymer," *Chemistry* 13 (2007): 4197–4202.

47. H. Wang, J. He, Y. Ding, and X. Xia, "Preparation and Characterization of Sulfonated Chitosan-Modified Gold Nanoparticles and Their Surface Electronic Payload of Charged Drugs," *Science China. Life Sciences* 61 (2018): 457–463.

48. M. C. Villalobos, M. Á. G. Castro, J. G. Serrano, and A. M. H. González, "Comparison of Polyampholyte Derivative of Chitosan With Bisphthalimides of Low Molecular Weight in the Green Synthesis of au Nanoparticles," *Gold Bulletin* 55 (2022): 41–51.

49. G. S. Tatykhanova, S. P. Hirvonen, Y. V. Bardadym, N. N. Gizatullina, and M. A. Saulimbay, "Fractionation and Characterization of Commercial Low Acyl Gellan Gum," *Macromolecular Symposia* 413 (2024): 2400001.

50. E. Dreveton, F. Monot, J. Lecourtier, D. Ballerini, and L. Choplin, "Influence of Fermentation Hydrodynamics on Gellan Gum Physico-Chemical Characteristics," *Journal of Fermentation and Bioengineering* 82 (1996): 272–276.

51. B. Shi, Z. Shen, H. Zhang, J. Bi, and S. Dai, "Exploring N-Imidazolyl-O-Carboxymethyl Chitosan for High Performance Gene Delivery," *Biomacromolecules* 13 (2012): 146–153.

52. H. Huang, Q. Yuan, and X. Yang, "Morphology Study of Gold-Chitosan Nanocomposites," *Journal of Colloid and Interface Science* 282 (2005): 26–31.

53. E. O. Shatabayeva, D. B. Kaldybekov, L. Ulmanova, et al., "Enhancing Mucoadhesive Properties of Gelatin Through Chemical Modification With Unsaturated Anhydrides," *Biomacromolecules* 25 (2024): 1612–1628.

54. W. Yinsong, L. Lingrong, W. Jian, and Q. Zhang, "Preparation and Characterization of Self-Aggregated Nanoparticles of Cholesterol-Modified O-Carboxymethyl Chitosan Conjugates," *Carbohydrate Polymers* 69 (2007): 597–606.

55. A. Zając, W. Sąsiadek, L. Dymińska, et al., "Chitosan and Its Carboxymethyl-Based Membranes Produced by Crosslinking With Magnesium Phytate," *Molecules* 28 (2023): 5987.

56. Q. Z. Wang, X. G. Chen, N. Liu, et al., "Protonation Constants of Chitosan With Different Molecular Weight and Degree of Deacetylation," *Carbohydrate Polymers* 65 (2006): 194–201.

57. E. Hassani, N. Hosseinpour, and H. Bidgoli, "Swelling Behavior of Carboxymethylchitosan-Based Nanocomposite Hydrogels in Response to Different Stimuli (Salinity, pH, and Temperature) and the Gels' Microfluidic Capability for Water Shut-Off Applications," *Energy and Fuels* 38 (2024): 3645–3655.

58. D. P. Shan and G. K. Jain, "Modification and Characterization of Gellan Gum," *Pharmaceutical Technology* 33 (2009): 48–58.

59. J. Silva-Correia, J. M. Oliveira, S. G. Caridade, et al., "Gellan Gum-Based Hydrogels for Intervertebral Disc Tissue-Engineering Applications," *Journal of Tissue Engineering and Regenerative Medicine* 5 (2011): e97–e107.

60. M. Zaman, H. Xiao, F. Chibante, and Y. Ni, "Synthesis and Characterization of Cationically Modified Nanocrystalline Cellulose," *Carbohydrate Polymers* 89 (2012): 163–170.

61. I. Giavasis, L. M. Harvey, and B. McNeil, "Gellan Gum," *Critical Reviews in Biotechnology* 20 (2000): 177–211.

62. J. Du and Y.-L. Hsieh, "Nanofibrous Membranes From Aqueous Electrospinning of Carboxymethyl Chitosan," *Nanotechnology* 19 (2008): 125707.

63. A. L. Bukzem, R. Signini, D. M. Dos Santos, L. M. Lião, and D. P. R. Ascheri, "Optimization of Carboxymethyl Chitosan Synthesis Using Response Surface Methodology and Desirability Function," *International Journal of Biological Macromolecules* 85 (2016): 615–624.

64. D. M. Dos Santos, A. L. De Bukzem, and S. P. Campana-Filho, "Response Surface Methodology Applied to the Study of the Microwave-Assisted Synthesis of Quaternized Chitosan," *Carbohydrate Polymers* 138 (2016): 317–326.

65. B. Klaykruayat, K. Siralertmukul, and K. Srikulkit, "Chemical Modification of Chitosan With Cationic Hyperbranched Dendritic Polyamidoamine and Its Antimicrobial Activity on Cotton Fabric," *Carbohydrate Polymers* 80 (2010): 197–207.

66. J. Luo, X. Wang, B. Xia, and J. Wu, "Preparation and Characterization of Quaternized Chitosan Under Microwave Irradiation," *Journal of Macromolecular Science, Part A Pure and Applied Chemistry* 47 (2010): 952–956.

67. A. B. Lowe and C. L. McCormick, "Synthesis and Solution Properties of Zwitterionic Polymers," *Chemical Reviews* 102 (2002): 4177–4189.

68. D. Lupa, W. Płaziński, A. Michna, et al., "Chitosan Characteristics in Electrolyte Solutions: Combined Molecular Dynamics Modeling and Slender Body Hydrodynamics," *Carbohydrate Polymers* 292 (2022): 119676.

69. G. S. Manning, "Counterion Binding in Polyelectrolyte Theory," *Accounts of Chemical Research* 12 (1979): 443–449.

70. Z. Adamczyk, K. Jamrozy, P. Batys, and A. Michna, "Influence of Ionic Strength on Poly(Diallyldimethylammonium Chloride) Macromolecule Conformations in Electrolyte Solutions," *Journal of Colloid and Interface Science* 435 (2014): 182–190.

71. Z. Adamczyk, M. Morga, D. Kosior, and P. Batys, "Conformations of Poly- l -Lysine Molecules in Electrolyte Solutions: Modeling and Experimental Measurements," *Journal of Physical Chemistry C* 122 (2018): 23180–23190.

72. S. E. Kudaibergenov, *Polyampholytes: Synthesis, Characterization, and Application*, ed. S. E. Kudaibergenov (New York, NY: Springer Science+Business Media, 2002).

73. S. E. Kudaibergenov, *Polyampholytes in Advanced Polymer Science and Emerging Technologies* (Boca Raton, FL: CRC Press, 2024).

74. S. Nath, "Complexation Behavior of Proteins With Polyelectrolytes and Random Acrylic Polyampholytes Using Turbidimetric Titration," *Journal of Chemical Technology and Biotechnology* 62 (1995): 295–300.

Supporting Information

Additional supporting information can be found online in the Supporting Information section.

ANIONIC POLYSACCHARIDE – GELLAN AS PERSPECTIVE POLYMER FOR POTENTIAL APPLICATION IN MEDICINE AND OIL RECOVERY: A MINI-REVIEW

Kudaibergenov S.E[1]., Tatykhanova G.S[1,2]., Gizatullina N.N[1]., Tuleyeva R.N[1,3]., Kaldybekov D.B[1,3]., Gussenov I.Sh[1,2]., Berzhanova R.Zh[3]., Mukasheva T.D[3]., Vamvakaki M[4]., Aseyev V.O[5]., Khutoryanskiy V.V[6].

[1]*Institute of Polymer Materials and Technology, Almaty, Kazakhstan, e-mail: skudai@mail.ru*
[2]*Satbayev University, Almaty, Kazakhstan, e-mail: gulnur-ts81@yandex.kz*
[3]*al-Farabi Kazakh National University, Almaty, Kazakhstan, e-mail: mtogzhan@mail.ru*
[4]*University of Crete, Heraklion, Greece, e-mail: vamvakak@iesl.forth.gr*
[5]*Department of Chemistry, University of Helsinki, Helsinki, Finland, e-mail: vladimir.aseyev@helsinki.fi*
[6]*University of Reading, Reading, UK, e-mail: v.khutoryanskiy@reading.ac.uk*

Abstract

Potential application of gellan in medicine and oil recovery based on literature survey and own results of authors has been presented in this mini-review. Purification and fractionation procedures of commercial gellan gum have been described. The application of gellan gum and its modified derivatives in medicine, in particular, as drug delivery systems accompanied by mucoadhesivity has been briefly considered. Gold nanoparticles immobilized within gellan and poly(2-ethyl-2-oxazoline)-grafted gellan have been demonstrated for photothermal treatment of Ehrlich cancer cell. Potential application of gellan in oil recovery has been considered. The prospect of organizing the gellan production in Kazakhstan has been outlined.

Keywords: high acyl gellan, low acyl gellan, drug delivery, gold nanoparticles, photothermal therapy, oil recovery, glucose-fructose syrup, fermentation, production of gellan.

Introduction

Gellan is abundant polysaccharide that is widely used in food industry [1], biotechnology [2], medicine [3], pharmacy [4], tissue engineering [5] and oil industry [6]. Gellan is a linear anionic heteropolysaccharide obtained from biomass by aerobic fermentation by the microorganism *Sphingomonas elodea* [7-9]. The repeating unit of gellan consists of four polysaccharide residues: 1,3-β-D-glucose, 1,4-β-D-glucuronicacid, 1,4-β-D-glucose, and 1,4-α-L-rhamnose at a ratio of 2:1:1 [1].

Specific gelling properties of gellan in different media led to the development of controlled release forms including oral, ophthalmic, nasal and other [10]. Gellan gum-based hydrogels exhibit excellent *in vivo* and *in vitro* biocompatibility [11], tunable physical mechanical and injectable properties for application in regeneration of cartilage [12, 13], cell encapsulation [14], nucleus pulposes regeneration [15]. Recent progress in the design of multifunctional hydrogels with participation of gellan gum in the context of biomedical engineering and regenerative medicine is discussed and summarized in recent review [16].

Authors [17, 18] developed gellan-based nanohydrogel systems to deliver multiple drugs: prednisolone and paclitaxel. Prednisolone was chemically linked to the carboxylic

groups of gellan while placitaxel was physically entrapped into gel matrix. The synergistic anti-inflammatory and anti-cancer effect were reached with respect to malignant cells and tumor inflammatory components. Analgesic, antipyretic and anti-flammatory drug – diclofenac sodium was immobilized into the matrix of poly(methacrylamide)-grafted-gellan gum and its sustained *in vitro* release kinetics was studied [19]. It was shown that the diclofenac sodium releases over a period of 8 h and the release profile is described by Higuchi square root kinetic model and release mechanism is governed by Fickian diffusion.

Gellan gum was chemically modified by the reaction with methacrylic anhydride to produce derivatives with 6, 14 and 49% methacrylation [20]. *In vitro* study performed with formulations of sodium fluorescein containing gellan gum and its methacrylated derivatives indicated that methacrylation enhances their retention on bovine conjunctival mucosa. *In vivo* experiments with the formulations of pilocarpine hydrochloride containing gellan gum and methacrylated derivatives have demonstrated that all polymers enhance the drug effect significantly, but best performance is observed for the polysaccharide with 6% methacrylation.

Gellan gum has been used to prepare polymeric carriers with prolonged retention on the eye surface for topical ocular drug delivery [21]. It was chemically modified with short poly(2-ethyl-2-oxazoline) (PEtOx) chains. The derivatives with three degrees of grafting were prepared by varying the in-feed mass ratio of PEtOx grafts over gellan. NMR and FTIR spectroscopies, thermogravimetric analysis, and SEC evidenced that the grafting had actually taken place. The graft copolymers (LAG-*g*-PEtOx) were found to be highly biocompatible with cells cultured under their induction at concentration of 0.01, 0.1 and 1 $mg \cdot mL^{-1}$ demonstrated a physiological morphology, as well as an increase in viability and proliferation.

Complex formation between a natural polysaccharide – gellanand an antimicrobial drug – ofloxacin was studied in aqueous and buffer solutions [22]. Conductimetric and potentiometric titration curves revealed that gellan and ofloxacin forms a water-soluble complex of composition 2:1 mol/mol stabilized by ionic and hydrogen bonds. The formation of the gellan-ofloxacin complex was confirmed by FTIR spectroscopy, dynamic light scattering, zeta-potential and thermogravimetric analysis. The average hydrodynamic size of the complex was found 307±5nm and its zeta-potential was negative and equal to -15 mV. Thin films of the gellan-ofloxacin complex, gelled in 0.3 wt.% of $CaCl_2$, were used to study the release kinetics of ofloxacin in distilled water and phosphate buffer. The drug release kinetics evaluated by UV-Vis spectroscopy at λ_{max} = 289 nm and calculated by the Ritger-Peppas model correspond to non-Fickian diffusion in distilled water and Case II transport (zero-order kinetics) in phosphate buffer. The cumulative release of ofloxacin from the gellan-ofloxacin films was equal to 96±2% and 36±2% in phosphate buffer and distilled water, respectively. It is expected that the gellan-ofloxacin complex is able to form *in situ* gel on the surface of the eye and to prolong the drug residence time in the tear fluid.

It is well known that cancer is one of the leading causes of mortality in the modern world, with more than 10 million new cases every year. Targeting nanoparticles that selectively recognize and destroy cancer cells in the body remain key concept in nanomedicine [23, 24]. Gold nanoparticles (AuNPs) with controlled geometrical, optical, and surface-chemical properties are the priority research of intensive studies and applications in cancer diagnosis, treatment and as drug delivery system.

AuNPs protected by poly(2-ethyl-2-oxazoline) (POZ) of different molecular weights (M_w = 5, 50, 200 and 500 kDa) were synthesised and characterised by dynamic light scattering, nanoparticle tracking analysis, zeta potential measurement and transmission electron microscopy [25]. It was established that the use of POZ with 50 kDa resulted in formation of AuNPs with low polydispersity while POZ with greater molecular weights led to formation of more polydisperse AuNPs. Fluorescent labelling of these nanoparticles was achieved through their reaction with poly(ethyleneglycol dithiol) (8-12 kDa) as a linker molecule with subsequent reaction with 6-(iodoacetamido)fluorescein. The fluorescent nature of obtained AuNPs was confirmed by the appearance of the fluorescence peak at 510 nm that is typical for fluorescein molecules and glowing of the aqueous solution under the UV irradiation. The fluorescently-labelled AuNPs are promising tool in biomedical application to monitor the biological systems using fluorescent microscopy.

Application aspects of polysaccharides in enhanced oil recovery (EOR) are well-known and were recently reviewed by authors [26,27]. Among a widely EOR application of polysaccharides the main attention was paid to xanthan [28-30], guar gum [31], scleroglucan [32], welan [33], carboxymethyl- and hydroxyethyl cellulose [34], starch [35], diutan, pullulan, [36, 37] carrageenan [38, 39] and in a less degree to gellan [40, 41]. Reservoir conditions like temperature, salinity, charges on the rock surfaces, and the nature of crude oil are important parameters of consideration for polymer flooding. Compared with water-soluble synthetic polymers traditionally used in oil production, biopolymers, in particular gellan gum, have the following advantages: 1) thermal stability, which in some cases reaches up to 150 °C, 2) mechanical stability, 3) salt resistance, 4) stability in a wide range of pH changes, 5) environmental safety.

During the last 10 years our research group comprehensively studied the applicability of gellan in EOR in the course of laboratory experiments [42-49] and oilfield tests [50-53]. The study of bulk gels derived from inorganic and polymeric precursors, including gellan, in order to plug high-permeability thief zones of oil reservoirs was reviewed in [54]. The plugging efficiency of gellan gel was compared with crosslinked by chromium (III) ions hydrolyzed poly(acrylamide) that is widely used in EOR.

Purification and fractionation of commercial gellan gum

Commercial gellan depending on the degree of deacylation of glycerate and acetate groups is distinguishedas high acyl (HAG) and low acyl gellan (LAG) (Table 1) [1].

Table 1

Structural formula and some properties of HAG and LAG

Gellan type	Average molecular weight, kDa	Solubility in water	Thermal stability
High acyl gellan (HAG)	$(1\text{-}2)\cdot10^3$	Well soluble in hot water	Heat-responsive
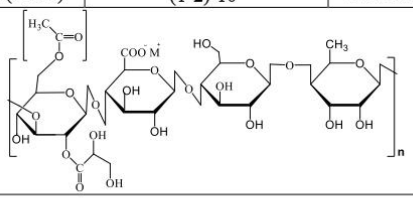			

Low acyl gellan (LAG)	$(0.5\text{-}1)\cdot10^3$	Well soluble in cold water	Stable to heat
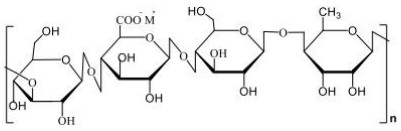			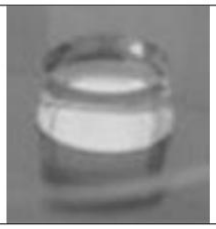

Commercial gellan gum produced by fermentation contain some amount of mono- and divalent cations that comes from the nutrient salts required for growth of the bacteria and/or introduced during post-fermentation processing [55].

Extremely high molecular weight of low acyl gellan gum (LAG) in the range of $(0.5\text{-}1)\cdot10^6$ restricts a wide application of gellan as drug delivery system. Aqueous solution of gellan due to presence of Na^+, K^+, Mg^{2+} and Ca^{2+}forms a fraction of soluble chains and a dispersed fraction of swollen gel-like multi molecular aggregates of gellan. We have developed the purification procedure of gellan as demonstrated in Ref. [21]. At first, LAG (1 w/v %) was dissolved for 3 h in deionized water at 50 °C (Figure 1). Turbid solution/dispersion was centrifuged for 30 min at 40 °C with a spinning rate of 5000 rpm. The clear supernatant fraction was collected and precipitated in acetone (1:4 v/v). LAG was separated from water-acetone mixture by vacuum filtration using Whatman Grade 541 filter paper and dried for ~30 min. Then, the separated LAG was redissolved in deionized water again, reprecipitated in acetone and dried. Dry GG was twice washed with isopropanol. Then, LAG was dissolved in deionized water and dialyzed against deionized water (cut off 12 – 14 kDa) for at least 24 h. The product was freeze-dried and collected as dry fluffy white fibers. The yield of purification was 45% – 50% of the original weight of LAG. FTIR and NMR spectroscopy did not reveal any significant differences between purified and pristine LAG. Thus, there was no indication that GG was incompletely deacetylated and that a fraction was removed during purification. This conclusion is also supported by the elemental analysis, which reveals equal carbon and hydrogen contents in both samples. Therefore, the most likely reason for the low yield of purification is divalent cations. Small amount of these metal cations binds gellan chains into particles, which are removed by centrifugation.

Chains scissoring of commercial LAG was carried out by means of ultrasound treatment to obtain LAG fractions of lower molecular weight. Ultrasonically treated at 50 °C during 10, 20, 30, 60, 90 and 120 min 1 wt.% gellan samples were centrifuged at 50 °C during 1 h. Every time the separated supernatant was precipitated by isopropyl alcohol, dialyzed several times and freeze-dried. The reduced viscosities of ultrasonically treated LAG samples were measured in aqueous solution containing 0.025M tetramethylammonium chloride (Figure 2). The viscosity average molecular weights (M_η)of LAG fractions calculated according to Mark-Kuhn-Houwink equationin 0.025M tetramethylammonium chloride $[\eta] = 7.48\cdot10^{-3}\cdot M_w^{0.91}$ [56] are shown in Table 2.

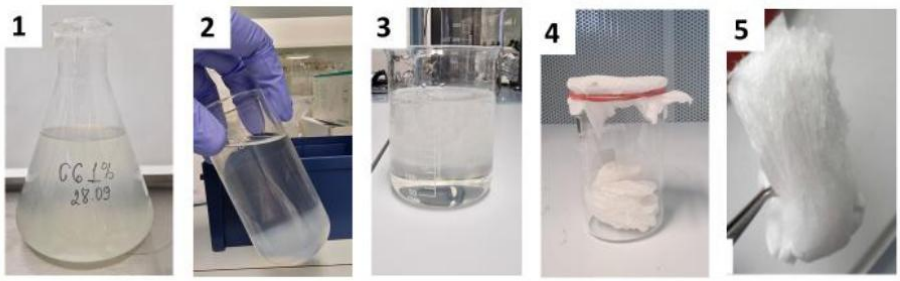

Figure 1. Removal of the insoluble fraction (*i.e.* multimolecular swollen particles) from commercial LAG: (1) turbid 1 w/v % "solution" of LAG in deionized water 3 h after dissolution at 50 °C; (2) LAG in water after centrifugation for 30 minutes at 40 °C with a spinning rate of 5000 rpm; (3) supernatant is extracted after centrifugation and precipitated in acetone (1:4 v/v); (4) precipitated LAG, which is separated from water-acetone mixture with vacuum filtration; (5) dry gellan gum after freeze-drying[21]

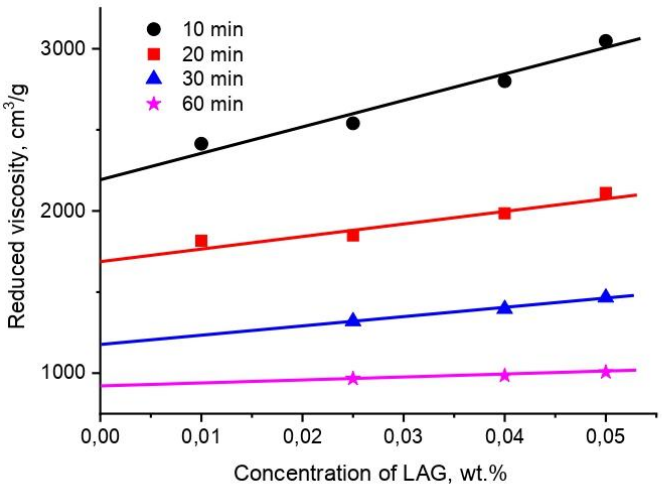

Figure 2. Concentration dependence of the reduced viscosity of LAG after 10, 20, 30 and 60 min treatment by ultrasonic source

Table 2

The intrinsic viscosity and M_η of LAG fractions

Ultrasonic treatment, min	Intrinsic viscosity, $cm^3 \cdot g^{-1}$	$M_\eta \cdot 10^{-5}$, Dalton
10	2200	10.0
20	1690	7.63
30	1180	5.12
60	920	3.92

It is seen that the ultrasonic treatment of LAG leads to gradually decreasing of both [η] and M_η. It is probably connected with cleavage of glycosidic linkages and degradation of LAG [2]. Proton NMR and FTIR spectra of LAG after 10 and 120 min ultrasound treatment show that both ^{1}H NMR and FTIR spectra of samples are the same confirming the absence of structural changes. ^{1}H NMR spectra of LAG contain CH groups of rhamnose (δ 5.27 ppm), CH groups of glucuronic acid (δ 5.09 ppm), and CH_3 groups of rhamnose (δ 1.86 ppm) [46].[1]In FTIR spectra the bands at 3568-3513 and 1419-1412 cm^{-1} correspond to stretching and bending vibrations of OH groups. The peaks at 2935-2920 and 2886-2870 cm^{-1} are due to the stretching CH bonds. The sharp peaks at 1612-1610 cm^{-1} and 1042-1041 cm^{-1} belong to asymmetric COO^-stretching and COC stretching bonds respectively.

Gellan gum immobilized gold nanoparticles for treatment of cancer cells

The unique properties of gellan gum, in particular, biocompatibility, low toxicity, biodegradability, commercial availability and low cost argue the successful application of this class of polysaccharide in nanomedicine [57].The cellular uptake and toxicity ofgold nanoparticles (AuNPs) stabilized by low acyl gellan gum (LAG-AuNPs) was studied on mouse embryonic fibroblast cells, NIH 3T3 and human glioma cell line LN-229 [58 71]. It was shown that in the cancerous cells the LAG-AuNPs were localized mainly in the cytoplasm and perinuclear region of the cells. Oral administration of LAG-AuNPs did not cause any toxicity in rats during 28 days and was no any significant difference in hematological, biochemical and histopathology of organs demonstrating potential of LAG-AuNPS as DDS.

The AuNPs stabilized by gellan gum was loaded by doxorubicin hydrochloride (DOX) – one of the potential and well-know anticancer drugs [59 72] was conjugated with sophorolipid (SL) [60 73] and their cytotoxicity were evaluated with respect to human glioma cell line LN 229 and human glioma stem cell line HNGC-2 (Figures 3,4).

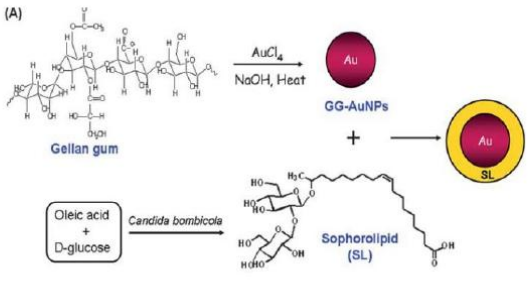

Figure 3. Synthesis of gellan gum reduced and stabilized AuNPs (GG-AuNPs) and sophorolipid-conjugated LAG-AuNPs [59]

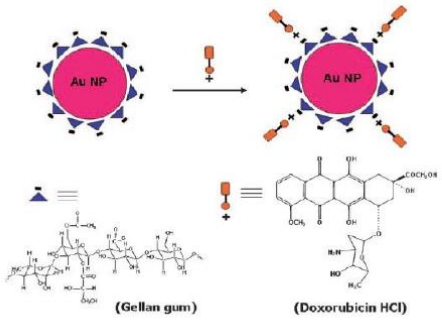

Figure 4. Stabilization of AuNPs by gellan gum and subsequent loading of LAG-AuNPs by doxorubicin [58]

Both SL-conjugated and DOX-loaded gellan gum containing AuNPs exhibited increased effectiveness against glioma tumors. The same authors [61] studied the antibacterial

activity of the dispersions of silver nanoparticles (AgNPs) stabilized by gellan gum (LAG-AgNPs), the cytotoxicity of LAG-AgNPs against mouse embryonic fibroplast cells NIH 3T3 and also evaluated the *in vitro* diffusion of AgNPs dispersions/gels across rat skin. The results show that LAG capping effectively passivates the AgNPs and does not display any cytotoxicity against NIH 3T3 and exhibits eligibility for topical treatments.

Photothermal damage of cells is currently one of the most promising research avenues in the treatment of cancer and infectious diseases. The essence of this phenomenon is as follows: AuNPs have an absorption maximum in the visible or near-IR (NIR) region and get very hot when irradiated with corresponding light. If, they are located inside or around the target cells (which can be achieved by conjugating gold nanoparticles to antibodies or other molecules), these cells die. The revolution in thermal cancer therapy is associated with 20-40 nm AuNPs that convert the 20 ns laser irradiation (514 nm) to local heat (up to 40-45 °C), and selectively kill the cancer cells. This method called plasmonic photothermal therapy (PPTT) [62] has extensively been researched and used for biomedical application [63]. The PPTT has much potential in diagnosis, treatment and evolution of diseases, in particular cancer [64]. In recent review [65] the advancements of plasmonic nanoparticles and films in the field of biomedicine was overviewed.

Among the numerous nanomaterials the best one are AuNPs because of their biocompatibility, low toxicity, ability to absorb in visible or NIR region, excellent photostability, and availability in various morphologies [66]. Among the gold nanoparticles the gold nanoshells [67] and nanorods (AuNRs) [68] are especially suitable for PPTT due to their tunable longitudinal plasmon band in the NIR region [63].

Small spherical AuNPs exhibit poor NIR absorption, therefore nanoaggregates, nanoshells, nanorods and nanomatryoshkas stabilized by functional polymers are suitable for PPTT [65]. Gellan gum coated gold nanorods (LAG-AuNRs) was fabricated by authors [69] and used for intracellular drug delivery and imaging. The preparation strategy of AuNRs includes several steps: at first the fine dispersed AuNRs is synthesized by a seed-mediated growth method using cationic surfactant – cetyltrimethylammonium bromide (CTAB) as surface passivant [70], then the layer-by-layer (LbL) technique is used for coating, and finally AuNRs are coated by gellan gum (Figure 5).

The cytotoxicity and osteogenic ability of gellan-coated AuNRs was tested with respect to SaOS-2 (Sarcoma osteogenic), a human osteoblast-like cell line commonly used as osteoblastic model [71]. It was found that AuNRs-LAG were not cytotoxic after 14 days of culturing and were localized inside lysosomes. NIR lasers are selected due to higher penetration of human tissue resulting in minimal damage. *In vitro* experiments show that heating of tumor tissues is observed in the presence of NIR-exposed AuNRs, however laser irradiation in the absence of AuNRs causes negligible damage of healthy tissues [65]. Without coating by biocompatible polymers, AuNRs can not infiltrate the blood vessels and therefore their concentration increases in plasma. *In vivo* tumor ablation requires a tissue temperature of around 48-50 °C for successful operation.

Spherical gold nanoparticles (AuNPs) and gold nanorods (AuNRs) was stabilized using LAG and poly(2-ethyl-2-oxazoline)-grafted gellan (LAG-*g*-PEtOx) and utilized as PTT agents for the treatment of Ehrlich cancer cells. As previously shown [72], gellan-coated AuNPs are monodisperse and their average hydrodynamic sizes are in the range of 4-25 nm. Polymer-protected AuNPs were produced using one-pot and growth seeding techniques in an aqueous solution [68]. These particles were observed to demonstrate temperature-dependent

conformational changes and high stability over a period of 36 days, thus making them suitable for PTT treatment.

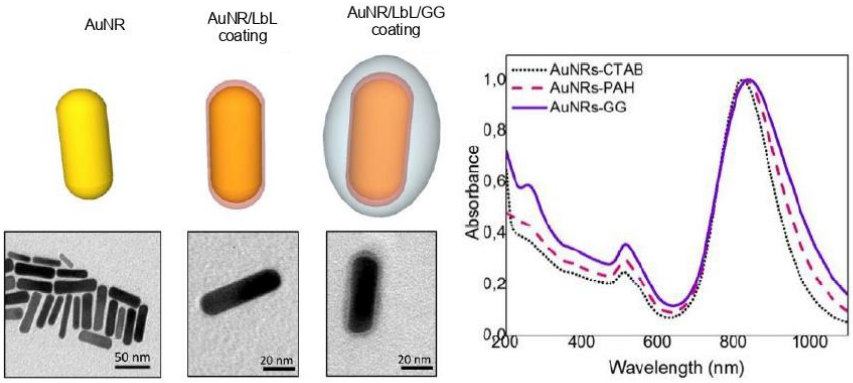

Figure 5. Covering and TEM images of AuNRs by layer-by-layer coatings (AuNRs/LbL) and coating by gellan gum of AuNRs/LbL (left) and visible spectra of AuNRs-CTAB, AuNRs-CTAB-LbL, AuNRs-LAG (right) [71]

All animal experiments were carried out in accordance with the protocol approved by the local ethical committee at the Kazakh Research Institute of Oncology and Radiology (Protocol No.5-2021, December 10, 2021). For the *in vivo* experiments, 18 CD-1 mice with a subcutaneous Ehrlich tumor were selected. The tumor transplantation into intact animals was carried out *via* subcutaneous injection of tumor cells at a dose of 5 million species. Experiments began 10 days later, when the tumors reached a size of around 4-5 mm in diameter. The mice were divided into 3 groups: Group 1 is 5 control individuals, with no colloidal AuNPs solution was injected or exposure of the mice to irradiation; Group 2 is 5 animals, a colloidal AuNPs solution was injected and no irradiation performed; and Group 3 is 5 animals, a colloidal AuNPs solution was injected and irradiation was carried out. Before the start of the experiment, hair removal of the surface of the tumor skin was performed, then intratumoral injection of 0.05 mL of colloidal AuNPs-PVP (40 kDa) was performed, at a concentration of AuNPs in suspension equal to 44.8 $\mu g \cdot mL^{-1}$. After 25 min, the tumor node was subjected to 30 min of laser exposure. The process was repeated daily for 7 days. Throughout the experiment, the size of the tumors was measured every day using a caliper. On day 9, the tumors were removed *via* dissection of the peritoneum and additional weighing was performed. In accordance with the Council for International Organizations of Medical Sciences (CIOMS) international guidelines for the conduct of biomedical research using animals, before removing the tumor, the mice were humanely sacrificed.

The prepared AuNPs and AuNRs were characterized by UV/Vis-spectroscopy, dynamic light scattering, zeta-potential, transmission electron microscopy (TEM), and optical microscopy. As seen from TEM images, the spherical AuNPs and rod-like AuNRs stabilized by gellan and LAG-*g*-PEtOx are uniformly distributed (Figure6).

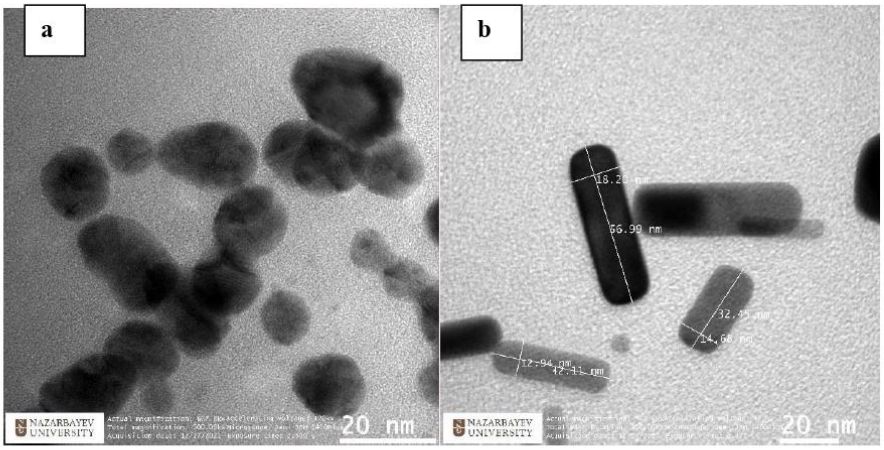

Figure 6. TEM images of spherical AuNPs (a) and rod like AuNRs (b) stabilized with gellan (a) andLAG-*g*-PEtOx (b)

The gellan-protected AuNPs exhibited light-to-heat conversion, raising the temperature from 37 to 43 °C upon irradiation by laser light at 530 nm. In the case of AuNPs, considerable damage to Ehrlich cancer cells was observed to occur over the 40 days following irradiation. However, with regards to AuNRs, the damage to Ehrlich's cancer cells was slightly lower than seen with AuNPs. *In vivo* experiments demonstrated that laser irradiation of tumors in mice after the addition of AuNPs leads to a statistically significant decrease in tumor size, as compared to those not irradiated and the control samples. Due to unique intrinsic biocompatibility, gellan-coated AuNPs and AuNRs may contribute to the enhancement of the efficacy of treatment of Ehrlich's cancer cells.

The prospect of organizing the production of gellan in Kazakhstan

Recently [73] the research team of the Institute of Polymer Materials and Technology (www.ipmt.kz) in collaboration with biotechnology lab of al-FarabiKazakh National University developed the gellan production technology from glucose-fructose syrup of Zharkent and Burunday corn starch plants of Kazakhstan (krahmalopatoka.kz). Fermentation of these products by *Sphingomonas paucimobilis* ATCC® 31461 leads to formation of HAG as described in [74] (Figure 7).

The main difference between the high- and low-acyl gellan is that the HAG contains acyl group positioned at O(2) and glyceride positioned at O(6) fragments and the presence of intensive absorption band at 1726 cm^{-1} is specific for these groups. FTIR spectra of commercial HAG purchased from "Xinjiang Fufeng Biotechnologies Co., Ltd.", China, and Kazakhstan HAG separated from the fermentation broth are compared in Figure 8. In all cases the appearance of intensive bands at 1724-1727 cm^{-1} is specific for acyl groups of HAG.

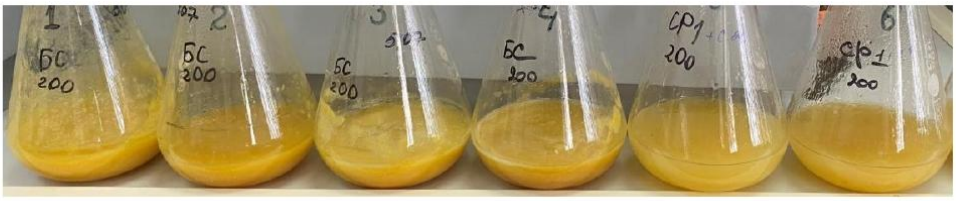

Figure 7. Biomasses obtained upon fermentation of glucose-fructose syrup by *Sphingomonas paucimobilis* ATCC® 31461

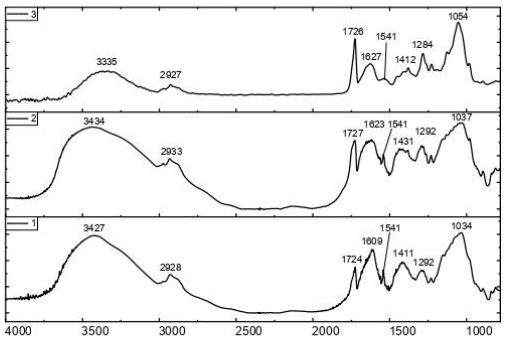

Figure 8. FTIR spectra of self-purified (1), technical (2) HAG produced by Xinjiang Fufeng Biotechnologies Co., Ltd. and Kazakhstan HAG (3) obtained by fermentation of glucose-fructose syrup

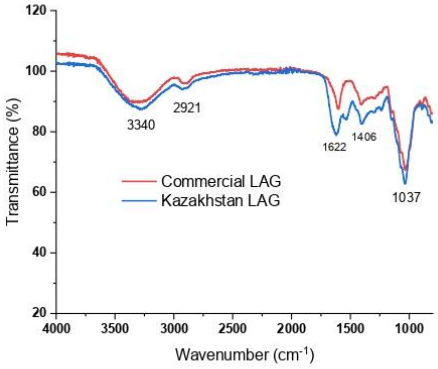

Figure 9. FTIR spectra of commercial LAG purchased from Xinjiang Fufeng Biotechnologies Co., Ltd. and Kazakhstan LAG obtained by deacylation of Kazakhstan HAG

In deacylated gellan gum, or LAG, the intensive peaks at 1724-1727 cm^{-1} disappear that confirms the elimination of acyl groups from HAG (Figure 9). The commercial and Kazakhstan LAG contains the bands at 3340, 1406, 2921, 1622 and 1037 cm^{-1} that belong to stretching and bending OH, stretching CH, C=O and C-O-C bonds, respectively. ^{1}H NMR spectra of LAG coincide well with our previous data [46] and show the characteristic peaks of CH of rhamnose (5.27 ppm), CH of glucuronic acid (5.09 ppm), and CH_3 of rhamnose (1.86 ppm) (Figures 10, 11).

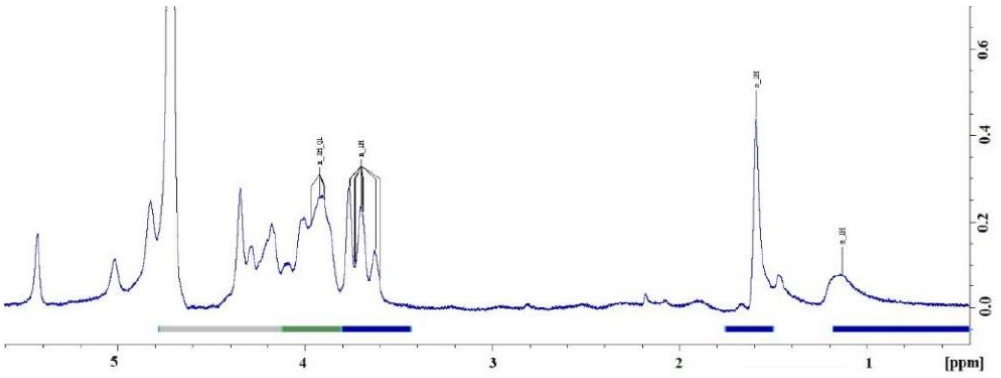

Figure 10. ^{1}H NMR spectrum of commercial LAG in D_2O at 60 ^{0}C. C = 10 mg·mL^{-1}

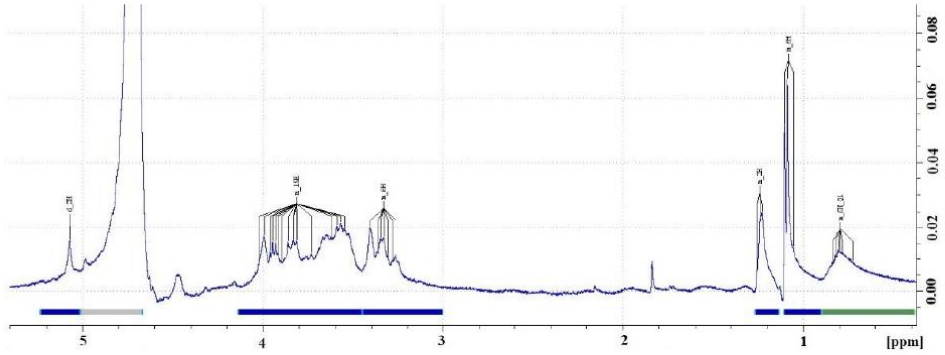

Figure 11. ^{1}H NMR spectrum of Kazakhstan LAG in D_2O at 60 ^{0}C. C = 10 mg·mL^{-1}

As seen from Figure 12, ^{13}C NMR spectra of commercial LAG and Kazakhstan LAG coincide well.

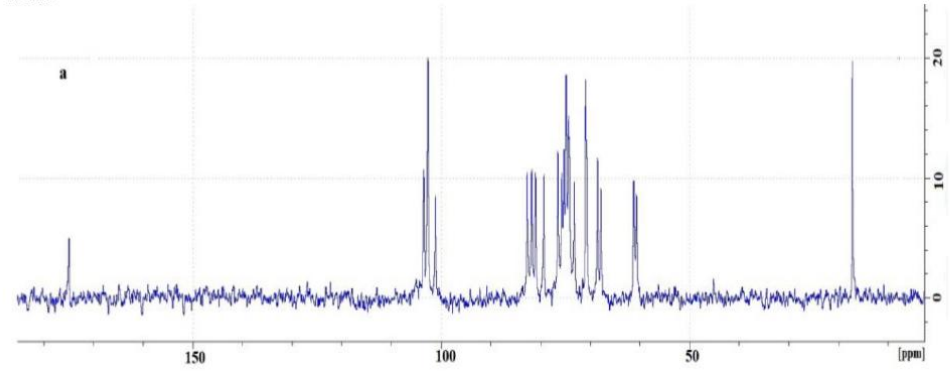

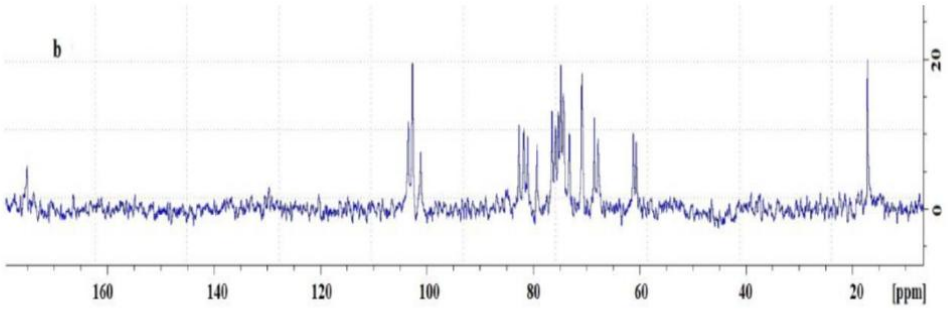

Figure 12. ^{13}C NMR spectra of commercial (a) and Kazakhstan (b) LAG at 60 °C

The thermogravimetric curves (TG) of commercial gellan and HAG produced by our research team coincide well, both samples decompose at approximately 250 °C.The values of weight-average molecular weight (M_w), number-average molecular weight (M_n) and polydispersity index (PDI) of HAG determined by GPC are represented Table 3.

Table 3

Molecular weights and PDI of Kazakhstan HAG prepared from glucose-fructose syrup of Zharkent corn starch plant

HAG produced from glucose-fructose syrupof Zharkent corn starch plant	Molecular mass, Dalton			PDI
	M_w	M_n	M_z	M_w/M_n
	343 500	333 000	360 000	1.03

The dynamic viscosities of biomass produced from different types of raw materials increase in the following order: Burunday glucose-fructose syrup >Zharkent glucose-fructose syrup > glucose. It is seen that the biomass obtained from Burunday glucose-fructose syrup is more suitable for HAG production and oil recovery (Table 4).

Table 4

Dynamic viscosities of the biomass obtained from various sources

Type of raw materials	Pure Glucose	Zharkent glucose-fructose syrup	Burunday glucose-fructose syrup
Dynamic viscosity,mPa·s	2280	3170	4420

Aqueous solutions 0.25 and 0.5% Kazakhstan LAG showed an excellent gelation property upon the addition of 0.01-1.0M NaCl and/or $CaCl_2$.

The potential application of HAG in EOR was demonstrated by Gao [41]. In our case, the fermented biomass obtained from Burunday glucose-fructose syrup with dynamic viscosity 4420 mPa·s was injected into the sand pack model (Figure 13). The monotonous increase in pressure is probably accounted for the gradually plugging of pores by fine gel particles that are screened out at the inlet of the model. The effluent samples obtained at the output of the sand pack model contain the fine gel particles coming from biomass. Injection of water into

the sand pack model after injection of biomass leads to sharp increase of pressure due to the displacement of gel particles by water (Figure 14).

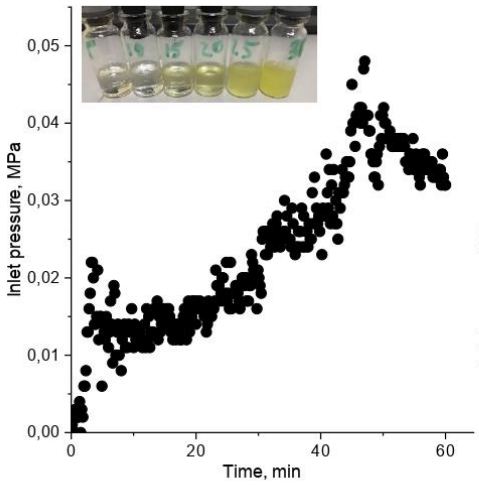

Figure 13. Change of the pressure upon injection of biomass into sand pack model. Insert is filtrate after injection of 30 mL biomass

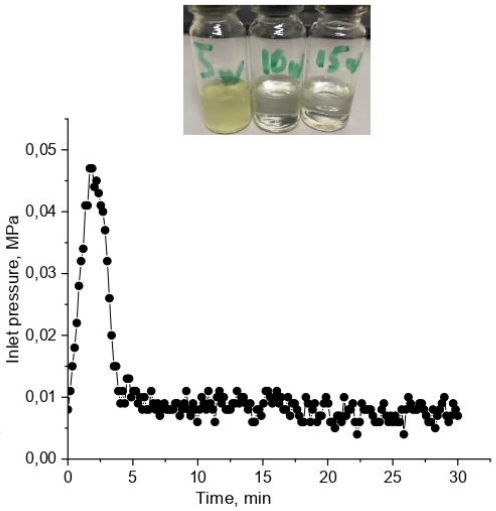

Figure 14. Change of the pressure upon injection of water into the sand pack model after injected biomass. Insert is filtrate after injection of 15 mL water

These experiments clearly demonstrate that injection of biomass directly into oil reservoir is less effective and such system will not penetrate into the reservoir matrix. The fine gel particles will be filtered out on the walls of the well. In fractures, these samples will not be able to reduce permeability, as they do not form a strong gel that bridges the fracture.

Conclusions

The most recent application aspects of gellan gum and its modified derivatives in medicine, in particular, as drug delivery systems accompanied bymucoadhesivity have been briefly surveyed. The immobilization protocol of anticancer drugs and gold nanoparticles within gellan matrix has been discussed. Release of anticancer drugs from gellan gel matrix to outer solution has been considered. The advancements of plasmonic photothermal therapy that has much potential in diagnosis and treatment of cancer cells have been overviewed.

Numerous laboratory experiments and oilfield tests reveal the gelation and plugging behavior induced by saline oilfield water as well as salt resistance, thermal and mechanical stability,environmental safetyputs forward the gellan gum as perspective natural biopolymer for enhanced oil recovery.

The high and low acyl gellan gums produced in Kazakhstanin laboratory condition by fermentation on glucose-fructose syrup of Zharkent and Burunday corn starch plants by *Sphingomonas paucimobilis*in future may be scaled up and used in food industry and oil recovery.

Acknowledgements

This work was financially supported by Science Committee of the Ministry of Science and High Education of the Republic of Kazakhstan (Grant No. AP13067773). Authors thank the Horizon 2020 research and innovation program of the European Union Maria Sklodowska-Curie (Grant agreement 823883-NanoPol-MSCA-RISE-2018) for financial support.

References

[1]. Morris E., R., Katsuyosh, N., Rinaudo M. (2012). Gelation of gellan – A review. *Food Hydrocolloids*, *28*, 373-411. http://dx.doi.org/10.1016/j.foodhyd.2012.01.004.

[2]. Deverton J., Wang C., Lai R.C., Su K., Zhang K., Wang D-A. (2009). An improved injectable polysaccharide hydrogel: Modified gellan gum for long-term cartilage regeneration in vitro. *J Mater Chem*, *19*, 1968-1977.http://dx.doi.org/10.1039/b818090c.

[3]. Osmalek T., Froelich A., Tasarek S. (2014). Application of gellan gum in pharmacy and medicine.*International Journal of Pharmaceutics*, *466*, 328-340. http://dx.doi.org/10.1016/j.ijpharm.2014.03.038.

[4]. D'Arrigo G., Di Meo C., Gaucci E., Chichiarelli S., Coviello T., Capitani D., Alhaaique P., Matricardi P. (2012). Self-assembled gellan gum nanohydrogel as a tool for prednisolone delivery. *SoftMatter*, 8, 11557-11564. http://dx.doi.org/10.1039/C2SM26178B.

[5]. Silva-Correa J., Oliveira J.M., Caridade S.G., Oliveira J.T., Sousa R.A., Mano J.F., Reis R.I. (2011). Gellan gum-based hydrogels for intervertebral disc tissue engineering applications. *J. Tissue Eng Regen Med*, *5*, e97-e107. https://doi.org/10.1002/term.363.

[6]. Kudaibergenov S., Adilov Zh., Nuraje N., Sagindykov A., Tatykhanova G., Ibragimov R., Gusenov, I. (2012). Laboratory test for enhanced oil recovery with gellan. *International Journal of Biology and Chemistry4*, 58-68.ISSN: 2218-7979 eISSN 2409-370X.

[7]. Bajaj I.B., Survase S.A., Saudagar P.S., and Singhal R.S. (2007). Gellan gum: Fermentative production, downstream processing and applications (Review). *Food Technol Biotechnol,45*, 341-354.ISSN 1330-9862

[8]. Giavasis I., Harvey L.M., McNeil B. (2000). Gellan gum. *Critical Reviews in Biotechnology*, *20*, 177-211. http://dx.doi.org/10.1080/07388550008984169.

[9]. O'Neill M.A., Selvendran R.R., Morris V.J. (1983). Structure of the acidic extracellular gelling polysaccharide produced by *Pseudomonas elodea*. *Carbohydr Res*, *124*, 123-133.https://doi.org/10.1016/0008-6215(83)88360-8.

[10]. Tatykhanova G., Aseyev V., Kudaibergenov S. (2020). Mucoadhesive properties of gellan and its modified derivatives. *Reviews and Advances in Chemistry*, *10*, 140-157. https://doi.org/10.1134/S207997802003005X.

[11]. Silva-Correa J., Zavan B., Vindignz,V., Silva T.H., Oliveira J.M., Abatangelo G., Reis R.L. (2013). Biocompatibility evaluation of ionic- and photo-crosslinked methacryalted gellan gum hydrogels: In vivo and in vitro study. *Adv Health Mater*, *2*, 568-575. https://doi.org/10.1002/adhm.201200256.

[12]. Oliveira J.T., Gardel L.S. Rada T., Martins L., Gomes M.E., Reis R.L. (2010). Injectable gellan gum hydrogels with autologous cells for the treatment of rabbit articular cartilage defects. *J Orthop Res*, *28*, 1193-1199.https://doi.org/10.1002/jor.21114.

[13]. Coutinho D.F., Sant S., Shin H., Oliveira J.T., Gomes M.E., Neves N.M., Khademhosseini A., Reis R.L. (2010). Modified gellan gum hydrogels with tunable physical and mechanical properties. *Biomaterials*, *31*, 7494-7502.https://doi.org/10.1016/j.biomaterials.2010.06.035.

[14]. Tsaryk R., Silva-Correia J., Oliveira J.M., Unger R.E. Landes C., Brochhausen C., Chanaati S., Reis R.L., Kirkpatrick C.J. (2017). Biological performance of cell-encapsulated methacrylated gellan gum-based hydrogels for nucleus pulposes regeneration. *J Tissue Eng Regen Med*, *11*(3), 637-648. https://doi.org/10.1002/term.1959.

[15]. Silva-Correa J., Miranda-Goncalves V., Salgado A.J., Sousa N., Oliveira J.M., Reis R.L. (2012). Angiogenic potential of gellan-gum-based hydrogels for application nucleus pulposes regeneration: In vivo study. *Tissue Eng Part A*, *18*, 1203-1212.https://doi.org/10.1089/ten.tea.2011.0632.

[16]. Hacker M.C., Nawaz H.A. (2015). Multi-functional macromers for hydrogel design in biomedical and regenerative medicine. *Int J Mol Sci*, *16*, 27677-27706. https://doi.org/10.3390/ijms161126056.

[17]. D'Arrigo G., Navarro G., Di Meo C., Matricardi P., Torchilin V. (2014). Gellan gum nanohydrogel containing anti-inflammatory and anti-cancer drugs: a multi-drug delivery system for a combination therapy in cancer treatment. *European Journal of Pharmaceutics and Biopharmaceutics, 87*(1), 208-216. https://doi.org/10.1016/j.ejpb.2013.11.001.

[18]. D'Arrigo G., Di Meo C., Gaucci E., Chichiarelli S., Coviello T., Capitani D., Alhaaique P., Matricardi P. (2012). Self-assembled gellan gum nanohydrogel as a tool for prednisolone delivery. *Soft Matter, 8*, 11557-11564.https://doi.org/10.1039/C2SM26178B.

[19]. Nandi G., Patra P., Priyadarshini K.S., Ghosh L.K. (2015). Synthesis, characterization and evaluation of methacrylamide grafted gellan as sustained release tablet matrix. *International Journal of Biological Macromolecules, 72*, 965-974. https://doi.org/10.1016/j.ijbiomac.2014.09.052.

[20]. Agibayeva L.E., Kaldybekov D.B., Porfiryeva N.N., Garipova V.R., Mangazbayeva R.A., Moustafine R.I., Semina I.I., Mun G.A., Kudaibergenov S.E., Khutoryanskiy V.V. (2020).Gellan gum and its methacrylated derivatives as in situ gelling mucoadhesive formulations of pilocarpine: In vitro and in vivo studies. *International Journal of Pharmaceutics*, *577*. https://doi.org/10.1016/j.ijpharm.2020.119093.

[21]. Lavikainen J., Dauletbekova M., Toleutay G., Kaliva M., Chatzinikolaidou M., Kudaibergenov S.E., Tenkovtsev A., Khutoryanskiy V.V., Vamvakaki M., Aseyev V. (2021). Poly(2-ethyl-2-oxazoline) grafted gellan gum for potential application in transmucosal drug delivery. *Polym. Adv. Technol*, 1–11. https://doi.org/10.1002/pat.5298.

[22]. Tatykhanova G., Aseyev V., Vamvakaki M., Khutoryanskiy V., Kudaibergenov S. (2022). Ophthalmic drug delivery system based on the complex of gellan and ofloxacin.*Chem. Bull. Kaz. Nat. Univ, 105*(2), 4-12. https://doi.org/10.15328/cb1239.

[23]. Peer D., Karp J.M, Hong S., Farokhzad O.C., Margalit R., Langer R. (2017). Nanocarriers as an emerging platform for cancer therapy. *Nat. Nanotechnol, 2*, 751-760.https://doi.org/10.1038/nnano.2007.387

[24]. Wilhelm S., Tavares A.J., Dai Q., Ohta S., Audet J., Dvorak H.F., Chan W.C.W. (2016). Analysis of nanoparticle delivery to tumors. *Nature Reviews/Materials, 1*, 1-12.https://doi.org/10.1038/natrevmats.2016.14.

[25]. Nurgaziyeva E., Kudaibergenov S., Mun G., Khutoryanskiy V. (2021). Synthesis of fluorescently-labelled poly(2-ethyl-2-oxazoline)-protected gold nanoparticles. *Chemical Bulletin of Kazakh National University*, *100*(1), 12-20. https://doi.org/10.15328/cb1185.

[26]. Wanfen Pu, Chao Shen, Bing Wei, Yang Yang, Yibo Li, (2018). A comprehensive review of polysaccharide biopolymers for enhanced oil recovery (EOR) from flask to field. *Journal of Industrial and Engineering Chemistry*, *61*, 1-11. https://doi.org/10.1016/j.jiec.2017.12.034.

[27]. Shunxiang Xia, Laibao Zhang, Artur Davletshin, Zhuoran Li, Jiahui You and Siyuan Tan.(2020). Application of polysaccharide biopolymer in petroleum recovery. *Polymers,12*, 1860.https://doi.org/10.3390/polym12091860.

[28]. Audibert A., Noik C., Lecourtier J. (1993).Behavior of polysaccharides under harsh conditions. *The Journal of Canadian Petroleum Technology, 32*(7), p.53-58.https://doi.org/10.2118/93-07-05.

[29]. Mothé C.G., Correia D.Z., de França F.P. Riga A.T. (2006).Thermal and rheological study of polysaccharides for enhanced oil recovery. *Journal of Thermal Analysis and Calorimetry, 85*(1), 31–36.

[30]. Yajun Li, Long Xu, Houjian Gong, Boxin Ding, Mingzhe Dong, Yanchao Li. (2017). A microbial exopolysaccharide produced by sphingomonas species for enhanced heavy oil recovery at high temperature and high salinity. *Energy Fuels, 31*, 3960−3969.https://doi.org/10.1021/acs.energyfuels.6b02923.

[31]. Shimaa M.E., Elsayed G.Z., Walaa A.E. Omar A.A.S., Attia M.A. (2021). Guar gum-based hydrogels as potent green polymers for enhanced oil recovery in high-salinity reservoirs. *ACS Omega,* 6(36), 23421–23431. https://doi.org/10.1021/acsomega.1c03352.

[32]. Kalpakci B., Jeans Y., Magri N., Padolewski J. (1990). Thermal stability of scleroglucan at realistic reservoir conditions. In:*SPE/DOE Enhanced Oil Recovery Symposium*, SPE.

[33]. Long Xu, Guiying Xu, Long Yu, Houjian Gong, Mingzhe Dong and Yajun Li. (2014). The displacement efficiency and rheology of welan gum for enhanced heavy oil recovery. *Polym. Adv. Technol*,*25*,1122 – 1129. https://doi.org/10.1002/pat.3364.

[34]. Marianny Y., Combariza A.P., Martínez-Ramírez CristianBlanco-Tirado. (2021). Perspectives in nanocellulose for crude oil recovery: A Minireview. *Energy Fuels,* https://doi.org/10.1021/acs.energyfuels.1c02230.

[35]. Weijia Cao, Kun Xie, Xiaoyan Wang, Xiangguo Lu, Xin He, Guorui Xu, Xiang Li. (2020). Starch graft copolymer and polymer gel applied in Bohai oilfield for water plugging and profile control and their mechanisms. *Geosystem Engineering*, 1-8.https://doi.org/:10.1080/12269328.2020.1732838.

[36]. Elshafie A., Joshi S.J., Al-Wahaibi Y.M., Al-Bahry S.N., Al-Bemani A.S., Al-Hashmi A., Al-Mandhari M.S. (2017). Isolation and characterization of biopolymer producing Omani aureobasidium pullulans strains and its potential applications in microbial enhanced oil recovery *SPE Oil and Gas India Conference and Exhibition*, Mumbai, India, April, Paper No: SPE-185326-MS. https://doi.org/10.2118/185326-MS.

[37]. Al-Araimi S.H., Elshafie A., Al-Bahry S.N., Al-Wahaibi Y.M., Al-Bemani A.S. (2020). Biopolymer production by *Aureobasidiummangrovei* SARA-138H and its potential for oil recovery enhancement. *Applied Microbiology and Biotechnology*,https://doi.org/10.1007/s00253-020-11015-x.

[38]. Ridout M.J., Garza S., Brownsey G.J., Morris V.J. Mixed iota-kappa carrageenan gels. (1996). *Int. J. Biol. Macromol, 18*, 5–8.http:// doi./10.1016/0141-8130(95)01037-8.

[39]. Stefan Iglauer, Yongfu Wu, Patrick Shuler, Yongchun Tang, William A. Goddard. (2011). Dilute iota- and kappa-Carrageenan solutions with high viscosities in high salinity brines. *Journal of Petroleum Science and Engineering, 75*, 304–311. http:// doi./10.1016/j.petrol.2010.11.025.

[40]. Elham Sharifpour, Mehdi Escrochi, Masoud Riazi, Shahab Ayatollahi. (2016). On the importance of gel rigidity and coverage in a smart water shutoff treatment in gas wells. *Journal of Natural Gas Science and Engineering, 31*, 808-818. http://dx.doi.org/10.1016/j.jngse.2016.03.001.

[41]. Chang Hong Gao. (2016). Unique rheology of high acyl gellan gum and its potential applications in enhancement of petroleum production. *J Petrol Explor Prod Technol, 6*,743–747. https://doi.org/10.1007/s13202-015-0212-8.

[42]. Ibragimov R., Gusenov I., Tatykhanova G., Adilov Zh., Nurxat Nuraje, Kudaibergenov S. (2013).Study of gellan for polymer flooding. *Journal of Dispersion Science and Technology, 34*, 1-8. https://doi.org/10.1080/01932691.2012.742766.

[43]. Gussenov I.Sh., Ibragimov R.Sh., Kudaibergenov S.E., Abilkhairov D.T., Kudaibergenov D.N. (2014). Application of polymer gellan for injectivity profile leveling. *SPE Annual Caspian Conference and Exhibition*, 1-7.https://doi.org/10.2118/172299-MS.

[44]. Kudaibergenov S., Nuraje N., Adilov Zh., Abilkhairov D., Ibragimov R., Gusenov I., Sagindykov A. (2015). Plugging behavior of gellan in porous saline media. *Journal of Applied Polymer Science, 132*,41256. https://doi:10.1002/app.41256.

[45]. Kudaibergenov S.E., Gussenov I.Sh., Zhappasbayev B.Zh., Shakhvorostov A.V. (2015). Application of polymer flooding technology for enhanced oil recovery. *Chemical Bulletin of Kazakh National University, 4*(80), 74-80.https://doi.org/10.15328/cb644.

[46]. Nurakhmetova Zh., Gussenov I.Sh.,Tatykhanova G.S., Kudaibergenov S.E. (2015). Behavior of gellan in aqueous-salt solutions and oilfield saline water. *Chemical Bulletin of Kazakh National University, 3*(79), 35-40.https://doi.org/10.15328/cb640.

[47]. Kudaibergenov S.E., Tatykhanova G.S., Sigitov V.B., Nurakhmetova Z.A., Blagikh E.V. Gussenov I.Sh., Seilkhanov T.M. (2016). Physico-chemical and rheological properties of gellan in aqueous-salt solutions and oilfield saline water. *MacromolSymp, 363*, 20-35. https://doi.org/10.1002/masy.201500139.

[48]. Gussenov, I., Zhappasbayev, B., Kudaibergenov, S. (2017). Permeability reduction of heterogeneous oil reservoirs by brine-triggered gellan gel. *Journal of Nanoscience and Nanotechnology, 17*, 9198-9201. https://doi.org/10.1166/jnn.2017.14295.

[49]. Nurakhmetova Zh., Gussenov I., Aseyev V., Sigitov V., Kudaibergenov S. (2018). Application of sol-gel transition of gellan and xanthan for enhanced oil recovery and as drilling fluids. *Journal of Chemical Technology and Metallurgy, 53*, 68-78.

[50]. Kudaibergenov S.E., Abilkhairov D.T., Gussenov I.Sh., Sagindykov A.A. (2015). Pilot tests of polymer flooding technology in oilfield Kumkol. *Oil & Gas, 3*, 75–82 (in Russian).

[51]. Kudaibergenov S.E., Gussenov I.Sh., Zhappasbayev B.Zh., Shakhvorostov A.V., Abilkhairov D.T. (2015). Gel-polymer treatment of oil reservoirs. High efficiency and duration of action. *Oil & Gas Russia, 12*, 76–81 (in Russian).

[52]. Abilkhairov D.T., Zhappasbayev B.Zh., Gussenov I.Sh., Shakhvorostov A.V., Kudaibergenov S.E. (2017). Gel-polymer treatment of exploitation well for water shut-off. *Oil & Gas, 1*, 47–58 (in Russian).

[53]. Gussenov, I., Kudaibergenov, S.E. (2022). Permeability reduction by gellan gum solutions. *Journal of Petroleum Science and Engineering, 208,* 109546. https://doi.org/10.1016/j.petrol.2021.109546.

[54]. Gussenov I., Nuraje N., Kudaibergenov S. (2019).Bulk gels for permeability reduction in fractured and matrix reservoirs. *Energy Reports, 5*, 733-746. https://doi.org/10.1016/j.egyr.2019.06.012.

[55]. Grasdalen H., Smidsrød O. (1987). Gelation of gellan gum. *Carbohydrate Polymers*, *7*, 371-393.https://doi.org/10.1016/j.foodhyd.2012.01.004

[56]. Dreveton E., Monot F., Lecourtier J., Ballerini D., Choplin L. (1996). Influence of fermentation hydrodynamics on gellan gum physic-chemical characteristics. *J. Fermentation and Bioeng*, *82(3)*, 272-276.

[57]. Wagner A.M., Spencer D.S., Peppas N.A. (2018). Advanced architectures in the design of responsive polymers for cancer nanomedicine. *J Appl Polym Sci, 135*, 46154. https://doi.org/10.1002/app.46154.

[58]. Dhar S., Mali V., Bodhankar S., Shiras A., Prasad B.L.V., Pokharkar V. (2011). Biocompatible gellan gum-reduced gold nanoparticles: cellular uptake and subacute oral toxicity studies. *J Appl Toxicol, 31*, 411-420.https://doi.org/10.1002/jat.1595

[59]. Dhar S., Reddy E.M., Pokharkar V., Prasad B.L.V. (2008). Natural gum reduced/stabilized gold nanoparticles for drug delivery formulations. *ChemEur J, 14*, 10244-10250. https://doi.org/10.1002/chem.200801093.

[60]. Dhar S., Reddy E.M., Prabhune A., Pokharkar V., Shiras A., Prasad B.L.V. (2011). Cytotoxicity of sophorolipid-gellan gum-gold nanoparticle conjugates and their doxorubicin loaded derivatives towards human glioma stem cell lines. *Nanoscale, 3*, 575-580.https://doi.org/10.1039/C0NR00598C.

[61]. Dhar S., Murawala P., Shiras A., Pokharkar V., Prasad B.L.V. (2012). Gellan gum capped silver nanoparticle dispersions and hydrogels: cytotoxicity and *in vivo* diffusion studies. *Nanoscale, 4*, 563-567.https://doi.org/10.1039/C1NR10957J

[62]. Huang X.H., Jain P.K. El-Sayed I.H., El-Sayed M.A. (2008). Plasmonic photothermal therapy (PPTT) using gold nanoparticles. *Lasers in Medical Science, 23*, 217-228. https://doi.org/10.1007/s10103-007-0470-x.

[63]. Huang X., Neretina S., El-Sayed M.A. (2009). Gold nanorods: From synthesis and properties to biological and biomedical applications. *Adv. Mater, 21*, 4880-4910.https://doi.org/10.1002/adma.200802789.

[64]. Huang X.H., Jain P.K. El-Sayed I.H., El-Sayed M.A. (2007). Gold nanoparticles: interesting optical properties and recent applications in cancer diagnostic and therapy. *Nanomedicine, 2*, 681-693. https://doi.org/10.2217/17435889.2.5.681.

[65]. Lim, W.Q., Gao, Z. (2016). Plasmonic nanoparticles in biomedicine. *Nano Today, 11*, 168-188. https://doi.org/10.1016/j.nantod.2016.02.002.

[66]. Jabeen, F., Najam-ul-Haq, M., Javeed, R., Huck, C.W., Bonn, G.K. (2014). Au-nanomaterials as a superior choice for near-infrared photothermal therapy. *Molecules, 19*, 20580-20593. https://doi.org/10.3390/molecules191220580.

[67]. Day E.S., Thompson P.A., Zhang L., Lewinski N.A., Drezek R.A., Blaney S.M., West J.L. (2011). Nanoshell-mediated photothermal therapy improves survival in a murine glioma model. *J Neurooncol, 104*, 55-63.https://doi.org/10.1007/s11060-010-0470-8

[68]. Mackey M.A., Ali M.R.K., Austin L.A., Near R.D., El-Sayed M.A. (2014). The most effective gold nanorod size for plasmonic photothermal therapy: Theory and in vivo experiments. *J Phys Chem B, 118*, 1319-1326.https://doi.org/10.1021/jp409298f.

[69]. Viera S., Vial S., Maia F., Carvalho M., Reis R.L., Granja P.L., Oliveira J.M. (2015). Gellan gum-coated gold nanorods: an intracellular nanosystem for bone tissue engineering. *RSC Adv*,https://doi.org/10.1039/C5RA13556G.

[70]. Nikoobakht B., El-Syed M.A. (2003).Preparation and growth mechanism of gold nanorods (NRs) using seed-mediated growth method.*Chem Mater, 15*, 1957-1962.https://doi.org/10.1021/cm0207321

[71]. Pautke C., Schieker M., Tischer T., Kolk A., Neth P., Mutschler W., Milz S. (2004). Characterization of osteosarcoma cell lines MG-63, Saos-2 and U-2 OS in comparison to human osteoblasts.*Anticancer Res, 24*(6), 3743-3748.

[72]. Nurakhmetova Zh.A., Azhkeyeva A.N., Klassen I.A., Tatykhanova G.S. (2020). Synthesis and stabilization of gold nanoparticles using water-soluble synthetic and natural polymers. *Polymers*, *12*, 2625. https://doi.org/10.3390/polym12112625.

[73]. Kudaibergenov S.E., Shakhvorostov A.V., Gussenov I. Sh., Tatykhanova G.S., Kunakbayev E.T., Mukasheva T.D., Berzhanova R. Zh., Akhmetova M.V. (2021). On the perspective of organization of polysaccharide – gellan from domestic raw materials for oil and gas industry. *Materials of International Online Conference "Innovation Technologies in Oil & Gas Sector. Implementation Experience and Perspectives of Development"*, Aktau, November 19, 55-168.

[74]. Guilan Zhu, Long Sheng, Qunyi Tong. (2013). A new strategy to enhance gellan production by two-stage culture in *Sphingomonas paucimobilis*. *CarbohydratePolymers,* 98, 829–834. https://doi.org/10.1016/j.carbpol.2013.06.060